

Structural studies on the ribosomal exit tunnel as a regulator of translation and target of antimicrobials.



Martino Morici

Hamburg, 2024

Dissertation zur Erlangung des Doktorgrades
eingereicht an der Universität Hamburg
Institut für Biochemie und Molekularbiologie
Fachbereich Chemie

1. Gutachter: **Prof. Dr. Daniel N. Wilson**, Universität Hamburg, Hamburg, Deutschland, Institut für Biochemie und Molekularbiologie, Fachbereich Chemie
2. Gutachter: **Prof. Dr. Yury Polikanov**, University of Illinois, Chicago, USA, Biological Sciences
3. Gutachter: **Prof. Dr. Matthieu G. Gagnon**, The University of Texas Medical Branch, Galveston, USA, Department of Microbiology & Immunology

Prüfungskommission:

Prof. Dr. Daniel N. Wilson, Universität Hamburg, Hamburg, Deutschland, Institut für Biochemie und Molekularbiologie, Fachbereich Chemie

Prof. Dr. Andrew Torda, Universität Hamburg, Hamburg, Deutschland, Zentrum für Bioinformatik

Prof. Dr. Tobias Beck, Universität Hamburg, Hamburg, Deutschland, Institut für Physikalische Chemie, Fachbereich Chemie

Disputation: 01/11/2024

Druckfreigabe: 06/11/2024

Die für die Dissertation notwendigen Arbeiten wurden zwischen Januar 2021 und Juni 2024 an der Universität Hamburg im Institut für Biochemie und Molekularbiologie am Fachbereich Chemie in der Arbeitsgruppe von Prof. Dr. Daniel N. Wilson durchgeführt.

List of Publications included in this thesis

Publication 1: RAPP-containing arrest peptides induce translational stalling by short circuiting the ribosomal peptidyltransferase activity

Martino Morici, Sara Gabrielli, Keigo Fujiwara, Helge Paternoga, Bertrand Beckert, Lars V. Bock, Shinobu Chiba and Daniel N. Wilson

Nat Commun. *15*, 2432 (2024)

Publication 2: The SecM arrest peptide traps a pre-peptide bond formation state of the ribosome

Felix Gersteuer*, Martino Morici*, Sara Gabrielli, Keigo Fujiwara, Haaris A. Safdari, Helge Paternoga, Lars V. Bock, Shinobu Chiba and Daniel N. Wilson

Nat Commun. *15*, 2431 (2024)

Publication 3: Structural basis for translation inhibition by the glycosylated drosocin peptide

Timm O. Koller*, Martino Morici*, Max Berger*, Haaris A. Safdari, Deepti S. Lele, Bertrand Beckert, Kanwal J. Kaur and Daniel N. Wilson

Nat Chem. Biol. *19*, 1072-1081 (2023)

List of Publications not included in this thesis

Publication 4: Structural conservation of antibiotic interaction with ribosomes

Helge Paternoga*, Caillan Crowe-McAuliffe*, Lars V. Bock, Timm O. Koller, Martino Morici, Bertrand Beckert, Alexander G. Myasnikov, Helmut Grubmüller, Jiří Nováček, Daniel N. Wilson

Nat Struct Mol Biol. *30*, 1380–1392 (2023).

Publication 5: The cyclic octapeptide antibiotic argyirin B inhibits translation by trapping EF-G on the ribosome during translocation

Maximiliane Wieland*, Mikael Holm*, Emily J. Rundlet*, Martino Morici, Timm O. Koller, Tinashe P. Maviza, Domen Pogorevc, Ilya A. Osterman, Rolf Müller, Scott C. Blanchard, Daniel N. Wilson

Proc Natl Acad Sci U S A. *119*, e2114214119 (2022).

Publication 6: Rest assured: Programmed translational stalling studied by MD simulations

Sara Gabrielli, Martino Morici, Keigo Fujiwara, Helge Paternoga, Bertrand Beckert, Lars V. Bock, Shinobu Chiba, Daniel N. Wilson

Biophys. J. *123*, 361a (2024).

Publication 7: Paenilamicins from the honey bee pathogen *Paenibacillus* larvae are context-specific translocation inhibitors of protein synthesis

Timm O. Koller*, Max J. Berger*, Martino Morici, Helge Paternoga, Timur Bulatov, Adriana Di Stasi, Tam Dang, Andi Mainz, Karoline Raulf, Caillan Crowe-McAuliffe, Marco Scocchi, Mario Mardirossian, Bertrand Beckert, Nora Vazquez-Laslop, Alexander Mankin, Roderich D. Suessmuth, Daniel N. Wilson

Nat Chem. Biol. *Online ahead of print* (2024).

Publication 8: The proline-rich antimicrobial peptide B7-005: low bacterial resistance, safe for human cells and effective in zebrafish embryo bacteraemia model

Adriana Di Stasi, Sara Bozzer, Sabrina Pacor, Luigi de Pascale, Martino Morici, Lara Favero, Mariagiulia Spazzapan, Silvia Pegoraro, Roberta Bulla, Daniel N. Wilson, Paolo Macor, Marco Scocchi, Mario Mardirossian

Open Biol. *In press* (Accepted in principle).

Publication 9: Mechanistic Divergence and Differential Antimicrobial Activity of the Proline-Rich Peptide B7-005: Membrane Disruption and Protein Synthesis Inhibition across ESKAPE+E Pathogens

Adriana Di Stasi, Sara Capolla, Martino Morici, Sara Bozzer, Max Berger, Sabrina Pacor, Thuy Duong Pham, Roberto Spurio, Attilio Fabbretti, Paolo Macor, Daniel N. Wilson, Marco Scocchi, Mario Mardirossian

Manuscript submitted.

Table of contents

List of Publications included in this thesis	4
List of Publications not included in this thesis	5
Acknowledgements	9
Abbreviations	23
Zusammenfassung	26
Summary	28
Introduction	30
The bacterial “Gene Machine”: focus on the prokaryotic ribosome	31
Bacterial translation cycle	33
Translation initiation	36
Translation elongation	39
Decoding	40
Peptide bond formation	43
Ribosome translocation	47
Translation termination	51
Ribosome recycling	55
The ribosome exit tunnel and its role in protein synthesis	57
Bacterial translation: the perfect antimicrobial target	64
Inhibitors of initiation	64
Inhibitors of elongation: decoding and accommodation	65
Inhibitors of elongation: peptide bond formation	66
Inhibitors of elongation: translocation	66
Inhibitors of termination and recycling	67
Focus on antimicrobial peptides	68
The case of proline-rich antimicrobial peptides	70

Objective of these studies: Structural insights into the fundamental role of the bacterial ribosome exit tunnel.....	76
Cumulative Thesis: Summary of Publications	78
Publication 1: RAPP-containing arrest peptides induce translational stalling by short circuiting the ribosomal peptidyltransferase activity	78
Publication 2: The SecM arrest peptide traps a pre-peptide bond formation state of the ribosome	79
Publication 3: Structural basis for translation inhibition by the glycosylated drosocin peptide	80
Discussion and Outlook.....	82
Arrest peptides short-circuiting the ribosome: a small hydrogen atom vs a titanic macromolecular machine	82
Add some sugar: a sweet desert at the end of translation. The case of the class II PrAMP drosocin	86
The ribosome is a ribozyme... which ribozyme? Insights into peptide bond formation from our structural studies	89
The ceiling of the A-site: an interesting pocket	91
Conclusion.....	92
References	94
Auflistung der Gefahrstoffe nach GHS.....	132
Declaration on Oath.....	134
Publications.....	135

Acknowledgements

Contrary to what one may think, this is not going to be the easiest section of my thesis to write. A doctorate is a path that lasts many years, important ones of the life of an individual. At least, they were very important for me. I feel the need to thank many people, and I want to do so not with sterile words, but by showing how much I owe to all the people I am going to list. This section is both in english and in italian, since many of you are more familiar with Dante's language.

Two people contributed the most to this time of my life, and I am going to mention one as the first and one as the last.

I want to start with the person which is at the beginning and at the end of this experience of mine: Prof. Daniel N. Wilson. Dear Daniel, I spent so much time thinking about what should I thank you for. It is indeed very difficult for me to faithfully express how much I am grateful to you. For a start, you offered me an opportunity that changed my life, and it did so for good. I left my country to join your group, and I never regretted. These years I really enjoyed working for you and discussing together always gave me the feeling that this was not my job, but was us working on a passion we share. You have been an excellent mentor, a person I could trust and a friend. You taught me so much and at the same time you helped me always, even in situations in which it was not your moral or professional duty. The time I worked as a PhD with you will strongly affect my career in a beneficial way, and this I will not forget. In your eyes I noticed a glimpse of genius: you have been the best guide for me, in this moment of my path. I will finish by mentioning the thing I should thank you for the most: freedom, which is the most important thing a scientist should ask for. You gave me everything I was looking for in a PhD. I hope that I left you something in exchange to what you left me and that we can continue working together somehow. I will always owe you.

Next I wish to thank all the members of my group. Doing science is not easy and your presence and help was crucial for my doctorate experience. I want to thank Bertrand, because despite the very short time he supervised me, he taught me a lot, and I am sure that beneath his rough ways there is a good heart. Timm deserves for sure special thanks: you are the one that helped me the most in the group, you taught me a lot of things with infinite patience and also assisted me in solving personal problems. Together with Max, who never missed the chance to encourage me, we share a paper and this was the result of a friendly synergy. Helge has been the senior in our group, and to be honest he was the best senior you could ask for. I cannot forget your infinite patience and wish to teach and help, often without asking for anything back. You are a really good person, Helge, I wish you the best for your future in science. I also want to thank Lucy: when I talk about you to other people, I always say that I wish to finish my carrier having become one tenth of how expert and efficient you are. I want to thank Karo, because you are an example of how someone can be gentle but strong at the same time. You have been a key presence that made the social environment more pleasant, always taking the lead in making PhD hats and organizing gifts. Among the people I

worked with, Felix has shown a remarkable set of skills and sharp mind. I am really thankful I had the chance to work with you, and it was a pleasure working together on the SecM project... you really are the golden boy. Haaris must be thanked for his continuous effort in making grids and collecting datasets: this was beneficial for the whole group. He was always ready to teach others, to help and to discuss projects. I am quite sure that for you this time here was not easy as well, being very far from home. However you resisted and made the best out of it. It is my wish to thank Martina, for the work we did together in Daniel's lab and for the experiences we shared in this city. Among my colleagues, Andrea is for sure the most passionate about ribosomes and cryo-EM, and I will always remember with pleasure the nights spent drinking wine and discussing about ribosomes. Your presence was a slice of Italy inside the lab. I want to thank Amanda for making the time in the lab and in the office funnier than usual, and for being a friend in good times and bad times. A visiting member of the lab, which became a hamburger and a friend, is Bi, which I want to thank for being my best viet cong. Despite not being part of our scientific team, Danny was a crucial element of the group, for everyone and also for me. You are a pillar of the group, always ready to help everyone with a smile.

Science is something you do together, so it is very important for me to thank all the collaborators in the projects I worked on. In particular I want to start with Prof. Shinobu Chiba and his postdoc Keigo Fujiwara, since their tremendous and beautiful amount of work was the base and the cement of all the projects on stallers in the lab, especially RAPP arrest peptides and SecM. To these projects, also Sara Gabrielli and Dr. Lars Bock gave a crucial contribution, and it was fun to get drunk together in Heidelberg. Essential was also the service for grid making and data collection, which is at the base of the work done in our lab. For this, it is important to particularly mention Dr. Jiří Nováček from Ceitec (Brno), Cornelia Cazey and Dr. Carolin Seuring from the CSSB (Hamburg). They were extremely professional and pleasant to work with.

I want to express my gratitude also to Dr. Mario Mardirossian and Dr. Marco Scocchi. Their precision and dedication made me proud of being an Italian scientist and it was a pleasure to talk for hours on the phone with Mario about ribosomes and peptides. A collaborator that deserves a special mention is Prof. Witold Szaflarski: Witek was not only a collaborator, but also a member of the lab, a colleague, a mentor and a friend which was always there, available and happy to collaborate with a smile. Similarly, Prof. Pohl Milon established with our lab a great collaboration we are all thankful for, and I always enjoyed discussing with him, who became also a good friend of mine.

There are also a few people I met here in Hamburg which made my stay in the city something I would miss. First of all Misha: dear Misha, we met in a very difficult and dark period of our lives, and we shared years together in this city. I found in you a honest friend and a brother I can always count on, despite we are very far and rarely in touch, but always thinking about each other. I wish you the best, and I am sure you will get it. It is my pleasure to mention the members of the Ignatova lab, especially Nikhil Bharti who is also my neighbor, for inviting me to hang out with them... those were

fun nights. I recently had the chance to meet Jorge, who became my friend very fast and spontaneously. You made me feel home, somehow, and I can tell that you are a very good scientist. I recognized this when we met. The time I spent here was also partially shared with Rossana, which I met before starting the PhD: thanks Ross for being a really good friend, always present for me and sorry for not reaching out so frequently.

There are then several people that were crucial for my scientific life not entirely related to Hamburg. Given the primary role that science plays for me, I want to thank them. In this list, the first is without any doubt Prof. Giorgio Pennacchiotti Cappannini. Dear Giorgio, I can hear you saying “one is born a scientist, doesn’t become one” while reading this, however let me tell you that for one time you are wrong. It is important for me to thank you from the bottom of my heart, because you were the sparkle of my scientific path. I will never forget your lessons and you have to be aware that you changed my life, and with mine the one of many generations of scientists you inspired. Martin Luther King once said that whatever job you are doing, you have to perform that so that if the angels of God come down and look at the outcome, they would be surprised for how good this was. This is how you gave your lessons, Giorgio, and you should be proud of that, because of that many people will never forget you.

Among these people, among your students, there is also the second person of this list: Prof. Attilio Fabbretti. If science is my second family, without any doubt Attilio would be my father. I remember when we met by chance in the corridors in Camerino... that evening changed my life. I am so thankful that you dedicated your time to teach me directly, and this was not solely beneficial for my skills, but mostly for my scientific mindset. I am proud that I am your student and you are the one who first trained me. This is priceless, and there are very few people I respect how I respect you, but I am quite sure you are aware of that... at the end of the day, you are the world’s best and most humble molecular biologist. Be aware that while fighting your war, you will always have a soldier in me.

Another very important person of this list is also a son of Camerino, and I am referring to Prof. Stefano Marzi. Dear Sté, I got to know you as a mentor during my very first experience outside Italy. Let me tell you that you did an amazing job, and in that very difficult moment of my personal life you have also been a friend, and both these roles stayed. You are one of the first people I call when I need a suggestion, because I like the way you think as a scientist and as an individual. I have always considered you and Angelita part of my extended family, and I can’t think of many people that had such a positive impact in my life. I owe you two in so many ways that these few lines would have never been sufficient, not even if Giacomo Leopardi would be writing them. Thank you so much, I am sure we will have many chances to work together and hang out in the future, which is always fun.

Before coming to Hamburg, I did my Master Degree in Pavia, where I was so lucky to be trained in the lab of Prof. Giovanna Riccardi, which I am happy to thank for the chance she gave me. Dear Prof., I have always had religious respect for you and I will

be always thankful for the time I spent in your lab. These were very important years for my training, which were possible also thank to Prof. Laurent Chiarelli and Dr. J. Camilla Sammartino. Thank you Laurent and Camilla, I remember and apply daily your teachings and dedication to science.

In Pavia I also had the possibility to attend two courses that strongly affected my path. I want to thank the teachers of these courses, Prof. Andrea Mattevi and Prof. Federico Forneris, who introduced me to structural biology and made me fall in love with this artistic slice of biology. In particular I want to mention how Prof. Forneris is the main reason why I decided to study Cryo-EM and this brought me to Hamburg. Very few people teach like you, and I think you really deserve the name of the Stupor Mundi.

In Pavia I also met Prof. Ermanno Gherardi, the dean of Collegio Volta, which hosted me in those happy years. Thank you Prof. Gherardi for being a stimulating dean and mentor, making the residence a fertile scientific environment.

I want to continue mentioning my friends, some of which I met thanks to science, some other were wonderful gifts I found in my path.

The first to be mentioned are my two snack buddies, aka Lorenzo Penna and Valentino Di Guglielmo.

Lorenzo, you have been my first best friend and my all time favourite artist. I think that you have been given a gift that you didn't waste, but cultivated. Art speaks through you, and I am so proud to be your friend. Thank you for always staying at my side, sorry if sometimes I am annoying, but this is my most sincere way to show my affection to you, but I am sure you are aware of this.

Dear Vale, there is no way I can express how much I feel lucky to be your friend. Many things I need to mention, but I want to cut it short saying that I appreciate so much how loyal and constant you have always been to me. You are part of my family and always there, when I am sad and when I am happy. The best hours of my life I have spent with you, and I will never forget these... you are always close, no matter which continent I am at the moment. Thanks Vale, I hope to be for you a friend as good as you have always been to me. I really love you.

Among my friends, there are some I want to mention because I was always fascinated by their beautiful mind, which matches the infinite power of their souls. I am talking about Giada Marinelli, Kevin Massani and Davide Lusito. The reason why you belong to the same paragraph is that you have taught me something: It is possible to be brothers also without being relatives. Because this is what you are to me: brothers, and you have deserved this position. The chance of us meeting were extremely low and I am so glad this happened. We are sparse in Europe, but there is something that will always connect us. I will always be there for you, do not forget.

One of my homes was Liceo Scientifico Leonardo Da Vinci, which not only made me meet a lot of good teachers, but also many good friends. Some of them stayed, and I want to mention Beatrice Abatelli, Marco Centanni and Elena Casagrande. Spending time with you is always a pleasure and despite me being always far, you are always in

my thoughts. I am sure you will achieve your dreams for which you have worked so much.

The web connecting most of the people I listed here is called University of Camerino. Camerino for me is like a old friend, like a woman I loved. It gave me so much and it will always be in my heart. Two of the most beautiful gifts I received there are for sure Andrea Della Valle and Lisa Armillei. You are exceptionally rare individual, which, despite your very difficult lives, shine like stars in a very dark sky. This is how I see you, and meeting you was unlikely, but among the best things happened in my life. Thank you for existing and being there for me.

Also Pavia gave me a lot. I would never miss to mention my two angels: Marta & Eleonora. I always think about you, and I am so proud of who you became. We are really far apart, but somehow I feel you as close as the people I see every day. Your pure souls and beauty is a sun shining on my life. Take care and don't make me worry about you.

Raffaella deserves special thanks: you have been really close to me during this last and difficult year of PhD. You have been the best friend one could ask for. I am sure one day you will realize how strong and precious you are. Your presence was positive and often essential during my difficult days here, and I hope I could match the important contribution you had in my life.

Many of you are aware that I don't sleep that much. For sure, another creature of the night is familiar with this. I am talking about Lara Romeo. Lara, you are an exceptional friend, always there to help me. Your point of view has often been something I was missing in my schematics and reasoning. Thank you for being my friend in these years and please do not forget that you are a rare flower.

I want to spend few lines also to thank some artists, because seriously: what is life without art? During each day of my life here, paintings and music played a primary role in making everything better. I would like to thank many, but I am going to keep my list short. I want to thank Vincent Van Gogh, for being an example of passion and dedication and for showing the world that madness is not a disease but only another pair of glasses to see reality. To this weird list also belongs Tarek Iurcich, also known as Rancore. I wish I can express my inner demon through my science as you do through your masterpieces, you have been a daily brother in arms. Finally I want to thank Michele Salvemini, aka Caparezza, for being my older brother and my friend since I could think, being there for me every day, when I was feeling good and when I was feeling bad. You have always been an active presence in my life.

The last section of this list is dedicated to my relatives, the first family I had. "Family is all" said someone, and Hamburg made me realize how much this is true. My family allowed me to study, and this is the best gift they could give me. They have always been there to support and help me, all of them, no matter what. They have been my life-long teachers.

Dear Mom, thank you for being the best parent I could ask for. Thank you for loving me so much, always and always more. I apologize if I make you suffer by being far away, but I hope one day you will understand that this is the only way I have to feel alive. I am sorry if I am a scorzo', but remember that I am the grandson of your father. This doesn't mean I don't love you back, but I am sure you know. You are always in my mind, and I honestly think that the world doesn't deserve a person as good as you... for sure I do not, but I am happy I have you, as all your students... I also am one of them.

Dear Dad, thank you for being the way you are and being always there to help, without hesitation and without taking the credit. Despite our differences, I think we are complementary and there is a bit of you in me and a bit of me in you. I am aware that it is not easy to be a father and that is even less easy to be my father. Sorry for often not being lovely and talkative, but we are Morici and we understand each other without words.

Maria, thank you for being my sister and for showing me brotherhood, even if my thoughts are very difficult to penetrate and I am restive in showing my love to you. This to be said, we all know that you are aware of that love being there, and that you understand how I am, in good and bad. It is always nice to receive a call from you, even if I pretend to be annoyed... but this you know, right?

Dear Zia Laura, I thank you for having given me two wonderful cousins that were always like little brothers to me. Jacopo and Giulio, I am so proud of you, and I become more proud as the days pass. Please, don't stop making me proud of you, and remember that I am not the only one always looking at your life from far away. Please, continue studying, this is the only thing I ask you.

Zio Cesare, you are also in this list. In the past I used to judge you and to dislike you, but let me confess that as the years pass, I understand you more and more. You didn't have a easy life, and despite that you always gift a smile to whoever surround you. I really think you have something more than the others, and remember: I am your only real nephew!

Dear Nonna, on this planet you are the person I respect and trust the most. To me you are a real hero. You always supported me in my life and my studies and loved me unconditionally. You are so important to me, because you were always my best teacher. This section is all about teachers, and nobody can match you, because you are always right, I don't know how this is possible. I hope one day you will forgive me for all the pain I caused you because I left home. It was not an easy decision, and I feel it on my skin every day of my life since years. However it was essential, and I am sure you are intelligent enough to understand this; for sure you love me enough to understand this.

I want to close this long list by thanking the person I loved the most in my life.

Dear Nonno, thank you for always being there for me, since the moment I was born. You didn't owe me anything and despite this you have always shown the special love you had for me. You have been a baby-sitter, a teacher, a mentor and a friend. You have thought me how to talk, how to walk, how to shave, how to drive and how to

behave. You gave me everything and you never asked for anything back. You decided to leave while I was here in Germany and I didn't have the chance and the strength to say goodbye. This is because I really feel like you never left. For me you are indeed a constant presence: I feel you so close and I like to think that you live in all the things I say and do, in all the people I meet, in all the experiences I have. This keeps me going, you keep me going; in any moment, even as I am writing, you are here. I hope I am making you proud of me, as a proof of the special love I had and have for you. I would like to remember you as you were, to think you as alive... I would like to think that you are still listening to me, and while doing so, smiling.

Ringraziamenti

Contrariamente a quanto si possa pensare, questa non sarà la sezione della tesi più facile da scrivere. Il dottorato è un percorso che dura molti anni importanti per la vita di un individuo. Perlomeno, per me sono stati molto importanti. Sento il bisogno di ringraziare molte persone e voglio farlo non con parole sterili, ma mostrando quanto devo a tutte le persone che elencherò. Questa sezione è sia in inglese che in italiano, poiché molti di voi hanno più familiarità con la lingua di Dante.

Due persone hanno contribuito maggiormente a questo periodo della mia vita e ne citerò una come prima e una come ultima.

Voglio iniziare con la persona che è all'inizio e alla fine di questa mia esperienza: il Prof. Daniel N. Wilson. Caro Daniel, ho passato tanto tempo a pensare per cosa avrei dovuto ringraziarti. È infatti molto difficile per me esprimere fedelmente quanto ti sono grato. Per cominciare mi hai offerto un'opportunità che ha cambiato la mia vita e lo ha fatto per sempre. Ho lasciato il mio Paese per unirmi al tuo gruppo e non me ne sono mai pentito. In questi anni mi è piaciuto molto lavorare per te e discutere insieme mi ha sempre dato la sensazione che questo non fosse il mio mestiere, ma che fossimo noi a lavorare su una passione che condividiamo. Sei stato un ottimo mentore, una persona di cui ho potuto fidarmi e un amico. Mi hai insegnato tanto e allo stesso tempo mi hai sempre aiutato anche in situazioni in cui non era tuo dovere morale o professionale. Il periodo in cui ho lavorato con te come dottorando influenzerà fortemente la mia carriera in modo positivo e questo non lo dimenticherò. Nei tuoi occhi ho scorto il barlume di genio: sei stato la migliore guida per me in questo momento del mio percorso. Concludo citando la cosa per cui devo ringraziarti di più: la libertà, che è la cosa più importante che uno scienziato dovrebbe chiedere. Mi hai dato tutto quello che cercavo in un dottorato. Spero di averti lasciato qualcosa in cambio di quello che tu hai lasciato a me e di poter continuare a lavorare insieme in qualche modo. Sarò sempre in debito con te.

Desidero poi ringraziare tutti i membri del mio gruppo. Fare scienza non è facile e la vostra presenza e il vostro aiuto sono stati fondamentali per la mia esperienza di dottorato. Voglio ringraziare Bertrand perché nonostante il brevissimo tempo in cui mi ha seguito mi ha insegnato molto e sono sicuro che sotto i suoi modi rudi c'è un cuore buono. Timm merita sicuramente un ringraziamento speciale: sei quello che mi ha aiutato di più nel gruppo mi hai insegnato tante cose con infinita pazienza, aiutandomi anche a risolvere problemi personali. Insieme a Max, che non ha mai perso l'occasione di incoraggiarmi, abbiamo condiviso un articolo e questo è stato il risultato di una sinergia amichevole. Helge è stato il senior del nostro gruppo e ad essere onesti è stato il miglior senior che si potesse chiedere. Non posso dimenticare la sua infinita pazienza e il suo desiderio di insegnare e aiutare spesso senza chiedere nulla in cambio. Sei davvero una brava persona, Helge e ti auguro il meglio per il tuo futuro nella scienza. Voglio ringraziare anche Lucy: quando parlo di te ad altre persone dico sempre che vorrei finire la mia carriera diventando un decimo di quanto sei esperta ed efficiente

tu. Voglio ringraziare Karo perché sei un esempio di come si possa essere gentili e forti allo stesso tempo. Sei stata una presenza fondamentale che ha reso più piacevole l'ambiente sociale prendendo sempre l'iniziativa di fare cappelli di dottorato e organizzare i regali. Tra le persone con cui ho lavorato, Felix ha dimostrato competenze notevoli e una mente acuta. Sono davvero grato di aver avuto la possibilità di lavorare con te ed è stato un piacere lavorare insieme al progetto SecM... sei davvero un ragazzo d'oro. Haaris deve essere ringraziato per il suo continuo impegno nel fare griglie e nella raccolta di dataset: questo è stato utile per l'intero gruppo. È stato sempre pronto a insegnare agli altri, ad aiutare e a discutere i progetti. Sono certo che anche per te questo periodo qui non è stato facile, essendo molto lontano da casa. Tuttavia hai resistito e ne hai tratto il meglio. Desidero ringraziare Martina per il lavoro svolto insieme nel laboratorio di Daniel e per le esperienze che abbiamo condiviso in questa città. Tra i miei colleghi, Andrea è sicuramente il più appassionato di ribosomi e cryo-EM e ricorderò sempre con piacere le serate passate a bere vino e a discutere di ribosomi. La sua presenza è stata un pezzo d'Italia all'interno del laboratorio. Voglio ringraziare Amanda per aver reso il tempo in laboratorio e in ufficio più divertente del solito e per essere stata un'amica nei momenti belli e in quelli brutti. Un membro ospite del laboratorio che è diventato una hamburger e una amica è Bi, che voglio ringraziare per essere il mio miglior viet cong. Nonostante non facesse parte del nostro team scientifico, Danny è stata un elemento fondamentale del gruppo per tutti e anche per me. Sei un pilastro del gruppo, sempre pronta ad aiutare tutti con un sorriso. La scienza è qualcosa che si fa insieme quindi è molto importante per me ringraziare tutti i collaboratori dei progetti su cui ho lavorato. In particolare vorrei iniziare con il Prof. Shinobu Chiba e il suo postdoc Keigo Fujiwara poiché la loro enorme e incredibile mole di lavoro è stata la base e il cemento di tutti i progetti sugli staller del laboratorio in particolare i peptidi RAPP e SecM. A questi progetti anche Sara Gabrielli e il dottor Lars Bock hanno dato un contributo fondamentale ed è stato divertente ubriacarsi insieme a Heidelberg. Essenziale è stato anche il servizio di produzione di griglie e raccolta dati che è alla base del lavoro svolto nel nostro laboratorio. Per questo è importante citare in particolare il dottor Jiří Nováček del Ceitec (Brno), Cornelia Cazey e la dottoressa Carolin Seuring del CSSB (Amburgo). Sono stati estremamente professionali e piacevoli. Voglio esprimere la mia gratitudine anche al dottor Mario Mardirossian e al dottor Marco Scocchi. La loro precisione e dedizione mi hanno reso orgoglioso di essere uno scienziato italiano ed è stato un piacere parlare per ore al telefono con Mario di ribosomi e peptidi. Un collaboratore che merita una menzione speciale è il Prof. Witold Szaflarski: Witek non è stato solo un collaboratore ma anche un membro del laboratorio, un collega, un mentore e un amico sempre presente, disponibile e felice di collaborare con un sorriso. Allo stesso modo il Prof. Pohl Milon ha stabilito con il nostro laboratorio una grande collaborazione di cui siamo tutti grati e mi è sempre piaciuto discutere con lui, che è diventato anche un mio buon amico.

Ci sono anche alcune persone che ho incontrato qui ad Amburgo e che hanno reso il mio soggiorno in questa città qualcosa che mi mancherà. Innanzitutto Misha: caro

Misha ci siamo incontrati in un periodo molto difficile e buio delle nostre vite e abbiamo condiviso anni insieme in questa città. Ho trovato in te un amico sincero e un fratello su cui posso sempre contare, nonostante siamo molto lontani e ci sentiamo raramente, ma pensiamo sempre l'uno all'altro. Ti auguro il meglio e sono sicuro che lo otterrai. Ho il piacere di menzionare i membri del laboratorio Ignatova, in particolare Nikhil Bharti, che è anche mio vicino di casa, per avermi invitato a uscire con loro... sono state serate divertenti. Di recente ho avuto l'occasione di conoscere Jorge, che è diventato mio amico molto velocemente e spontaneamente. Mi hai fatto sentire a casa in qualche modo e posso dire che sei un ottimo scienziato. L'ho capito quando ci siamo incontrati. Il tempo che ho trascorso qui è stato in parte condiviso anche con Rossana, che ho conosciuto prima di iniziare il dottorato: grazie Ross per essere un'ottima amica sempre presente per me e scusami se non scrivo spesso.

Ci sono poi diverse persone che sono state fondamentali per la mia vita scientifica non del tutto legate ad Amburgo. Dato il ruolo primario che la scienza svolge per me, voglio ringraziarle.

In questo elenco il primo è senza dubbio il Prof. Giorgio Pennacchietti Cappannini. Caro Giorgio, leggendo queste righe mi sembra di sentirti dire "scienziati si nasce, non si diventa", ma permettimi di dirti che per una volta ti sbagli. È importante per me ringraziarti dal profondo del mio cuore, perché sei stato la scintilla del mio percorso scientifico. Non dimenticherò mai le tue lezioni e devi sapere che hai cambiato la mia vita, e con la mia quella di molte generazioni di scienziati che hai ispirato. Martin Luther King una volta disse che qualunque lavoro tu stia facendo, devi farlo in modo tale che se gli angeli del Signore scendessero e guardassero il risultato, sarebbero sorpresi per quanto è stato fatto bene. È così che tu davi le tue lezioni, Giorgio, e dovresti esserne orgoglioso, perché per questo motivo molte persone non ti dimenticheranno mai.

Tra queste persone, tra i tuoi studenti, c'è anche la seconda persona di questa lista: il Prof. Attilio Fabbretti. Se la scienza è la mia seconda famiglia, senza alcun dubbio Attilio sarebbe mio padre. Ricordo quando ci siamo incontrati per caso nei corridoi di Camerino... quella sera ha cambiato la mia vita. Sono così grato che tu abbia dedicato il tuo tempo per insegnarmi direttamente, e questo non è stato solo utile per le mie competenze, ma soprattutto per la mia mentalità scientifica. Sono orgoglioso di essere tuo studente e sei tu che mi hai formato per primo. Questo è inestimabile, e ci sono pochissime persone che rispetto come rispetto te, ma sono abbastanza sicuro che tu lo sappia già... dopotutto, sei il miglior e più umile biologo molecolare del mondo. Sappi che nel combattere la tua guerra, avrai sempre un soldato.

Anche un'altra persona molto importante di questa lista è figlia di Camerino, e mi riferisco al Prof. Stefano Marzi. Caro Sté, ti ho conosciuto come mentore durante la mia prima esperienza fuori dall'Italia. Permettimi di dirti che hai fatto un lavoro straordinario, e in quel momento molto difficile della mia vita personale sei stato anche un amico, ed entrambi questi ruoli sono rimasti. Sei una delle prime persone che chiamo quando ho bisogno di un consiglio, perché mi piace il modo in cui pensi come

scienziato e come individuo. Ho sempre considerato te e Angelita parte della mia famiglia allargata, e non riesco a pensare a molte persone che abbiano avuto un impatto così positivo sulla mia vita. Vi devo tanto in così tanti modi che queste poche righe non sarebbero mai sufficienti, nemmeno se Giacomo Leopardi le stesse scrivendo. Grazie mille, sono sicuro che avremo molte occasioni per lavorare insieme e vederci in futuro, che è sempre divertente.

Prima di venire ad Amburgo, ho conseguito la mia laurea magistrale a Pavia, dove sono stato così fortunato da essere formato nel laboratorio della Prof.ssa Giovanna Riccardi, che sono felice di ringraziare per l'opportunità che mi ha dato. Cara Prof.ssa, ho sempre avuto un rispetto religioso per lei e sarò sempre grato per il tempo trascorso nel suo laboratorio. Questi sono stati anni molto importanti per la mia formazione, resi possibili anche grazie al Prof. Laurent Chiarelli e alla Dott.ssa J. Camilla Sammartino. Grazie Laurent e Camilla, ricordo e applico quotidianamente i vostri insegnamenti e la vostra dedizione alla scienza.

A Pavia ho anche avuto la possibilità di frequentare due corsi che hanno fortemente influenzato il mio percorso. Voglio ringraziare i docenti di questi corsi, il Prof. Andrea Mattevi e il Prof. Federico Forneris, che mi hanno introdotto alla biologia strutturale e mi hanno fatto innamorare di questo lato artistico della biologia. In particolare, voglio menzionare come il Prof. Forneris sia la ragione principale per cui ho deciso di studiare cryo-EM e questo mi ha portato ad Amburgo. Pochissime persone insegnano come te, e penso che ti meriti davvero il nome dello Stupor Mundi.

A Pavia ho anche incontrato il Prof. Ermanno Gherardi, il rettore del Collegio Volta, che mi ha ospitato in quegli anni felici. Grazie Prof. Gherardi per essere un rettore e mentore stimolante, rendendo il Collegio un ambiente scientifico fertile.

Voglio continuare menzionando i miei amici, alcuni dei quali ho conosciuto grazie alla scienza, altri sono stati meravigliosi doni che ho trovato lungo il mio cammino.

I primi da menzionare sono i miei due compagni di merende, alias Lorenzo Penna e Valentino Di Guglielmo.

Lorenzo, sei stato il mio primo migliore amico e il mio artista preferito di sempre. Penso che tu abbia ricevuto un dono che non hai sprecato, ma coltivato. L'arte parla attraverso di te, e sono così orgoglioso di essere tuo amico. Grazie per essere sempre stato al mio fianco, scusa se a volte sono fastidioso, ma questo è il mio modo più sincero per mostrarti il mio affetto, ma sono sicuro che tu ne sia consapevole.

Caro Vale, non c'è modo di esprimere quanto mi sento fortunato ad essere tuo amico. Ci sono molte cose che dovrei menzionare, ma voglio essere breve dicendo che apprezzo moltissimo quanto sei sempre stato leale e costante con me. Sei parte della mia famiglia e sempre presente, quando sono triste e quando sono felice. Le migliori ore della mia vita le ho passate con te, e non le dimenticherò mai... sei sempre vicino, non importa in quale continente mi trovi in quel momento. Grazie Vale, spero di essere per te un amico buono quanto tu lo sei sempre stato per me. Ti voglio davvero bene.

Tra i miei amici, ce ne sono alcuni che voglio menzionare perché sono sempre stato affascinato dalla loro mente, che fa da specchio all'infinita potenza delle loro anime.

Sto parlando di Giada Marinelli, Kevin Massani e Davide Lusito. La ragione per cui appartenete allo stesso paragrafo è che mi avete insegnato qualcosa: è possibile essere fratelli anche senza essere parenti. Perché questo è ciò che siete per me: fratelli, e avete meritato questo ruolo. Le possibilità di incontrarci erano estremamente basse e sono così felice che sia successo. Siamo sparsi per l'Europa, ma c'è qualcosa che ci conetterà sempre. Sarò sempre lì per voi, non dimenticatelo.

Una delle mie case è stata il Liceo Scientifico Leonardo Da Vinci, che non solo mi ha fatto incontrare molti bravi insegnanti, ma anche molti buoni amici. Alcuni di loro sono rimasti, e voglio menzionare Beatrice Abatelli, Marco Centanni ed Elena Casagrande. Passare del tempo con voi è sempre un piacere e nonostante io sia sempre lontano, siete sempre nei miei pensieri. Sono sicuro che realizzerete i vostri sogni per cui avete lavorato tanto.

La rete che connette la maggior parte delle persone elencate qui si chiama Università di Camerino. Camerino per me è come un vecchio amico, come una donna che ho amato. Mi ha dato tanto e sarà sempre nel mio cuore. Due dei regali più belli che ho ricevuto lì sono sicuramente Andrea Della Valle e Lisa Armillei. Siete individui eccezionalmente rari, che, nonostante le vostre vite molto difficili, brillano come stelle in un cielo molto scuro. È così che vi vedo, e incontrarvi era improbabile, ma tra le migliori cose accadute nella mia vita. Grazie per esistere e per essere lì per me.

Anche Pavia mi ha dato tanto. Non potrei mai non menzionare i miei due angeli: Marta & Eleonora. Penso sempre a voi, e sono così orgoglioso di ciò che siete diventate. Siamo davvero lontani, ma in qualche modo vi sento vicine come le persone che vedo ogni giorno. Le vostre anime pure e la vostra bellezza sono un sole che brilla sulla mia vita. Prendetevi cura di voi e non fatemi preoccupare.

Raffaella merita ringraziamenti speciali: sei stata davvero vicina a me durante quest'ultimo e difficile anno di dottorato. Sei stata la migliore amica che si potesse chiedere. Sono sicuro che un giorno ti renderai conto di quanto sei forte e preziosa. La tua presenza è stata positiva e spesso essenziale durante i miei giorni difficili qui, e spero di aver ricambiato l'importante contributo che hai avuto nella mia vita.

Molti di voi sanno che non dormo molto. Di sicuro, un'altra creatura della notte lo sa bene. Sto parlando di Lara Romeo. Lara, sei un'amica eccezionale, sempre pronta ad aiutarmi. Il tuo punto di vista è spesso qualcosa che mi manca nei miei schemi e ragionamenti. Grazie per essere stata mia amica in questi anni e per favore non dimenticare che sei un fiore raro.

Voglio spendere qualche riga anche per ringraziare alcuni artisti, perché seriamente: che cos'è la vita senza arte? Durante ogni giorno della mia vita qui, i dipinti e la musica hanno svolto un ruolo primario nel rendere tutto migliore. Vorrei ringraziare molti, ma limiterò la mia lista. Voglio ringraziare Vincent Van Gogh, per essere un esempio di passione e dedizione e per aver mostrato al mondo che la follia non è una malattia, ma solo un altro paio di occhiali per vedere la realtà. A questa strana lista appartiene anche Tarek Iurcich, noto anche come Rancore. Vorrei poter esprimere il mio demone interiore attraverso la mia scienza come tu fai attraverso i tuoi capolavori, sei stato un

fratello d'armi in questi anni. Infine voglio ringraziare Michele Salvemini, alias Caparezza, per essere il mio fratello maggiore e il mio amico da quando ho iniziato a pensare, essendo lì per me ogni giorno, quando mi sentivo bene e quando mi sentivo male. Sei sempre stato una presenza attiva nella mia vita.

L'ultima sezione di questa lista è dedicata ai miei parenti, la prima famiglia che ho avuto. "La familia es todo", ha detto qualcuno, e Amburgo mi ha fatto capire quanto questo sia vero. La mia famiglia mi ha permesso di studiare, e questo è il miglior regalo che potessero farmi. Sono sempre stati lì per supportarmi e aiutarmi, tutti loro, indipendentemente da tutto. Sono stati i miei insegnanti per tutta la vita.

Cara Mamma, grazie per essere il miglior genitore che potessi chiedere. Grazie per amarmi così tanto, sempre e sempre di più. Mi scuso se ti faccio soffrire stando lontano, ma spero che un giorno capirai che questo è l'unico modo che ho per sentirmi vivo. Mi dispiace se sono uno scorzo', ma ricorda che sono il nipote di tuo padre. Questo non significa che non ti ami, ma sono sicuro che lo sai. Sei sempre nei miei pensieri, e penso sinceramente che il mondo non meriti una persona buona come te... di certo io non ti merito, ma sono felice di averti, come tutti i tuoi studenti... anch'io sono uno di loro.

Caro Babbo, grazie per essere come sei e per essere sempre lì ad aiutare, senza esitazione e senza prenderne il merito. Nonostante le nostre differenze, penso che siamo complementari e che c'è un po' di te in me e un po' di me in te. So che non è facile essere un padre e che è ancora meno facile essere mio padre. Scusa se spesso non sono affettuoso e loquace, ma noi Morici ci capiamo senza parole.

Maria, grazie per essere mia sorella e per mostrarmi sempre fratellanza, anche se i miei pensieri sono molto difficili da penetrare e se sono restio a mostrarti il mio amore. Detto questo, sappiamo tutti che sei consapevole che quell'amore c'è, e che sai come sono, nel bene e nel male. È sempre bello ricevere una tua chiamata, anche se faccio finta di esserne infastidito... ma questo lo sai, vero?

Cara Zia Laura, ti ringrazio per avermi dato due meravigliosi cugini che sono sempre stati come fratellini per me. Jacopo e Giulio, sono così orgoglioso di voi, e divento più orgoglioso man mano che i giorni passano. Per favore, non smettete di rendermi orgoglioso di voi, e ricordate che non sono l'unico a guardare sempre la vostra vita da lontano. Per favore, continuate a studiare, questo è l'unica cosa che vi chiedo.

Zio Cesare, anche tu sei in questa lista. In passato ti giudicavo e non mi piacevi, ma lascia che ti confessi che col passare degli anni ti capisco sempre di più. Non hai avuto una vita facile, e nonostante ciò regali sempre un sorriso a chiunque ti circonda. Penso davvero che tu abbia qualcosa in più degli altri, e ricorda: sono il tuo unico vero nipote!

Cara Nonna, su questo pianeta sei la persona che rispetto e di cui mi fido di più. Per me sei un vero eroe. Mi hai sempre sostenuto nella mia vita e nei miei studi e mi hai amato incondizionatamente. Sei così importante per me, perché sei sempre stata la mia migliore insegnante. Questa sezione è tutta sugli insegnanti, e nessuno può eguagliarti, perché hai sempre ragione, non so come sia possibile. Spero che un giorno mi perdonerai per tutto il dolore che ti ho causato per aver lasciato casa. Non è stata una

decisione facile, e la sento sulla mia pelle ogni giorno della mia vita da anni. Tuttavia era essenziale, e sono sicuro che sei abbastanza intelligente da capirlo; sicuramente mi ami abbastanza da capirlo.

Voglio chiudere questa lunga lista ringraziando la persona che ho amato di più nella mia vita.

Caro Nonno, grazie per essere sempre stato lì per me, dal momento in cui sono nato. Non mi dovevi nulla e, nonostante ciò, hai sempre mostrato l'amore speciale che avevi per me. Sei stato un baby-sitter, un insegnante, un mentore e un amico. Mi hai insegnato come parlare, come camminare, come farmi la barba, come guidare e come comportarmi. Mi hai dato tutto e non hai mai chiesto nulla in cambio. Hai deciso di andartene mentre ero qui in Germania e non ho avuto la possibilità né la forza di dirti addio. Questo perché sento che non te ne sei davvero mai andato. Per me sei infatti una presenza costante: ti sento così vicino e mi piace pensare che vivi in tutte le cose che dico e faccio, in tutte le persone che incontro, in tutte le esperienze che ho. Questo mi fa andare avanti, Tu mi fai andare avanti; in ogni momento, anche mentre sto scrivendo questo, sei qui. Spero di renderti orgoglioso di me, per dimostrarti l'amore speciale che avevo e che ho per te.

Voglio ricordarti com'eri, pensare che ancora vivi... voglio pensare che ancora mi ascolti e che come allora sorridi.

Abbreviations

Å	Ångstrom
A-site	Amino acyl-site
aa	amino acyl
AMP	Antimicrobial peptide
ASD	anti-Shine-Dalgarno
ASL	anticodon stem loop
C-terminus	Carboxyl terminus
Cam	Chloramphenicol
Cln	Clindamycin
cryo-EM	Cryogenic electron microscopy
CTD	C-terminal domain
CTF	Contrast transfer function
Dal	Dalfopristin
DC	Decoding center
ddH ₂ O	nuclease-free deionized water
DDM	Dodecyl-β-D-maltoside
DNA	Deoxyribonucleic acid
Dro	Drosocin
E-site	Exit-site
Ec (Eco)	<i>Escherichia coli</i>
EF	Elongation factor
Ery	Erythromycin
Fig	Figure
Fluc	Firefly luciferase
fMet	N-formylmethionine
FSC	Fourier shell correlation
FWD	forward
GDP	Guanosine diphosphate
GGQ (-motif)	Glycine-Glycine-Glutamine (-motif)
GTP	Guanosine triphosphate
h/H	helix
IC	Initiation complex
IC	Inhibitory concentration
IF	Initiation factor
Klb	Klebsazolicin

LD	lethal dose
Lnc	Lincomycin
Lnz	Linezolid
LSU	large subunit
MIC	minimal inhibitory concentration
mRNA	messenger RNA
Mtu	<i>Mycobacterium tuberculosis</i>
N-terminus	Amino terminus
NC	nascent chain
NPET	nascent peptide exit tunnel
NTD	N-terminal domain
OD	optical density
P-site	peptidyl-site
PCR	Polymerase chain reaction
PDB	Protein data bank
P _i	inorganic phosphate
PIC	Preinitiation complex
PrAMPs	Proline-rich antimicrobial peptides
PTC	Peptidyl transferase center
px	pixel
Qin	Quinupristin
REV	reverse
RF	Release factor
RNA	Ribonucleic acid
RRF	Ribosome recycling factor
rRNA	ribosomal RNA
SD	Shine-Dalgarno
SQ	Squires
SRL	Sarcin ricin loop
SSU	small subunit
Sup.Fig.	supplementary figure
TC	Ternary complex
TcmX	Tetracenomycin X
Tel	Telithromycin
Tia	Tiamulin
tRNA	transfer RNA
UTR	untranslated region
Vg	Virginiamycin

W
wt

Water
wildtype

For amino acids the standardized and commonly accepted single- and triple-letter and for nucleotides the single-letter nomenclature is used. For bacteria the genus is used abbreviated after the first entry.

Zusammenfassung

Die Proteinsynthese ist ein wesentlicher Prozess in allen lebenden Systemen, der hauptsächlich während der Translation durch das Ribosom stattfindet. Während der Translation polymerisieren die Ribosomen eine naszierende Polypeptidkette, die sich in den Ausgangstunnel erstreckt. Dieser Tunnel ist eine strukturelle Schlüsselkomponente des Ribosoms und ein entscheidender Akteur im Prozess, der die Proteinfaltung, das Targeting und die Regulierung der Genexpression in verschiedenen Szenarien beeinflusst. Die kumulativen Forschungsarbeiten haben bedeutende strukturelle Einblicke in die Rolle des bakteriellen ribosomalen Ausgangstunnels bei der Translationsregulation und sein Potenzial als Ziel für antimikrobielle Peptide geliefert. In dieser Arbeit wird die Kryo-EM umfassend genutzt, um detaillierte Mechanismen der durch spezifische Arrestpeptide ausgelösten Translationsblockade aufzudecken, was zu unserem Verständnis der bakteriellen Genexpressionsregulation und der Wirkung von Antibiotika beiträgt.

Es wurde festgestellt, dass RAPP-haltige Arrest-Peptide die Translation abwürgen, indem sie in die Aktivität der ribosomalen Peptidyltransferase eingreifen. Die Studie untersucht speziell ApdA, das effizient grampositive bakterielle Ribosomen abwürgt, und ApdP, das sowohl grampositive als auch gramnegative bakterielle Ribosomen abwürgt, obwohl es bei gramnegativen Arten konserviert ist. Hochauflösende Kryo-EM-Strukturen von Ribosomen aus *Bacillus subtilis* und *Escherichia coli*, die durch ApdA bzw. ApdP blockiert werden, zeigen, dass diese Peptide die Bildung der nachfolgenden Peptidbindung verhindern, indem sie ein einzelnes Wasserstoffatom an der Pro-tRNA in der A-Seite stabilisieren. Dieser Mechanismus verdeutlicht die Rolle des RAPP-Motivs als wesentliches "Arrestmodul" und des N-terminalen Abschnitts als "Regulatoremodul" und liefert ein detailliertes mechanistisches Verständnis dafür, wie diese Peptide die ribosomale Translation aufhalten. Dieser Mechanismus ist analog zu dem durch das SecM-Peptid induzierten Abwürgen.

Das SecM-Arrest-Peptid reguliert die Genexpression in *E. coli* durch Abwürgen der Translation. Die Studie korrigiert frühere Modelle, indem sie mittels Cryo-EM zeigt, dass SecM das Ribosom abwürgt, indem es die Pro-tRNA in der A-Stelle stabilisiert und die Bildung einer Peptidbindung mit der Peptidyl-tRNA in der P-Stelle verhindert. Diese Forschung zeigt eine Verdichtung der naszierenden SecM-Kette zu einer α -Helix innerhalb des ribosomalen Tunnels, im Gegensatz zu früheren Erkenntnissen. Molekulardynamiksimulationen deuten darauf hin, dass die von SecA auf die naszierende Kette ausgeübten Zugkräfte den Translationsstillstand aufheben können, indem sie eine lokale Entfaltung bewirken, wodurch die Translation fortgesetzt werden kann. Diese Forschungsarbeit bietet neue Einblicke in die strukturelle Grundlage des SecM-induzierten Translationsstopps und unterstreicht die konservierte Strategie der Translationsregulation bei verschiedenen Bakterienarten.

Der ribosomale Ausgangstunnel ist auch das Ziel für die Bindung vieler antimikrobieller Verbindungen. Das glykosylierte prolinreiche antimikrobielle Peptid

(PrAMP) Drosocin wird von Drosophila-Arten zur Bekämpfung bakterieller Infektionen produziert. Im Gegensatz zu vielen PrAMPs ist Drosocin an Threonin 11 O-glykosyliert, was seine antimikrobielle Aktivität verstärkt. Die Kryo-EM-Analyse von Drosocin-SRC zeigt, dass sich das glykosylierte Drosocin im Polypeptid-Ausgangstunnel des Ribosoms bindet und den Freisetzungsfaktor RF1 abfängt, wodurch eine ordnungsgemäße Beendigung der Proteinsynthese verhindert wird. Die Glykosylierung an Thr11 interagiert mit U2609 der 23S rRNA und verursacht Konformationsänderungen, die die Basenpaarung mit A752 stören, wodurch der gebundene RF1 stabilisiert und die Translation gehemmt wird. Diese Studie unterstreicht das Potenzial für die Entwicklung neuer antimikrobieller Wirkstoffe auf der Grundlage der strukturellen Merkmale von glykosyliertem Drosocin und bietet eine Grundlage für die Entwicklung synthetischer Derivate mit verbesserten antimikrobiellen Eigenschaften und geringer Toxizität.

Insgesamt liefert diese Arbeit umfassende strukturelle und mechanistische Erkenntnisse darüber, wie spezifische Arrestpeptide und antimikrobielle Wirkstoffe mit dem bakteriellen Ribosom interagieren, um die Translation zu regulieren. Die Ergebnisse unterstreichen die Bedeutung des ribosomalen Exit-Tunnels als kritische Stelle für die Translationskontrolle und als vielversprechendes Ziel für neuartige Antibiotika und tragen damit zu einem breiteren Verständnis der bakteriellen Genexpression und der Mechanismen der Antibiotikaresistenz bei.

Summary

Protein synthesis is an essential process in all living systems, primarily occurring during translation by the ribosome. During translation, ribosomes polymerize a nascent polypeptide chain that extends into the exit tunnel. This tunnel is a key structural component of the ribosome and a crucial player in the process, influencing protein folding, targeting, and the regulation of gene expression across various scenarios. The cumulative research undertaken has provided significant structural insights into the role of the bacterial ribosomal exit tunnel in translation regulation and its potential as a target for antimicrobial peptides. This work extensively utilizes cryo-EM to reveal detailed mechanisms of translational stalling induced by specific arrest peptides, further contributing to our understanding of bacterial gene expression regulation and antibiotic action.

RAPP-containing arrest peptides have been identified to induce translational stalling by interfering with the ribosomal peptidyltransferase activity. The study specifically examines ApdA, which efficiently stalls Gram-positive bacterial ribosomes, and ApdP, which stalls both Gram-positive and Gram-negative bacterial ribosomes despite being conserved among Gram-negative species. High-resolution cryo-EM structures of ribosomes from *Bacillus subtilis* and *Escherichia coli* stalled by ApdA and ApdP, respectively, reveal that these peptides prevent the formation of the subsequent peptide bond by stabilizing a single hydrogen atom on the Pro-tRNA in the A-site. This mechanism elucidates the role of the RAPP motif as an essential "arrest module" and the N-terminal stretch as a "regulator module," providing a detailed mechanistic understanding of how these peptides halt ribosomal translation. This mechanism is found to be analogous to the stalling induced by the SecM peptide.

SecM arrest peptide regulates gene expression in *E. coli* by stalling translation. The study corrects previous models by demonstrating through cryo-EM that SecM stalls the ribosome by stabilizing the Pro-tRNA in the A-site, preventing peptide bond formation with the peptidyl-tRNA in the P-site. This research reveals a compaction of the nascent SecM chain into an α -helix within the ribosomal tunnel, contrary to previous structural findings. Molecular dynamics simulations suggest that pulling forces exerted by SecA on the nascent chain can relieve the translational arrest by causing local unfolding, thereby allowing translation to proceed. This research provides new insights into the structural basis of SecM-induced translational stalling and highlights the conserved strategy of translational regulation among diverse bacterial species.

The ribosomal exit tunnel also constitutes the target for the binding of many antimicrobial compounds. The glycosylated proline-rich antimicrobial peptide (PrAMP) drosocin is produced by *Drosophila* species to combat bacterial infections. Unlike many PrAMPs, drosocin is O-glycosylated at threonine 11, which enhances its antimicrobial activity. Cryo-EM analysis of drosocin-SRC reveals that glycosylated

drosocin binds within the polypeptide exit tunnel of the ribosome and traps release factor RF1, preventing proper termination of protein synthesis. The glycosylation at Thr11 interacts with U2609 of the 23S rRNA, causing conformational changes that disrupt its base-pairing with A752, thus stabilizing the bound RF1 and inhibiting translation. This study highlights the potential for developing new antimicrobial agents based on the structural features of glycosylated drosocin and provides a basis for designing synthetic derivatives with enhanced antimicrobial properties and low toxicity.

Overall, this body of work provides comprehensive structural and mechanistic insights into how specific arrest peptides and antimicrobial agents interact with the bacterial ribosome to regulate translation. The findings underscore the importance of the ribosomal exit tunnel as a critical site for translational control and a promising target for novel antibiotics, thereby contributing to the broader understanding of bacterial gene expression and antibiotic resistance mechanisms.

Introduction

In biological entities, the flow of biochemical information is described by the central dogma of molecular biology (Crick, 1958): DNA is the macromolecular species which has been selected during molecular evolution for long-term storage and propagation of information by the means of biological process of DNA replication, carried out by DNA-dependent DNA polymerases.

Linear stretches of DNA encoding for discrete polypeptides are referred to as “genes”, collectively constituting the genome of the organism.

DNA also works as a template for the second crucial biological process, namely, transcription. During transcription, DNA-dependent RNA polymerases synthesize a strand of RNA complementary and antiparallel to a certain linear portion of DNA.

RNA molecules may retain different biological functions, on the basis of which they can be categorized in two groups: some are involved in the mechanism of regulation of gene expression, while others are the components involved in the third key biological process of the central dogma, which is translation.

By the means of translation, information transcribed from DNA genes into messenger RNA (mRNA) molecules are translated into sequences of amino acid residues composing polypeptides (Crick *et al.*, 1961), which are the major direct effectors of the phenotype in living systems.

In this process, transfer RNA (tRNA) molecules are short RNA molecules characterized by a peculiar folding referred to as “cloverleaf structure” working as adaptors, since they link an amino acid, bound to the 3’ acceptor end of the tRNA to the anticodon: a sequence of 3 nucleotides complementary to codons (nucleotides triplets) linearly arranged along mRNAs (Kim *et al.*, 1973).

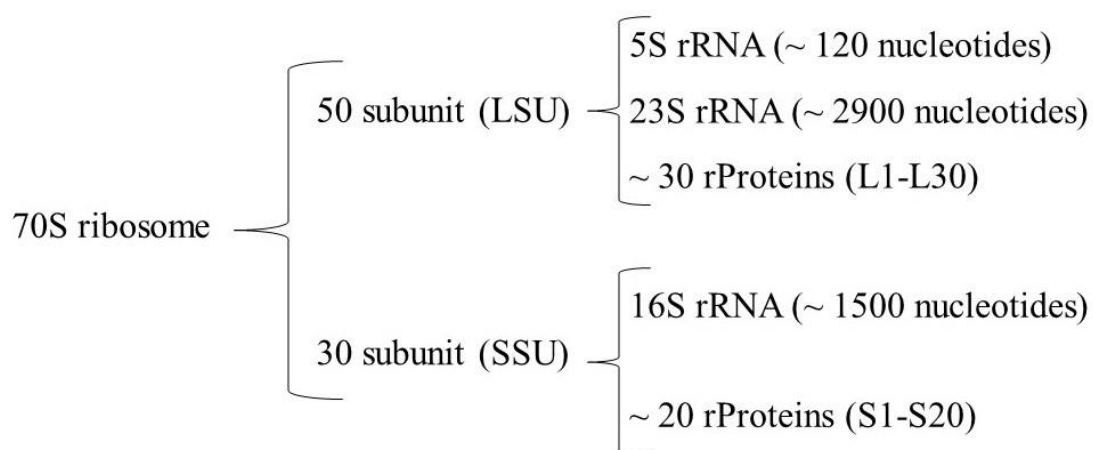
The interaction between an mRNA and tRNA adaptors takes place within the main player of translation: the ribosome.

The ribosome is a ribonucleoprotein complex constituted of ribosomal proteins (rProteins) and ribosomal RNA (rRNA) molecules, the former retaining mainly a structural stabilizing role, the latter being responsible for the catalytic activity. This macromolecule works as a scaffold during the process of translation, having a fundamental role to optimally position two tRNAs simultaneously bound to two adjacent codons of mRNA. This is followed by the catalysis of peptidyl-transferase reaction. This reaction associates the growing polypeptide chain to the amino acid bound to the tRNA on the A-site of the ribosome (Ramakrishnan, 2001).

The process of translation is divided in three steps, namely initiation, elongation and termination, all of which are extremely conserved and tightly regulated to finely tune gene expression. Moreover, given the biological relevance of translation for the fitness of the cell, the factors involved are the targets of most of the known antibiotics (Arenz *et al.*, 2016).

The bacterial “Gene Machine”: focus on the prokaryotic ribosome

The eubacterial ribosome is a 2.5 megadalton (MDa) ribonucleoprotein particle constituted of two subunits: a small subunit (SSU), also referred to as 30S subunit, and a large subunit (LSU), also referred to as 50S subunit, which during the process of translation assemble to form a 70S ribosome (Wilson and Nierhaus, 2005). Each of the two subunits is a complex of RNA molecules, namely, ribosomal RNA (rRNA) and ribosomal proteins (rProteins) (Scheme 1, Fig. 1a) (Nierhaus, 1991).



Scheme 1: Composition of the bacterial ribosome (70S) and of its subunits (Nierhaus, 1991). “S” stands for Svedberg unit, a non-SI metric unit for sedimentation coefficient of particles; 1S is equivalent to 100 fs when measuring a particle’s sedimentation rate. rProteins are labeled with an “L” if they belong to the LSU and with an “S” if they belong to the SSU, followed by a number.

Ribosomal proteins are mostly extended over the surface of the ribosome, reaching the inside portion by means of long tendrils; in the complex, the main role of these extensions is the one of stabilizing the rRNA structure (Brodersen *et al.*, 2002; Klein *et al.*, 2004) (Fig. 1a), albeit some rProteins have been shown to participate in the regulation of translation kinetics (Duval *et al.*, 2013), especially those lining the exit tunnel in the large subunit (Seidelt *et al.*, 2009). On the other hand, rRNA molecules constitute the bulk of the two particles, exposed over the intersubunit interface and responsible for the ribosome’s core functions of decoding and peptide bond formation (Cech, 2000). This is possible due to the fact that rRNAs acquire complex and defined three-dimensional folds, including secondary structures, such as helices, and tertiary structures, including domains: the SSU comprises four domains, the 5’ domain or body, the central domain or platform, the 3’ major domain or head and the 3’ minor domain, that includes helices h44-h45 (Schlunzen *et al.*, 2001), while the LSU is composed of six domains, named from I to VI (Ban *et al.*, 2000).

The two subunits retain different roles during translation (Ramakrishnan, 2002).

The SSU is responsible for decoding: a cleft localized at the interface between the head and the body constitutes the channel for the mRNA to be translated; the entry of such channel where the mRNA lies is shaped by proteins S3, S4 and S5, while the exit point is enveloped by proteins S11, S18 and S21, together with the 3’ end of the 16S rRNA

(Yusupova *et al.*, 2001). The portion enclosed by these two sites is called decoding center (DC), since it is the region where mRNA codons and tRNA anticodons basepair (Schmeing and Ramakrishnan, 2009) (Fig. 1b), thereby allowing translation to be dictated by the universal genetic code. The peptidyl-transferase center (PTC) is localized inside the LSU, performing the catalysis of peptide bond formation during ribosomal protein synthesis (Ban *et al.*, 2000; Harms *et al.*, 2001; Nissen *et al.*, 2000; Hansen *et al.*, 2002; Schmeing *et al.*, 2002; Schlunzen *et al.*, 2001) (Fig. 1b). Since both the DC and the PTC are almost totally constituted by rRNA, the ribosome can be classified as ribozyme (Cech, 2000; Noller, 2012).

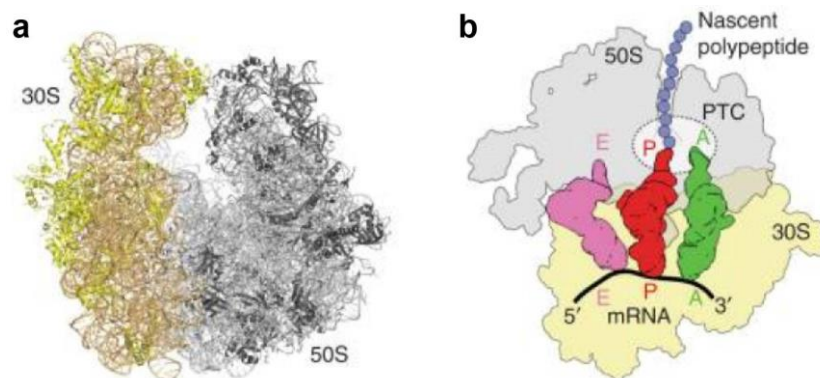


Figure 1: Arrangement of the bacterial ribosome. (a). Ribbons structure of the bacterial ribosome is divided in two subunits, being the SSU or 30S (yellow) and the LSU or 50S (grey). Both are constituted of a functional rRNA core (dark gold for the 30S and light grey for the LSU) and several stabilizing rProteins (yellow for the 30S and dark grey for the LSU). (b). Scheme for the arrangement of the translating ribosome before peptide bond formation, with the 30S in yellow and the 50S in grey. mRNA (black) is wrapped around the head of the 30S, where the decoding center displays the E- (pink), P- (red) and A- (green) tRNA binding sites, to which the corresponding tRNAs (same colours) are bound. The CCA ends of the P- and A-site tRNAs come in close proximity at the PTC of the 50S (circled); the P-site tRNA is acylated with the nascent polypeptide chain (blue balls), which runs inside the exit tunnel of the LSU, and the A-site tRNA is acylated with the aminoacid decoded by the A-site codon (green ball). Panels adapted from Arenz and Wilson, 2016.

Inside the 70S ribosome, the intersubunit space between the DC and the PTC hosts tRNA molecules; in particular, there are three tRNA-binding sites, each of which allowing the association of a 3-nucleotide codon of the mRNA and the anticodon of a tRNA in correspondence to the DC (Ogle *et al.*, 2001; Yusupova *et al.*, 2001; Vanloock, 2000 *et al.*; Carter *et al.*, 2000). The A-site (acceptor site) is the one in which the incoming aminoacyl-tRNA (A-tRNA) from the surrounding cellular environment enters and is positioned at the beginning of each elongation cycle. The P-site (peptidyl site) is next to the A-site and harbours the peptidyl-tRNA (P-tRNA) (or the initiator tRNA during initiation), which is the tRNA to which the growing polypeptide chain is attached (Fig. 1b).

Both bound A-tRNA and P-tRNA extend into the PTC on the LSU where their 3'-ends are stabilized by the interactions with A-loop (nts 2547-2561) and P-loop (nts 2246-

2259) of the 23S rRNA, respectively: C75 within the 3'-end of the A-site tRNA basepairs with G2553 and C74 and C75 within the 3'-end of the P-site tRNA basepair with G2252 and G2251 (*E. coli* numbering is exclusively used in this thesis, unless specified) (Moazed and Noller, 1989; Kim and Green 1999). These key interactions stabilize the aminoacyl acceptor stem and in doing so, they force the attached amino acids into an optimal configuration with respect to PTC, which is strictly necessary for an efficient peptide bond formation reaction to occur (Samaha *et al.*, 1995; Nissen *et al.*, 2000). Upon completion of peptide bond formation, the tRNA in the P-site is deacylated, since the nascent chain is now bound through the newly-formed peptide bond to the amino acid attached to the tRNA on the A-site (Nissen *et al.*, 2000; Hansen *et al.*, 2002).

After peptide bond formation, translocation occurs, a process that is modulated by EF-G. During translocation, the deacylated tRNA moves to the E-site (exit site), from which it will then leave the ribosome. Concomitantly, the peptidyl-tRNA, whose chain is now one amino acid residue longer, moves from the A-site to the P-site (Yusupov *et al.*, 2001; Schuwirth *et al.*, 2005; Selmer *et al.*, 2006). The A-site is now empty and ready to accommodate the next incoming A-tRNA.

While the nascent chain elongates, it emerges from the translational machinery by gradually extending through an exit tunnel in the LSU. The exit tunnel spans from the PTC to the back of the 50S subunit, and is ~100 Å long, corresponding to ~30 amino acids of growing protein, and 10-30 Å wide, since the width is not uniform along the conduit (Nissen *et al.*, 2000) (Fig 1b). Most of the tunnel lining is made up of rRNA, however a constriction generated by proteins L4 and L22 narrows the tunnel close to the PTC. Near the exit, the tunnel widens to form a funnel, the surface of which is built not only by rRNA, but also by ribosomal proteins L24, L25 and L29 (Nissen *et al.*, 2000). These two regions seem to be involved in assisting the folding of the growing polypeptide chain (Notari *et al.*, 2018; Javed *et al.*, 2017; Liutkute *et al.*, 2020) and in regulating gene expression (Seidelt, 2009).

Bacterial translation cycle

The portion of a mRNA being translated into a sequence of amino acid residues constituting a protein is referred to as an open reading frame (ORF). Within the messenger's nucleotide sequence, the ORF is enclosed and delimited by a start codon, which is mostly an AUG codon (Blattner *et al.*, 1997; Kunst *et al.*, 1997), and by a stop, or nonsense, codon, usually UAG, UGA or UAA (Caskey *et al.*, 1968). The sequence from the 5' to 3' of nucleotide triplets (codons) inside the ORF dictates the identity of the amino acid residues arranged along the sequence of the polypeptide being synthesized (Crick *et al.*, 1961). At the 5' and 3' of the ORF there are untranslated regions (UTRs) that may harbor regulatory elements. Among the most common regulatory elements of bacterial mRNAs is the Shine-Dalgarno (SD) sequence, which is located in the 5' UTR (~39% of messengers in *E. coli*). The SD

sequence is generally four to seven nucleotides upstream the start AUG (Shine and Dalgarno, 1974; Chen *et al.*, 1994). The SD sequence plays several important roles: its sequence and spacing from the start codon affects the efficiency of an mRNA's translation (Mironova *et al.*, 1999; Komarova *et al.*, 2020), moreover, it assists in the placement of the SSU at the correct start codon in correspondence with the P-site, thereby ensuring the correct frame (Shine and Dalgarno, 1974).

The whole cycle of ribosomal protein synthesis proceeds through four major steps: initiation, elongation, termination and ribosome recycling (Fig. 2).

Translation initiation is the most regulated step (Laursen, 2005) and is fulfilled when the SSU has been correctly placed thanks to the mediation of the SD, the initiator tRNA associates at the P-site, basepairing with the start codon and subsequently the LSU assembles to form the whole 70S ribosome (Fig. 2).

In bacteria, the initiator tRNA is a fMet-tRNA_i^{fMet}, so the first amino acid of a polypeptide chain is the formylated methionine (Kozak, 1983). Formylation is required to distinguish the methionine amino acids to be used for initiation, whose tRNA is recognized by initiation factor 2 (IF2), from those being incorporated during elongation, whose tRNA is recognized by elongation factor Tu (EF-Tu) (Kozak, 1983). Moreover, during initiation, the formylation blocks the N-terminus of the amino acid residue, thereby preventing any non-canonical reactions (Guillon *et al.*, 1992; Kozak, 1983), such as aberrant peptide bond formation (Gualerzi and Pon, 1990).

The process proceeds with elongation, which occurs in rounds: during each round, the translational machinery extends the nascent polypeptide chain by C-terminally incorporating an amino acid brought by an incoming tRNA at the A-site, decoded by the codon downstream and then the ribosome translocates 3 nts toward the 3' of the mRNA being translated. Such processing allows 4 to 22 amino acids per second to be incorporated into the growing polypeptide chain (Wohlgemuth *et al.*, 2010; Fluitt *et al.*, 2007) (Fig. 2).

Translation termination is initialized whenever a stop codon is read at the A-site. Stop codons are also called “non-sense” codons, since they are not complementary to any natural anticodon; Instead, they are recognized by release factors (RF), which are protein factors that are able to enter the A-site cleft and subsequently hydrolyze the synthesized peptide chain from the P-tRNA. The translated peptide leaves the machinery and enters the cellular environment (Korostelev, 2011) (Fig. 2).

The subsequent step is termed ribosome recycling: Here, the two subunits of the 70S are split and separated from the mRNA template. This is necessary to recycle both the ribosomal subunits and the mRNA, so that they can participate in a new translation event (Zhou *et al.*, 2020) (Fig. 2).

The next chapter is dedicated to the detailed description of the individual steps of bacterial translation, focusing on the role of each molecular actor involved in such process.

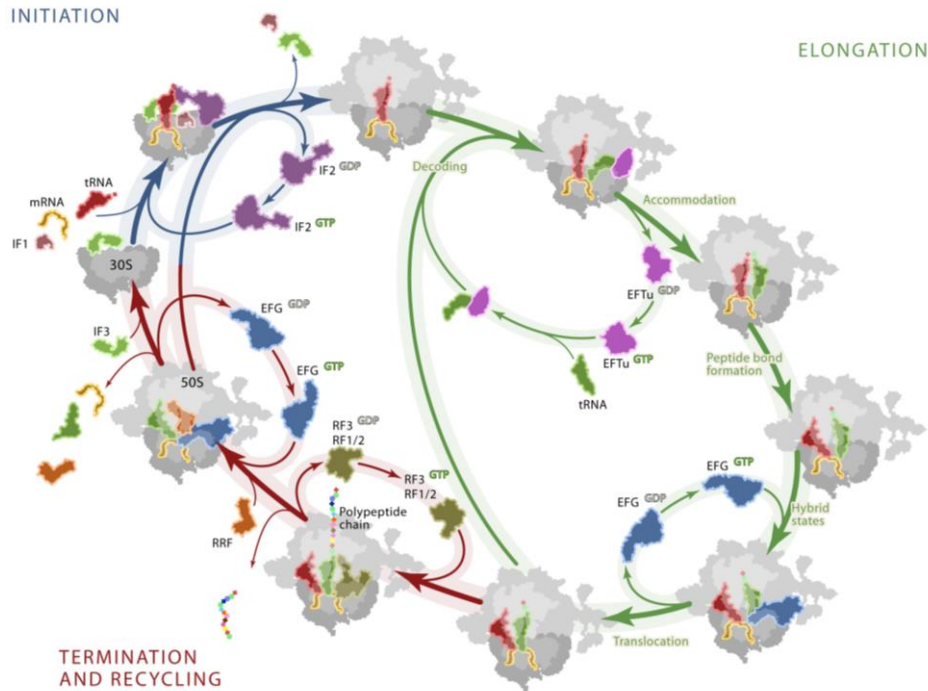


Figure 2: Bacterial translation cycle. The first step is initiation (top left, blue), during which the free 30S (dark grey) in the cellular pool interacts with IF1 (dark salmon) and IF3 (light green) to correctly position the mRNA (gold), so that the GTPase IF2 (dark purple) can correctly position the initiator fMet-tRNA^{fMet} (red) on the P-site so that codon:anticodon recognition takes place, allowing the assembly of the 50S, concomitant with the release of IFs, to form a functional 70S IC, able to enter elongation. During the elongation phase (green), each elongation cycle consists of consecutive decoding, accommodation, peptide bond formation and translocation and this is required to elongate the nascent chain of one aminoacid decoded at the A-site at the beginning of each cycle, repeated iteratively until a non-sense codon is reached. During decoding, the GTPase EF-Tu (light violet) carries an acylated tRNA (dark green) to the A-site, until codon:anticodon basepairing is succesful, GTP hydrolysis occurs on the elongation factor and the aa-tRNA is correctly positioned at the A-site. Subsequently, peptide bond formation is catalyzed by the ribosome PTC, so that the nascent chain become acylated to the A-site tRNA, with the most C-terminal residue being now part of it. The 30S costantly rotates around the 50S, producing a state referred to as “hybrid”, which also concerns the tRNAs, whose ASL stays on the corresponding site, but the CCA end rotates to the nearby site (the deacylated P-site tRNA toward the empty A-site, the acylated A-site tRNA pointing toward the P-site cleft of the 50S); this hybrid state constitutes the substrate for the GTPase EF-G (light blue), that interacts with the complex to allow translocation, consisting in the mRNA (together with the bound tRNAs) to slide of 3 nucleotides, moving the deacylated P-tRNA to the E-site (now being a E-site tRNA, prone to leave the complex) and the peptidyl-A-tRNA to the P-site, (now being the P-site tRNA). In this way the nascent chain has grown and the substrate for another decoding step is generated, with the subsequent (more 3’) mRNA codon exposed now at the A-site. When an in-frame stop codon is decoded at the A-site, termination step (red) is initialized. Depending on the stop codon encountered, either RF1 or RF2 (olive) enters and read the A-site, stimulating the hydrolysis of the nascent chain from the P-site tRNA, which is released as a polypeptide. The GTPase RF3 is required to interact with the complex and free RF1/2 upon GTP hydrolysis. At this point the complex components (LSU, SSU, deacylated tRNA, mRNA) must be recycled to replenish the cellular pool and this is achieved by the association of RRF (orange), followed by the activity of EF-G, which disassemble the complex to release the single components to the solvent. Figure adapted from Sohmen *et al.*, 2009.

Translation initiation

Initiation is the first step of the cycle and it is the most regulated one, thereby being the rate-limiting step of translation (Laursen *et al.*, 2005). This step is required to achieve the correct positioning of the fMet-tRNA_i^{fMet} in the P-site cleft, where it is base-paired with the start codon AUG (Milon and Rodnina, 2012a). The first stage of initiation results in a so-called 30S preinitiation complex (30S PIC), followed by the conversion to a 30S initiation complex (30S IC) and finally the joining of the 50S subunit to form an elongation-competent 70S initiation complex (70S IC) (Laursen *et al.*, 2005; Milon and Rodnina, 2012a; Simonetti *et al.*, 2008) (Fig. 2; Fig. 3a-b). The first two intermediate stages (30S PIC and 30S IC) involve not only the SSU, the mRNA and the fMet-tRNA_i^{fMet}, but also the initiation factors (IF) 1, 2 and 3 (Milon and Rodnina, 2012a). The binding of initiation factors during initiation exerts a fundamental favorable effect on the kinetics of the molecular interactions taking place (Gualerzi *et al.*, 2001). Nevertheless, the kinetics of the placement of the SSU on the mRNA strongly depends on the messenger's concentration and nucleotides sequence (Milon and Rodnina, 2012a).

Structural features of the mRNA around the start site affects its selection: in particular, the local secondary structures dictated by intrastrand base-pairing play a key role in determining the accessibility of the SSU to the 5'-UTR (de Smit and van Duin, 1990; Mustoe *et al.*, 2018; Kudla *et al.*, 2019). As a matter of fact, biochemical and computational data show that mRNAs are more frequently less structured in region surrounding their initiation site (Bentele *et al.*, 2013; Del Campo *et al.*, 2015). Also, 5'-UTRs generally display A/U-rich regions (Komarova *et al.*, 2005) which are less likely to give rise to stable mRNA folding. The A/U-rich regions also interact with the rProtein S1 (Boni *et al.*, 1991; Byrgazov *et al.*, 2015), thereby recruiting the ribosome for assembly on the messenger (Duval *et al.*, 2013). This early initiation event may be aided by the interaction between the SD sequence of the mRNA and the anti-SD (aSD) sequence localized nearby the 3' of the 16S rRNA (Shine and Dalgarno, 1974). The association of IF1 and IF3 to the SSU may assist in the binding of mRNA, by making the A-site more exposed and the entry of the mRNA tunnel wider (Hussain *et al.*, 2016). Such 30S-PIC is then proposed to recruit the fMet-tRNA_i^{fMet}, whose interaction with the SSU is promoted by the rotated conformation acquired by the head in that state (Hussain *et al.*, 2016) (Fig. 3a).

The structure of IF1 displays a oligonucleotide-binding (OB) fold (Sette *et al.*, 1997; Murzin, 1993) allowing it to bind to the SSU A-site, positioned next to S12, the G530 loop and 16S helix 44 (Carter *et al.*, 2001; Dahlquist and Puglisi, 2000; Simonetti *et al.*, 2008). The presence of IF1 generates a steric clash at the A-site that prevents the binding of any tRNA there (Laursen *et al.*, 2005). Moreover, IF1 has also an allosteric effect, facilitating the binding of IF2 and IF3 to the 30S (Milon *et al.*, 2012b) (Fig. 3c).

IF2 is a six domain (in *E. coli*, named domain I-VI) translational guanosine-5'-triphosphatase (trGTPase) (Mortensen *et al.*, 1998) that is necessary for the recruitment of fMet-tRNA_i^{fMet} to the 30S PIC and critical to ensure a correct LSU joining

(Simonetti *et al.*, 2013; Sprink *et al.*, 2016; Milon *et al.*, 2010). While the three N-terminal domains (I-III) are variable across bacterial species and dispensable (Laursen *et al.*, 2005; Caserta *et al.*, 2006), the three C-terminal ones (IV-VI) are characterized by a high conservation; in particular, domain IV retains the GTPase activity and it displays high homology with those of the other trGTPases (Sorensen *et al.*, 2001), such as EF-Tu and release factor 3 (RF3). All these G proteins bind the ribosome in GTP-bound state and their hydrolase activity is dependent on the interaction with the LSU (Maracci and Rodnina, 2016) (Fig. 3c). Domain V makes contact with the SSU and IF1, thereby anchoring IF2 to the 30S-PIC (Simonetti *et al.*, 2013) (Fig. 3c).

IF3 comprises an N-terminal domain (NTD) and a C-terminal domain (CTD), which are connected by a flexible linker (Biou *et al.*, 1995). Its structural conformation changes during the various stage of initiation, allowing the correct dynamic of the initiation step (Hussain *et al.*, 2016) (Fig. 3c). In the 30S PIC, the NTD of IF3 is anchored to the platform of the SSU (Dallas and Noller, 2001; Fabbretti *et al.*, 2007; McCutcheon *et al.*, 1999; Hussain *et al.*, 2016), so that the CTD can interact with IF1 (Hussain *et al.*, 2016). The main role of IF3, being in proximity to the P-site, is the one of discriminating against elongation-tRNAs by monitoring for the specific presence of the three previously mentioned consecutive G:C base pairs in the anticodon stem of tRNA_i^{fMet} (Hartz *et al.*, 1990; Hartz *et al.*, 1989; O'Connor *et al.*, 2001). Upon arrival of fMet-tRNA_i^{fMet}, the NTD detaches from the platform of the SSU to interact with the elbow of the incoming initiator tRNA, assisting its positioning at the P-site (Hussain *et al.*, 2016) and monitoring the correct anticodon:start codon base pairing (Risuleo *et al.*, 1976; Sussman *et al.*, 1996; Milon *et al.*, 2008) (Fig. 3d).

The initiator tRNA_i^{fMet} has peculiar, characterizing structural elements in the anticodon stem and the acceptor stem, absent in elongator tRNA^{Met} (Rajbhandary, 1994). The initiator tRNA_i^{fMet} lacks the 1:72 Watson-Crick base pair in the acceptor stem that is present in elongator tRNA^{Met} (Dube *et al.*, 1968; Woo *et al.*, 1980; Wrede *et al.*, 1979). The lacking 1:72 basepair is the signal for the N-formylation of Met-tRNA_i^{fMet} to fMet-tRNA_i^{fMet}, catalyzed by methionyl-tRNA transformylase (Lee *et al.*, 1991; Lee *et al.*, 1992; Schmitt *et al.*, 1998). Such formylation of the Met residue acylated to the tRNA_i^{fMet} is essential for the recognition by IF2 (Sundari *et al.*, 1976; Wu and Rajbhandary, 1997; Allen *et al.*, 2005). Moreover, the anticodon stem of tRNA_i^{fMet} displays three consecutive G:C base pairs, which provides less flexibility to the anticodon loop (with respect to the one of elongator tRNA_{Met}) (Dube *et al.*, 1968; Woo *et al.*, 1980; Seong and Rajbhandary, 1987a) and participates in the accommodation of the tRNA at the P-site, being indirectly recognized by IF3 (Seong and Rajbhandary, 1987b; Dallas and Noller, 2001; Hussain *et al.*, 2016) (Fig. 3c).

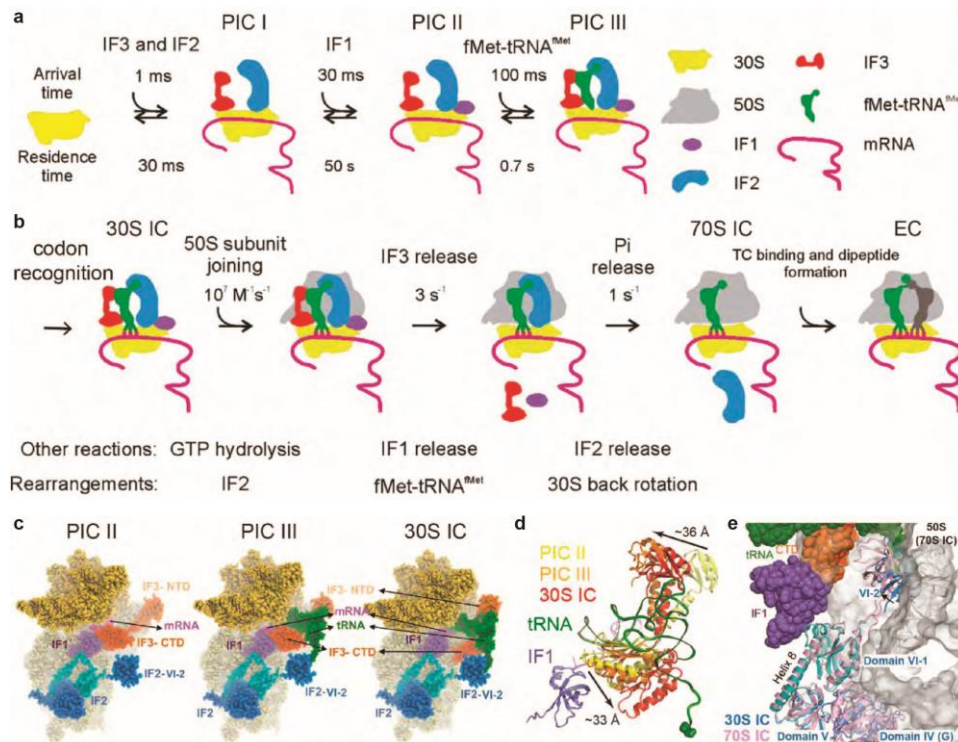


Figure 3: Kinetics and structural model of bacterial initiation. (a). Kinetics steps of 30S IC formation; the mRNA (magenta) can bind at any time in this stage. (b). Kinetic representation of the progression to the 70S IC, with transition to an elongation complex (EC) by delivery of an aa-tRNA to the A-site in form of a ternary complex (TC). Legend for factors' shape and colours at the right side of panel (a). (c). Binding of initiation factors to the SSU during PIC to 30S IC transition (IF1, purple; IF2, blue; IF3, red; mRNA magenta; SSU, yellow). (d). Structural rearrangement of IF3 in different stages of initiation (PIC II, yellow, PDB: 5LMP; PIC III, orange, PDB: 6LMT; 30S IC, red, fMet-tRNA green, IF1 purple, PDB: 5LMV), the fMet moiety of the tRNA is shown as spheres. (e). Superimposition of IF2 in the 30S IC (blue, PDB: 5LMV) and of IF2 in the 70S IC (pink, PDB: 3JCJ). Panels (a) and (b) are adapted from Milon and Rodnina (2012), panels (c-e) are adapted from Hussain *et al.*, 2016.

Such recognition between the anticodon of fMet-tRNA_i^{fMet} and the start codon of the mRNA in the channel of the SSU is the molecular event marking the transition of a 30S PIC to a 30S IC (Milon and Rodnina, 2012a) (Fig. 3b). Up to this moment, IF3 has the fundamental role of preventing a premature LSU joining: the positioning of its CTD generates a steric clash with H69 of the 50S subunit (Grunberg-Manago *et al.*, 1975; Grigoriadou *et al.*, 2007b; McCutcheon *et al.*, 1999; Hussain *et al.*, 2016). The accommodation of tRNA at the P-site causes a net conformational change of IF3, whose CTD moves away from the SSU neck and this sets aside the previously mentioned steric hindrance, virtually allowing the interaction between H69 of the 50S subunit and h44 of the 30S subunit, which is a key intersubunit bridge in the subsequent LSU joining (Hussain *et al.*, 2016) (Fig. 3c-d). The placement of the 50S subunit is also made possible by rotations within the SSU concomitant with the molecular events occurring during the stages going through the 30S PIC and the 30S IC (Milon *et al.*, 2012b).

IF2, its bound GTP and the initiator fMet-tRNA_i^{fMet} constitute a ternary complex which works as a scaffold for a more extensive interaction between the two ribosomal subunit,

so that the LSU reversibly joins the complex (Simonetti *et al.*, 2013, Simonetti *et al.*, 2008). The positioning of the LSU involves a close proximity between its sarcin-ricin loop (SRL) and the G-domain of IF2 (La Teana *et al.*, 2001; Qin *et al.*, 2009), which rearranges the catalytic histidine of the GTPase (His448) into an active orientation, so that GTP is hydrolyzed to GDP and an inorganic phosphate (Pi) (Sprink *et al.*, 2016). The dissociation of Pi triggers the detachment of IF2 from the initiator tRNA, which stably accommodates in the P-site cleft (La Teana *et al.*, 1996; Myasnikov *et al.*, 2005). IF2-GDP retains much lower affinity for the ribosome, and thus dissociates, followed by IF1 and finally by IF3 (Kaledhonkar *et al.*, 2019; Milon *et al.*, 2008; Goyal *et al.*, 2015) (Fig. 3e). Once the IFs are released, the translational complex matures to an elongation-competent 70S IC, whose P-site is charged with fMet- tRNA_i^{fMet} and A-site is vacant (Kaledhonkar *et al.*, 2019; Goyal *et al.*, 2015) (Fig. 3b). The translational machinery is now able to enter the second step of ribosomal protein synthesis, namely, elongation.

Translation elongation

The step of translation initiation is accomplished with the formation of an elongation-competent 70S IC, as previously described. Translation elongation consists in the polymerization of the polypeptide chain encoded in the mRNA being translated by successive addition of single amino acid residue units. Each single residue is linked C-terminally to the nascent chain by means of a “elongation cycle”, consisting of three stages: decoding, peptide bond formation and translocation. Such a cycle is re-iterated for each codon of the mRNA, proceeding from the 5' to 3' until an in-frame nonsense codon enters the A-site, thus initializing the next step, termination, which will be discussed in a later paragraph. Therefore, a elongation competent ribosome displays a vacant A-site, while the P-site is occupied either by fMet-tRNA_i^{fMet} (at the beginning of the very first cycle) or by a peptidyl-tRNA (after the first cycle has taken place) (Fig. 2).

Translation elongation requires the participation of protein factors, termed “elongation factors”, which interact with the ribosome to ensure the fidelity and kinetics of such key process. At the beginning of each cycle, during the first stage, the A-tRNA entering the complex is the one decoded by the codon of the ORF at the A-site. The aminoacyl moiety corresponds to one of the 20 proteogenic amino acids (Fig. 2). The protein responsible for the delivery of aa-tRNAs during elongation is the trGTPase elongation factor thermounstable (EF-Tu): a ternary complex composed of EF-Tu, its bound GTP and an aa-tRNA enters the A-site and accommodates inside the pocket so that the decoding codon:anticodon at the DC of the SSU is possible. If the decoding is successful, GTP hydrolysis is triggered and EF-Tu leaves the complex, while the A-site tRNA has achieved an optimal positioning for the ribosome catalysis, otherwise the whole ternary complex is rejected. After a successful decoding, the PTC of the LSU induces peptide bond formation: the peptidyl moiety attached to the P-site tRNA is transferred to the aminoacyl moiety attached to the A-site tRNA (Fig. 2).

The third and last stage of the elongation cycle is translocation. Upon translocation, the ribosome slides along the mRNA of three nts toward the 3' and the mRNA-bound tRNAs move together with the messenger. In this way, the uncharged tRNA occupies the E-site, the peptidyl-tRNA is at the P-site and the A-site now hosts the downstream in-frame mRNA codon. This stage is mechanically and kinetically assisted by elongation factor GTPase (EF-G), by means of the hydrolysis of its bound GTP. The translocation event is made possible also by crucial conformational changes involving the ribosome, the factors and the bound tRNAs (Fig. 2). Once translocation is achieved, the subsequent elongation cycle can start.

Decoding

The order with which amino acids are being introduced in the polypeptide chain is encoded in the sequence of codons of the mRNA (Crick *et al.*, 1961) which resides in the channel of the 30S subunit (Yusupova *et al.*, 2001). The decoding event that translates a codon into an amino acid residue is modulated by tRNAs, which have the role of adaptors. At the beginning of this stage, the ternary complex EF-Tu·GTP·aa-tRNA enters the complex by interacting solely with the ribosome, in particular, with the rProtein L7/12 (Wieden *et al.*, 2001; Kothe *et al.*, 2004; Diaconu *et al.*, 2005) (Fig. 4a). The structure of EF-Tu consists of three domains: domain I is the catalytic G-domain, while domains II and III make interaction with the aminoacylated CCA-end of the tRNA when the factor is GTP-bound; the final tract of the CCA-end with its associated aminoacyl moiety accommodates in a cleft shaped at the interface of domains I and II of EF-Tu (Nissen *et al.*, 1995; Nissen *et al.*, 1999) (Fig. 4b). At this stage, no interactions between the ASL of aa-tRNA and EF-Tu exist, making the former able to reach and make contact with the codon at the A-site (Loveland *et al.*, 2017).

Correct codon:anticodon basepairing is proofread first by codon sampling (Thompson and Stone, 1977; Gromadski and Rodnina, 2004): inside the *E. coli* ribosome there are four copies of L7/12, each able to interact with a EF-Tu, in turn engaged in a ternary complex (Diaconu *et al.*, 2005; Mustafi and Weisshaar, 2018); this configuration allows a rapid codon sampling (1 codon scanned each 1-2 ms) (Mustafi and Weisshaar, 2018). This is at the base of the fidelity of translation, since it permits the accommodation of cognate ternary complexes, while determining the dissociation of non-cognate ones (Pape *et al.*, 1999; Gromadski and Rodnina, 2004; Wohlgemuth *et al.*, 2010). However, there are still near-cognate complexes that are occasionally able to bypass the proofreading rejection, since their nitrogenous base at the anticodon tautomerize and thereby mimicking Watson-Crick base pairing and therefore manage to accommodate (Rozov *et al.*, 2015; Rozov *et al.*, 2016a; Rozov *et al.*, 2016b, Rozov *et al.* 2018, Fislage *et al.*, 2018).

The configuration of codon recognition involves the SSU in an open conformation that accommodates the incoming aa-tRNA in the so-called A*/T state: the CCA-end is in

association with the EF-Tu and the body of the tRNA is bent toward the A-site in order to sample the mRNA codon, although no Watson-Crick pairing is formed yet (Loveland *et al.*, 2017; Fislage *et al.*, 2018).

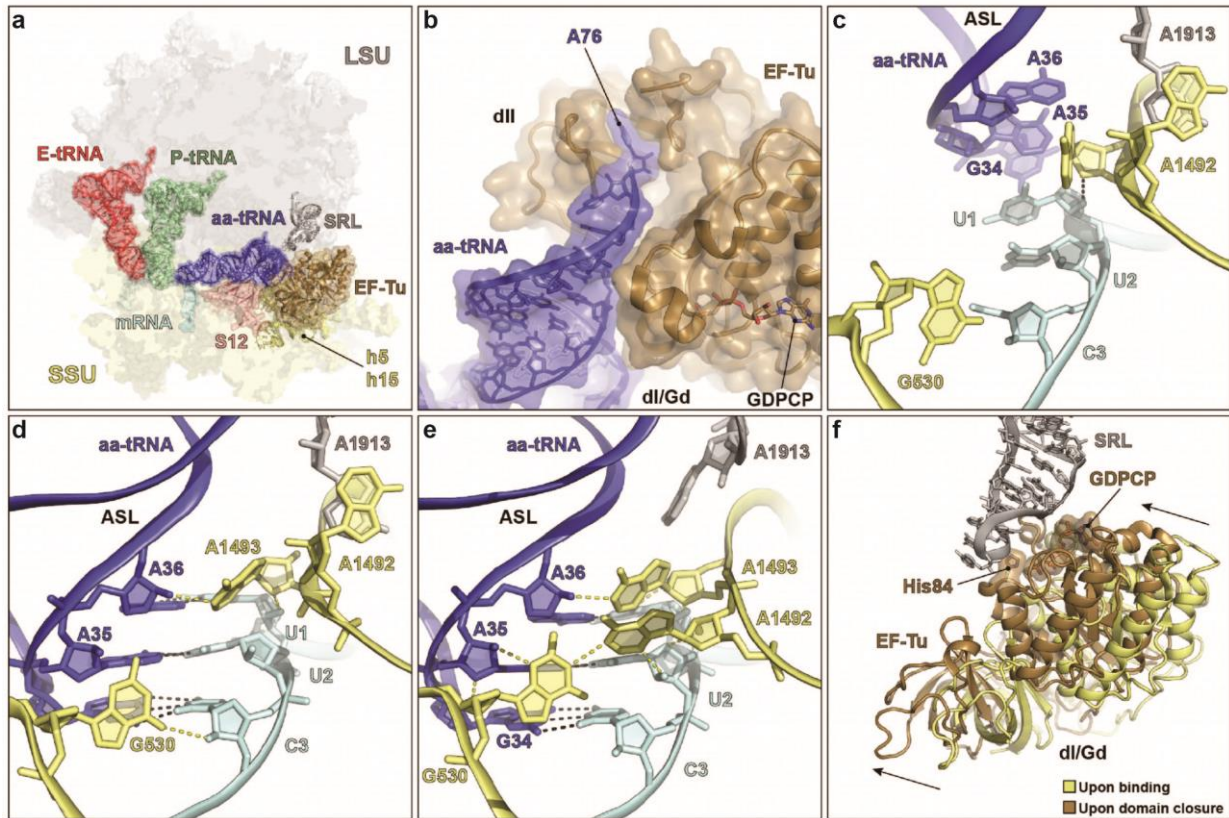


Figure 4: Molecular scale events of aa-tRNA delivery and decoding. (a). EF-Tu (brown) delivers aa-tRNA (blue) to the A-site mRNA codon (cyan) in the translating 70S ribosomal complex, with P-tRNA (green) and E-tRNA (red). The association of EF-Tu with the ribosomal particle is assisted by h5 (yellow), h15 (yellow) and S12 (salmon) of the 30S (pale yellow) and by the SRL (grey) of the LSU (pale grey). (b). Association of the CCA-end of unaccommodated tRNA (blue) with EF-Tu domain II (brown). (c-e). The DC performs decoding. (c). Conformation of DC nucleotides before of codon-anticodon base-pairing with A1492 and G530 being in an inactive conformation. The tRNA ASL is in a relaxed conformation. (d). Conformation of DC nucleotides (yellow) upon establishment of codon-anticodon interactions between mRNA codon (cyan) and A-tRNA anticodon (blue). To achieve this, ASL adopts a kinked conformation and then G530 and A1493 start monitoring codon-interactions. (e). DC with all nucleotides in active conformation. A-minor interactions are being monitored for the codon-anticodon helix. The kinked conformation of the A-tRNA ASL (blue) is maintained. Hydrogen bonds are indicated by black dashed lines. Polar contacts are indicated by yellow dashed lines. (f) Accommodation of the G-domain of EF-Tu upon domain closure. The proximity of the G-domain with the SRL (grey) positions the catalytic histidine (His84) for GTP hydrolysis. The position of the G-domain upon initial binding is shown in yellow. The position of the G-domain after domain closure is shown in brown. Panels adapted from Loveland *et al.*, 2017.

The ribosome is a key contributor of codon:anticodon sampling. In particular, four highly conserved decoding bases participate in the monitoring: 16S rRNA bases A1492 and A1493 of helix 44 (h44) in the SSU body, base G530 belonging to h18 (530 loop in the SSU shoulder) and 23S rRNA base A1913 of H69 (in the LSU) (Ogle *et al.*, 2001; Ortiz-Meoz and Green, 2011; Loveland *et al.*, 2017; Fislage *et al.*, 2018).

Before the arrival of a ternary complex at the A-site, these decoding bases are found to be in a OFF/inactive state: A1492 and A1493 are localized within the core of h44, with A1492 stacked on A1913 and G530 in *syn*-conformation (Fig. 4c). When a ternary complex enters the A-site, the ASL starts probing for Watson-Crick basepairing with the mRNA codon; the anticodon nucleotides flip out and the ASL conformation kinks (A/T tRNA state). This mechanically switches the decoding bases to their ON/active state: A1492, A1493 flip out of h44, A1913 flips out of H69, as G530 acquires an *anti*-conformation (Fig. 4d-e). Such an active configuration is competent for monitoring of correct codon:anticodon complementary match. In particular, A1913 interacts with the ASL, A1493 and G530 interrogates the first codon position, while the second one is verified by A1492 and G530, thereby establishing an extensive hydrogen-bond network with the minor groove of the codon:anticodon helix and with the ASL (Ogle *et al.*, 2001; Loveland *et al.*, 2017; Fislage *et al.*, 2018; Yusupov *et al.*, 2001) (Fig. 4e). In general, the establishment of this network does not involve the third position of the codon:anticodon interaction, and as a result decoding bases do not exclude noncanonical base pairing, termed “Wobble base pairing”. The direct consequence is that different codons recognizes the same tRNA species, bearing the same aminoacyl moiety, thereby making the genetic code degenerate (Crick *et al.*, 1966).

Stable acceptance of the ternary complex occurs upon the formation of such hydrogen bond network resulting from Watson-Crick basepairing (Fig. 4e). This triggers SSU closure where the head and the shoulder come closer together, making the latter less distant from the body (Ogle *et al.*, 2001; Ogle *et al.*, 2002; Loveland *et al.*, 2017; Fislage *et al.*, 2018). This further encases the tRNA in the A-site cleft, favouring the A/T state. EF-Tu is associated with the SSU shoulder, and as the latter slides, the EF-Tu G-domain is pushed closer to the SRL of the LSU, which works as GTPase activating protein (GAP) for trGTPases (Stark *et al.*, 1997; Ogle *et al.*, 2002; Moazed *et al.*, 1988; Voorhees *et al.*, 2010; Loveland *et al.*, 2017; Fislage *et al.*, 2018). This event moves the catalytic histidine of the EF-Tu G-domain (His84) near to A2662 of the SRL (Voorhees *et al.*, 2010; Loveland *et al.*, 2017; Fislage *et al.*, 2018) allowing the formation of hydrogen bonds that lock the His residue such that it coordinates a water molecule that participates in the nucleophilic attack on the γ -phosphate of the GTP (Cool and Parmeggiani, 1991; Daviter, 2003; Voorhees *et al.*, 2010; Loveland *et al.*, 2017; Fislage *et al.*, 2018) (Fig. 4f). In this way the GTPase catalysis is accomplished, and the GTP bound to EF-Tu is hydrolyzed to GDP and P_i. GTP hydrolysis is accompanied by a change in conformation, subsequently to which EF-Tu, once GDP-bound, loses affinity for the tRNA and for the surrounding ribosome; EF-Tu releases the CCA-end of tRNA (Pape *et al.*, 1998; Pape *et al.*, 1999; Kothe and

Rodnina, 2006), which switches to a A/A state, a configuration required for subsequent peptide bond formation (Pape *et al.*, 1998; Pape *et al.*, 1999; Gromadski and Rodnina, 2004, Sanbonmatsu *et al.*, 2005). Then EF-Tu·GDP leaves the translational machinery (Morse *et al.*, 2020).

Near-cognate tRNAs which have escaped the sampling selection by decoding bases are associated with a GTPase activation that is 100-fold slower with respect to the one observed for cognate tRNAs, so that SSU closure and GTP hydrolysis is accomplished just by a minor fraction of non-cognate ternary complexes (Pape *et al.*, 1998; Pape *et al.*, 1999; Zhang *et al.*, 2015a; Loveland *et al.*, 2017; Fislage *et al.*, 2018). Moreover, also in case of GTPase activation, the subsequent optimal accommodation tRNA at the PTC is much slower, since tRNA dissociation is favoured (Pape *et al.*, 1998; Pape *et al.*, 1999; Demeshkina *et al.*, 2013; Rozov *et al.*, 2015; Rozov *et al.*, 2016a; Rozov *et al.*, 2016b). This difference in kinetics allows a further discrimination between cognate and non-cognate ternary complexes, constituting a second proofreading step during translation elongation (Pape *et al.*, 1999; Geggier *et al.*, 2010; Jeong *et al.*, 2016). In addition to this, Morse *et al.* have demonstrated (Morse *et al.*, 2020) that those tRNAs placed at the A-site that are unable to participate efficiently in peptide-bond formation, as this proofreading takes place, engage with EF-Tu·GTP from solution, forming back the ternary complex on the ribosome. This proposed proofreading model may involve multiple GTP hydrolysis events (Morse *et al.*, 2020). Only near-cognate tRNAs escaping both proofreadings are included in the chain, resulting in a decoding error rate of around 10^{-3} (Wohlgemuth *et al.*, 2010; Manickam *et al.*, 2014). However, considering that an average *E. coli* protein is 300 amino acids long, the frequency of misincorporation is negligible and does not impact biological fitness in a significant way (Allan Drummond and Wilke, 2009).

Peptide bond formation

As previously mentioned, the ribosome is a ribozyme (Cech, 2000; Noller, 2012): its catalysis is peptide bond formation involving as substrates the carbonyl of the C-terminal amino acid residue of the nascent chain connected to the P-tRNA and the amino group of the amino acid carried by the A-tRNA. The catalytic center is referred to as the peptidyl transferase center (PTC) and all its components are part of domain V of the 23S rRNA, whose ribonucleotides sequence is highly conserved (Ban *et al.*, 2000; Nissen *et al.*, 2000; Hansen *et al.*, 2002), with the closest rProtein in bacteria being bL27, whose N-terminus is 8-10 Å away from any functional components (Voorhees *et al.*, 2009; Polikanov *et al.*, 2014a) and whose role in the catalysis is still debated (Polikanov *et al.*, 2014a; Maracci *et al.*, 2015). It has been shown that peptide bond formation can be catalysed solely by the 50S subunit, requiring just functional tRNA substrates or charged tRNA fragments, without the need for the 30S and translation factors (Monro, 1967; Maden and Monro, 1968; Schmeing *et al.*, 2002; Wohlgemuth *et al.*, 2006). The ribosome achieves peptide bond formation by playing a dual role: on one hand, it allows the substrate P-tRNA and A-tRNA to acquire an

optimal geometry for the reaction to occur, and indeed it is said to be an entropic trap (Sievers *et al.*, 2004), and, on the other hand, it provides a local chemistry that enhances the reaction rate (Schmeing *et al.*, 2005b; Polikanov *et al.*, 2014a). Both are going to be discussed in the following paragraphs.

The optimal placement of the CCA-ends of the P-tRNA and the A-tRNA ensured by the ribosome is crucial to lower the activation energy required for peptidyl transfer to happen. This occurs through aminolysis from the P-tRNA onto the amino acid of the A-tRNA, so that the rate is 10^5 - 10^7 -fold higher compared to such a reaction in solution (Sievers *et al.*, 2004). Such aminolysis is the consequence of the α -amino group of the aminoacyl-tRNA in the A-site nucleophilically attacking the carbonyl carbon of the ester group that anchors the nascent chain to the P-tRNA (Nissen *et al.*, 2000). In particular, the CCA end of the P-tRNA is stabilized in position by the formation of Watson-Crick base pairing between C74 and C75 with G2551 and G2552 belonging to the P-loop (H80) of the 23S rRNA; A76 is interacting by hydrogen bonding with A2450 and by stacking with the ribose of A2451. Nearby, the A-loop (H92) of the 23S rRNA is essential to place the CCA-end of the A-tRNA: C74 forms stacking interaction with U2555 and C75 base pairs with G2553, while A76 forms an A-minor motif with G2583. This last interaction leads to the disruption of the previously existing Wobble base pairing between G2583 and U2506, so that U2506 flips and U2584 and U2585 shift. Such change of local arrangement contributes to the optimization of the reactivity between the substrates: while the A-site is vacant, U2585 protects the peptidyl-tRNA at the P-site from premature hydrolysis in absence of A-tRNA, while upon A-tRNA accommodation its shift makes the ester bond connecting the nascent chain to the P-tRNA exposed for the nucleophilic attack from the amino acid residue at the A-site, meanwhile A2602 positions between the CCA-ends of the two accommodated tRNAs (Nissen *et al.*, 2000; Hansen *et al.*, 2002; Schmeing *et al.*, 2005a; Schmeing *et al.*, 2005b; Voorhees *et al.*, 2009; Polikanov *et al.*, 2014a). Such a change in conformation resulting from the optimal accommodation of the A-tRNA shifts the PTC from an uninduced to an induced state; once induced, the PTC also chemically contributes to the catalysis. The chemistry of peptide bond formation in the PTC is still debated in the field.

Historically, the first model proposed for peptide bond formation consisted in an acid-base catalysis: the crystal structure of the LSU of *Haloarcula marismortui* with CCA-end analogues led to the suggestion that the N3 atom of A2451, being in H-bonding distance from the α -amino group of the residue at the A-site tRNA, would act as a base, extracting an H-bond from it and consequently favouring the nucleophilic attack to the carbonyl carbon at the P-site. Mutation and deletion of A2451, however, subsequently showed that this residue was not essential for peptide bond formation (Polacek *et al.*, 2001; Youngman *et al.*, 2004; Erlacher *et al.*, 2005), and, more generally, it was observed that the ribosome catalysis was not pH dependent (Bieling *et al.*, 2006), making this model outdated. Subsequently, a proton relay model was first proposed by Schmeing *et al.* (2005a) from the interpretation of *H. marismortui* LSU in complex

with substrate, referred to as eight-membered proton shuttle. Here, the nucleophilic attack of the substrate α -amino group at the A-site to the C-terminal residue of the nascent chain is ignited by the 2'-OH moiety of A76 of the P-tRNA, which extracts a proton from the substrate nitrogen and at the same time donates one to the 3'-OH of the same ribose via a water molecule (Schmeing *et al.*, 2005a) (Fig. 5a).

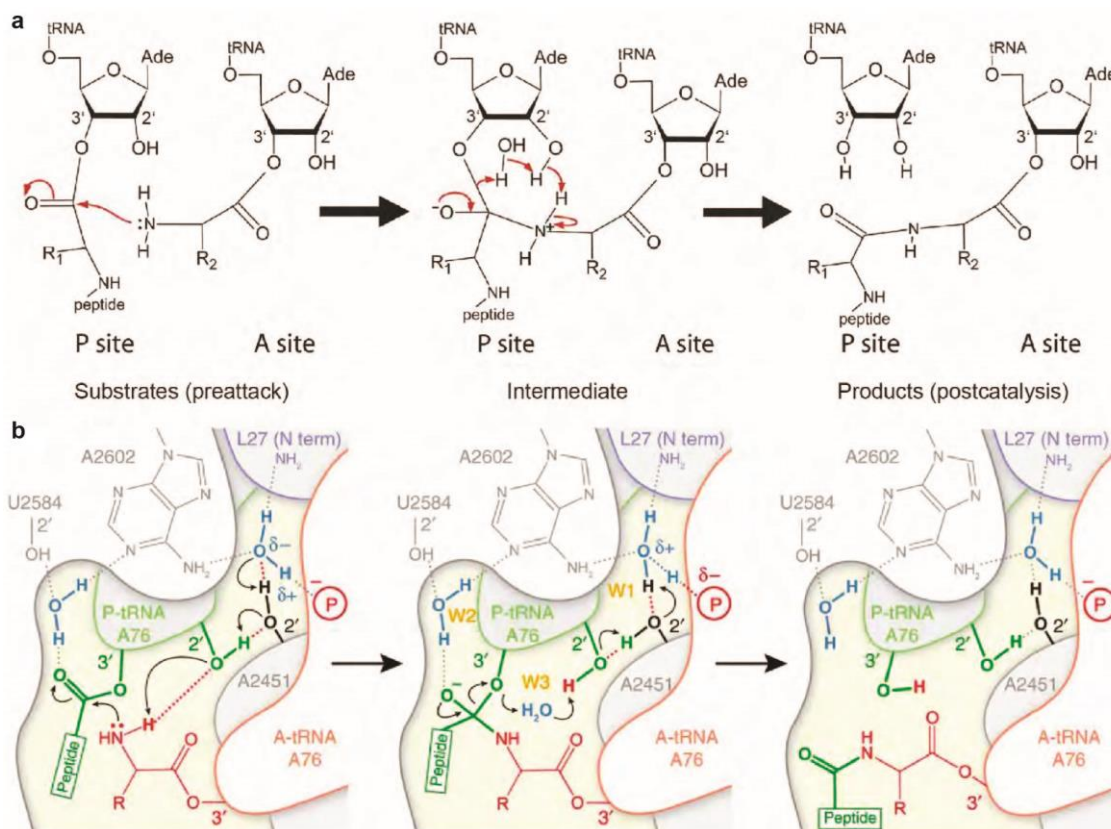


Figure 5: Overview of two model mechanisms for peptide bond formation. (a). Eight-membered proton shuttle. Panels adapted from Schmeing *et al.*, 2005a. (b). Proton wire. Panels adapted from Polikanov *et al.*, 2014a. Both mechanisms involve the formation of a tetrahedral intermediate as a consequence of the nucleophilic attack of the α -amino group in the A-site to the carbonyl carbon in the P-site. Breakdown of the intermediate via different proton transfer routes eventually results in the transfer of the peptidyl- from the P-tRNA to the α -amino group of the amino acid attached to the A-tRNA.

A more recent model was proposed by Polikanov *et al.* (2014a), based on atomic resolution structures of *T. thermophilus* 70S ribosomal complexes pre- and post-peptide bond formation, in which several components of the PTC, including a protein residue and stable water molecules, constitute a relay called a “proton wire” (Polikanov *et al.*, 2014a) (Fig. 5b). Three water molecules are involved in the process: water 1 (W1) is stabilized locally by the phosphate backbone of A-tRNA nucleotide A76, N6 of A2602 and the 2'-OH group of A2451 of the LSU, together with the N-terminal amino group of L27; water 2 (W2) is kept in position by N1 of A2602 and the 2'-OH group of U2584; water 3 (W3) is interacting with the 2'-OH groups of A76 of the P-tRNA and C2063 (Polikanov *et al.*, 2014a) (Fig. 5b). The negative phosphate backbone

of A76 of the P-tRNA and the basic character of the nitrogen at the N-terminus of L27 attract the hydrogens of W1, orienting its oxygen and giving it a partial negative charge (δ^-) which is responsible for initializing the proton wire: W1 oxygen transiently subtracts a hydrogen from the 2'-OH of A2451, which in turn accepts the one from the 2'-OH of the A76 of the P-tRNA; the latter is now able to acquire the hydrogen of the α -amino group of the aminoacyl residue at the A-site. This makes the nitrogen to which the hydrogen has been subtracted extremely nucleophilic, forcing the attack from its lone pair of electrons to the carbonyl carbon of the C-terminal residue of the nascent chain (Fig. 5b). The accomplishment of such nucleophilic attack leads to the formation of a new bond between the nitrogen of the amino group of the amino acid connected to the A-tRNA and the attacked carbonyl, so that a highly unstable tetrahedral intermediate state is achieved (Fig. 5b). The tetrahedral intermediate has its oxyanion negative charge stabilized by W2. Hiller *et al.* (2011) has shown by kinetic isotope studies that in a second step the ribosome catalyzes the rapid breakdown of such tetrahedral intermediate and this timing prevents premature translation termination by hydrolysis. The hydrogen from W1 flows back through the wire, going through A2451, the 2'-OH of P-tRNA and eventually to W3, from which it is acquired by the oxygen of the ester linkage between the P-tRNA and the intermediate, breaking it and reaching the reaction coordinate endpoint (Polikanov *et al.*, 2014a) (Fig. 5b).

The geometry described by Polikanov *et al.* has a better efficiency for proton transfer respect to the one of the proton shuttle. The model of the proton wire suggests an involvement of ribosomal protein L27 in the catalysis of the ribosome. However, the actual contribution and requirement of proteic components in peptide bond formation is still a matter of discussion and controversy. Ribosomal protein bL27 was already connected to the efficiency of peptide bond formation by Maguire *et al.* (2005), since the deletion of the first 3-6 N-terminal residues negatively affect the rate of the catalysis; Moreover the presence of this protein also seems to stabilize the substrate tRNAs, assisting in their optimal positioning (Voorhees *et al.*, 2009; Polikanov *et al.*, 2014a). On the other hand, the group of Marina Rodnina (Maracci *et al.*, 2015) clearly showed that the deletion of bL27 does not impair translation, causing only a non-lethal decrease in the rate. The distribution of bL27 itself among the domains of life does not suggest an essential role in the ancestral process of translation: while it is conserved among bacteria (Ban *et al.*, 2014), this is not the case for archaea and eukaryotes. The structure of the eukaryotic wheat-germ ribosome from Armache *et al.*, (2010) shows that protein L10e (uL16) has a conserved loop extending deep to the PTC, whose role in the ribosome catalysis is not clear yet; such loop is however flexible in *H. marismortui* ribosome (Ban *et al.*, 2000; Nissen *et al.*, 2000; Hansen *et al.*, 2002; Schmeing *et al.*, 2005a; Schmeing *et al.*, 2005b).

In conclusion, there is no universal definitive model for peptide bond formation to date, its conservation among the domains of life should still be completely elucidated by complementary biochemical, kinetics and structural approaches.

Ribosome translocation

After peptide bond formation has been accomplished, a deacylated tRNA is at the P-site, while the nascent chain, now elongated of one residue (the one encoded by the A-site mRNA codon) is loaded on the tRNA at the A-site. Ribosome translocation is required to move the tRNA at the P-site to the E-site, and the peptidyl-tRNA from the A-site to the P-site. Given the codon-anticodon pairing, the mRNA also slides in a concerted way. After a successful translocation, the A-site pocket becomes empty again, displaying the downstream (3') mRNA codon, allowing a subsequent decoding event and peptide bond to form, thus making the elongation phase iterative (Fig. 2). The state after peptide bond formation is referred to as a PRE state (pre-translocation), while the one achieved after translocation is called POST (post-translocation) (Fig. 6a).

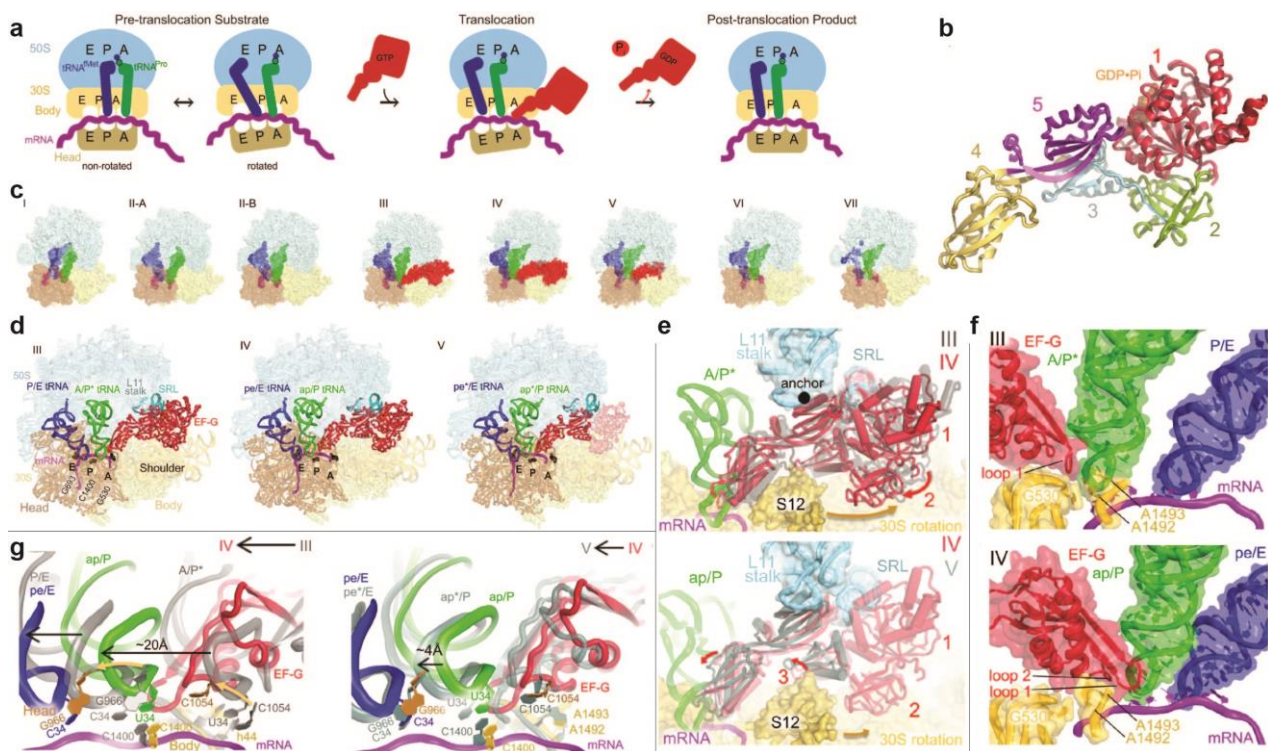


Figure 6: Ribosome translocation at a glance. (a). Schematics for ribosome translocation with 30S yellow (Head dark, body pale), 50S turquoise, P-site tRNA in blue and A-site tRNA in green, EF-G in red and mRNA in purple. (b). Architecture of EF-G, divided in 5 domains, numbered. (c). Segmented cryo-EM maps of the captured states of the translocation reaction. The components of the complex for each state are colored with the same code used in (a). (d). Structures III, IV and V with EF-G. 16S nucleotides at the A, P, and E sites (G530, C1400 and G693, respectively) are shown as black surfaces. (e). Rearrangement of EF-G relative to the 30S subunit from (top) Structure III (gray) to IV (colored) and (bottom) from Structure IV (colored) to V (blue-gray). Structures are aligned on 16S rRNA. (f). Positions of EF-G and tRNAs relative to the decoding center (yellow) in Structures (top) III and (bottom) IV. (g). Transitions of tRNA and EF-G between (left) Structures III and IV and (right) Structures IV and V. Panels adapted from Carbone *et al.*, 2021.

As the ribosomal translating complex is in the PRE state, the SSU rotates continuously with respect to the LSU, switching from a classical to a rotated/hybrid state, with an estimated rate of around 40 oscillations per second (Moazed and Noller, 1989; Blanchard *et al.*, 2004; Agirrezabala *et al.*, 2008; Cornish *et al.*, 2008; Chen *et al.*, 2011; Chen *et al.*, 2013a; Adio *et al.*, 2015; Sharma *et al.*, 2016). When going from classical to rotated state, the placement of the 30S occurs in concert with the tRNA conformations: the SSU rotates by 6° counter clockwise respect to the LSU and the head is swiveled by 6° (Frank and Agrawal, 2000; Agirrezabala *et al.*, 2008; Julian *et al.*, 2008; Agirrezabala *et al.*, 2012; Chen *et al.*, 2013b; Tourigny *et al.*, 2013); as a consequence of such a rotation, the tRNAs also enter a state said to be hybrid, in which the ASL remains placed on the respective A- and P-site of the 30S, while being into the P- and E-site with their respective acceptor stems. In this conformation, the tRNAs are in A/P- and P/E-hybrid states (Fig. 6a). Also the periphery of the LSU undergoes structural rearrangement, since in this phase the L1 stalk is found to be rotated of 30° toward the E-site in its “closed” state, in which it contacts the 30S head and the elbow of the P/E-tRNA. This spontaneous intersubunit rotation is an essential step of translocation, as it was shown that preventing it by anchoring the two subunits via cross-linking renders the process non-functional (Horan and Noller, 2007).

After the 30S has rotated and the tRNAs have entered the hybrid state, the accomplishment of translocation may also occur spontaneously, however, the low rate would not be compatible with life (Gavrilova and Spirin, 1971; Fredrick and Noller, 2003; Shoji *et al.*, 2006). In order to make translocation efficiency able to sustain the cellular metabolism, the ribosome requires the translational GTPase EF-G (Fig. 6b); EF-G is composed of 5 domains, among which domain I is the G-domain, responsible for GTPase activity requiring the highly conserved and essential His92 at the catalytic pocket. Domains I and II are also part of other translational GTPases (trGTPases), while domains III-V are only found in EF-G (Nishizuka and Lipmann, 1966; Ævarsson *et al.*, 1994; Czworkowski *et al.*, 1994; Rodnina *et al.*, 1997; Chen *et al.*, 2013b; Cunha *et al.*, 2013; Pulk and Cate, 2013; Tourigny *et al.*, 2013; Adio *et al.*, 2015) (Fig. 6b). The translocation rate in presence of EF-G-GTP is four orders of magnitude higher respect to that of the spontaneous event, and such rate is further increased by 40-fold upon GTP hydrolysis (Rodnina *et al.*, 1997; Munro *et al.*, 2010). EF-G displays two major conformations: a compact conformation that seems to be the preferred one in solution, as it was shown by FRET analysis by Salsi *et al.* (2015), and an elongated one, which is the one observed when the factor is in complex with the ribosome. In the latter, the extended form of EF-G bound to the ribosome structurally resembles that of the EF-Tu-GTP-tRNA ternary complex, since domain IV is mimicking the ASL of the tRNA (Ævarsson *et al.*, 1994; Czworkowski *et al.*, 1994; Nissen *et al.*, 1995) (Fig. 6b) and binds in a cleft defined by the head and the body of the 30S, close to the A-site, to contact the ASL of the A-tRNA (Brilot *et al.*, 2013). As with EF-Tu, the association of EF-G with the ribosomal GTPase center (GAC) occurs via the L7/L12 stalk (Diaconu *et al.*, 2005; Helgstrand *et al.*, 2007). The binding of EF-G can occur at any state of the 30S, however, the preferred substrate is the rotated state and it was shown that EF-G

binding favours the switch to the rotated state (Spiegel *et al.*, 2007; Chen *et al.*, 2011; Chen *et al.*, 2013a; Adio *et al.*, 2015; Belardinelli *et al.*, 2016a).

The activity of EF-G and the role of GTP hydrolysis is the subject of several recent kinetic and structural studies (Carbone *et al.*, 2021, Petrychenko *et al.*, 2021, Rundlet *et al.*, 2021). The group of Korostelev (Carbone *et al.*, 2021) performed time-resolved cryo-EM on a reconstituted ribosomal complex featuring deacylated P-tRNA and a nascent chain on the A-tRNA to which EF-G-GTP is provided (Fig. 6c). This led to the observation of several states along the translocation trajectory: a first state (Structure I) with unrotated 30S and canonical A/A and P/P tRNAs continuously interconverts with three variants of the second state, all of them displaying a rotated 30S (Structures IIA-C). In structure IIA the acceptor arm of the deacylated tRNA at the P-site occupies the E-site pocket of the 50S (P/E state), while the A-tRNA maintains a canonical A/A state; in structure IIB both tRNAs are in hybrid state (A/P and P/E), while in structure IIB also the elbow of A/P-tRNA is moved into the P-site pocket, forming a A/P* state. In the structural states described until now, EF-G is not part of the complex and while the 30S rotates and the tRNAs' arm and elbow move, the association between anticodons and their respective codons stays stable and unchanged. The complex observed in structure IIC is the substrate of EF-G, which is present in structure III (Fig. 6c): indeed structures I, IIA and IIB are incompatible with EF-G binding because of steric clash with the tRNAs, which are positioned the same way in structures IIC and III. In structure III, EF-G is associated to the ribosome in an extended conformation (Fig. 6d (left)): domain I binds close to the sarcin-ricin loop of the 50S, domains II and III anchor the factor to the 30S body and shoulder and domain V is hooked to the L11 stalk (Fig. 6e (top)). Such placement orients the domain IV with its tip entering the space shaped by the 30S shoulder, head and the ASL of A/P*-tRNA. In particular, Loop 1 of domain IV (aa 507-514) extends between the tRNA at the A-site and the decoding center, contacting G530 of the 30S shoulder, a crucial component locking the A-tRNA anticodon to its codon; at the same time, Loop 2 (aa 582-588) sticks into the minor groove of helix 34 of the 16S rRNA at C1209 as the head is in a pre-swiveled conformation (Fig. 6f (top)). This fit of domain 4 creates a thread that structurally couples the swivelling of the 30S to the unlocking of the codon-anticodon pairing at the A-site. In structure IV (Fig. 6c, d (middle)), the 30S has back-rotated from 11.6° (Structure III) to 5° and the head has swiveled of 17° toward the 50S; as a consequence, domains II to IV of EF-G is moved into the A-site (Fig. 6e (top)), so that domain IV now detaches the nucleotides of the tRNA at the A-site from those of the mRNA codon (Fig. 6f (top)). Also the tRNAs slip along the 30S, so that now the U34 of the A-site anticodon stacks on C1400 of the 16S and C34 of the P-site anticodon stacks with G966 of the 16S, in a chimeric state referred to as ap/P- and pe/E-tRNA, respectively (Fig. 6g (left)). The interdomain movements of EF-G when shifting from structure III to structure IV fits the spontaneous fluctuations of the factor in solution and in crystal structures of EF-G homologs, therefore, the capability of EF-G to move the tRNAs along the translocation trajectory of around 20 Å from structure III to IV are the result

of the factor's intrinsic stochastic rearrangement in the context of a ribosomal complex whose 30S is rotating.

In structure V, the 30S goes back to a rotation of 1.1° and the head further swivels to 18.1° (Fig 6c, d (right)). In such a state, the tRNAs are translocated another 3-5 Å so that the tRNA previously at the A-site is now more into the P-site of the decoding center in an ap*/P state (Fig 6g (right)); on the other end, the EF-G domain 4 is placed on the A-site, with the factor still hinged through domain V to the L11 stalk and domain III density much weaker (Fig 6e (bottom)), while those of domains I and II disappeared (sterically hindered by the new placement of S12) (Fig. 6e (bottom)), meaning that in this late translocation state, EF-G has extended even deeper into the 30S and the GTPase domain has detached from the SRL, with overall loss of contacts between the factor and the ribosome. From structure III to structure V, the association between EF-G GTPase center and the ribosome decreases while the contacts formed by the translocase superdomain increases drastically. The factor's density disappears in structure VI (Fig. 6c), whose tRNAs states are the same of those in structure V; structure VII displays a head with a completely reverse swivel of 20° to form a non-swivelled non-rotated state having canonical P-tRNA at the P-site bearing an elongated nascent chain and weak density of deacylated E-site tRNA, most of which already left the ribosomal complex (Fig. 6c).

In structure III, the GTPase domain of EF-G is sandwiched between the two ribosomal subunits and are in an active conformation due to the local rearrangement of catalytic His92 favoured by ribosome association. Together with ribosomal components, switch loop I (sw-I) of EF-G stabilizes GDP and switch loop II (sw-II) contacts the nearby inorganic phosphate (Pi), meaning that in this state GTP hydrolysis has already taken place. In structure IV, the GTPase domain has already partially dissociated from the SRL and the density for sw-II disappeared, as a result of the loop becoming flexible due to release Pi while GDP is still in the pocket. The analysis of such structures led to a model explaining the role of GTP hydrolysis in translocation: Carbone *et al.* proposed that the hydrolysis of GTP to GDP + Pi is not coordinated with translocation, but it occurs very fast, while the timing of the subsequent Pi release, possible by the rearrangement of sw-I and sw-II, fits and coordinates with the progression of tRNAs along the translocation trajectory, while the factor's GTPase domain completely loses contact with the ribosome. This explains why, despite positively contributing to the directionality of the process, GTP hydrolysis is not essential for translocation to efficiently occur. In this model, EF-G is accelerating translocation by acting as a nearly-rigid rod, that causes inherent ribosomal rearrangements to achieve tRNA movement on the 30S subunit. The GTPase activity of the factor is a mere switch allowing EF-G to efficiently detach and leave the ribosome.

The same time-resolved cryo-EM study was carried out by Petrychenko *et al.* (2021), that proposes an alternative contribution of EF-G, mostly dependent on GTP

hydrolysis. In particular, the GTPase activity resulting from the placement of EF-G close by the SRL leads to a change in conformation of the factor, that like a loaded spring being released pushes the tRNA hybrids along the translocation coordinates, to accomplish the step. Here, the behaviour of EF-G is similar to that described for EF-Tu upon A-tRNA release (Loveland *et al.*, 2017). In this study, however, the kinetics of the ribosome may be biased by the presence of the drug apramycin, which is used to slow down the reactions during late translocation (Petrychenko *et al.*, 2021).

The group of Blanchard (Rundlet *et al.*, 2021) also studied translocation by means of time-resolved Cryo-EM and complemented their data with sm-FRET. Their observations fit with those of Carbone *et al.*, 2021 and Petrychenko *et al.*, 2021, and they were also able to capture a state in which EF-G is still bound to GTP pre-hydrolysis. The role of EF-G in translocation offered by these data fits that of Korostelev (Carbone *et al.*, 2021).

Translation termination

The decoding of a stop codon (UAA, UAG, UGA) at the A-site initializes the termination phase, upon which the nascent chain is released from the P-tRNA to leave the translating complex as a polypeptide (Brenner *et al.*, 1965; Capecchi, 1967; Weigert and Garen, 1965). The process is possible by the activity of two classes of release factors: class I, which includes RF1 and RF2 and class II, which consists of RF3 in prokaryotes (Fig. 2,7).

Class I release factors are the first to enter into play, since they have the role of recognizing the stop codon at the DC and subsequently releasing the nascent chain from the P-tRNA (Capecchi, 1967; Zhou *et al.*, 2012a) (Fig. 7a-b). Both RF1 and RF2 have four domains (Fig. 7c): domain I, folding into three helices, has a stabilizing role, contacting the SSU; domain II and domain IV together form the superdomain having the function of decoding the stop codon at the A-site; domain III is shaped as a long helix with a loop containing the essential GGQ motif, that reaches into the PTC and mediates the hydrolysis of the bond linking the NC to the tRNA at the P-site (Zhou *et al.*, 2012a, Vestergaard *et al.*, 2001; Shin *et al.*, 2004; Zoldak *et al.*, 2007) (Fig. 7a-d). Upon association and placing of a class I RF at the 30S decoding center, crucial residues acquire a conformation that contribute to the decoding of the stop codon, namely, within a β -sheet belonging to domain II of the release factor: A1492 flips out of h44, A1493 maintains its position and stacks on A1913 from the large subunit, the latter having the role of substituting A1493; G530 and the third position of the stop codon stack (Korostelev *et al.*, 2008; Laurberg *et al.*, 2008; Ogle *et al.*, 2001; Selmer *et al.*, 2006; Weixlbaumer *et al.*, 2008) (Fig. 7e). RF1 and RF2 have a difference sequence motif in the β -sheet of domain II devoted to stop codon decoding and this leads to their capability of recognizing different stop codons:

RF1 is characterized by a Pro-Val-Thr (PVT) sequence that recognize UAG and UAA, while RF2's motif is Ser-Pro-Phe (SPF) allowing the factor to recognize UAA and UGA (Ito *et al.*, 2000).

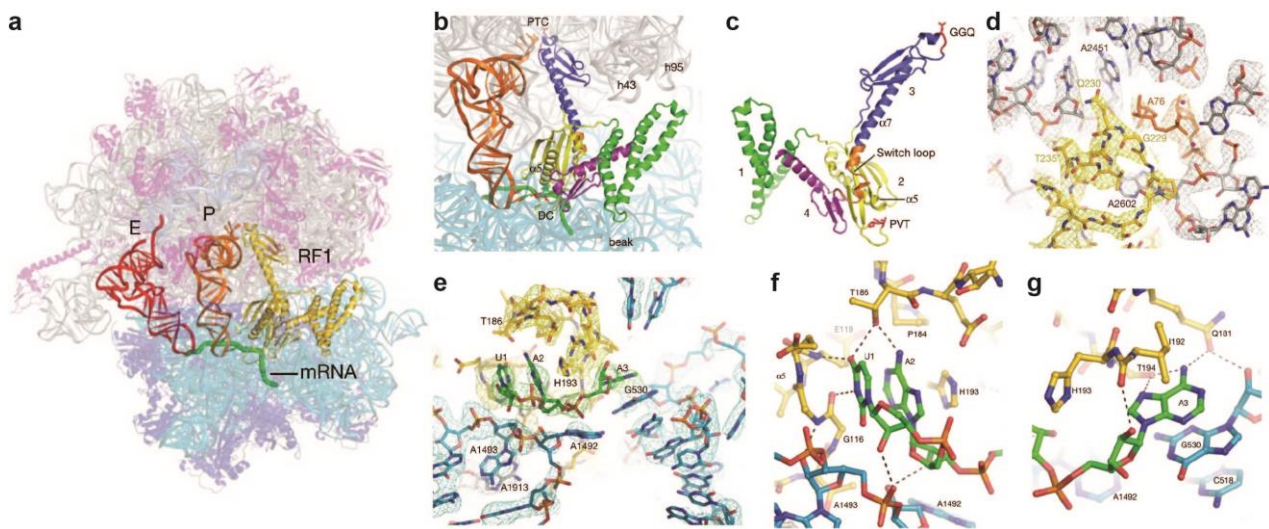


Figure 7: Activity of RF1 during translation termination. (a). Positioning of RF1 (yellow) upon presence of a nonsense codon (UAA or UAG) at the A-site of the 70S. P-tRNA is orange, E-tRNA is red and mRNA is green. (b). Focus of (a) in the pocket defined by the DC (bottom) and the PTC (top) of the ribosome. P-tRNA is orange, RF1 is coloured by domains (Domain 1 green, domain 2 yellow, domain 3 blue, domain 4 purple, switch loop shiny orange) and the GGQ and PVT motifs are red. (c). View of isolated RF1, rotated of 180° with respect to the orientation in (b). The colouring is the same as in (b). (d). Molecular model of the complex at the PTC with surrounding density. 23S rRNA is grey, P-tRNA is orange and RF1 is yellow. (e). Molecular model of the complex at the DC with surrounding density. 16S rRNA is light blue, RF1 is yellow, the mRNA is green. (f). Recognition of U1 and A2 of the UAA stop codon by RF1 elements. (g). Recognition of the third base A3 by RF1. (f-g) are coloured as in (e). Panels adapted from Laurberg *et al.*, 2008.

The first base of a stop codon at the A-site is decoded in both factors using the N-terminus of α -helix 5 forming two hydrogen bonds to recognize a uridine at first position (Korostelev *et al.*, 2008; Laurberg *et al.*, 2008; Petry *et al.*, 2005; Weixlbaumer *et al.*, 2008) (Fig. 7f). RF1 contacts the second codon through the threonine of its PVT motif by forming one hydrogen bond with adenine (Korostelev *et al.*, 2010; Laurberg *et al.*, 2008) (Fig. 7f); analogously, serine of RF2 SPF motif forms two hydrogen bonds with a purine at the second position (A or G) (Korostelev *et al.*, 2008; Weixlbaumer *et al.*, 2008), and such differential selectivity explains why RF1 can not recognize UGA. The recognition of the third codon is mediated by a Thr and a Gln in RF1 (Korostelev *et al.*, 2010; Laurberg *et al.*, 2008) (Fig 7g) and by a Val in RF2 (Korostelev *et al.*, 2008; Weixlbaumer *et al.*, 2008), which monitor the Hoogsteen edges of the third base (Zhou *et al.*, 2012a). While these contacts are essential to determine the specificity of the two factors for stop codons, there are also other interactions that provide additional structural stabilization for the interaction and the subsequent termination event, such as His197 in RF1 (Laurberg *et al.*, 2008) and His214 in RF2 (Weixlbaumer *et al.*, 2008) by stacking upon the purine base of the nucleotide in the second position.

Deciphering the stop codon successfully triggers alterations in the switch loop of RF1/2 (Youngman *et al.*, 2008; Zhou *et al.*, 2012a). This leads to RF1/2 domain III fitting into the PTC of the LSU due to the switch loop reorganization (Youngman *et al.*, 2008; Zhou *et al.*, 2012a) (Fig. 7b). Domain III contains a tripeptide Gly-Gly-Gln (GGQ) motif that is crucial in releasing the nascent chain (Fig. 7c). This motif is conserved across RF1, RF2, and the evolutionarily unrelated eukaryotic termination release factor eRF1 (Frolova *et al.*, 1999; Mora *et al.*, 2003; Seit-Nebi *et al.*, 2001; Shaw and Green, 2007; Zavialov *et al.*, 2002). Consequently, RF1 and RF2 employ a common mechanism for polypeptide chain release: a water molecule serves as an acceptor for the nascent peptide, determining its release from the ribosome (Tate and Brown, 1992). This water molecule plays a role analogous to the deprotonated α -amine during transpeptidation, since it attacks the carbonyl linking the peptidyl moiety to the P-site tRNA (Kuhlenkoetter *et al.*, 2011; Trobro and Aqvist, 2009). Trobro and Aqvist (2009) shown by molecular dynamic simulations that the conserved GGQ motif positions the crucial water molecule in the PTC adjacent to nucleotide A76 of the P-site tRNA bearing the peptidyl moiety and this also likely involves the 23S rRNA residue A2451, the 2'-hydroxyl of A76, and the backbone NH group of the glutamine residue (Fig.7d). It was demonstrated that the glycine residues in the first two positions of the GGQ motif are more important for water molecule placement than the glutamine in the third position: indeed, mutations in either glycine significantly impact translation termination (Mora *et al.*, 2003; Shaw and Green, 2007; Zavialov *et al.*, 2002). This results from the unique conformation of the GGQ motif, which is constrained by the achiral nature of glycine residues and their specific torsion angles (Zhou *et al.*, 2012a). The absence of the glycine residues disrupts the positioning of the GGQ motif and the water molecule within the PTC (Mora *et al.*, 2003; Shaw and Green, 2007; Zavialov *et al.*, 2002). By contrast, alterations to the glutamine have only minor effects (Shaw and Green, 2007; Zavialov *et al.*, 2002), while glutamine (*E. coli* Gln235) is suggested to be crucial for nucleophile specificity (Shaw and Green, 2007). Nonetheless, the backbone NH group plays a role in coordinating the water molecule and appears essential for stabilizing a tetrahedral intermediate and the final product (Laurberg *et al.*, 2008).

The formation of the tetrahedral intermediate occurs when the coordinated water molecule undergoes nucleophilic attack, likely displaying an oxyanion stabilized by the NH-group (Laurberg *et al.*, 2008). Following successful cleavage, the peptidyl moiety is liberated from the ribosome while the deacyl-tRNA remains bound. Hydrogen bonding with the 3'-hydroxyl of A76 stabilizes the deacyl-tRNA through interaction with the backbone NH-group (Laurberg *et al.*, 2008). Since the side chain's significance is minimal, substitution of Gln with other amino acids, such as alanine, is permissible and mainly influences the release rate (Mora *et al.*, 2003; Seit-Nebi *et al.*, 2001; Shaw and Green, 2007; Zavialov *et al.*, 2002), as the presence of the amino-group remains unaltered (Laurberg *et al.*, 2008). Nevertheless, under physiological conditions, RF1 and RF2 carry a post-translational modified GGQ motif: N5 of the Gln

side chain is methylated by the methyltransferase HemK (Dincbas-Renqvist *et al.*, 2000; Heurgue-Hamard *et al.*, 2002; Pierson *et al.*, 2016; Zeng and Jin, 2018) and such methylation of the Gln side chain may play a more crucial role in coordinating water alongside the backbone NH-group of the glutamine residue (Shaw and Green, 2007). X-ray crystallography research, elucidating the precise conformation of the methylated Gln side chain, supports this notion (Zeng and Jin, 2018): from the structure, it is clear that in the presence of Gln methylation the side chain adopts a conformation facilitating the precise positioning of the carbonyl carbon for coordinating the nucleophilic water molecule (Zeng and Jin, 2018).

Upon nascent peptide release, both RF1/2 and deacyl-tRNA remain bound to the ribosome. Termination release factor 3 (RF3), a class II RF, is necessary at this point to dissociate ribosome-bound RF1/2 and return them to the pool of translation factors available for protein synthesis (Freistroffer *et al.*, 1997; Goldstein and Caskey, 1970) (Fig. 2,8).

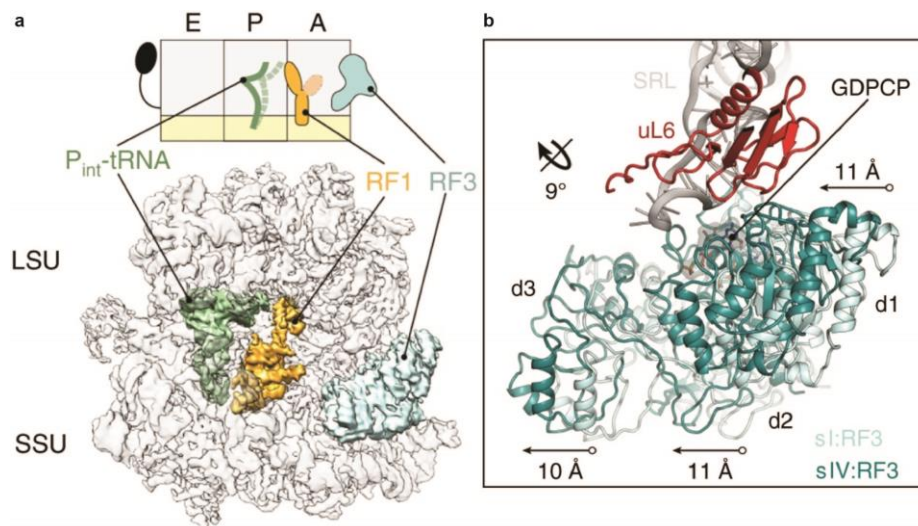


Figure 8: Activity of RF3 during translation termination. (a). Association of RF3 (cyan) to the termination complex. In this segmented map, the RF1 is yellow, the P-tRNA is in green, the rest of the complex is in grey. At the top, a schematic of the complex. (b). An intersubunit rotation of 9° brings the RF3 closer (pale cyan before rotation, teal after rotation) to the ribosome SRL (grey). Movements of domain 2 (d2) and domain 3 (d3) are indicated by the arrows. uL6 is in red. Panels are adapted from Graf *et al.*, 2018.

RF3, a three-domain protein, exhibits high structural similarity to other translational GTPases, such as EF-G, EF-Tu, and IF2 (Gao *et al.*, 2007; Jin *et al.*, 2011; Kihira *et al.*, 2012; Zhou *et al.*, 2012b) (Fig. 8a). Its G-domain (Domain I) hosts the GTPase activity, activated upon contact with the SRL (Lin *et al.*, 2015; Loveland *et al.*, 2017; Zhou *et al.*, 2012b), domains II and III, connected by a flexible linker, establish contacts with the SSU, enabling RF3 binding, particularly with S12 and 16S rRNA helices h5 and h15 (Gao *et al.*, 2007; Zhou *et al.*, 2012b; Jin *et al.*, 2011) (Fig. 8b). RF3 binding doesn't necessitate an mRNA signal in the A-site and likely occurs in its GTP-bound form to 70S ribosomes regardless of termination factors and deacyl or

peptidyl-tRNA presence, likely facilitated by L7/L12 (Carlson *et al.*, 2017; Pallesen *et al.*, 2013, Adio *et al.*, 2018; Koutmou *et al.*, 2014; Peske *et al.*, 2014). RF3 binding may even precede nascent chain release from ribosomes (Pre-hydrolysis 70S ribosome) (Adio *et al.*, 2018) and although RF3-GDP binding was not excluded, it seems unlikely due to the substantial GTP excess over GDP under native conditions (Adio *et al.*, 2018; Bennett *et al.*, 2009, Li *et al.*, 2024). The actual substrate for RF3-GTP action is, however, a post-hydrolysis 70S ribosome containing deacyl-tRNA in the P-site and RF1/2 in the A-site.

As far as it was observed, the mechanism of factor dissociation seems driven by RF3 that induces R-state ribosome formation through SSU rotation (Adio *et al.*, 2018; Ermolenko *et al.*, 2007a; Koutmou *et al.*, 2014; Graf *et al.*, 2018). As a result, disengagement of RF1/2 domain III and superdomain II/IV from the ribosome occurs (Gao *et al.*, 2007; Jin *et al.*, 2011; Kihira *et al.*, 2012; Pallesen *et al.*, 2013; Zhou *et al.*, 2012b; Graf *et al.*, 2018).

Structural studies investigating RF3-GDP((C/N)P) bound to various ribosomal complexes support this perspective (Gao *et al.*, 2007; Jin *et al.*, 2011; Kihira *et al.*, 2012; Pallesen *et al.*, 2013; Zhou *et al.*, 2012b; Graf *et al.*, 2018). In 70S-RF3 complexes, both in the presence of deacyl-tRNA and in its absence along with other ligands/factors, rotational movement of the SSU by up to 9° and SSU head swiveling of 4-14° were observed (Jin *et al.*, 2011; Zhou *et al.*, 2012b). Regardless of the ribosome rotational state, overlaying RF1/2 structures on their binding site and corresponding RF3 structures reveals no steric hindrance for simultaneous binding of class I and class II release factors. Hence, rotation-driven dissociation of RF1/2 appears to be the most plausible mechanism of RF3 to dissociate the class I release factors (Gao *et al.*, 2007; Jin *et al.*, 2011; Kihira *et al.*, 2012; Pallesen *et al.*, 2013; Zhou *et al.*, 2012b; Graf *et al.*, 2018). However, previous studies have not fully elucidated the mechanism underlying subunit rotation induction and whether RF3 undergoes significant conformational changes before GTPase activation. Additionally, it is still not clear whether GTP hydrolysis is necessary for the actual process of RF1/2 recycling or rather for RF3 dissociation from the ribosome (Adio *et al.*, 2018; Peske *et al.*, 2014), differently from EF-Tu and EF-G. A recent study from the group of Dr. Gagnon (Li *et al.*, 2024) suggests that RF1/2 release is independent from GTP hydrolysis, which is likely to occur upon a subsequent 30S rotation.

Ribosome recycling

Ribosomes and the factors engaged in protein synthesis are not disposable entities, meaning that there are system to place for mRNA release and the retrieval of post-termination ribosomes, termed “ribosome recycling” (Janosi *et al.*, 1994; Karimi *et al.*, 1999). Recycling itself is not essential for the correct outcome of protein synthesis by means of translation, but it is critical for replenishing the pool of ribosomal subunits available for mRNA recruitment and thereby for maintaining the cell metabolism. This step is mediated by the translation elongation factor EF-G and an additional specialized factor called the ribosome recycling factor (RRF), both of which essential and operating

synergistically in a GTP-dependent manner (Hirokawa *et al.*, 2006; Hirokawa *et al.*, 2005; Peske *et al.*, 2005; Zavialov *et al.*, 2005). Recycling necessitates RRF binding to the post-termination complex (PoTC) in the intersubunit space followed by EF-G association (Borg *et al.*, 2016; Dunkle *et al.*, 2011; Prabhakar *et al.*, 2017). Multiple structures depict RRF bound to 70S ribosomes (Fu *et al.*, 2016; Kim *et al.*, 2000; Nakano *et al.*, 2003; Saikrishnan *et al.*, 2005; Selmer *et al.*, 1999; Toyoda *et al.*, 2000; Yokoyama *et al.*, 2012; Yoshida *et al.*, 2001). Notably, two of these structures include both RRF and EF-G concurrently bound to 70S-PoTC (Fu *et al.*, 2016; Yokoyama *et al.*, 2012). RRF comprises two domains connected by a flexible linker, contributing to the interdomain kinetics of the factor (Fu *et al.*, 2016; Weixlbaumer *et al.*, 2007). Characteristic of RRF's structure is a three-helix bundle (domain I) extending up to the PTC (Dunkle *et al.*, 2011); the loop at the bundle's tip interacts with the LSU P-loop (Dunkle *et al.*, 2011), while α -helix 3 engages in ribosome binding by contacting H71 of the 23S rRNA (Dunkle *et al.*, 2011). RRF's domain II interacts with the SSU via protein S12 (Dunkle *et al.*, 2011; Fu *et al.*, 2016; Gao *et al.*, 2005). The association of RRF to PoTC stabilizes R-states containing P/E hybrid state deacyl-tRNAs (Dunkle *et al.*, 2011), prompting $\sim 9^\circ$ SSU body/platform counterclockwise rotation and $\sim 4^\circ$ head swivel (Dunkle *et al.*, 2011). Concurrent positioning of RRF and either tRNA in a P/P-state (Dunkle *et al.*, 2011) or RF1/2 (Pavlov *et al.*, 1997) is hindered by RRF's three-helix bundle, which extends to the PTC and blocks the A- and P-site cleft on the LSU (Dunkle *et al.*, 2011) and this evolved so that binding is restricted to complexes after peptide chain release and RF1/2 dissociation. Ribosome splitting is likely facilitated through domain II (Dunkle *et al.*, 2011; Yokoyama *et al.*, 2012), which can adopt different conformations in the presence or absence of EF-G: upon EF-G binding and subsequent GTP hydrolysis, RRF's domain II reorients toward domain I, proximal to intersubunit bridge B2a (H69 and h44) (Fu *et al.*, 2016; Wilson *et al.*, 2005). Interactions between RRF and EF-G differ from EF-G/tRNA interactions (Yokoyama *et al.*, 2012), with no tRNA contact observed in the RRF-EF-G structure (Yokoyama *et al.*, 2012). Instead, interactions occur between the junction of EF-G domain II-III and RRF domain II (Yokoyama *et al.*, 2012). The conformational changes induced by EF-G in domain II are proposed to distort subunit bridges like B2a (Fu *et al.*, 2016; Wilson *et al.*, 2005; Yokoyama *et al.*, 2012), leading to 70S ribosome dissociation into LSU and SSU. Subsequent IF3 binding to the SSU obstructs LSU interactions and serves as a starting point for another round of translation initiation (Hirokawa *et al.*, 2005; Peske *et al.*, 2005; Prabhakar *et al.*, 2017) and its association may also contribute to tRNA and mRNA dissociation from the SSU (Karimi *et al.*, 1999; Prabhakar *et al.*, 2017). Ribosome recycling thus links translation termination with initiation, facilitating seamless transitions between both phases of the cycle.

The ribosome exit tunnel and its role in protein synthesis

As peptide bond formation occurs in the PTC, amino acids are processively and iteratively polymerized into a nascent chain, which extends into a tunnel of the LSU spanning from the site of the catalysis to the outside solvent. The tunnel is 80-100 Å in length in bacteria, and therefore able to accommodate a polypeptide chain of 30-40 amino acid residues (Ban *et al.*, 2000; Voss *et al.*, 2006; Malkin and Rich, 1967; Hardesty *et al.*, 1993) (Fig. 9a). The walls of the tunnel are mostly constituted of rRNA nucleotides and its average diameter is 20 Å, however its shape, dimensions and composition are far from homogeneous along its length: starting from the PTC, the first tract of the tunnel is referred to as “upper tunnel” and it is delineated by a constriction formed by the loops of protein L4 and L22 that locally shrink the diameter to 10 Å. As the tunnel continues to its central and lower tracts, another proteic component exposing its surface to constitute the tunnel walls is L23.

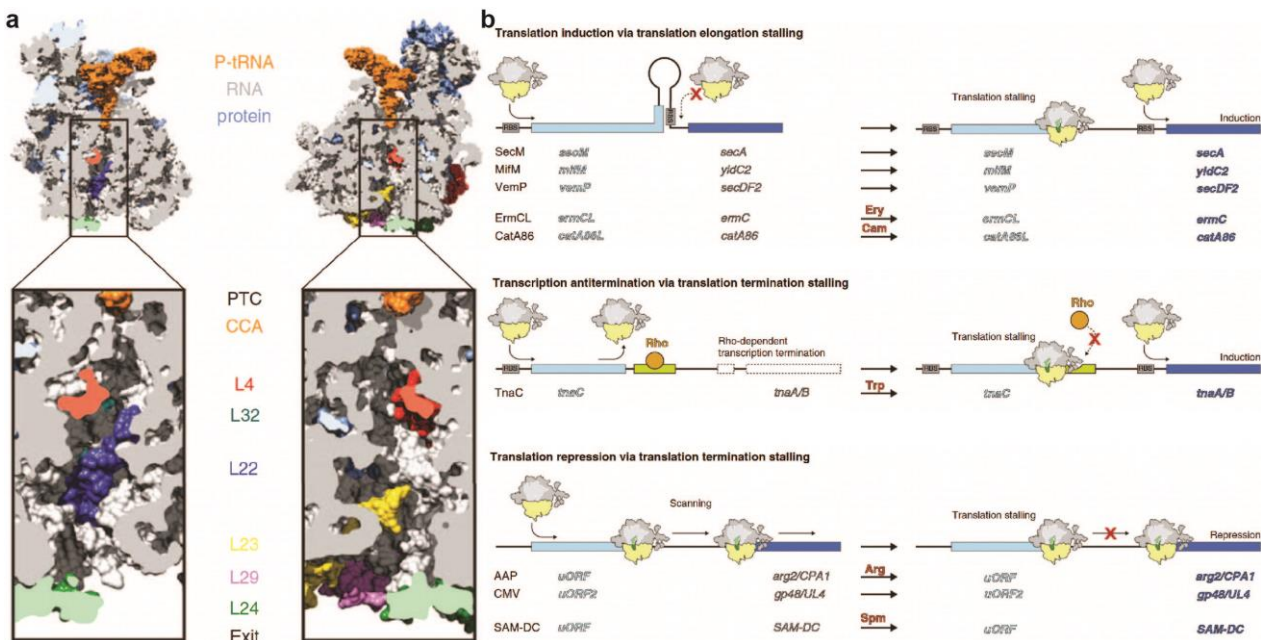


Figure 9: The ribosomal exit tunnel as a regulatory element. (a). Transverse sections through the bacterial large ribosomal subunit to reveal the tunnel components. Peptidyl-tRNA (orange), rRNA (gray) and r-proteins (light blue), except r-proteins L4 (red), L22 (dark blue), L23 (yellow), L29 (purple) and L24 (green) and L32 (dark green). Panel adapted from Wilson and Beckmann, 2011. (b). (Top) Stalling during translation elongation of SecM, MifM, VemP, ErmCL, and CatA86 leader peptides causes the ribosome to block stem-loop formation and exposes the ribosome binding site (RBS) of the downstream cistrons, allowing their expression; (Middle) Translation termination stalling on the TnaC leader peptide causes the ribosome to block Rho binding sites and thus preventing Rho-dependent transcription termination. Transcription of the downstream *tnaA/B* genes allows their expression via internal translation initiation. (Bottom) Stalling during translation termination of upstream open reading frames (uORFs) of arginine attenuator peptide (AAP), cytomegalovirus (CMV) and S-adenosyl-methionine decarboxylase (SAM-DC) prevents scanning and therefore represses expression of the respective downstream genes. Panel adapted from Wilson *et al.*, 2016.

At the end, the tunnel opens up to the outside environment as a funnel, forming the so-called “vestibule”, which is designated by proteins L23, L24 and L29 (Nissen *et al.*, 2000; Harms *et al.*, 2001; Schuwirth *et al.*, 2005, Selmer *et al.*, 2006) (Fig. 9a). For many years the tunnel was considered a crucial, albeit passive, conduit of the ribosome, but growing evidence suggests the tunnel acts as an active player in the regulation of protein synthesis, having an essential role in:

- Assisting the very early secondary structure (local) folding events of the polypeptide being synthesized: It was observed how the size and shape of the tunnel allows the early folding events of the nascent chain, as it is polymerized at the C-terminus, into both α -helices and β -sheets. This is crucial, since the environment of the tunnel and its composition, shields a relevant stretch of the nascent chain from the outer environment and its composition. This limits the potential interactions and biophysical events that could involve those residues locally, strongly affecting the final secondary structure of the polypeptide. As a consequence, the tertiary structure and therefore the physiology of the protein product and its related phenotype are also impacted (Cabrita *et al.*, 2016).
- Regulating molecular events taking place while, or soon after, the NC has been synthesized: certain sequences in the nascent peptide can interact with the exit tunnel walls, affecting the rate of translation. This can be part of a regulatory mechanism where specific sequences act as signals to slow down or pause translation, often for regulatory purposes such as facilitating co-translational folding or targeting (Nakatogawa and Ito, 2002).
- Interacting and signaling with various factors, such as chaperones and modification enzymes, which aid in folding and post-translational modifications as the NC exits the ribosome (Kaiser *et al.*, 2011).

The most evident phenomenon highlighting the regulatory role of the exit tunnel is the evolution of so-called NC arrest peptides (APs), which have been studied biochemically and structurally (Ito and Chiba, 2013; Wilson and Beckmann, 2011; Wilson *et al.*, 2016; Ramu *et al.*, 2009). APs prompt translational stalling to regulate the expression of downstream genes. Unlike translation inhibitors, like proline-rich antimicrobial peptides (PrAMPs, discussed in the next chapter), that inhibit translation by binding within the ribosomal tunnel *in trans*, APs act *in cis* during their own translation to induce stalling (Fig. 9b). Typically, an AP contains a segment of about 20 amino acids that interacts directly with ribosomal tunnel components to stall translation (Wilson *et al.*, 2016). Depending on the AP, translation arrest can occur during elongation when a sense codon is in the A-site (Fig. 9b (top)), as seen with SecM (Muto *et al.*, 2006; Garza-Sanchez *et al.*, 2006), MifM (Chiba and Ito, 2012), VemP (Ishii *et al.*, 2015), CatA86L (Wilson *et al.*, 2016), and ErmCL (Vazquez-Laslop and Mankin, 2014; Vazquez-Laslop *et al.*, 2008), or during termination when a stop codon is present (Fig. 9b (middle and bottom)), as observed with TnaC (Gong *et al.*, 2001), AAP (Wang *et al.*, 1998) and CMV (Bushan *et al.*, 2010). For elongation, the stall can occur at a specific site, as in ErmCL (Vazquez-Laslop and Mankin, 2014;

Vazquez-Laslop *et al.*, 2008) and VemP (Ishii *et al.*, 2015), or at multiple sites, as in MifM (Chiba and Ito, 2012).

Given the conserved nature of the ribosome, it is unsurprising that APs from one species can often induce stalling in another species' ribosomes. For instance, stalling during translation of *Arabidopsis thaliana* CGS1 or AAP from *Neurospora crassa* is also observed in rabbit reticulocyte and wheat germ ribosomes (Spevak *et al.*, 2010; Fang *et al.*, 2004). Similarly, the gp48/UL4 uORF2 from human cytomegalovirus (hCMV) induces stalling in human ribosomes as well as in rabbit, wheat germ, *Drosophila*, and yeast systems. However, some APs show species-specific stalling, such as MifM, which stalls in *Bacillus subtilis* but not in *Escherichia coli*, and SecM, which has the opposite effect (Chiba *et al.*, 2011).

In bacteria, stalling during translation of upstream open reading frames (uORFs) typically leads to upregulation of downstream gene expression. This can occur via anti-termination, where translation arrest blocks the Rho transcription terminator binding sites, allowing transcription and subsequent translation of downstream genes, as with TnaC. Alternatively, it can induce mRNA conformational changes that expose the Shine-Dalgarno sequence, enabling ribosome binding and translation of downstream genes, as seen with SecM, MifM, VemP, ErmCL, and Cat86L. In eukaryotes, stalling during uORF translation generally represses downstream gene expression by preventing ribosome scanning and initiation, as observed with AAP and CMV (Wilson *et al.*, 2016).

The ability of leader peptides to induce stalling may, or may not, depend on additional co-effector molecules:

- AAP and TnaC require arginine and tryptophan, respectively, while Cat86L and ErmCL require the antibiotics chloramphenicol and erythromycin, respectively. In these cases, stallers function as sensors of that specific co-effector molecule in the cell environment and regulate the expression of genes whose function is relevant in the metabolism of, or in the resistance against, the co-effector (Wilson *et al.*, 2016).
- SecM and MifM leads to a stalling event which is not influenced by any metabolite. In this scenario, stallers are sensors of pulling force exerted by protein translocator in the cell membrane which also recognize these APs nascent chain as substrate as they emerge from the exit tunnel, relieving the stalling. Such stalling regulate the expression of genes encoding for translocator components, which are often encoded in operons whose expression is extremely expensive for the cell metabolism (Wilson *et al.*, 2016).

A well-known example is the SecM arrest peptide, which controls the *secA* gene expression in Gram-negative bacteria like *Escherichia coli* (Nakatogawa and Ito, 2001; Nakatogawa *et al.*, 2004) (Fig. 9b (Top), 10a). Without SecM-mediated stalling, a stem-loop structure in the mRNA hides the ribosome-binding site (RBS) of the *secA*

gene, preventing SecA protein translation. When SecM causes stalling, it changes the mRNA conformation, exposing the RBS and enabling SecA translation. SecA, an ATPase, works with the SecYEG channel to target secretory proteins to the cytoplasmic membrane. The SecM arrest peptide includes an N-terminal signal sequence and is a SecA substrate. Interaction between SecA and SecM's signal sequence relieves SecM-induced stalling, establishing an autoregulatory system: low SecA levels prolong SecM stalling, upregulating *secA* expression, while restored SecA levels relieve stalling, repressing *secA* expression (Ito and Chiba, 2013; Nakatogawa *et al.*, 2004) (Fig. 10a).

Biochemical studies show that the SecM arrest peptide stalls the ribosome with SecM NC attached to tRNA^{Gly165} in the P-site and Pro¹⁶⁶-tRNA in the A-site (Garza-Sanchez *et al.*, 2006, Muto *et al.*, 2006). Alanine scanning mutagenesis identified Arg163 and Pro166 in SecM as crucial for stalling, leading to the SecM arrest motif 150FxxxxWIxxxxGIRAGP166 (Nakagawa and Ito, 2002) (Fig. 10a (Bottom right)). While this motif alone can induce stalling, the full-length SecM sequence is more effective, suggesting additional contributions from regions N-terminal to the motif (Nakagawa and Ito, 2002; Yang *et al.*, 2015, Muta *et al.*, 2020) (Fig. 10b). Biophysical studies suggest SecM adopts a compact conformation in the exit tunnel, with certain mutations (F150A, W155A, R163A) reducing stalling despite maintaining compaction (Fig. 10c). This indicates compaction is necessary, but not solely sufficient for translational arrest (Woolhead *et al.*, 2006). Mutations in 23S rRNA nucleotides and alterations in ribosomal proteins like uL22, which form the ribosomal tunnel, also reduce SecM-mediated stalling (Nakagawa and Ito, 2002) (Fig. 10d). Specific residues of SecM have been crosslinked to uL22, indicating critical interactions between SecM NC and the ribosome (Lawrence *et al.*, 2008; Yap and Bernstein, 2009).

Early SecM-stalled ribosomal complex (SRC) structures proposed that SecM shifts the P-site tRNA, interfering with peptide bond formation with the A-site Pro-tRNA (Bhushan *et al.*, 2011). Later cryo-EM structures of SecM-SRC at higher resolution suggested that SecM induces conformational changes in the peptidyltransferase center (PTC), leading to ribosome inactivation, and that Arg163 in SecM blocks Pro-tRNA accommodation in the A-site (Zhang *et al.*, 2015b) (Fig. 10e). However, this was contrary to biochemical studies indicating the A-site was occupied by Pro-tRNA (Muto *et al.*, 2006; Garza-Sanchez *et al.*, 2006), and that SecM NC was compacted in the tunnel, not extended (Woolhead *et al.*, 2006, Bracken and Woolhead 2019). Notably, this structure used only 17 SecM residues, with other regions replaced, so interactions of N-terminal regions were not assessed (Zhang *et al.*, 2015b). The SecM-SRC was purified with chloramphenicol, an elongation-inhibiting antibiotic, which may have affected the observed functional state (Zhang *et al.*, 2015b).

Besides stalling mechanisms, the SecM arrest peptide is widely used for generating ribosome-nascent chain complexes (RNCs) for functional studies (Evans *et al.*, 2015; Schaffitzel and Ban, 2007; Jha and Komar, 2012), including ribosome display

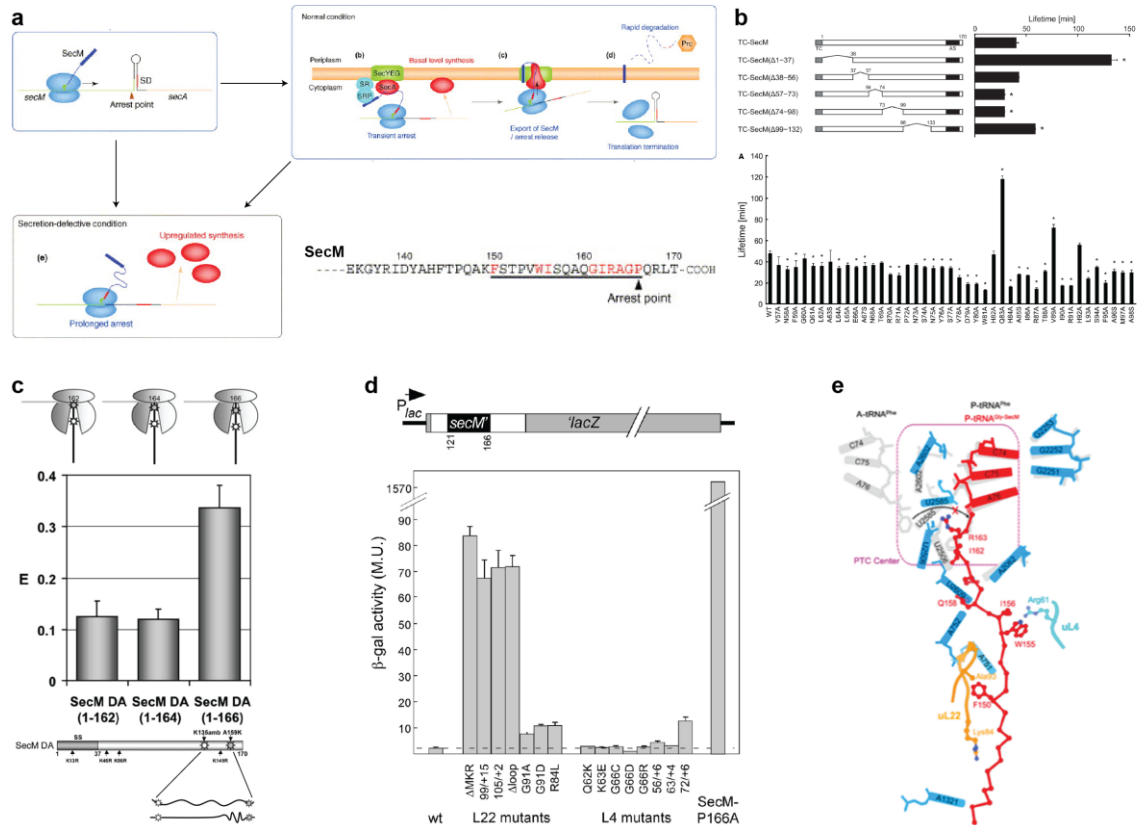


Figure 10: The bacterial staller SecM. (a). Mechanism of translational regulation of gene expression by SecM. (Bottom right) C-terminal sequence of SecM, with the arrest sequence essential for stalling (150-166) underlined. Essential residues are in red. Panels adapted from Nakatogawa *et al.*, 2004. (b). (Top) Left: Cartoon representation of TC-SecM and segment deletion mutants (TC = tag; AS = arrest sequence); Right: Lifetimes of translation arrest for the constructs on the left. Values represent the mean and standard deviation of three independent experiments. Panels adapted from Muta *et al.*, 2020. (c) (Top) Ribosome-nascent chain complexes containing different stretches of SecM being purified; (Middle) Measure of the efficiency of energy transfer (E) of the complexes depicted above. Error bars represent the standard deviation from three or more independent experiments; (Bottom) Schematics for the construct used, indicating where the fluorescent probes were incorporated, used to monitor the level of compaction of the nascent chain. Panels adapted from Woolhead *et al.*, 2006. (d). (Top) Construct used to monitor the efficiency of pausing, with white stretches being multicloning site sequence, black stretch corresponding to SecM sequence (wt or loss of function mutant, see below) and grey being the lacZ reporter sequence; (Bottom) Quantitation of SecM/β-galactosidase fusion protein synthesis measured from the activity of the enzyme (in Miller units, M.U.) in strains bearing mutations/deletion in L22 or L4. The wt strain is used as positive control, the SecM P166A loss of function mutant as negative control. Each value is the average of at least three independent cultures, with assay performed in duplicate for each culture; The standard error of the mean is depicted for each bar. Panel adapted from Lawrence *et al.*, 2008. (e). Model proposed for the mechanism of stalling of SecM, deduced from PDB: 3jbu. The ribosomal components rearranged by the staller are in blue (canonical arrangement in grey). Panel adapted from Zhang *et al.*, 2015b.

(Contreras-Martinez and DeLisa, 2007; Chung *et al.*, 2022)., real-time monitoring *in vivo* (Takahashi *et al.*, 2009), single-molecule imaging (Uemura *et al.*, 2008, Tsai *et al.*, 2014), and co-translational protein folding and targeting investigations (Notari *et al.*, 2018; Marsden *et al.*, 2018; Nilsson *et al.*, 2017; Nilsson *et al.*, 2016; Nilsson *et al.*, 2015; Houwman *et al.*, 2015; Jomaa *et al.*, 2016; Marino *et al.*, 2016; Jensen *et al.*, 2020; Elfageih *et al.*, 2020; Cymer and von Heijne, 2013; Cabrita *et al.*, 2016; Deckert

et al., 2021; Ahn *et al.*, 2022; Chan *et al.*, 2022; Bertolini *et al.*, 2021; Ismail *et al.*, 2012; Pellowe *et al.*, 2020).

Molecular dynamics simulations based on SecM structures have explored how pulling forces relieve translational arrest (Nilsson *et al.*, 2017; Gumbart *et al.*, 2012; Rychkova *et al.*, 2013; Zimmer *et al.*, 2021). Given SecM's extensive use in diverse studies, understanding the conformation of full-length SecM within the ribosomal tunnel, the number of SecM residues traversing the tunnel, and the exact mechanism by which SecM inhibits elongation is crucial.

Bioinformatic analysis has identified three additional classes of arrest peptides in bacterial genomes (Fig. 11). These include ApcA and ApdA in actinobacteria and ApdP in α -proteobacteria, which are located upstream of protein localization machinery components like YidC2 and SecDF (Sakiyama *et al.*, 2021) (Fig. 11a). ApcA and ApdA selectively arrest translation elongation on *B. subtilis* ribosomes but not on *E. coli* ribosomes, while ApdP can arrest translation on both (Sakiyama *et al.*, 2021) (Fig. 11b). All three arrest peptides cause translation arrest at a conserved RAP(P/G) motif, similar to the RAG motif in SecM (Sakiyama *et al.*, 2021).

Biochemical studies revealed that these arrest peptides stall the ribosome with a peptidyl-RAP-tRNA in the P-site and Pro-tRNA (for ApdA and ApdP) or Gly-tRNA (for ApcA) in the A-site (Sakiyama *et al.*, 2021) (Fig. 11c). This suggests that these peptides, like SecM, could interfere with A-site tRNA accommodation and peptide bond formation (Zhang *et al.*, 2015b). Mutagenesis studies have shown that the Arg in the RAP motif is crucial for stalling, though the exact mechanism for ApcA, ApdA, and ApdP remains to be determined (Sakiyama *et al.*, 2021) (Fig. 11b).

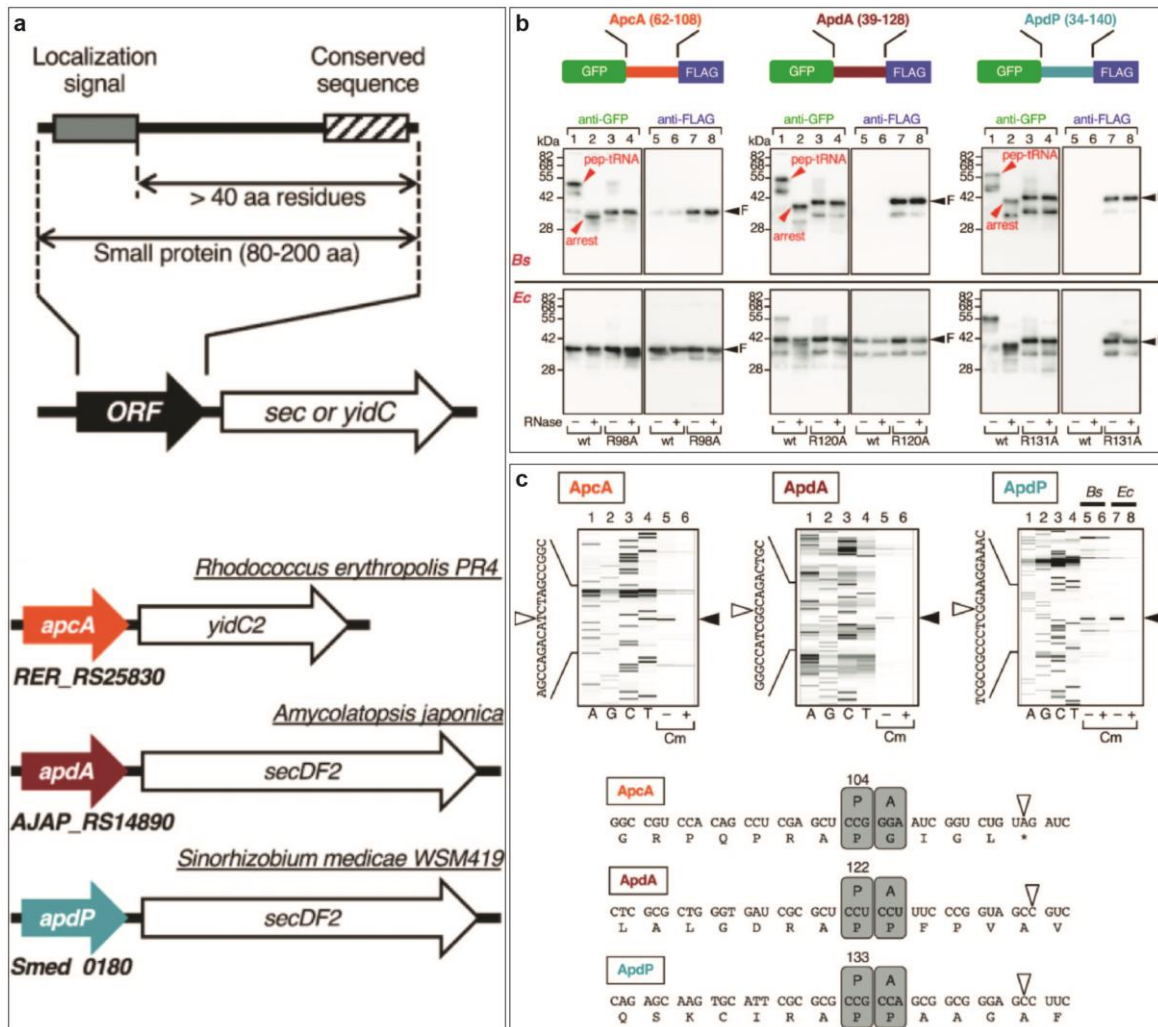


Figure 11: Identification and characterization of potential novel stalling ORFs. (a). Top: Schematic representation of the bioinformatic research for ORFs located upstream the *sec* or *yidC* genes, encoding a stretch of 80-200 amino acids, containing a N-terminal signal for extra-cytosolic localization and a consensus sequence at the C-terminus; Bottom: Schematic representation of the consensus of *apcA*, *apdA* and *apdP* with downstream *sec/yidC* genes. (b). In order to observe translation arrest *in vitro*, the sequences of *apcA* (left), *apdA* (middle) and *apdP* (right) were sandwiched between a N-terminal GFP and a C-terminal FLAG-tag. At the bottom, the products of *in vitro* translation by *Bacillus subtilis* (Bs) hybrid and by *Escherichia coli* (Ec) PURE translation system of these constructs were tested by running them on a SDS-PAGE (with neutral pH gel system) and subsequently immunoblotting with anti-GFP (green) and with anti-FLAG (blue). To remove the tRNA moiety from the peptidyl-tRNA species, a sample aliquot was treated with RNaseA before electrophoresis (lanes with even numbers, +). In the same experiment, also loss of function arginine (R) mutations were tested for each ORF. In the panel, pep-tRNA = peptidyl-tRNA species, arrest = arrested peptide species, F = full-length polypeptide species. (c). Top: Toeprint analysis of *apcA* (left), *apdA* (middle) and *apdP* (right) using the Bs hybrid system (lanes 5,6) and the Ec PURE system (lanes 7,8) in the presence (+) or absence (-) of chloramphenicol (Cm). In the panel, the white arrowheads mark the last nucleotide translated, the black arrowheads mark the major toeprint signals. (Bottom) Cartoon representation of the elongating ribosome stalling site for the three ORFs mRNA transcripts. Grey boxes marked as P and A represent the residence of the P-site and A-site of the ribosome, respectively. In the panel, the numbers above the box “P” indicate the P-site codons, the white arrowheads indicate the last nucleotides of the reverse transcription products observed in the toeprints above. Panels adapted from Sakiyama *et al.*, 2021.

Bacterial translation: the perfect antimicrobial target

Bacterial translation is a highly conserved and essential process, resulting from the interactions of many factors, forming relatively large ribonucleoprotein complexes and occurring in several steps, each characterized by its own kinetics and structural arrangement and it is significantly different from its eukaryotic counterpart. This makes it a major target for antimicrobial compounds (Arenz and Wilson, 2016). As a matter of fact, most of the known antimicrobials target bacterial translation, with every single step of the process being a target of a set of specific inhibitors (Fig. 12) (Arenz and Wilson, 2016). In this section, inhibitors for each translation step will be discussed, focusing on their mechanism of action and structural role.

Inhibitors of initiation

A variety of antibiotics are known as translation initiation inhibitors (Fig. 12 (green)). These include kasugamycin, pactamycin, edeine, and GE81112, which target the SSU (Fig. 12 (green)), and the orthosomycins evernimicin and avilamycin, which interact with the LSU (Fig. 12 (green)). Thermorubin, however, binds to both the SSU and LSU (Brandi *et al.*, 2008; Wilson, 2009; Bulkley *et al.*, 2012). Kasugamycin occupies the E site of the SSU, overlapping with the mRNA's path (Schlunzen *et al.*, 2006; Schuwirth *et al.*, 2006), thereby blocking the binding of the initiator fMet-tRNA^{fMet} to the 30S-PIC (Schlunzen *et al.*, 2006; Schuwirth *et al.*, 2006). Similarly, pactamycin interferes with 30S-PIC formation by altering the mRNA's path through the E site (Brodersen *et al.*, 2000), though later research suggested it acts by inhibiting translocation rather than initiation (Dinos *et al.*, 2004). In contrast, edeine and GE81112 obstruct the 30S-PIC formation by directly blocking the fMet-tRNA^{fMet} binding site (Pioletti *et al.*, 2001; Dinos *et al.*, 2004; Brandi *et al.*, 2006). Thermorubin binds within a pocket formed by h44 of the SSU and H69 of the LSU (Bulkley *et al.*, 2012), inhibiting 30S-PIC formation through conformational changes that disrupt IF binding (Bulkley *et al.*, 2012). Evernimicin and avilamycin are thought to prevent the 30S-PIC association with the LSU by blocking IF2 accommodation on the LSU during subunit joining (Belova *et al.*, 2001).

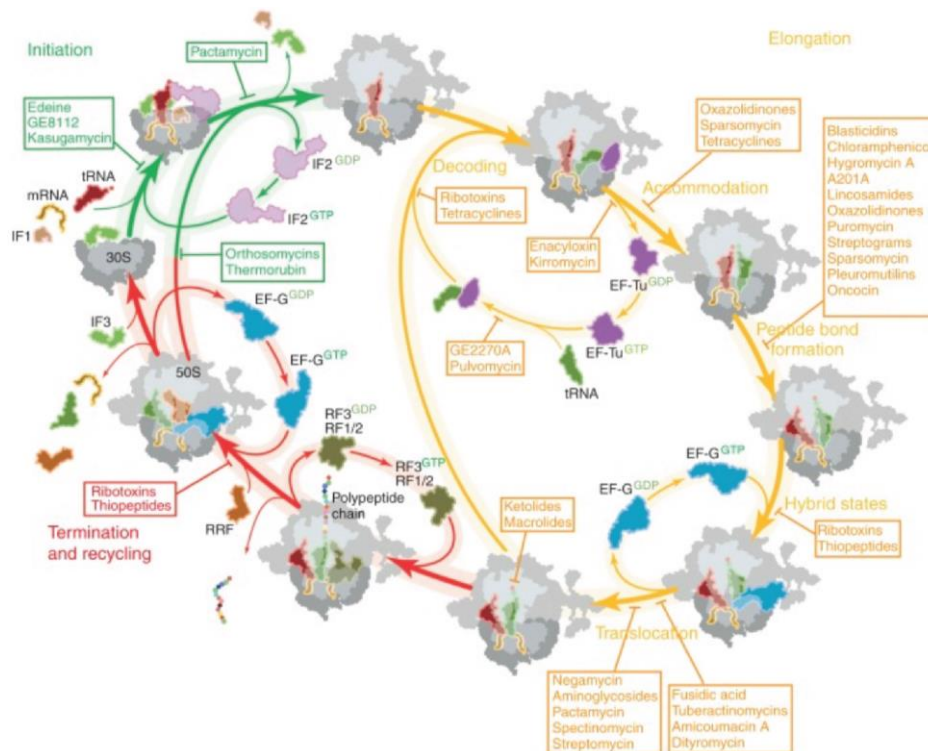


Figure 12: Overview of antimicrobials targeting the process of bacterial translation, listed into boxes associated to the different steps of initiation (green), elongation (yellow) and termination/recycling (red). Figure adapted from Arenz and Wilson, 2016.

Inhibitors of elongation: decoding and accommodation

A variety of antibiotics inhibit the delivery and accommodation of aminoacyl-tRNA on the ribosome (Wilson, 2009) (Fig. 12 (yellow)). These inhibitors include those that interact with EF-Tu, such as GE2270A and kirromycin, and those that directly interact with the ribosome, like thiostreptons and tetracyclines (Fig. 12 (yellow)). Additionally, antibiotics from the negamycin and aminoglycoside classes bind to the ribosome, disrupting the decoding process (Fig. 12 (yellow)). Thiopeptide antibiotics, including GE2270A and derivatives like LFF571, bind to EF-Tu, preventing it from forming a complex with aminoacyl-tRNA. In contrast, kirromycin binds to the EF-Tu-aa-tRNA complex and traps it on the ribosome (Wilson, 2009). Thiostrepton-like antibiotics interact with the large ribosomal subunit and interfere with the binding of translational GTPases, including EF-Tu and elongation factor G (EF-G) (Wilson, 2009). The tetracycline family of antibiotics, including third-generation glycylicyclines like tigecycline, bind to the SSU, blocking codon recognition on the mRNA by the anticodon of the aa-tRNA sterically (Nguyen, *et al.* 2014). Although negamycin and aminoglycosides have different binding sites on the SSU, both stabilize the binding of aa-tRNAs, including near-cognate aa-tRNAs, causing misreading and stop-codon suppression (Wilson, 2009; Olivier *et al.*, 2014; Polikanov *et al.*, 2014b).

Inhibitors of elongation: peptide bond formation

Antibiotics that disrupt peptide bond formation typically do so by hindering the proper positioning of the aminoacylated-CCA end of the A-tRNA at the peptidyl transferase center (PTC) (Fig. 12 (yellow)). Consequently, these antibiotics are considered to inhibit a final stage of aminoacyl-tRNA accommodation at the A-site. Notable examples include phenicols (such as chloramphenicol), oxazolidinones (like linezolid), pleuromutilins (such as tiamulin), and lincosamides (including clindamycin) (Wilson, 2009, 2014) (Fig. 12 (yellow)). More recently, this has also been observed for hygromycin A, the nucleoside antibiotic A201A (Polikanov *et al.*, 2015), and the antimicrobial peptide oncocin (Roy *et al.*, 2015; Seefeldt *et al.*, 2015) (Fig. 12 (yellow)). Additionally, some larger macrolide antibiotics, like josamycin, tylosin, and spiramycin, impede peptide bond formation by disrupting A-tRNA accommodation at the PTC (Wilson, 2009) (Fig. 12 (yellow)). Generally, macrolides are believed to bind within the ribosomal tunnel, thereby obstructing the elongation of the nascent polypeptide chain (Kannan *et al.*, 2014). However, recent findings indicate that certain polypeptides can evade the drug within the tunnel and even complete synthesis despite the presence of the antibiotic (Kannan and Mankin, 2012a; Kannan *et al.*, 2012b).

Inhibitors of elongation: translocation

Numerous antibiotics disrupt the translocation process in various ways (Fig. 12 (yellow)). Examples include aminoglycosides like kanamycin and gentamicin, which bind to h44 of the SSU and stabilize the pretranslocation state (Wilson, 2009) (Fig. 12 (yellow)). Additionally, neomycin binds to H69 of the LSU, trapping intermediate hybrid states and hindering translocation (Wang *et al.*, 2012) (Fig. 12 (yellow)). Viomycin and capreomycin span the ribosomal interface between h44 and H69, stabilizing a distinct intermediate hybrid state (Stanley *et al.*, 2010; Ermolenko *et al.*, 2007b) (Fig. 12 (yellow)). Spectinomycin binds to the neck region of the SSU, locking a rotated conformation of its head and trapping an intermediate state during translocation (Carter *et al.*, 2000; Borovinskaya *et al.*, 2007; Pan *et al.*, 2007) (Fig. 12 (yellow)). Recently characterized translocation inhibitors include negamycin, which interacts with A-tRNA and stabilizes it in the A-site (Olivier *et al.*, 2014; Polikanov *et al.*, 2014b) (Fig. 12 (yellow)). Amicoumacin A interacts with mRNA in the E-site, preventing its movement and thus blocking translocation (Polikanov *et al.*, 2014c) (Fig. 12 (yellow)). Dityromycin and its analogue GE82832 bind exclusively to ribosomal protein S12 on the SSU, preventing EF-G from adopting the final state necessary for tRNA and mRNA translocation (Bulkley *et al.*, 2014) (Fig. 12 (yellow)).

Inhibitors of termination and recycling

Currently, no clinically relevant antibiotics specifically targeting the termination and recycling phases of translation. Many antibiotics act during elongation by inhibiting factor binding (e.g., thiostrepton) or preventing peptide bond formation (e.g., chloramphenicol), which also affect RF binding or peptidyl-tRNA hydrolysis (Wilson, 2009). However, a few antibiotics are suggested to preferentially act during termination rather than elongation (Fig. 12 (red)). Blastocidin S and fusidic acid have been identified in this regard (Svidritskiy *et al.* 2013; Savelsbergh *et al.*, 2009) (Fig. 12 (yellow)). Fusidic acid binds not to free EF-G, but to EF-G-GTP when complexed with the ribosome. While allowing GTP hydrolysis, fusidic acid prevents the necessary EF-G conformational changes for dissociation, thereby trapping EF-G on the ribosome. This inhibition during ribosome recycling, rather than elongation, is particularly sensitive to fusidic acid's action (Savelsbergh *et al.*, 2009). Blastocidin S binds to the P-site of the LSU and overlaps with the binding site of C75 of the CCA-end of P-tRNA (Hansen, *et al.*, 2003; Svidritskiy *et al.*, 2013). Blastocidin S reduces the rate of peptide bond formation and is notably effective at inhibiting peptidyl-tRNA hydrolysis by RF1 (Svidritskiy *et al.*, 2013).

Focus on antimicrobial peptides

Antimicrobial peptides (AMPs) serve as crucial agents in combating bacterial infections by targeting bacterial ribosomes and disrupting protein synthesis. Their mechanisms of action and binding sites vary, offering diverse approaches to inhibit bacterial growth (Fig. 13).

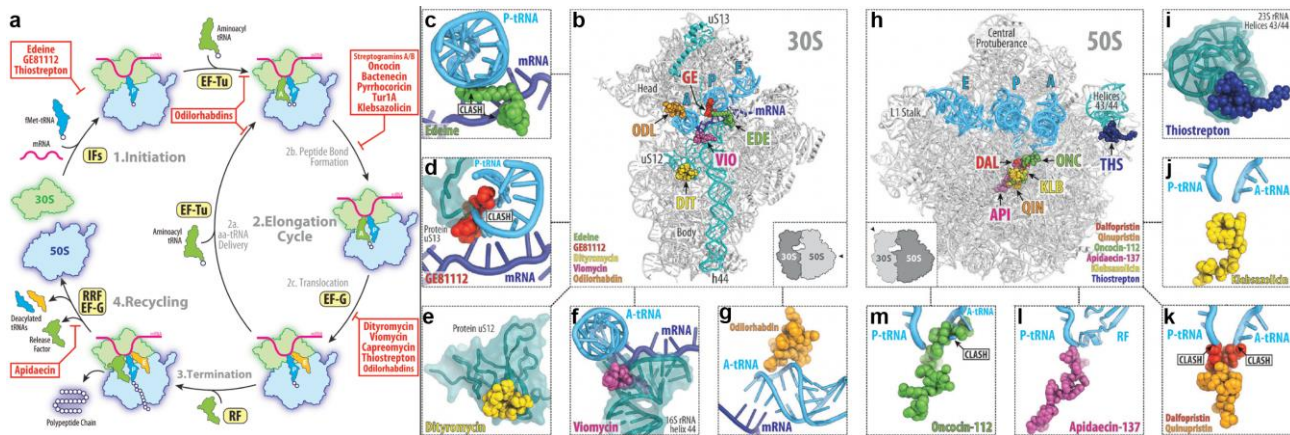


Figure 13: Antimicrobial peptides targeting translation. (a). Overview of antimicrobials peptides targeting the process of bacterial translation, listed into boxes associated to the different steps of initiation, elongation and termination/recycling. (b-g) (b) Binding sites of antimicrobial peptides in the 30S, with a focus on (c) Edeine (EDE, green), (d) GE81112 (GE, red), (e) Dityromycin (DIT, yellow), (f) Viomycin (VIO, violet) and (g) Odilorhabdin (ODL, gold). (h-m) (h) Binding sites of antimicrobial peptides in the 50S, with a focus on (i) Thiostrepton (dark blue), (j) Klebsazolicin (KLB, yellow), (k) Dalfopristin (DAL, red) and Qino-pristin (QIN, orange), (l) Apidaecin-137 (API, grape), (m) Oncocin-112 (ONC, green). Panels adapted from Polikanov *et al.*, 2018.

Edeine (Fig. 13a-c) and GE81112A (Fig. 13a,b,d) have been discussed in the previous section. These peptides inhibit translation by blocking the formation of a competent 70S initiation complex necessary for translation to proceed (Pioletti *et al.*, 2001; Dinos *et al.*, 2004; Brandi *et al.*, 2006) (Fig. 13a). Also dityromycin is mentioned above, it targets the ribosomal protein uS12 on the 30S subunit (Fig. 13a,b,e). This interaction inhibits the translocation of tRNA and mRNA, essential for protein elongation, by trapping elongation factor G (EF-G) in a compact conformation on the ribosome (Bulkley *et al.*, 2014).

Viomycin and capreomycin are cyclic pentapeptides from the tuberactinomycin family (Thomas *et al.*, 2003). They exhibit potent activity against *Mycobacterium tuberculosis*, including multidrug-resistant strains (Jain and Dixit, 2008). As anticipated above, these antibiotics bind to a site spanning the 30S and 50S ribosomal subunits, particularly interacting with nucleotides A1492 and A1493 in the 16S rRNA (Stanley *et al.*, 2010) (Fig. 13a,b,f). This binding stabilizes a rotated ribosomal conformation with hybrid tRNA states (Peske *et al.*, 2004; Shoji *et al.*, 2006; Ermolenko *et al.*, 2007b; Pan *et al.*, 2007; Cornish *et al.*, 2008; Ly *et al.*, 2010; Wang *et al.*, 2012), effectively trapping the ribosome in an intermediate state during translocation and inhibiting EF-G release (Holm *et al.*, 2016; Brilot *et al.*, 2013).

Odilorhabdins are a novel class of antimicrobial peptides produced by symbiotic bacteria associated with entomopathogenic nematodes (Pantel *et al.*, 2018). They target the decoding center of the 30S ribosomal subunit, specifically binding to the 16S rRNA (Fig. 13a,b). This interaction induces miscoding during translation, leading to the incorporation of incorrect amino acids and the production of dysfunctional proteins (Pantel *et al.*, 2018). Odilorhabdins' unique binding site overlaps with those of other antibiotics like paromomycin and tetracycline but extends to adjacent regions (Fig. 13g), causing pronounced miscoding effects. By disrupting the ribosome's proofreading mechanisms, odilorhabdins increase translation errors, compromising bacterial viability. Structural studies have shown that odilorhabdins bind at a unique site within the A-site of the 30S subunit, inducing translational stress without completely blocking ribosomal function (Wang *et al.*, 2012; Olivier *et al.*, 2014; Polikanov *et al.*, 2014b; Pantel *et al.*, 2018). Their effectiveness against a wide range of bacterial pathogens, including multidrug-resistant strains, highlights their potential as new antibiotics. The distinct mechanism of action of odilorhabdins, inducing translational errors, makes them a promising candidate for developing therapies to combat antibiotic resistance.

Thiopeptides, such as thiostrepton, nosiheptide, and micrococcin, interact directly with the ribosome (Bagley *et al.*, 2005; Nicolaou *et al.*, 2009) (Fig. 13a,h). These antibiotics bind in a cleft between the N-terminal domain of ribosomal protein uL11 and the 23S rRNA helices, preventing the proper functioning of essential translation factors (IF2, EF-Tu and EF-G) (Harms *et al.*, 2008) (Fig. 13h-i). Despite their efficacy against Gram-positive bacteria and malarial parasites, their poor solubility and bioavailability limit their use in clinical settings (Wilson, 2009).

Klebsazolicin (KLB) is a notable protein synthesis inhibitor from *Klebsiella pneumoniae* (Metelev *et al.*, 2017). Structural studies of the ribosome-KLB complex show that KLB binds in the nascent peptide exit tunnel, overlapping with binding sites of other antibiotics like macrolides (Metelev *et al.*, 2017) (Fig. 13a,h,j). KLB adopts a compact, globular conformation. KLB's interaction with the ribosome mainly involves stacking with rRNA bases (Metelev *et al.*, 2017). Its ability to be expressed in a surrogate *E. coli* host opens possibilities for rational drug design by altering the amino acid sequence of the KLB precursor to modify the properties of the final compound (Metelev *et al.*, 2017).

Streptogramins are a class of antibiotics produced by *Streptomyces* species, divided into two subclasses: group A and group B (Li and Seiple, 2017). Group A streptogramins, such as madumycin II and virginiamycin M, target the peptidyl transferase center (PTC) of the bacterial ribosome, spanning the A-site cleft and extending into the P site (Osterman *et al.*, 2017; Schmeing *et al.*, 2005b; Hansen *et al.*, 2003; Tu *et al.*, 2005; Noeske *et al.*, 2014) (Fig. 13a,h,k). They inhibit peptide bond formation by preventing the correct positioning of tRNA CCA-ends into the PTC. This binding induces rearrangements in the 23S rRNA, creating a catalytically inactive state

(Osterman *et al.*, 2017; Schmeing *et al.*, 2005b). Group B streptogramins, including pristinamycin IA and quinupristin, bind within the nascent peptide exit tunnel, overlapping with macrolide binding sites and obstructing the passage of nascent peptides (Harms *et al.*, 2004; Tu *et al.*, 2005; Noeske *et al.*, 2014) (Fig. 13a,h,k). The synergy between streptogramin A and B compounds arises from their binding to adjacent but non-overlapping sites on the ribosome, effectively halting protein synthesis by dual mechanisms (Osterman *et al.*, 2017; Hansen *et al.*, 2003; Tu *et al.*, 2005; Noeske *et al.*, 2014; Tu *et al.*, 2005; Harms *et al.*, 2004; Vannuffel and Cocito, 1996) (Fig. 13k). This synergistic action has been harnessed in clinical treatments, notably in Synercid, a combination of dalfopristin (group A) and quinupristin (group B), used against multidrug-resistant bacterial infections. Despite its intravenous-only formulation and narrow spectrum, Synercid is valuable for treating severe infections like those caused by vancomycin-resistant *Enterococcus faecium* and methicillin-resistant *Staphylococcus aureus* (MRSA) (Noeske *et al.*, 2014; Manzella, 2001).

Apidaecin-137 (Fig. 13a,h,l) and Oncocin-112 (Fig. 13a,h,m) are discussed in the next paragraph.

In summary, these AMPs exhibit diverse mechanisms of action, from blocking the initiation of protein synthesis and translocation to promoting miscoding. Their specific interactions with ribosomal components highlight their potential as targeted antimicrobial agents, providing a basis for developing new antibiotics to combat resistant bacterial strains.

The case of proline-rich antimicrobial peptides

Proline-rich antimicrobial peptides (PrAMPs) are a class of antimicrobial agents that play a crucial role in the innate immune system by targeting bacterial protein synthesis. These peptides, found across various species, are particularly noted for their ability to inhibit bacterial growth through non-lytic mechanisms, while generally AMPs act by disrupting the bacterial membrane. PrAMPs are classified into two main types based on their source and structural properties: type I and type II (Graf *et al.*, 2017) (Fig. 14a). Type I PrAMPs are primarily derived from mammals and feature a high content of proline and arginine residues (Fig. 14a). They typically inhibit protein synthesis by binding to the bacterial ribosome, particularly within the ribosomal exit tunnel of the 50S subunit and impeding the initial elongation cycles soon after initiation (Graf *et al.*, 2017) (Fig. 14b). Type II PrAMPs, on the other hand, are predominantly found in insects and are also rich in proline residues. These peptides adopt an elongated conformation within the ribosomal exit tunnel and inhibit protein synthesis through specific interactions with the 23S rRNA, freezing the translating complex at the termination step (Graf *et al.*, 2017).

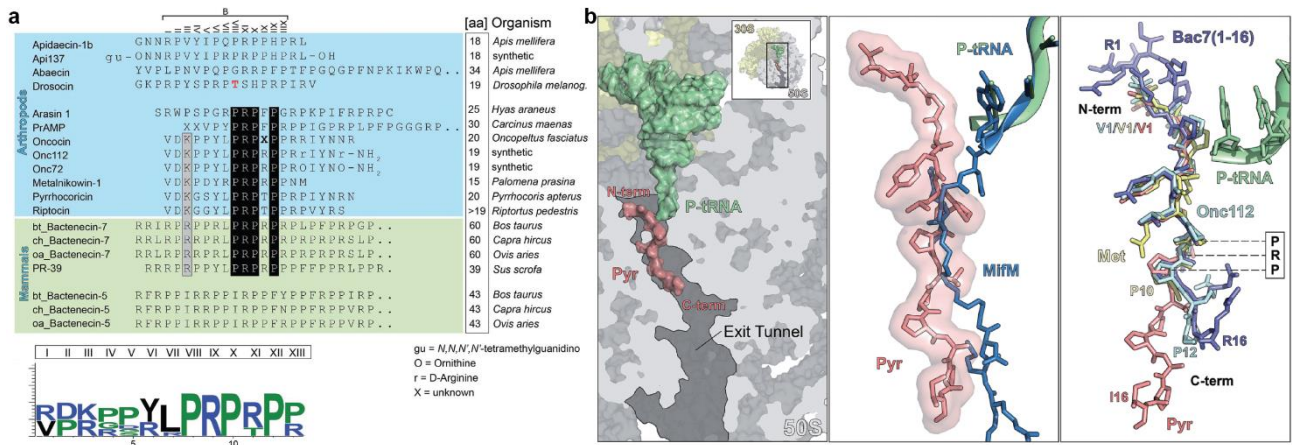


Figure 14: A glance at PrAMPs. (a). Sequence alignments of PrAMPs; Top: sequences of naturally occurring and synthetic PrAMPs derived from arthropods (insects and crustaceans, blue) and mammals (green). The central PrAMPs were aligned first based on ribosome-bound structures of Onc112, Pyr, Met and Bac7 and then on sequence similarity. Similar and identical residues are shown in grey and black, respectively. The red T of drosocin indicates the O-glycosylation at Thr11, the X indicates the unknown position 11 of oncocin. Bottom: Sequence conservation of the core residues I to XIII of the natural PrAMPs listed in the central region above between oncocin and PR-39. (b). Binding site of Class I PrAMPs. Left: pyrrhocoricin (Pyr, pink) is shown as an example. The 50S (section) is light grey, with the tunnel cavity darker grey, the 30S is yellow and the P-tRNA is green. Middle: relative orientation of Pyr (pink) to the nascent chain of MifM (dark blue), acylated to the P-tRNA (green). The two polypeptide chains are positioned with opposite C→N orientation inside the exit tunnel, and this is the case for all the PrAMPs belonging to class I. Right: superimposition of mammalian Bac7(1-16) (light blue) and insect derived PrAMPs Onc112 (cyan), metalnikowin-1 (Met, yellow), and Pyr (pink), with their conserved PRP motif highlighted. Panels adapted from Graf *et al.*, 2017.

Class I PrAMPs bind to the ribosome in an inverted orientation compared to nascent polypeptides, with their N-terminus in the A-site and the C-terminus extending into the polypeptide exit tunnel (Fig. 14b (middle)). The binding site is divided into sections within the A-site binding pocket, the A-site crevice, and the upper region of the exit tunnel (Fig. 14b (left)). The N-terminal residues in the A-site are critical for inhibition, while the C-terminal residues in the exit tunnel are less crucial. In several studies, the C-terminal residues were unresolved, and deleting up to 19 C-terminal amino acids from Bac7 did not affect activity (Gagnon *et al.*, 2016; Mardirossian *et al.*, 2018; Roy *et al.*, 2015; Seefeldt *et al.*, 2015, 2016; Benincasa *et al.*, 2004). Conversely, removing N-terminal residues from oncocins reduced activity significantly, highlighting the importance of the N-terminus (Gagnon *et al.*, 2016). PrAMP binding is facilitated by numerous polar contacts and stacking interactions within the exit tunnel. A conserved PRP motif is found in all class I PrAMPs, consistently located in the same position and conformation across all resolved complexes (Gagnon *et al.*, 2016; Mardirossian *et al.*, 2018; Roy *et al.*, 2015; Seefeldt *et al.*, 2015, 2016) (Fig. 14b (right)). The differences among class I PrAMPs lie in their amino acid composition, number of residues, and contacts within the A-site binding pocket. Insect PrAMPs like Onc112, Met, and Pyr have four N-terminal amino acids reaching the A-site binding pocket, while mammalian PrAMPs like Bac7 and Tur1A have seven additional amino acids forming

a short loop that acts as an A-site anchor, specific to mammalian PrAMPs (Gagnon *et al.*, 2016; Mardirossian *et al.*, 2018; Roy *et al.*, 2015; Seefeldt *et al.*, 2015, 2016) (Fig. 14b (right)). Insect PrAMPs such as Onc112, Pyrrhocoricin (Pyr), and Metalnikowin (Met) share a conserved amino acid sequence at their N-terminus. Binding within the A-site pocket involves polar and stacking interactions, where Asp2 interacts with C2507 and G2553. Lys3 forms a hydrogen bond with A2453 of 23S rRNA, while Val1's backbone interacts with C2573 and C2507 (Seefeldt *et al.*, 2015, 2016). Tyr6 is crucial in A-site binding and antimicrobial activity due to its stacking interaction with C2452; its substitution drastically reduces activity (Knappe *et al.*, 2011). Positions 5 and 7 show variability among PrAMPs affecting hydrogen bonding patterns in the A-site. The C-terminus of insect PrAMPs varies in length and contributes minimally to binding, with observed interactions involving Arg9 (Seefeldt *et al.*, 2015, 2016). The mammalian PrAMPs Bac7 and Tur1A bind to the A-site binding pocket and crevice of eubacterial 70S ribosomes via polar contacts involving peptide backbone and amino acid side chains (Mardirossian *et al.*, 2018; Seefeldt *et al.*, 2016). Key interactions include hydrogen bonding and stacking involving arginine residues, particularly Arg2 with C2573, replacing Val1's backbone interaction seen in insect PrAMPs. Residues eight to ten in mammalian PrAMPs correspond to positions five to seven in insect PrAMPs, with residue nine contributing to stacking interactions similar to Tyr6 in insects. Bac7 and Tur1A exhibit enriched stacking interactions within the polypeptide exit tunnel, involving multiple arginine residues (Mardirossian *et al.*, 2018; Seefeldt *et al.*, 2016). Class I PrAMPs obstruct the A-site crevice and binding pocket with their N-terminal residues (Gagnon *et al.*, 2016; Mardirossian *et al.*, 2018; Roy *et al.*, 2015; Seefeldt *et al.*, 2015, 2016). This allows the placement of fMet-tRNA^{fMet} during translation initiation but interferes with the delivery of the first aa-tRNA by EF-Tu (Mardirossian *et al.*, 2018; Seefeldt *et al.*, 2015, 2016). While decoding on the SSU can occur, further accommodation after EF-Tu release is blocked due to the steric hindrance from the N-terminal residues of PrAMPs. Superimposed pre-attack 70S ribosomes with an accommodated aa-tRNA in the A-site show that the A-tRNA CCA-end and N-terminal residues of PrAMPs are incompatible (Graf *et al.*, 2017). This steric clash also prevents PrAMP binding during translation elongation, requiring PrAMP binding to occur between translation termination and initiation to avoid clashes with peptidyl-tRNA (Graf *et al.*, 2017). Class I PrAMPs inhibit the transition from translation initiation to elongation, as shown by biochemical experiments (Mardirossian *et al.*, 2018; Seefeldt *et al.*, 2015, 2016). Toeprinting assays confirm that translation in the presence of class I PrAMPs causes ribosomal stalling at the AUG start codon, preventing further elongation (Mardirossian *et al.*, 2018; Seefeldt *et al.*, 2015, 2016).

Api137, a class II PrAMP derived from wild-type apidaecin 1b of *Apis mellifera*, binds to the polypeptide tunnel like a nascent chain (Florin *et al.*, 2017) (Fig. 15).

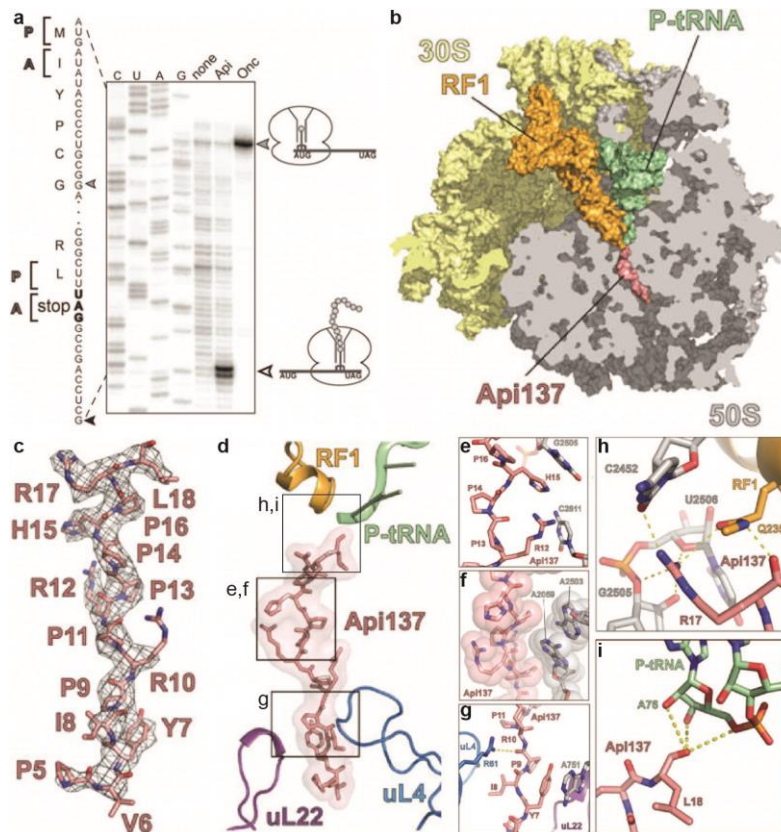


Figure 15: Api137 belongs to class II PrAMPs. (a). Toeprinting analysis comparing the effect on translation of the model RNA template *yrbA* gene of Onc112 (Onc) and Api137 (Api). A black arrow indicates the stalling band at the initiation site caused by Onc112, a white arrow indicates the stalling band at the stop codon caused by Api137, with a schematic of the predicted stalled complex on the right. (b). Transverse section of the 50S (grey) to show the binding site of Api137 (salmon) on the terminating 70S ribosome (30S is yellow), containing RF1 (orange) and P-tRNA (green). (c). Cryo-EM density (mesh) and molecular model (salmon) for residues 5-18 of Api137. (d). Positioning of Api137 (salmon) in the exit tunnel relative to RF1 (yellow), P-tRNA (green), uL4 (blue) and uL22 (purple). Boxed areas are zoomed in the following panels, as indicated on the side. (e-f). Interactions of Api137 (salmon) with nucleotides of the 23S rRNA (grey). (g). Contacts between Api137 (salmon) and uL4 residues (blue). Also nucleotide A751 (grey) and uL22 (purple) are shown. (h). Interactions of Api137 (salmon) with RF1 residues (yellow) and 23S rRNA nucleotides (grey). (i). Interactions of Api137 (salmon) with the CCA end of the P-tRNA (green). Panels adapted from Florin *et al.*, 2017.

Unlike class I PrAMPs, class II PrAMPs like Api137 trap ribosomes with a stop codon in the A-site, affecting translation termination (Florin *et al.*, 2017) (Fig. 15a). The C-terminal residues Arg17 and Leu18 are positioned in the A-site crevice, but do not extend into the A-site binding pocket, a placement crucial for Api137's function (Fig 15b-d). Substituting Arg17 with Ala reduces activity against *E. coli* ribosomes (Castle *et al.*, 1999). The N-terminal residues travel down the polypeptide tunnel, where binding is primarily facilitated by stacking interactions (Florin *et al.*, 2017; Seefeldt *et al.*, 2015, 2016). These interactions include Tyr7 with A751, Arg12 with C2611, and

His15 with G2505 (Florin *et al.*, 2017) (Fig. 15e-g). Polar contacts also occur in the PTC with RF1 and deacylated P-site tRNA, with Arg17 forming hydrogen bonds with 23S rRNA residues and Gln235 of the RF1 GGQ motif, and Leu18 interacting with A76 of deacyl-P-tRNA (Florin *et al.*, 2017) (Fig. 15h-i). Api137 does not hinder RF binding or the RF-mediated release of the nascent chain, but instead prevents RF dissociation from the ribosome. This inhibition is due to interactions where Leu18 binds with the ribose of A76 in the P-site and Arg17 forms hydrogen bonds with 23S rRNA and Gln235 of RF1 (Florin *et al.*, 2017) (Fig. 15i). Consequently, RF1 dissociation is blocked, even in the presence of RF3, leading to RF depletion and stalling ribosomes during termination, indirectly causing stop codon read-through (Florin *et al.*, 2017). Given its size, Api137 likely accesses its binding site in the polypeptide tunnel via the tunnel exit rather than the PTC, due to steric hindrance. Its action requires binding after peptide chain release and before RF1/2 departure from the post-hydrolysis 70S ribosome (Florin *et al.*, 2017). The proline residues might help maintain an extended peptide conformation, facilitating diffusion within the ribosomal tunnel (Nissen *et al.*, 2000).

Besides producing classical membrane-targeting AMPs, such as defensins, cecropins, and dipterocins, *Drosophila* also generates a PrAMP named drosocin (Bulet *et al.*, 1993, 1999) (Fig. 14a). This 19-amino acid peptide, rich in proline and arginine, is highly effective against Gram-negative bacteria like *Escherichia coli* (Bulet *et al.*, 1993, 1999). Unlike most PrAMPs, drosocin is O-glycosylated at Thr11, with either N-acetylgalactosamine (α -d-GalNAc) or a disaccharide of galactose linked to N-acetylgalactosamine (β -Gal(1 \rightarrow 3)- α -d-GalNAc) (Bulet *et al.*, 1993; Uttenweiler-Joseph *et al.*, 1998) (Fig. 14a). Additionally, a double-glycosylated form exists, with glycosylation on both Ser7 and Thr11 (Rabel *et al.*, 2004). Both forms appear in *Drosophila* hemolymph within 6 hours post-infection, increasing to 40 μ M within 24 hours (Uttenweiler-Joseph *et al.*, 1998). The disaccharide form disappears after 2 weeks, whereas the monosaccharide remains for up to 3 weeks (Uttenweiler-Joseph *et al.*, 1998). Synthetic drosocin without O-glycosylation shows reduced activity, underscoring the importance of this modification for full activity (Bulet *et al.*, 1993, 1999; Hoffmann *et al.*, 1999; Gobbo *et al.*, 2002). Various synthetic derivatives of drosocin with different sugar moieties retain good antimicrobial activity, often surpassing the unmodified form (Gobbo *et al.*, 2002; Marcaurelle *et al.*, 1998; Rodriguez *et al.*, 1997; Otvos *et al.*, 2000; Ahn *et al.*, 2011a, 2011b; Talat *et al.*, 2011; Lele *et al.*, 2015a). Though both modified and unmodified drosocin adopt extended conformations in solution (Gobbo *et al.*, 2002; Talat *et al.*, 2011; Lele *et al.*, 2015a), glycosylation likely helps maintain this conformation for effective intracellular target binding (Bulet *et al.*, 1999; Gobbo *et al.*, 2002). Glycosylation also enhances solubility, serum stability, and broadens biological activity, though its exact role is still unknown (Bulet *et al.*, 1999). Drosocin inhibits protein synthesis both *in vivo* and *in vitro*, but the precise mechanism remains unclear (Lele *et al.*, 2015b; Ludwig *et al.*, 2022). Pyrrhocoricin, a type I insect PrAMP, is also O-glycosylated at Thr11 with a minor disaccharide form (Cociancich *et al.*, 1994) (Fig. 14a). Due to sequence similarity,

drosocin was initially thought to act similarly to pyrrocoricin and metalnikowins rather than to apidaecins and abaecins (Bulet *et al.*, 1999). However, several observations indicate that drosocin is more akin to apidaecins. Unlike drosocin, the unmodified form of pyrrocoricin is slightly more active than its modified version (Hoffmann *et al.*, 1999). In ribosome-binding antibiotic competition assays, drosocin competes more effectively with Api137 than with the oncocin derivative Onc112 (Krizsan *et al.*, 2015). Additionally, the deletion of the carboxy-terminal Arg18–Val19 nearly abolishes drosocin's antimicrobial activity (Hoffmann *et al.*, 1999), similar to Api137 (Berthold and Hoffmann, 2014), whereas N-terminal truncations inactivate type I PrAMPs like Bac7 (Seefeldt *et al.*, 2016; Benincasa *et al.*, 2004).

Objective of these studies: Structural insights into the fundamental role of the bacterial ribosome exit tunnel

As ribosomes perform translation, they polymerize a nascent polypeptide chain that extends into the exit tunnel. This tunnel is not only an essential architectural component of the ribosome, but it is also a crucial active player in the process, affecting protein folding, targeting and mediating translational regulation of gene expression across many different scenarios. The main objective of our studies was to structurally characterize the bacterial exit tunnel with respect to its role in translation regulation as well as a target of antimicrobial peptides.

Recent work from the lab of Prof. Shinobu Chiba (Sakiyama *et al.*, 2021) has localized by bioinformatics consensus sequences upstream the *secDF* operon. These sequences are conserved in the genome of several actinobacteria (*apdA*) and α -proteobacteria (*apdP*), being characterized by polypeptide features typical of arrest peptides and a highly conserved RAPP motif. In the same study, these sequences were biochemically shown to strongly arrest translation elongation *in vitro* and *in vivo*, with ApdA being particularly efficient in stalling *B. subtilis* (Gram positive) ribosomes, while ApdP being efficient in stalling both *B. subtilis* (Gram positive) and *E. coli* (Gram negative) ribosomes. However, ApdP is conserved among Gram negative species. Our aim was to obtain high resolution cryo-EM structures of ApdA-stalled *B. subtilis* ribosomal complex and of ApdP-stalled *E. coli* ribosomal complex, in order to describe the mechanism of translational stalling of these two arrest peptides (**Publication 1**). The results of such work and the comparison of our structures with the previous structure of SecM-Stalled ribosomal complex (SRC) (Zhang *et al.*, 2015b), together with the incompatibility between the model for stalling mechanism proposed by Zhang *et al.* (2015b) and the previous literature, on SecM prompted us to generate a SecM-SRC. We employed the same methods used in Publication 1, to obtain a high resolution cryo-EM structure required to define a more updated stalling mechanism (**Publication 2**). Such studies are essential to further characterize the phenomenon of translational stalling, which is not only a natural gene expression regulation strategy, but a few stallers, like SecM, are also used as a tool to arrest the ribosome in many biochemical and biophysical studies (Evans *et al.*, 2015; Schaffitzel and Ban, 2007; Jha and Komar, 2012; Contreras-Martinez and DeLisa, 2007; Chung *et al.*, 2022; Takahashi *et al.*, 2009; Uemura *et al.*, 2008, Tsai *et al.*, 2014; Notari *et al.*, 2018; Marsden *et al.*, 2018; Nilsson *et al.*, 2017; Nilsson *et al.*, 2016; Nilsson *et al.*, 2015; Houwman *et al.*, 2015; Jomaa *et al.*, 2016; Marino *et al.*, 2016; Jensen *et al.*, 2020; Elfageih *et al.*, 2020; Cymer and von Heijne, 2013; Cabrita *et al.*, 2016; Deckert *et al.*, 2021; Ahn *et al.*, 2022; Chan *et al.*, 2022; Bertolini *et al.*, 2021; Ismail *et al.*, 2012; Pellowe *et al.*, 2020).

Given its essential role in translation, the exit tunnel is also one of the main targets of antimicrobials, such as macrolides (Arenz and Wilson, 2016), streptogramins (Polikanov *et al.*, 2018) and PrAMPs (Graf *et al.*, 2017). PrAMPs are divided in two classes: class I PrAMPs inhibit translation during the early phase of elongation, while class II PrAMPs inhibit translation termination by trapping the RF1/2 in the terminating

complex, depleting the essential factor in the cell; both of these classes bind inside the upper tunnel tract (Graf *et al.*, 2017). While class I PrAMPs have been extensively characterized under the biochemical and structural points of view (Graf *et al.*, 2017), before our study only a single PrAMP (Api137) had been characterized as belonging to class II (Florin *et al.*, 2017). Another candidate for a class II PrAMP was Drosocin, a PrAMP produced by *Drosophila melanogaster*, displaying activity against Gram negative bacteria and bearing a unique glycosylation at Thr11 (Bulet *et al.*, 1993, 1999). While displaying analogies with the class I pyrrolicin (Bulet *et al.*, 1993, 1999; Cociancich *et al.*, 1994), drosocin was suspected to be a class II PrAMP since it competes with Api137 and mutational studies on it are indicative of a class II PrAMP mechanism of action (Krizsan *et al.*, 2015; Hoffmann *et al.*, 1999). In order to resolve this discrepancy, our study aimed to produce a high-resolution structure of Drosocin-SRC (**Publication 3**). This is relevant to characterize an understudied PrAMP and the role of its glycosylation in the interaction with the bacterial ribosome; drosocin is characterized by optimal solubility, bioavailability, stability and toxicity parameters, making it a potential clinical candidate. Its detailed structural characterization may also be relevant in the future for structure-based drug design studies.

Cumulative Thesis: Summary of Publications

Publication 1: RAPP-containing arrest peptides induce translational stalling by short circuiting the ribosomal peptidyltransferase activity

Martino Morici, Sara Gabrielli, Keigo Fujiwara, Helge Paternoga, Bertrand Beckert, Lars V. Bock, Shinobu Chiba and Daniel N. Wilson

Nat Commun. 15, 2432 (2024)

Previous research has shown that nascent polypeptide chains (NCs) can interact with the ribosomal tunnel to modulate translation rates or induce arrest (Sauna and Kimchi-Sarfaty, 2011; Wilson *et al.*, 2016) Specifically, arrest peptides like SecM in *E. coli* regulate the expression of essential proteins by stalling translation (Nakatogawa and Ito, 2001; Nakatogawa *et al.*, 2004). A recent bioinformatic study followed by biochemical characterization by Sakiyama *et al.* (2021) localized RAPP-containing arrest peptides able to induce translational stalling in bacterial ribosomes; in particular ApdA is efficiently stalling Gram positive bacterial ribosomes, ApdP is efficiently stalling both Gram positive and Gram negative bacterial ribosomes, despite being conserved among Gram negative species.

In this study, we determined cryo-EM structures of ribosomes from *Bacillus subtilis* stalled by ApdA and ribosomes from *Escherichia coli* stalled by ApdP at 2.3 Å and 2.2 Å, respectively. These structures revealed that the RAPP motifs allow full accommodation of the A-site tRNA, but prevent the formation of the subsequent peptide bond. The data supports a model where the RAP in the P-site stabilizes a single hydrogen atom on the Pro-tRNA in the A-site, preventing the optimal geometry required for the correct catalysis of peptide bond formation by the ribosome to occur. The RAPP motif is essential for stalling to occur, since it is the direct responsible for the arrangement that eventually precludes nucleophilic attack in the PTC, constituting a “arrest module”. The N-terminal stretch is tuning the stalling efficiency and species specificity, despite not being crucial for the stalling phenotype; such tract can be referred to as “regulator module”.

In conclusion, this study provides a detailed mechanistic understanding of how RAPP-containing arrest peptides stall ribosomal translation. This mechanism is analogous to that of SecM, as studied in the related manuscript (**Publication 2**), indicating a conserved strategy among diverse bacterial species to regulate protein synthesis through translational stalling (Ito and Chiba, 2013).

Publication 2: The SecM arrest peptide traps a pre-peptide bond formation state of the ribosome

Felix Gersteuer*, Martino Morici*, Sara Gabrielli, Keigo Fujiwara, Haaris A. Safdari, Helge Paternoga, Lars V. Bock, Shinobu Chiba and Daniel N. Wilson

Nat Commun. 15, 2431 (2024)

SecM (secretion monitor) is an arrest peptide which regulates gene expression by stalling translation. This mechanism is crucial for the expression of the SecA ATPase, which cooperates with the SecYEG translocon to facilitate protein insertion or translocation across the cytoplasmic membrane in *E. coli* (Ito and Chiba, 2013). A previous study on SecM (Zhang *et al.*, 2015b) suggested a model in which the placement of Arg163, belonging to the characterizing RAGP motif, hampers the entrance of Prolyl-tRNA at the A-site, effectively halting translation elongation. However, such model is in contrast with many previous findings in the literature, indicating an occupied A-site in the stalled complex (Garza-Sanchez *et al.*, 2006, Muto *et al.*, 2006). Functionally relevant N-terminal residues not part of the stalling motif but affecting stalling efficiency (Nakagawa and Ito, 2002; Yang *et al.*, 2015, Muta *et al.*, 2020), were either not observed in this structure or not cloned in the construct. A compaction of the SecM nascent chain in the tunnel (Woolhead *et al.*, 2006) contributing to the stalling phenotype was not observed in the structure from Zhang *et al.* (2015b), whose chain is extended. Moreover, the authors of this manuscript used chloramphenicol during the isolation of the complex, a drug sitting in the A-site pocket, that could potentially bias the resulting structural analysis.

Given this and the striking similarity with the stalling motifs from the previously discussed ApdA and ApdP, our study aims to elucidate the structural basis of SecM-induced translational stalling. Furthermore, in collaboration with Sara Gabrielli and Dr. Lars V. Bock from the Göttingen Max Planck Institute, we investigated how pulling forces on the nascent chain can relieve this arrest.

In our study, we obtained a high-resolution structure (2.0 Å) of a ribosome stalled during the translation of the full-length *E. coli* SecM arrest peptide. The structure reveals that SecM induces stalling by stabilizing the Pro-tRNA in the A-site in a manner that prevents peptide bond formation with the SecM-peptidyl-tRNA in the P-site, with a mechanism analogous to the one described for *apdA* and *apdP* in the related manuscript (**Publication 1**). Moreover, the nascent chain seems to be highly compacted, folding into a α -helix in the upper tunnel, completely shifting the register of the residues along the tunnel, and therefore establishing a network of interactions between the nascent chain and the tunnel elements completely different from the one previously described by Zhang *et al.* (2015b).

Molecular dynamics simulations suggest that a pulling force exerted by SecA on the SecM nascent chain can relieve the translational arrest. This is achieved by upstream local unfolding of the observed SecM α -helix because of the tension generated, which is then propagated throughout the rest of the nascent chain to reach the C-terminus, thereby disrupting the peculiar local geometry that prevents peptide bond formation to occur; as a result, stalling is relieved and translation can proceed.

The N-terminal residues that have been proven to be affecting the stalling efficiency, also localized in the α -helix folding in the upper tunnel, are part of the previously mentioned “regulator module”, that affect the final stalling strength mediated by the “arrest module”. These structural and mechanistic insights extend to other arrest peptides that regulate components of the protein localization machinery across various bacterial lineages, including human pathogens.

Publication 3: Structural basis for translation inhibition by the glycosylated drosocin peptide

Timm O. Koller*, Martino Morici*, Max Berger*, Haaris A. Safdari, Deepti S. Lele, Bertrand Beckert, Kanwal J. Kaur and Daniel N. Wilson

Nat Chem. Biol. *19*, 1072-1081 (2023)

The proline-rich antimicrobial peptide (PrAMP) drosocin is produced by *Drosophila* species to combat bacterial infections (Bulet *et al.*, 1993, 1999). Unlike many PrAMPs, drosocin is O-glycosylated at threonine 11, which enhances its antimicrobial activity (Bulet *et al.*, 1993, 1999). Several findings suggest that drosocin could belong to class II PrAMPs: it competes with Api137 rather than with Onc112 in ribosome binding assays (Krizsan *et al.*, 2015) and C-terminal residues deletions are loss of function (Hoffmann *et al.*, 1999), similarly to Api137

To elucidate the mechanism of action of drosocin and the interactions it has with the bacterial ribosome, we generated drosocin-SRC, which were subjected to cryo-EM analysis, yielding high resolution structure of the complex (2.3 Å).

Our study revealed that glycosylated drosocin binds within the polypeptide exit tunnel of the ribosome and traps RF1, preventing the proper termination of protein synthesis, with a binding site and a orientation analogous to Api137 (Florin *et al.*, 2017). We could show that the glycosylation of drosocin not only affects its cellular uptake, but also its interaction with the ribosome. Specifically, the sugar moiety at Thr11 of Drosocin establishes multiple interactions with U2609 of the 23S rRNA, causing conformational changes that disrupt its base-pairing with A752. This disruption stabilizes the bound RF1, thus inhibiting translation.

These findings highlight the potential for developing new antimicrobial agents based on the structural features of glycosylated drosocin. Moreover, the study's insights into the ribosome-drosocin interactions may inform the design of synthetic derivatives with enhanced antimicrobial properties while maintaining low toxicity.

Discussion and Outlook

The structures determined in these studies have provided a better characterization of the bacterial ribosome exit tunnel. In particular, the work done on ApdA, ApdP and SecM arrest peptides shows how interactions established between the nascent chain of these staller and the components of the exit tunnel wall result in a geometry at the PTC that is not productive for peptide bond formation to be initiated, a stalling mechanism not previously described before.

The exit tunnel is also the target of PrAMPs, including drosocin, that was characterized under the structural and biochemical point of view in our work. Here we defined drosocin as a class II PrAMP that is able to trap RF1 on a terminating ribosome, a mechanism in which its glycosylation plays a critical functional role.

Arrest peptides short-circuiting the ribosome: a small hydrogen atom vs a titanic macromolecular machine

In this study, we determined the structures of ribosomes stalled during translation by the RAPP-containing arrest peptides ApdA and ApdP at 2.3 Å and 2.2 Å resolution, respectively. These structures, along with MD simulations and prior biochemistry (Sakiyama *et al.*, 2021), enabled us to propose a model explaining how RAPP arrest peptides freeze translation by impeding peptide bond formation. Normally, peptide bond formation occurs when the α -amino group of the aminoacyl-tRNA at the A-site attacks the carbonyl-carbon of the peptidyl-tRNA's amino acid at position 0 (linked to A76 of the P-tRNA); such a nucleophilic attack requires proton extraction from the α -amino group, mediated by the 2' O of A76 ribose (Polikanov *et al.*, 2014a) (Fig. 16a). During ApdA and ApdP polymerization, translation stalls with the peptidyl-RAP-tRNA in the P-site and Pro-tRNA in the A-site. Strikingly, the ribosome's PTC is induced, accommodating the substrate Pro-tRNA fully, yet the nucleophilic attack does not ensue. The observed geometry and the results of MD simulation suggest that this is due to a hydrogen bond between the Pro nitrogen at the A-site and the carbonyl-oxygen of the Ala in the RAP motif at the P-site, thereby preventing proton extraction by A76 (Fig. 16b). Moreover, an additional hydrogen bond seems to be formed between the 2'-OH oxygen of A76 and the nitrogen of the amino group of the prolyl moiety at the A-site, involving the oxygen donating, instead of extracting, a hydrogen from the nitrogen lone pair (Fig. 16b). This lone pair, that normally would perform the nucleophilic attack (Polikanov *et al.*, 2014a) (Fig. 16a), is therefore trapped in a geometry that eventually prevents peptide bond formation.

This model fits with the fact that mutations of the RAP motif's Pro or Arg alleviate stalling (Sakiyama *et al.*, 2021) (Fig. 16e). Indeed, unlike non-stalling peptides with β -strand geometry (Syroegin *et al.*, 2023), the RAP motifs of ApdA and ApdP do not

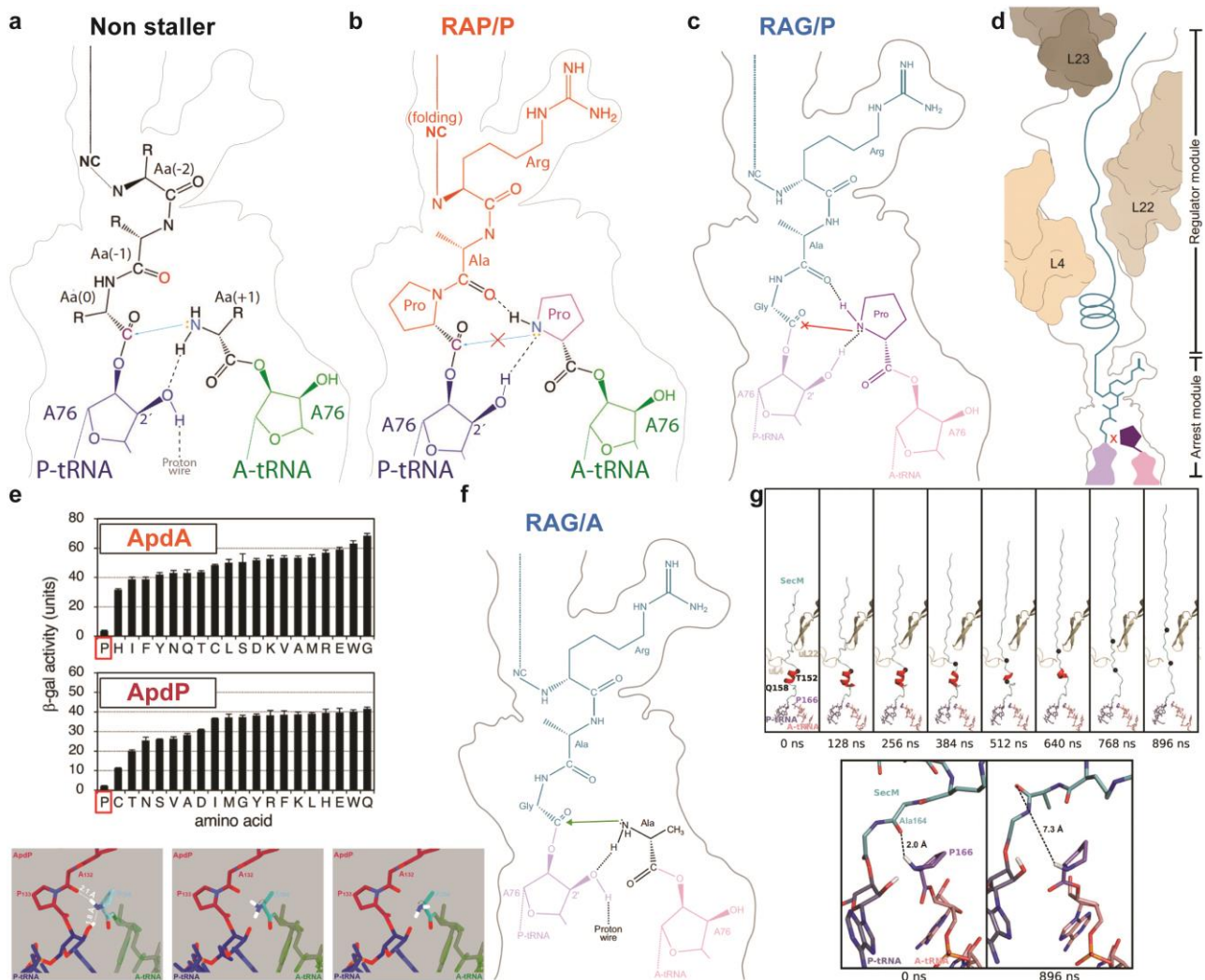


Figure 16: Stalling mechanism and relief of ApdA, ApdP and SecM. (a-c). Schematic representations of the PTC for (a) canonical non-stalling nascent polypeptide chains, where the lone pair electrons on the α -amino group of the aminoacyl moiety attached to the A-site tRNA performs a nucleophilic attack (blue arrow) on the carbonyl-carbon of the peptidyl-tRNA in the P-site. The nucleophilicity of the α -amino group is enhanced by the extraction of a proton by the 2'OH of ribose of A76 of the P-tRNA. (b). RAPP-mediated translation stalling by ApdA or ApdP (RAP/P motif), where the nucleophilic attack of the nitrogen of the A-site Pro on the carbonyl-carbon of the peptidyl-tRNA cannot occur because (i) the hydrogen of the nitrogen of Pro is involved in a hydrogen bond with the carbonyl-oxygen of Ala of the RAP motif in the P-site, and (ii) the 2'O of the ribose of A76 donates hydrogen to form a hydrogen bond with the lone pair electron, rather than extracting the proton as required for peptide bond formation. (c). Same schematic as (b), but for SecM (RAG/P motif). (d). ApdA, ApdP and SecM stalling is strongly driven by their RAP/P or RAG/P arrest module; however, the N-terminal regulator module also contributes by fine tuning the stalling efficiency and specificity. (e). Impact of amino acids encoded by the A-site codons for the efficiency of the elongation arrest of ApdA (top) and ApdP (middle). In the graph, the y-axis stands for β -galactosidase activity, that is inversely proportional to the stalling strength, since the staller is cloned upstream *lacZ*. The wt is boxed in red. Each bar stands for the mean and SD for $n = 3$. (Bottom) Arrangement at the PTC for (left) ApdP, with the formation of two hydrogen bonds that make nucleophilic attack impossible. Whenever Pro at the A-site is mutagenized to any other residue (middle, right), the bond between the α -carbon and the amino nitrogen rotates, making the proton wire possible, thereby preventing stalling. (f). Same schematic as (c), but for RAG/A motif, a geometry that would allow the nucleophilic attack. (g). (Top) Geometry of SecM NC in the tunnel as a pulling force is applied in time, from 0 to 896 ns. The α -helix (red) is gradually unfolded. (Bottom) As a result of the pulling force applied on SecM NC, the propagated tension affects the orientation of the carbonyl oxygen to disrupt the H-bond responsible for stalling, eventually resulting in stalling relief. Panels (a), (b) and (e, bottom) are adapted from Publication 1; Panels (c), (d), (f), (g) are adapted from Publication 2; Panel (e, top) is adapted from Sakiyama *et al.*, 2021.

adopt this structure, which would prevent the non-productive conformations inhibiting peptide bond formation (Syroegin *et al.*, 2023; Polikanov *et al.*, 2014a). On the other hand, the proline at the P-site tilts the nascent chain to fit the arginine in the tunnel pocket shaped by nucleotides 2503-2506 and 2061, where this residue forms extensive interactions, positioning the three amino acid C-terminal stretch so that upon arrival of the decoded prolyl-tRNA at the A-site, the hydrogen bond can readily form between its nitrogen and the carbonyl oxygen of Ala of the motif (Fig. 16b). Without A-site tRNA, the RAP motif in ApdA and ApdP loses most of its structural stability, another finding suggesting that Pro-tRNA at the A-site stabilizes the RAPP motif geometry, since it forms two additional hydrogen bonds, locking everything in place. Mutating the A-site Pro completely disrupts the stalling phenotype (Sakiyama *et al.*, 2021) (Fig. 16e, top) and, based on our model, this is because proline is the only amino acid with a secondary amine among the proteogenic ones. Other amino acids have a primary amine, and therefore the bond connecting the α carbon and the nitrogen of the amino group is able to freely rotate, while it is constrained in proline (Fig 16e, bottom). This means that, despite a RAP at the P-site C-terminus, aminoacyl-tRNAs at the A-site that are different from proline can adopt geometries favorable for nucleophilic attack and peptide bond formation, thereby preventing stalling (Fig 16e, bottom).

ApdP stalls translation in *B. subtilis* and *E. coli* ribosomes, while ApdA stalls only in *B. subtilis* ribosomes (Sakiyama *et al.*, 2021). Chimeric studies identified a region in ApdP near the RAP motif that confers such species-specificity. Although the tunnel region around these residues is conserved, how they contribute to species specificity remains unclear. Mutations in ribosomal proteins influencing MifM specificity (Sohmen *et al.*, 2015) did not affect ApdA and ApdP, suggesting that possible contribution from elements deeper in the tunnel would be indirect.

From our study and previous biochemistry (Sakiyama *et al.*, 2021), N-terminal region's role in RAPP stalling-specificity seems to be significant. The group of A. Buskirk (Woolstenhulme *et al.*, 2013) localized R/HxPP motifs causing stalling of bacterial translation elongation in a library of artificially and randomly generated amino acid sequences in a past study. In this research, they have shown that the N-terminal region indeed influenced or alleviated stalling (Woolstenhulme *et al.*, 2013), despite RAPP being able to stall without any additional N-terminal stretch.

These findings and our structures suggest that RAPP stallers can be divided in two modules: the RAPP "arrest module", attached to P-tRNA that is essential for elongation arrest, and an N-terminal "regulator module" that was selected to fine-tune the stalling strength and specificity (Fig. 16d).

Although ApdA and ApdP are both characterized by an RAP/P motif, their stalling mechanism differ completely from the one proposed for SecM's RAG/P motif by Zhang *et al.* (2015b) where accommodation of the Pro-tRNA at the A-site is sterically blocked (Zhang *et al.*, 2015b). By contrast, our re-determined SecM structure revealed that SecM in fact uses a similar stalling mechanism as ApdA and ApdP, and which is

also distinct from other stallers like MifM (Sohmen *et al.*, 2015) and VemP (Su *et al.*, 2017) that disrupt A-site tRNA accommodation.

Our cryo-EM structure of an *E. coli* ribosome stalled using the full-length SecM sequence at 2.0 Å resolution revises the known mechanism of SecM-induced translational arrest proposed by Zhang *et al.* (2015b). In such stalled complex, SecM nascent chain traps the ribosome in a pre-peptide bond formation state, with SecM-peptidyl-Gly-tRNA in the P-site and Pro166-tRNA in the A-site. The geometry observed at the PTC between the RAG motif at the P-site and the incoming Pro at the A-site is identical to the one previously observed in ApdA and ApdP stalled complexes (Fig 16b-c). This suggests that the mechanism preventing the nucleophilic attack is the same and is the direct consequence of the extra hydrogen bond formed between the donating nitrogen of the Pro amino group and the carbonyl oxygen of the Ala at -1. This also explains why Pro166 is critical for stalling in SecM, analogous to the previously described RAP/P motif, and contrary to what was proposed before (Zhang *et al.*, 2015b), i.e. that the shape of the proline would clash with Arg163 (Fig. 16f).

Additionally, the folding of an α -helix was evident in the upper tunnel, involving residues whose contribution to the stalling efficiency was previously proved, and this is in agreement with the observation of compaction of the nascent chain in the tunnel affecting the stalling phenotype of the SecM AP (Woolhead *et al.*, 2006). Therefore, we used MD simulations to apply a pulling force on SecM's N-terminus with the same intensity exerted by SecA. We verified that this indeed relieves stalling by eventually disrupting the local arrangement at the PTC between Ala164 and Pro166 (Fig. 16g). However, the α -helix of SecM needs to unfold first, so that the nascent chain can be stretched across the tunnel constriction and therefore the tension can be propagated to the C-terminus, where the “arrest module” is situated (Fig. 16g). This implies that SecM's secondary structure acts as an additional safe guard that fine-tunes the stalling efficiency by modulating the required force to relieve stalling: As for RAPP staller, the N-terminal region of SecM also seems to constitute a “regulator module” (Fig. 16d), which may also affect species specificity. Indeed, SecM stalling is efficient in *E. coli* but not *B. subtilis* (Chiba *et al.*, 2011), and this might be due to tunnel differences, especially in ribosomal proteins uL4 and uL22, which line the N-terminal stretch (Fig. 16d).

The differences evident between our structural findings and those from Zhang *et al.* (2015b) on SecM most likely depend on the use of chloramphenicol during the purification of the complex. This antimicrobial is known to block translation by binding in the A-site pocket and preventing incoming tRNA accommodation. This explains why their structure displays a vacant A-site and why their NC is less structured, given that Pro-tRNA would force it into place as it happens in RAPP APs. Moreover, the genetic construct used in the previous study to arrest translation lacks most of the N-terminal region of the wt AP, which was substituted by artificial tags (Zhang *et al.*, 2015b).

Our work on ApdA, ApdP and SecM structurally rationalizes the mechanism of stalling of many consensus sequences containing RAPP, RGPP, HAPP and RAGP spread among the genome of many microorganisms (Fujiwara *et al.*, 2024) (Fig. 16b-c). The essential role of the last Pro in stalling has been previously discussed, and it is related to its restrained geometry, being a secondary amino acid. The nature of the penultimate residue is one of orienting the nascent chain so that the first residue of the motif enters the tunnel pocket above the A-site as previously mentioned. The only two amino acids that would allow this path of the NC are Pro and Gly, since they can be polymerized to the nascent chain in *cis* configuration. The second residue is the one at -1, whose carbonyl oxygen should be oriented toward the nitrogen of the incoming proline (last in the motif). It seems that residues with absent or very reduced lateral chains were selected at this position: Gly and Ala have been observed, Ser does not impair stalling (Sakiyama *et al.*, 2021). This can be explained by the fact that a bulky residue there could clash with the walls of the tunnel at the P-site, preventing the correct positioning of the carbonyl oxygen. The Arg at first position seems to be essential (Sakiyama *et al.*, 2021) and it is a common feature of the three studied staller. Its long lateral chain allows the formation of an extended network of interaction with the tunnel cavity, including two water-mediated interactions. Interestingly, the motif identified by Buskirk (Woolstenhulme *et al.*, 2013) and Chiba (Fujiwara *et al.*, 2024) also include a His at first position. The two nitrogens of the His side chain, analogously to the two nitrogens of the Arg side chain, could coordinate the two water molecules to locally reproduce the interactions between the NC and the tunnel.

Add some sugar: a sweet desert at the end of translation. The case of the class II PrAMP drosocin

The mechanism of action of drosocin, including the role of its peculiar O-glycosylation, was elucidated by our biochemical and structural studies. We verified that indeed drosocin belongs to class II PrAMPs, analogously to Api137 (Florin *et al.*, 2017; Graf *et al.*, 2018), inhibiting translation at the step of termination, by trapping RF1 on the ribosome subsequently to NC release (Fig. 17a-b). This is also reflected by the weak inhibition of translation *in vitro*, as it happens for Api137 (Florin *et al.*, 2017). RF1 and RF2 are limiting in the cell pool and essential for the translation cycle to be terminated and the factors involved recycled. Drosocin, like Api137 (Florin *et al.*, 2017), depletes RFs of class I, eventually leading to cell death.

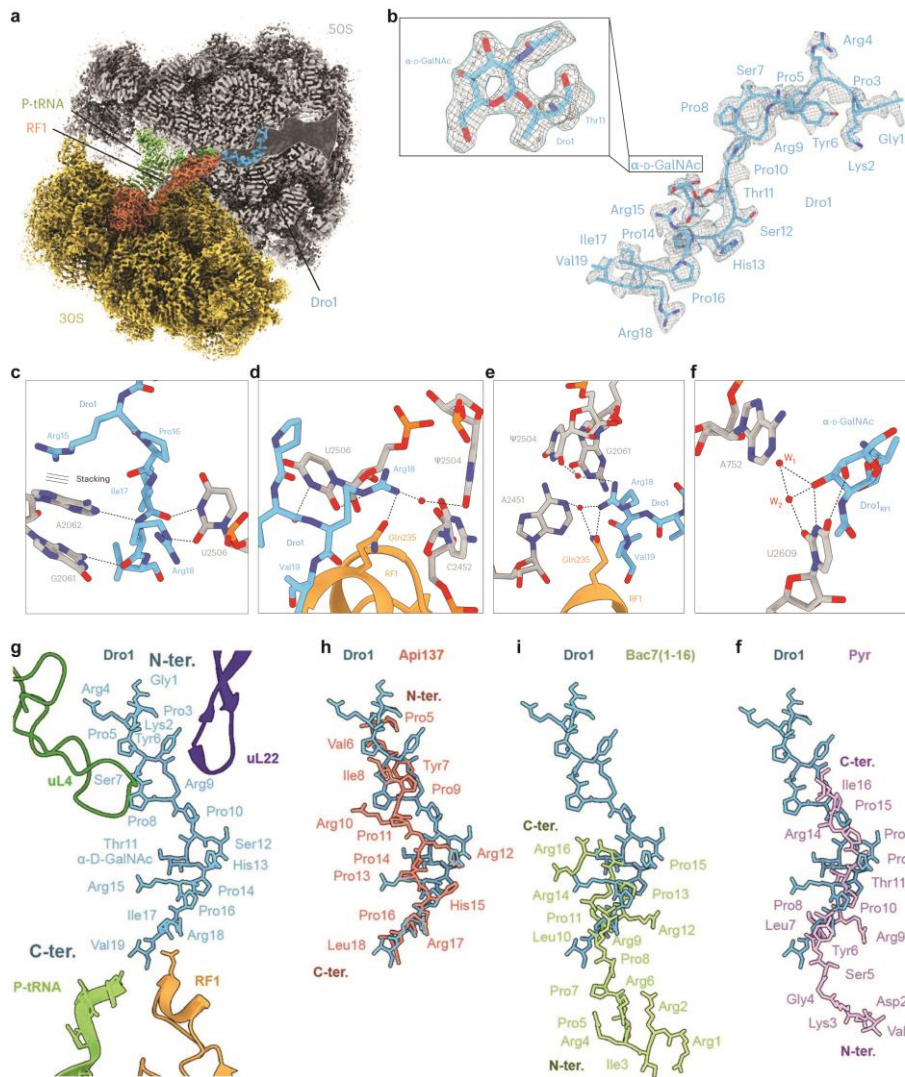


Figure 17: Structural analysis of the PrAMP drosocin. (a). Cryo-EM map of drosocin bound to termination complex with transverse section of the 50S (gray) to reveal drosocin (cyan) binding site within the exit tunnel. The P-tRNA is coloured green, the RF1 is coloured in orange and the 30S is yellow. (b). Cryo-EM density (gray mesh) with molecular model for drosocin (cyan) with zoom on the glycosylation α -D-GalNAc. (c-e). Interactions of drosocin (cyan) with 23S rRNA nucleotides (gray) and RF1 (orange); waters are represented as red balls. (f). Interaction of the glycosylation α -D-GalNAc (cyan) with the 23S rRNA base pairing involving A752 and U2609 (gray); waters are represented as red balls. (g). Relative position of drosocin (cyan) compared to P-tRNA (lime), RF1 (orange), uL4 (green) and uL22 (dark blue) within the drosocin-bound termination complex. (h). Superimposition of drosocin (cyan) from (g) with (h) Api137 (salmon) from the Api137-ArfB complex (PDB: 6YSS), (i) Bac7(1–16) (lime) from the Bac7-70S complex (PDB: 5F8K) and (f) Pyrrhocoricin (Pyr, purple) from the Pyr-70S complex (PDB: 5FDV). Panels adapted from Publication 3; in the panels, drosocin is labelled Dro1.

We observed that the C-terminal Arg18 of drosocin interacts directly with Gln235 in RF1 GGQ motif, a critical interaction as mutating Arg18 to alanine eliminates the peptide's inhibitory effect (Fig. 17c-e). Drosocin also undergoes O-glycosylation at Thr11 (Bulet *et al.*, 1993) (Fig. 17b), where the α -D-GalNAc modification forms multiple hydrogen bonds with U2609 of 23S rRNA (Fig. 17f), enhancing ribosome binding. This supports our findings and past observations that glycosylated drosocin

exhibits stronger antimicrobial activity than its unmodified counterpart (Gobbo *et al.*, 2002; Marcaurelle *et al.*, 1998; Rodriguez *et al.*, 1997; Otvos *et al.*, 2000; Ahn *et al.*, 2011a, 2011b; Talat *et al.*, 2011; Lele *et al.*, 2015a). Through the sugar moiety, drosocin causes U2609 to shift, disrupting its base pair with A752, normally (Svetlov *et al.*, 2020) (Fig. 17f) formed in *E. coli*. Indeed, mutations at these nucleotide positions affect the glycosylated form's activity but not the unmodified form. Interestingly, in some bacteria like *Mycobacterium tuberculosis*, U2609 and A752 are naturally unpaired (Yang *et al.*, 2017), potentially making these ribosomes more susceptible to glycosylated drosocin.

Besides the termination complex, drosocin binds to a vacant 50S subunit and to the elongating ribosome. This suggests drosocin might interact with the 50S subunit after ribosome recycling when the 70S ribosomes split. On the vacant 50S, α -D-GalNAc still disrupts the U2609-A752 base pair, but the C-terminus of drosocin remains flexible given the lack of RF1's interaction. This is perfectly reflecting the structural behaviour of Ap137, whose C-terminus is also stabilized by RF1 (Florin *et al.*, 2017).

Given the absence of stable initiation states in our structures, fMet-tRNA can bind at the P-site unimpeded by drosocin. However, we observed a significant population of drosocin-bound ribosomes in an elongation state, with deacylated-tRNA^{fMet} in the P-site and fMet-Leu-tRNA^{Leu} in the A-site. This suggests drosocin temporarily hinders the first translocation event, involving fMet-Leu-tRNA^{Leu} moving into the P-site. Despite this, toeprinting experiments showed ribosomes eventually translate the entire ORF, getting trapped at the termination codon.

In the elongation state, drosocin is flexible, with α -D-GalNAc density poorly resolved and U2609 present in both paired and unpaired forms. We propose that drosocin and fMet-Leu-tRNA^{Leu} compete for the P-site, with successful translocation eventually displacing drosocin. Drosocin can rebind only when the nascent chain is released at the termination codon.

Interestingly, while drosocin and apidaecin inhibit translation similarly by trapping RFs on the ribosome (Florin *et al.*, 2017) (Fig. 17g-h), their binding modes and interactions differ. O-glycosylation is peculiar and crucial for drosocin but absent in apidaecin. Other PrAMPs like pyrrococin (Bulet *et al.*, 1999) are also glycosylated at the same position as drosocin, suggesting similar ribosome interactions (Thr11 modification). Pyrrococin, however, belongs to class I PrAMPs: it inhibits the first stages of elongation after initiation and it runs in the exit tunnel with a N \rightarrow C orientation opposite to the one of a growing NC (Gagnon *et al.*, 2016), contrary to drosocin and apidaecin (Florin *et al.*, 2017) (Fig. 17i-f).

Our study shows drosocin traps RF1 decoding the UAA stop codon similarly to canonical translation, with higher resolution revealing previously unseen water-mediated interactions, enhancing our understanding of stop codon recognition in translation termination.

The ribosome is a ribozyme... which ribozyme? Insights into peptide bond formation from our structural studies

The ribosome performs the catalysis of peptide bond formation. Different models for its molecular mechanism have been proposed, the most recent one is the so-called “proton wire” by Polikanov *et al.* (2014a). As previously discussed, the ribosome optimally positions the amino group of the A-site tRNA residue and the carbonyl carbon of the most C-terminal residue of the nascent chain. In such geometric arrangement, one of the hydrogens of the amino group is temporarily subtracted and fed into a proton relay, making the nitrogen much more nucleophilic and forcing the attack from its lone pair to the carbonyl carbon, forming as a result a tetrahedral intermediate between the NC, the P-site tRNA, the aminoacyl residue at the A-site and its tRNA. The subtracted proton is taken by the 2'-OH of A76 of the P-tRNA and then passed to A2451 and eventually to W1. The proton then flows back, going from W1 to A2451, then to 2'-OH and W3, from which it is fueled to the tetrahedral intermediate, breaking it; this results in the nascent chain being elongated of one amino acid, now loaded onto the tRNA at the A-site, with the P-site tRNA deacylated. This model has two limits:

- It proposes how peptide bond formation is catalyzed starting from a non-protonated form of the aminoacyl at the A-site. However, several data suggest that at the pH conditions encountered in the cytosol, the aminoacyl moiety amino group is likely in its protonated form, with the amino group being a NH_3^+ , rather than a NH_2 (NH_2^+ , rather than NH for a proline) (Green *et al.*, 2002; Johansson *et al.*, 2010). This means that the lone pair that should perform the nucleophilic attack is instead possibly a hydrogen. It is important to state, however, that at the moment of writing this, there is no model explaining ribosome-catalyzed peptide bond formation starting from a protonated aminoacyl-tRNA at the A-site, nor there is a model explaining how that extra proton is first removed from the aminoacyl moiety.
- The molecular models that suggested the proton wire path by Polikanov *et al.* (2014a) are characterized by the elements involved in the relay being isolated from the bulk solvent. This would make the proton flow very efficient, without potential dissipation of the proton to the outside environment. W3 was assigned to an elongated density, proposing that such water would occupy two different coordinates in time, becoming stabilized upon proton transfer.

Our work on ApdA, ApdP and SecM SRC led us to the generation of high resolution cryo-EM structures being pre-attack states, in which the translating ribosome is frozen in the situation reproduced by Polikanov by using non-hydrolyzable aa-NH-tRNA^{aa} at the A-site. In all our structures we could observe the elements of the proton wire as described by Polikanov *et al.* (2014a). The density associated with W3, however, is very defined in our maps and close to a second defined density for a fourth molecule of water, which we refer to as W4 (Fig. 18, W3b is actually W4).

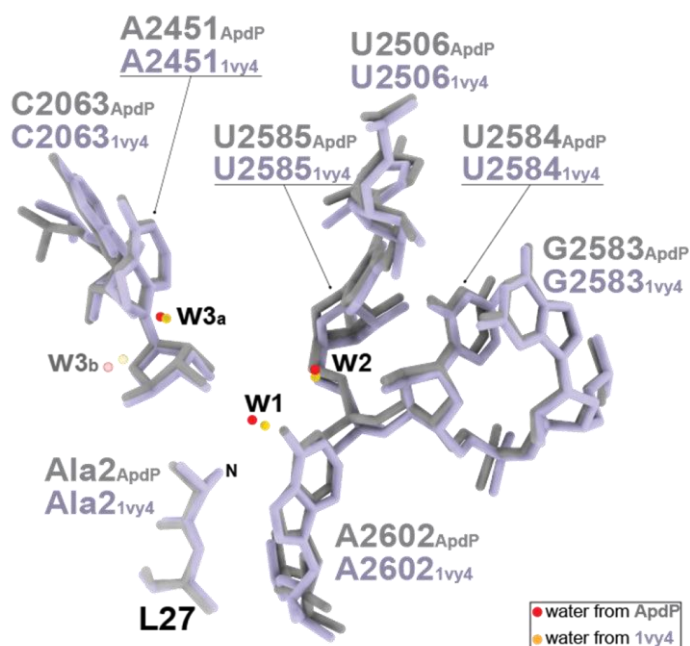


Figure 18: Overlay of the components of the proton wire from the preattack state of Polikanov *et al.* (2014a, PDB: 1vy4, violet/yellow) and from ApdP-SRC (Publication 1, grey/red). W3b is shown in pale, and it is referred to the alternative minor conformation of W3 in the preattack of Polikanov *et al.* (2014a), while we refer at it as W4 in this section of the thesis. The arrangement is identical in ApdA-SRC (Publication 1) and in SecM-SRC (Publication 2). Panel generated using ChimeraX and adobe illustrator, most updated versions.

This suggests that in their structures, because of resolution limits, Polikanov and collaborators were not able to resolve W3 from W4, assigning the smeared density to a single water molecule. The presence of a W4 is also confirmed in recent X-ray structures of pre-attack states from the Polikanov group (Syroegin *et al.*, 2023). W4 is in hydrogen bond distance from W3 and it would therefore bridge the proton wire to the bulk solvent. This means that the ribosome could be able to extract a proton from the α -amino at the A-site that would be discharged to the bulk solvent. Imagining a protonated aa-tRNA positioning at the A-site, it is possible that a first proton enters the wire, reaching W1, from which it flows back to W3, then hops to W4 from which it is released to the bulk solvent. In this way the amino group at the A-site is not protonated anymore, and peptide bond formation could occur mediated by the proton wire as described by Polikanov and colleagues (2014a). In this model, the ribosome would ultimately work as a proton pump that processively extract protons from the nitrogen at the A-site, thereby explaining how the first proton is removed from the amino group in an enzymatic efficient fashion. The ribosome would then partially perform an acid-base catalysis. This fits with the fact that given its relevance, in an RNA world, acid-base catalysis ribozyme can be expected to have arisen early during molecular evolution (Doudna and Cech, 2002). However, extensive studies by the group of Rodnina (Bieling *et al.*, 2006) have shown that the efficiency of peptide bond formation

is not dependent on pH in the range 6 to 9. As it is discussed in this study, while the role of the 2'-OH of A76 have been proposed to be of primary importance in ribosome catalysis (Weinger *et al.*, 2004), with the role of extracting a proton from the amino group, it seems that this hydroxyl group can be an acid-base catalyst only in the context of the ribosome (Sharma *et al.*, 2005). This means that rather than its intrinsic chemistry (pKa), this OH is a crucial component of the hydrogen bond network allowing proton flow because of its optimal geometry, favoured by the ribosome cage. In this setting, it is possible that the pH of the outside environment is not able to affect the efficiency of proton extraction by the ribosome, whose wire is somehow energetically shielded from the solvent and characterized by a local and peculiar chemistry.

The ceiling of the A-site: an interesting pocket

It is remarkable that the ribosome cavity in which the essential arginine is placed from the RAPP and RAGP motifs is the same as that exploited by the crucial Arg18 of Drosocin (see Publication 1 Fig.3, Publication 2 Fig. 4, This thesis Fig. 17c-e). This is the case also for Api137 (Florin *et al.*, 2017) (Fig. 17h), making it a feature of all the structurally described class II PrAMPs.

This cavity is localized in a crucial functional site of the ribosome, very close to the A-site cavity and to the PTC in general, where it offers charges and surfaces for interactions: this made it the target for many antimicrobial classes, including phenicols, lincosamides and macrolides (Schlünzen *et al.*, 2001) and eukaryotic ribosomes inhibitors, such as anisomycin and T-2 toxin (Garreau de Loubresse *et al.*, 2014). We have underlined that it also plays a crucial role for inhibitors of termination, like drosocin and Api137 (Publication 3; Florin *et al.*, 2017).

The fact that this pocket is relevant in RAPP and RAGP stalling (Publications 1 and 2) gives it importance also in the context of physiological translation regulation. It is interesting to point out that several of the inhibitory compounds previously mentioned have been shown to have a certain context-specificity (Syroegin *et al.*, 2022) and are also involved in regulation of expression of certain genes (Ramu *et al.*, 2009). Moreover, some of them have been shown to have an effect on bacterial physiology and proteome without drastically hampering cell growth or being bactericidal, at subinhibitory concentrations (Wood *et al.*, 2023; Meydan *et al.*, 2019); these concentrations are often in the range observed in nature. These observations raise the possibility that this cavity is not only a mere optimal target for inhibitors of translation, but it could have evolved as a sensor of molecular effectors acting in *cis* (like APs) or in *trans* (like drugs at subinhibitory concentrations) to ultimately regulate translation.

As it was exploited as a partner of interactions by nature, it could be the subject of structure-based drug design studies to fight antimicrobial resistance, given it is highly conserved and prone for such purpose.

Conclusion

The technical advancement of the last two decades, together with the improvement of related hardware and software, has made cryo-EM the technique of choice to achieve atomic resolution. Given its size and intrinsic stability, the ribosome has always been an optimal object of structural studies using this technique. In this work, cryo-EM was applied to structurally characterize NC stalling-mediated regulation of gene expression at the translational level and the binding of translation inhibitors to the bacterial ribosome.

The complementary research reported in Publication 1 and Publication 2 allowed us to not only describe a previously uncharacterized stalling mechanism mediated by RAPP-containing motif, but to also demonstrate that such a stalling mechanism is the one acting in the well-studied SecM AP. Until now, the previous structures of SecM-RNC were either characterized at relatively low resolution and resulted from purifying the complex in presence of the drug chloramphenicol, completely biasing the biology of the phenomenon (Bhushan *et al.*, 2011; Zhang *et al.*, 2015b). Our re-determined structure of SecM allowed us to describe in atomic details the geometry of the complex. We concluded that the stalling mechanism of SecM RAG/P motif is in fact the same as that of the ApdA and ApdP RAP/P motif. This means that these three stallerers are likely to be evolutionary related and their divergence in the N-terminal region accounts for the different stalling intensities as well as the species-specificity. In general, these AP uORFs can be conceived as being divided into two parts, a divergent N-terminal “regulator module” and a highly conserved C-terminal “arrest module”. Hundreds of uORFs containing RAP/P or RAG/P motif have been bioinformatically localized, and are spread amongst the genomes of countless microbial species, suggesting that they play a central role in regulating gene expression in bacteria (Fujiwara *et al.*, 2024). This also encompasses many human pathogens, which may exploit RAPP-mediated stalling to regulate their fitness. For example, *Bordetella pertussis*, the causative agent of whooping cough, has been shown to possess an operon required for copper intake having a uORF containing a conserved RAPP motif (Roy *et al.*, 2022). Mutagenesis of this motif disrupts the regulation of the operon (Roy *et al.*, 2022), suggesting that NC-mediated stalling regulates the operon translation, as described for ApdA, ApdP and SecM.

APs regulating gene expression at the translational level is a strategy also observed in eukaryotic systems (Wilson *et al.*, 2016). More generally, the stalling or slowing down of the ribosome can affect mRNA stability and protein folding, thereby having clinical consequences (Sauna and Kimchi-Sarfaty, 2011). Such phenomenon may therefore not only have a fundamental relevance, but also potential medical applications in the future.

Our cryo-EM study on drosocin-stalled ribosomal termination complex provided a structural and mechanistic understanding of this PrAMP in Publication 3. The study we performed succeeded to define drosocin as a class II PrAMP. The peptide binds in the tunnel, with a N→C orientation identical to that of a nascent chain, and it forms extensive interactions with the tunnel walls. Its presence traps RFs of class I (RF1 or RF2 depending on the stop codon). This mechanism is the same as Api137 (Florin *et al.*, 2017) and eventually leads to cell death by depleting the limiting RFs, required for a healthy translation cycle. This is reflected by the low inhibition in cell-free translation system and the good activity *in vivo*, characteristic of class II PrAMPs (Florin *et al.*, 2017). This study enriched the knowledge on antimicrobials specifically acting at the stage of termination, which is still quite limited (Arenz and Wilson, 2016; Polikanov *et al.*, 2018). Drosocin is characterized by a peculiar glycosylation at position Thr11, namely, a α -D-GalNAc (Bulet *et al.*, 1999). This modification is known to enhance the peptide stability and solubility (Bulet *et al.*, 1999), providing it with a good pharmacokinetic profile. The glycosylation also likely contributes to favour an extended conformation of the peptide, which facilitates the association to the ribosome exit tunnel (Bulet *et al.*, 1999). Moreover, the glycosylated form of drosocin is characterized by better activity *in vitro* and *in vivo* with respect to the unmodified one, and this is rationalized by the fact that the sugar indeed contributes to the binding of drosocin to its ribosomal target (Publication 3). The base-pair with which α -D-GalNAc interacts suggests that drosocin could display enhanced activity against *M. tuberculosis*, a pathogen representing a primary threat nowadays, and this PrAMP could potentially enrich the arsenal against multidrug-resistant strains (Yang *et al.*, 2017).

Like other PrAMPs, drosocin is synthesized by ribosomal translation in the producer (Bulet *et al.*, 1999). The unmodified form is released from the eukaryotic ribosome and exported from the cell into the extracellular matrix after the glycosylation is added (Bulet *et al.*, 1999). Given the high protein synthesis efficiency of *D. melanogaster* cell lines and the ribosomal synthesis of drosocin, it would be possible to artificially produce the modified form of drosocin, which would be excreted in the medium, with high yield.

More generally, PrAMPs are characterized by low cytotoxicity, given the fact that they do not permeabilize the cell membrane and are acting specifically on prokaryotic ribosomes (Scocchi *et al.*, 2011). As suggested by our studies on drosocin, the addition of a glycosylation could contribute to make PrAMPs more potent and at the same time better candidates to enter clinical trials, with an efficient production and storage.

In conclusion, our research contributed in adding drosocin to the potential arsenal to fight infections in the near future and in considering the novel strategy of adding glycosylations to antimicrobials to make them better clinical candidates.

References

Adio, S., Senyushkina, T., Peske, F., Fischer, N., Wintermeyer, W., and Rodnina, M.V. (2015). Fluctuations between multiple EF-G-induced chimeric tRNA states during translocation on the ribosome. *Nature Communications* 6, 7442.

Adio, S., Sharma, H., Senyushkina, T., Karki, P., Maracci, C., Wohlgemuth, I., Holtkamp, W., Peske, F., and Rodnina, M.V. (2018). Dynamics of ribosomes and release factors during translation termination in *E. coli*. *Elife* 7.

Ævarsson, A., Brazhnikov, E., Garber, M., Zheltonosova, J., Chirgadze, Y., al-Karadaghi, S., Svensson, L.A., and Liljas, A. (1994). Three-dimensional structure of the ribosomal translocase: elongation factor G from *Thermus thermophilus*. *EMBO J* 13, 3669-3677.

Agirrezabala, X., Lei, J., Brunelle, J.L., Ortiz-Meoz, R.F., Green, R., and Frank, J. (2008). Visualization of the hybrid state of tRNA binding promoted by spontaneous ratcheting of the ribosome. *Mol Cell* 32, 190-197.

Agirrezabala, X., Liao, H.Y., Schreiner, E., Fu, J., Ortiz-Meoz, R.F., Schulten, K., Green, R., and Frank, J. (2012). Structural characterization of mRNA-tRNA translocation intermediates. *Proc Natl Acad Sci U S A* 109, 6094-6099.

Ahn, M., Murugan, R.N., Nan, Y.H., Cheong, C., Sohn, H., Kim, E.H., Hwang, E., Ryu, E.K., Kang, S.W., Shin, S.Y., Bang, J.K. (2011a). Substitution of the GalNAc- α -O-Thr¹¹ residue in drosocin with O-linked glyco-peptoid residue: effect on antibacterial activity and conformational change. *Bioorg Med Chem Lett* 21, 6148-6153.

Ahn, M., Sohn, H., Nan, Y.H., Murugan, R.N., Cheong, C., Ryu, E., Kim, E., Kang, S., Kim, E., Shin, S., Bang, J.K. (2011b). Functional and structural characterization of drosocin and its derivatives linked O-GalNAc at Thr11 residue. *Bull. Korean Chem Soc* 32, 3327–3332.

Ahn, M., Włodarski, T., Mitropoulou, A., Chan, S.H.S., Sidhu, H., Plessa, E., Becker, T.A., Budisa, N., Waudby, C.A., Beckmann, R., Cassaignau, A.M.E., Cabrita, L.D., Christodoulou, J. (2022). Modulating co-translational protein folding by rational design and ribosome engineering. *Nat Commun* 13, 4243.

Allan Drummond, D., and Wilke, C.O. (2009). The evolutionary consequences of erroneous protein synthesis. *Nature Reviews Genetics* 10, 715.

Allen, G.S., Zavialov, A., Gursky, R., Ehrenberg, M., and Frank, J. (2005). The cryo-EM structure of a translation initiation complex from *Escherichia coli*. *Cell* 121, 703-712.

Arenz, S. and Wilson D.N.(2016). Bacterial protein synthesis as a target for antibiotic inhibition. *Cold Spring Harb Perspect Med.* 6, a025361.

Armache, J.-P., Jarasch, A., Anger, A.M., Villa, E., Becker, T., Bhushan, S., Jossinet, F., Habeck, M., Dindar, G., Franckenberg, S., Marquez V., Mielke T., Thomm M., Berninghausen O., Beatrix B., Söding J., Westhof E., Wilson D.N., Beckmann R. (2010). Localization of eukaryotes specific ribosomal proteins in a 5.5-Å cryo-EM map of the 80S eukaryotic ribosome. *Proceedings of the National Academy of Sciences* 107, 19754.

Bagley, M., Dale, J., Merritt, E., and Xiong, X. (2005). Thiopeptide antibiotics. *Chem Rev* 105, 685–714.

Ban, N., Nissen, P., Hansen, J., Moore, P.B., and Steitz, T.A. (2000). The complete atomic structure of the large ribosomal subunit at 2.4 Å resolution. *Science* 289, 905-920.

Ban N., Beckmann R., Cate J.H., Dinman J.D., Dragon F., Ellis S.R., Lafontaine D.L., Lindahl L., Liljas A., Lipton J.M., McAlear M.A., Moore P.B., Noller H.F., Ortega J., Panse V.G., Ramakrishnan V., Spahn C.M., Steitz T.A., Tchorzewski M., Tollervey D., Warren A.J., Williamson J.R., Wilson D.N., Yonath A., Yusupov M. (2014) A new system for naming ribosomal proteins. *Curr Opin Struct Biol* 24,165-169.

Belardinelli, R., Sharma, H., Caliskan, N., Cunha, C.E., Peske, F., Wintermeyer, W., and Rodnina, M.V. (2016a). Choreography of molecular movements during ribosome progression along mRNA. *Nature Structural & Molecular Biology* 23, 342-348.

Belova, L., Tenson, T., Xiong, L.Q., McNicholas, P.M., Mankin, A.S. (2001). A novel site of antibiotic action in the ribosome: Interaction of evernimicin with the large ribosomal subunit. *Proc Natl Acad Sci* 98, 3726–3731.

Benincasa, M., Scocchi, M., Podda, E., Skerlavaj, B., Dolzani, L., Gennaro, R. (2004). Antimicrobial activity of Bac7 fragments against drug-resistant clinical isolates. *Peptides* 25, 2055–2061.

Benincasa, M., Runti, G., Mardirossian, M., Gennaro, R., Scocchi, M. (2017). Methods for Elucidating the Mechanism of Action of Proline-Rich and Other Non-lytic Antimicrobial Peptides. *Methods Mol Biol* 1548, 283-295.

Bennett, B.D., Kimball, E.H., Gao, M., Osterhout, R., Van Dien, S.J., and Rabinowitz, J.D. (2009). Absolute metabolite concentrations and implied enzyme active site occupancy in *Escherichia coli*. *Nature Chemical Biology* 5, 593-599.

Bentele, K., Saffert, P., Rauscher, R., Ignatova, Z., and Blüthgen, N. (2013). Efficient translation initiation dictates codon usage at gene start. *Molecular Systems Biology* 9, 675.

Berthold, N. & Hoffmann, R. (2014). Cellular uptake of apidaecin 1b and related analogs in Gram-negative bacteria reveals novel antibacterial mechanism for proline-rich antimicrobial peptides . *Protein Pept Lett* 21, 391–398.

Bertolini, M., Fenzl, K., Kats, I., Wruck, F., Tippmann, F., Schmitt, J., Auburger, J.J., Tans, S., Bukau, B., Kramer, G. (2021). Interactions between nascent proteins translated by adjacent ribosomes drive homomer assembly. *Science* 371, 57-64.

Bhushan, S., Meyer, H., Starosta, A.L., Becker, T., Mielke, T., Berninghausen, O., Sattler, M., Wilson, D.N., Beckmann, R. (2010). Structural basis for translational stalling by human cytomegalovirus and fungal arginine attenuator peptide. *Mol Cell* 40, 138-146.

Bhushan, S., Hoffmann, T., Seidelt, B., Frauenfeld, J., Mielke, T., Berninghausen, O., Wilson, D.N., Beckmann, R. (2011). SecM-stalled ribosomes adopt an altered geometry at the peptidyl transferase center. *PLoS Biol* 9, e1000581.

Bieling, P., Beringer, M., Adio, S., and Rodnina, M.V. (2006). Peptide bond formation does not involve acid-base catalysis by ribosomal residues. *Nature Structural & Molecular Biology* 13, 423-428.

Biou, V., Shu, F., and Ramakrishnan, V. (1995). X-ray crystallography shows that translational initiation factor IF3 consists of two compact alpha/beta domains linked by an alpha-helix. *EMBO J* *14*, 4056-4064.

Blanchard, S.C., Kim, H.D., Gonzalez, R.L., Jr., Puglisi, J.D., and Chu, S. (2004). tRNA dynamics on the ribosome during translation. *Proc Natl Acad Sci U S A* *101*, 12893-12898.

Blattner F.R., Plunkett G. 3rd, Bloch C.A., Perna N.T., Burland V., Riley M., Collado-Vides J., Glasner J.D., Rode C.K., Mayhew G.F., Gregor J., Davis N.W., Kirkpatrick H.A., Goeden M.A., Rose D.J., Mau B., Shao Y. (1997). The complete genome sequence of *Escherichia coli* K-12. *Science* *277*, 1453-1462.

Boni, I.V., Isaeva, D.M., Musychenko, M.L., and Tzareva, N.V. (1991). Ribosome-messenger recognition: mRNA target sites for ribosomal protein S1. *Nucleic Acids Res* *19*, 155-162.

Borg, A., Pavlov, M., and Ehrenberg, M. (2016). Complete kinetic mechanism for recycling of the bacterial ribosome. *RNA* *22*, 10-21.

Borovinskaya, M.A., Shoji, S., Holton, J.M., Fredrick, K., Cate, J.H. (2007). A steric block in translation caused by the antibiotic spectinomycin. *ACS Chem Biol* *2*, 545–552.

Bracken, H.A. & Woolhead, C.A. (2019). Increased freedom of movement in the nascent chain results in dynamic changes in the structure of the SecM arrest motif. *Biosci rep* *39*, BSR20181246.

Brandi, L., Fabbretti, A., Pon, C.L., Dahlberg, A.E., Gualerzi, C.O. (2008). Initiation of protein synthesis: A target for antimicrobials. *Expert Opin Ther Targets* *12*, 519–534.

Brenner, S., Stretton, A.O.W., and Kaplan, S. (1965). Genetic Code: The ‘Nonsense’ Triplets for Chain Termination and their Suppression. *Nature* *206*, 994-998.

Brilot, A.F., Korostelev, A.A., Ermolenko, D.N., and Grigorieff, N. (2013). Structure of the ribosome with elongation factor G trapped in the pretranslocation state. *Proc Natl Acad Sci U S A* *110*, 20994-20999.

Brodersen, D.E., Clemons, W.M., Carter, A.P., Morgan-Warren, R.J., Wimberly, B.T., Ramakrishnan, V. (2000). The structural basis for the action of the antibiotics tetracycline, pactamycin, and hygromycin B on the 30S ribosomal subunit. *Cell* 103, 1143–1154.

Brodersen D.E., Clemons W.M. Jr, Carter A.P., Wimberly B.T., Ramakrishnan V. (2002). Crystal structure of the 30 S ribosomal subunit from *Thermus thermophilus*: structure of the proteins and their interactions with 16 S RNA. *J Mol Biol.* 316,725-768.

Bulet, P., Dimarcq, J.L., Hetru, C., Lagueux, M., Charlet, M., Hegy, G., Van Dorselaer, A., Hoffmann, J.A. (1993). A novel inducible antibacterial peptide of *Drosophila* carries an O-glycosylated substitution. *J Biol Chem* 268,14893-14897.

Bulet, P., Hetru, C., Dimarcq, J.L., Hoffmann D. (1999) Antimicrobial peptides in insects; structure and function. *Dev Comp Immunol* 23, 329-344.

Bulkley, D., Johnson, F., Steitz, T.A. (2012). The antibiotic thermorubin inhibits protein synthesis by binding to intersubunit bridge B2a of the ribosome. *J Mol Biol* 416, 571–578.

Bulkley, D., Brandi, L., Polikanov, Y.S., Fabbretti, A., O'Connor, M., Gualerzi, C.O., Steitz, T.A. (2014). The antibiotics dityromycin and GE82832 bind protein S12 and block EF-G catalyzed translocation. *Cell Rep* 6, 357–365.

Byrgazov, K., Grishkovskaya, I., Arenz, S., Coudeville, N., Temmel, H., Wilson, D.N., Djinovic-Carugo, K., and Moll, I. (2015). Structural basis for the interaction of protein S1 with the *Escherichia coli* ribosome. *Nucleic Acids Res* 43, 661-673.

Cabrita L.D., Cassaignau A.M.E., Launay H.M.M., Waudby C.A., Wlodarski T., Camilloni C., Karyadi M.E., Robertson A.L., Wang X., Wentink A.S., Goodsell L., Woolhead C.A., Vendruscolo M., Dobson C.M., Christodoulou J. (2016). A structural ensemble of a ribosome-nascent chain complex during cotranslational protein folding. *Nat Struct Mol Biol* 23, 278-285.

Capecchi, M.R. (1967). Polypeptide chain termination in vitro: isolation of a release factor. *Proc Natl Acad Sci U S A* 58, 1144-1151.

Carbone C.E., Loveland A.B., Gamper H.B. Jr, Hou Y.M., Demo G., Korostelev A.A. (2021). Time-resolved cryo-EM visualizes ribosomal translocation with EF-G and GTP. *Nat Commun* 12, 7236.

Carlson, M.A., Haddad, B.G., Weis, A.J., Blackwood, C.S., Shelton, C.D., Wuerth, M.E., Walter, J.D., and Spiegel, P.C., Jr. (2017). Ribosomal protein L7/L12 is required for GTPase translation factors EF-G, RF3, and IF2 to bind in their GTP state to 70S ribosomes. *FEBS J* 284, 1631-1643.

Carter, A.P., Clemons, W.M., Brodersen, D.E., Morgan-Warren, R.J., Wimberly, B.T., and Ramakrishnan, V. (2000). Functional insights from the structure of the 30S ribosomal subunit and its interactions with antibiotics. *Nature* 407, 340-348.

Carter, A.P., Clemons, W.M., Jr., Brodersen, D.E., Morgan-Warren, R.J., Hartsch, T., Wimberly, B.T., and Ramakrishnan, V. (2001). Crystal structure of an initiation factor bound to the 30S ribosomal subunit. *Science* 291, 498-501.

Caserta, E., Tomšić, J., Spurio, R., La Teana, A., Pon, C.L., and Gualerzi, C.O. (2006). Translation Initiation Factor IF2 Interacts with the 30 S Ribosomal Subunit via Two Separate Binding Sites. *Journal of Molecular Biology* 362, 787-799.

Caskey, C.T., Tompkins, R., Scolnick, E., Caryk, T., and Nirenberg, M. (1968). Sequential translation of trinucleotide codons for the initiation and termination of protein synthesis. *Science* 162, 135-138.

Castle, M., Nazarian, A., Yi, S.S., Tempst, P. (1999) Lethal effects of apidaecin on *Escherichia coli* involve sequential molecular interactions with diverse targets. *J Biol Chem* 1999 274, 32555-32564.

Cech, T.R. (2000). Structural biology. The ribosome is a ribozyme. *Science* 289, 878-879.

Schlunzen, F., Zarivach, R., Harms, J., Bashan, A., Tocilj, A., Albrecht, R., Yonath, A., and Franceschi, F. (2001). Structural basis for the interaction of antibiotics with the peptidyl transferase centre in eubacteria. *Nature* *413*, 814-821.

Chan, S.H.S., Włodarski, T., Streit, J.O., Cassaignau, A.M.E., Woodburn, L.F., Ahn, M., Freiherr von Sass, G.J., Waudby, C.A., Budisa, N., Cabrita, L.D., Christodoulou, J. (2022). The ribosome stabilizes partially folded intermediates of a nascent multi-domain protein. *Nat Chem* *14*, 1165-1173.

Chen, C., Stevens, B., Kaur, J., Cabral, D., Liu, H., Wang, Y., Zhang, H., Rosenblum, G., Smilansky, Z., Goldman, Yale E., *et al.* (2011). Single-Molecule Fluorescence Measurements of Ribosomal Translocation Dynamics. *Molecular Cell* *42*, 367-377.

Chen, H., Bjercknes, M., Kumar, R., and Jay, E. (1994). Determination of the optimal aligned spacing between the Shine-Dalgarno sequence and the translation initiation codon of *Escherichia coli* mRNAs. *Nucleic Acids Res* *22*, 4953-4957.

Chen, J., Petrov, A., Tsai, A., O'Leary, S.E., and Puglisi, J.D. (2013a). Coordinated conformational and compositional dynamics drive ribosome translocation. *Nat Struct Mol Biol* *20*, 718-727.

Chen, Y., Feng, S., Kumar, V., Ero, R., and Gao, Y.-G. (2013b). Structure of EF-G-ribosome complex in a pretranslocation state. *Nature Structural & Molecular Biology* *20*, 1077-1084.

Chiba, S., Kanamori, T., Ueda, T., Akiyama, Y., Pogliano, K., Ito, K. (2011). Recruitment of a species-specific translational arrest module to monitor different cellular processes. *Proc Natl Acad Sci U S A* *108*, 6073-6078.

Chiba, S., Ito, K. (2012). Multisite ribosomal stalling: a unique mode of regulatory nascent chain action revealed for MifM. *Mol Cell* *47*, 863-872.

Chung, S.S., Bidstrup, E.J., Hershewe, J.M., Warfel, K.F., Jewett, M.C., DeLisa, M.P. (2022). Ribosome Stalling of *N*-Linked Glycoproteins in Cell-Free Extracts. *ACS Synth Biol* *11*, 3892-3899.

Cociancich, S., Dupont, A., Hegy, G., Lanot, R., Holder, F., Hetru, C., Hoffmann, J.A., Bulet, P. (1994). Novel inducible antibacterial peptides from a hemipteran insect, the sap-sucking bug *Pyrrhocoris apterus*. *Biochem J* *300* (Pt 2), 567-575.

Contreras-Martinez, L.M. & DeLisa, M.P. (2007). Intracellular ribosome display via SecM translation arrest as a selection for antibodies with enhanced cytosolic stability. *J Mol Biol* 372, 513–524.

Cool R.H., Parmeggiani A. (1991). Substitution of histidine-84 and the GTPase mechanism of elongation factor Tu. *Biochemistry* 30, 362-366.

Cornish, P.V., Ermolenko, D.N., Noller, H.F., and Ha, T. (2008). Spontaneous intersubunit rotation in single ribosomes. *Mol Cell* 30, 578-588.

Crick, F.H. (1958). On protein synthesis. *Symp Soc Exp Biol* 12, 138-163.

Crick, F.H., Barnett, L., Brenner, S., and Watts-Tobin, R.J. (1961). General nature of the genetic code for proteins. *Nature* 192, 1227-1232.

Cunha, C.E., Belardinelli, R., Peske, F., Holtkamp, W., Wintermeyer, W., and Rodnina, M.V. (2013). Dual use of GTP hydrolysis by elongation factor G on the ribosome. *Translation (Austin)* 1, e24315.

Cymer, F. & von Heijne, G. (2013). Cotranslational folding of membrane proteins probed by arrest-peptide-mediated force measurements. *Proc Natl Acad Sci USA* 110, 14640–14645.

Czworkowski, J., Wang, J., Steitz, T.A., and Moore, P.B. (1994). The crystal structure of elongation factor G complexed with GDP, at 2.7 Å resolution. *EMBO J* 13, 3661-3668.

Dahlquist K.D., Puglisi J.D. (2000). Interaction of translation initiation factor IF1 with the *E. coli* ribosomal A site. *J Mol Biol* 299, 1-15.

Dallas, A., and Noller, H.F. (2001). Interaction of translation initiation factor 3 with the 30S ribosomal subunit. *Mol Cell* 8, 855-864.

de Smit, M.H., and van Duin, J. (1994). Translational initiation on structured messengers: Another role for the shine-dalgarno interaction. *Journal of Molecular Biology* 235, 173-184.

Deckert, A., Cassaignau, A.M.E., Wang, X., Włodarski, T., Chan, S.H.S., Waudby, C.A., Kirkpatrick, J.P., Vendruscolo, M., Cabrita, L.D., Christodoulou, J. (2021). Common sequence motifs of nascent chains engage the ribosome surface and trigger factor. *Proc Natl Acad Sci U S A* 118, e2103015118.

Del Campo C., Bartholomäus A., Fedyunin I., Ignatova Z. (2015). Secondary Structure across the Bacterial Transcriptome Reveals Versatile Roles in mRNA Regulation and Function. *PLoS Genet* *11*, e1005613.

Demeshkina, N., Jenner, L., Westhof, E., Yusupov, M., and Yusupova, G. (2013). New structural insights into the decoding mechanism: translation infidelity via a G.U pair with Watson-Crick geometry. *FEBS Lett* *587*, 1848-1857.

Diaconu, M., Kothe, U., Schlunzen, F., Fischer, N., Harms, J.M., Tonevitsky, A.G., Stark, H., Rodnina, M.V., and Wahl, M.C. (2005). Structural basis for the function of the ribosomal L7/12 stalk in factor binding and GTPase activation. *Cell* *121*, 991-1004.

Dincbas-Renqvist, V., Engstrom, A., Mora, L., Heurgue-Hamard, V., Buckingham, R., and Ehrenberg, M. (2000). A post-translational modification in the GGQ motif of RF2 from *Escherichia coli* stimulates termination of translation. *EMBO J* *19*, 6900-6907.

Dinos, G., Wilson, D.N., Teraoka, Y., Szaflarski, W., Fucini, P., Kalpaxis, D., Nierhaus, K.H. (2004). Dissecting the ribosomal inhibition mechanisms of edeine and pactamycin: The universally conserved residues G693 and C795 regulate Psite tRNA binding. *Mol Cell* *13*, 113–124.

Doudna, J., Cech, T. 2002. The chemical repertoire of natural ribozymes. *Nature* *418*, 222–228.

Dube, S.K., Marcker, K.A., Clark, B.F.C., and Cory, S. (1968). Nucleotide Sequence of NFormyl-methionyl-transfer RNA. *Nature* *218*, 232-233.

Dunkle, J.A., Wang, L., Feldman, M.B., Pulk, A., Chen, V.B., Kapral, G.J., Noeske, J., Richardson, J.S., Blanchard, S.C., and Cate, J.H.D. (2011). Structures of the Bacterial Ribosome in Classical and Hybrid States of tRNA Binding. *Science* *332*, 981.

Duval M., Korepanov A., Fuchsbauer O., Fechter P., Haller A., Fabbretti A., Choulier L., Micura R., Klaholz B.P., Romby P., Springer M., Marzi S. (2013). *Escherichia coli* ribosomal protein S1 unfolds structured mRNAs onto the ribosome for active translation initiation. *PLoS Biol.* *11*, e1001731.

Elfageih, R., Karyolaimos, A., Kemp, G., de Gier, J.W., von Heijne, G., Kudva, R. (2020). Cotranslational folding of alkaline phosphatase in the periplasm of *Escherichia coli*. *Protein Sci* *29*, 2028-2037.

Erlacher, M.D., Lang, K., Shankaran, N., Wotzel, B., Hüttenhofer, A., Micura, R., Mankin, A.S., and Polacek, N. (2005). Chemical engineering of the peptidyl transferase

center reveals an important role of the 2' -hydroxyl group of A2451. *Nucleic Acids Research* 33, 1618-1627.

Ermolenko, D.N., Majumdar, Z.K., Hickerson, R.P., Spiegel, P.C., Clegg, R.M., and Noller, H.F. (2007a). Observation of intersubunit movement of the ribosome in solution using FRET. *J Mol Biol* 370, 530-540.

Ermolenko, D.N., Spiegel, P.C., Majumdar, Z.K., Hickerson, R.P., Clegg, R.M., Noller, H.F. (2007b). The antibiotic viomycin traps the ribosome in an intermediate state of translocation. *Nat Struct Mol Biol* 14, 493–497.

Evans, M.S., Ugrinov, K.G., Frese, M.A. & Clark, P.L. (2005). Homogeneous stalled ribosome nascent chain complexes produced *in vivo* or *in vitro*. *Nat Methods* 2, 757–762.

Fabbretti, A., Pon, C.L., Hennelly, S.P., Hill, W.E., Lodmell, J.S., and Gualerzi, C.O. (2007). The real-time path of translation factor IF3 onto and off the ribosome. *Mol Cell* 25, 285-296.

Fang, P., Spevak, C., Wu, C., Sachs, M. (2004). A nascent polypeptide domain that can regulate translation elongation. *Proc Natl Acad Sci U S A* 101,4059-4064.

Fislage, M., Zhang, J., Brown, Z.P., Mandava, C.S., Sanyal, S., Ehrenberg, M., and Frank, J. (2018). Cryo-EM shows stages of initial codon selection on the ribosome by aa-tRNA in ternary complex with GTP and the GTPase-deficient EF-TuH84A. *Nucleic Acids Research* 46, 5861-5874.

Florin, T., Maracci, C., Graf, M., Karki, P., Klepacki, D., Berninghausen, O., Beckmann, R., Vázquez-Laslop, N., Wilson, D.N., Rodnina, M.V., Mankin, A.S. (2017). An antimicrobial peptide that inhibits translation by trapping release factors on the ribosome. *Nat Struct Mol Biol* 24, 752-757.

Fluitt A., Pienaar E., Viljoen H. (2007). Ribosome kinetics and aa-tRNA competition determine rate and fidelity of peptide synthesis. *Comput Biol Chem* 31, 335-346.

Frank, J., and Agrawal, R.K. (2000). A ratchet-like inter-subunit reorganization of the ribosome during translocation. *Nature* 406, 318-322.

Fredrick, K., and Noller, H.F. (2003). Catalysis of ribosomal translocation by sparsomycin. *Science* 300, 1159-1162.

Freistroffer, D.V., Pavlov, M.Y., MacDougall, J., Buckingham, R.H., and Ehrenberg, M. (1997). Release factor RF3 in E.coli accelerates the dissociation of release factors RF1 and RF2 from the ribosome in a GTP-dependent manner. *EMBO J* 16, 4126-4133.

Frolova, L.Y., Tsivkovskii, R.Y., Sivolobova, G.F., Oparina, N.Y., Serpinsky, O.I., Blinov, V.M., Tatkov, S.I., and Kisselev, L.L. (1999). Mutations in the highly conserved GGQ motif of class 1 polypeptide release factors abolish ability of human eRF1 to trigger peptidyl-tRNA hydrolysis. *RNA* 5, 1014-1020.

Fu, Z., Kaledhonkar, S., Borg, A., Sun, M., Chen, B., Grassucci, R.A., Ehrenberg, M., and Frank, J. (2016). Key Intermediates in Ribosome Recycling Visualized by Time-Resolved Cryoelectron Microscopy. *Structure* 24, 2092-2101.

Fujiwara, K., Tsuji, N., Yoshida, M., Takada, H., Chiba, S. (2024). Patchy and widespread distribution of bacterial translation arrest peptides associated with the protein localization machinery. *Nat Commun* 15, 2711.

Gagnon, M.G., Roy, R.N., Lomakin, I.B., Florin, T., Mankin, A.S., Steitz, T.A. (2016). Structures of proline-rich peptides bound to the ribosome reveal a common mechanism of protein synthesis inhibition. *Nucleic Acids Res* 44, 2439-2450.

Gao, N., Zavialov, A.V., Li, W., Sengupta, J., Valle, M., Gursky, R.P., Ehrenberg, M., and Frank, J. (2005). Mechanism for the disassembly of the posttermination complex inferred from cryo-EM studies. *Mol Cell* 18, 663-674.

Gao, N., Zavialov, A.V., Ehrenberg, M., and Frank, J. (2007). Specific Interaction between EF-G and RRF and Its Implication for GTP-Dependent Ribosome Splitting into Subunits. *Journal of Molecular Biology* 374, 1345-1358.

Garreau de Loubresse, N., Prokhorova, I., Holtkamp, W., Rodnina, M.V., Yusupova, G. and Yusupov, M. (2014). Structural basis for the inhibition of the eukaryotic ribosome. *Nature* 513, 517-522.

Garza-Sanchez, F., Janssen, B.D. & Hayes, C.S. (2006). Prolyl-tRNA(Pro) in the A-site of SecM-arrested ribosomes inhibits the recruitment of transfer-messenger RNA. *J Biol Chem* 281, 34258-34268.

Gavrilova, L.P., and Spirin, A.S. (1971). Stimulation of "non-enzymic" translocation in ribosomes by p-chloromercuribenzoate. *FEBS Lett* 17, 324-326.

Geggier, P., Dave, R., Feldman, M.B., Terry, D.S., Altman, R.B., Munro, J.B., and Blanchard, S.C. (2010). Conformational Sampling of Aminoacyl-tRNA during Selection on the Bacterial Ribosome. *Journal of Molecular Biology* 399, 576-595.

Gobbo, M., Biondi, L., Filira, F., Gennaro, R., Benincasa, M., Scolaro, B., Rocchi, R. (2002). Antimicrobial peptides: synthesis and antibacterial activity of linear and cyclic drosocin and apidaecin 1b analogues. *J Med Chem* 45, 4494-4504.

Goldstein, J.L., and Caskey, C.T. (1970). Peptide Chain Termination: Effect of Protein S on Ribosomal Binding of Release Factors. *Proceedings of the National Academy of Sciences* 67, 537.

Gong, F., Ito, K., Nakamura, Y., Yanofsky, C. (2001). The mechanism of tryptophan induction of tryptophanase operon expression: tryptophan inhibits release factor-mediated cleavage of TnaC-peptidyl-tRNA^{Pro}. *Proc Natl Acad Sci USA* 98, 8997-9001.

Goyal, A., Belardinelli, R., Maracci, C., Milon, P., and Rodnina, M.V. (2015). Directional transition from initiation to elongation in bacterial translation. *Nucleic Acids Res* 43, 10700-10712.

Graf, M., Mardirossian, M., Nguyen, F., Seefeldt, A.C., Guichard, G., Scocchi, M., Innis, C.A., Wilson, D.N. (2017). Proline-rich antimicrobial peptides targeting protein synthesis. *Nat Prod Rep* 34, 702-711.

Graf, M., Huter, P., Maracci, C., Peterek, M., Rodnina, M.V. & Wilson, D.N. (2018). Visualization of translation termination intermediates trapped by Apidaecin 137 peptide during RF3-mediated recycling of RF1. *Nat Commun* 9, 3053.

Green, R., Lorsch, J.R. (2002). The path to perdition is paved with protons. *Cell* 110, 665-668.

Grigoriadou, C., Marzi, S., Pan, D., Gualerzi, C.O., and Cooperman, B.S. (2007b). The translational fidelity function of IF3 during transition from the 30 S initiation complex to the 70 S initiation complex. *J Mol Biol* 373, 551-561.

Gromadski, K.B., and Rodnina, M.V. (2004). Kinetic determinants of high-fidelity tRNA discrimination on the ribosome. *Mol Cell* 13, 191-200.

Grunberg-Manago, M., Dessen, P., Pantaloni, D., Godefroy-Colburn, T., Wolfe, A.D., and Dondon, J. (1975). Light-scattering studies showing the effect of initiation factors on the reversible dissociation of *Escherichia coli* ribosomes. *J Mol Biol* 94, 461-478.

Gualerzi, C.O., Pon, C.L. (1990). Initiation of mRNA translation in prokaryotes. *Biochemistry*. 29:5881-5889.

Gualerzi, C.O., Brandi, L., Caserta, E., Garofalo, C., Lammi, M., La Teana, A., Petrelli, D., Spurio, R., Tomsic, J., and Pon, C.L. (2001). Initiation factors in the early events of mRNA translation in bacteria. *Cold Spring Harb Symp Quant Biol* 66, 363-376.

Guillon, J.M., Meinel, T., Mechulam, Y., Lazennec, C., Blanquet, S., and Fayat, G. (1992). Nucleotides of transfer RNA Governing the Specificity of *Escherichia coli* Methionyl-transfer RNA(Met)f Formyltransferase. *J Mol Biol* 224, 359-367.

Gumbart, J., Schreiner, E., Wilson, D.N., Beckmann, R. & Schulten, K. (2012). Mechanisms of SecM-mediated stalling in the ribosome. *Biophys J* 103, 331–341.

Hansen, J.L., Schmeing, T.M., Moore, P.B., and Steitz, T.A. (2002). Structural insights into peptide bond formation. *Proc Natl Acad Sci U S A* 99, 11670-11675.

Hansen, J.L., Moore, P.B., Steitz, T.A. 2003. Structures of five antibiotics bound at the peptidyl transferase center of the large ribosomal subunit. *J Mol Biol* 330, 1061–1075.

Hardesty, B., Odom, O.W., Kudlicki, W., and Kramer, G. (1993). Extension and folding of nascent peptides on ribosomes. In *The Translation Apparatus*. Nierhaus, K.H., Franceschi, F., Subramanian, A.R., Erdmann, V.A., and Wittmann-Liebold, B.

Harms, J.M., Schlunzen, F., Zarivach, R., Bashan, A., Gat, S., Agmon, I., Bartels, H., Franceschi, F., and Yonath, A. (2001). High resolution structure of the large ribosomal subunit from a mesophilic eubacterium. *Cell* 107, 679-688.

Harms, J.M., Schlunzen, F., Fucini, P., Bartels, H., and Yonath, A. (2004). Alterations at the peptidyl transferase centre of the ribosome induced by the synergistic action of the streptogramins dalbavancin and quinupristin. *BMC Biol* 2, 4.

Harms, J.M., Wilson, D.N., Schlunzen, F., Connell, S.R., Stachelhaus, T., Zaborowska, Z., Spahn, C.M., Fucini, P. (2008). Translational regulation via L11:

molecular switches on the ribosome turned on and off by thiostrepton and micrococcin. *Mol Cell* 30, 26–38.

Hartz, D., McPheeters, D.S., and Gold, L. (1989). Selection of the initiator tRNA by *Escherichia coli* initiation factors. *Genes Dev* 3, 1899-1912.

Hartz, D., Binkley, J., Hollingsworth, T., and Gold, L. (1990). Domains of initiator transfer RNA and initiation codon crucial for initiator transfer RNA selection by *Escherichia coli* IF3. *Gene Dev* 4, 1790-1800.

Helgstrand, M., Mandava, C.S., Mulder, F.A., Liljas, A., Sanyal, S., and Akke, M. (2007). The ribosomal stalk binds to translation factors IF2, EF-Tu, EF-G and RF3 via a conserved region of the L12 C-terminal domain. *J Mol Biol* 365, 468-479.

Heurgue-Hamard, V., Champ, S., Engstrom, A., Ehrenberg, M., and Buckingham, R. (2002). The *hemK* gene in *Escherichia coli* encodes the N(5)-glutamine methyltransferase that modifies peptide release factors. *EMBO J* 21, 769-778.

Hirokawa, G.O., Nijman, R.M., Raj, V.S., Kaji, H., Igarashi, K., and Kaji, A. (2005). The role of ribosome recycling factor in dissociation of 70S ribosomes into subunits. *RNA* 11, 1317-1328.

Hirokawa, G., Demeshkina, N., Iwakura, N., Kaji, H., and Kaji, A. (2006). The ribosome-recycling step: consensus or controversy? *Trends Biochem Sci* 31, 143-149.

Hoffmann, R., Bulet, P., Urge, L., Otvös, L. Jr. (1999). Range of activity and metabolic stability of synthetic antibacterial glycopeptides from insects. *Biochim Biophys Acta* 1426, 459-467.

Holm, M., Borg, A., Ehrenberg, M., and Sanyal, S. (2016). Molecular mechanism of viomycin inhibition of peptide elongation in bacteria. *Proc Natl Acad Sci U.S.A.* 113, 978–983.

Horan, L.H., and Noller, H.F. (2007). Intersubunit movement is required for ribosomal translocation. *Proceedings of the National Academy of Sciences* 104, 4881.

Houwman, J.A., Westphal, A.H., van Berkel, W.J. & van Mierlo, C.P. (2015). Stalled flavodoxin binds its cofactor while fully exposed outside the ribosome. *Biochim Biophys Acta* 1854, 1317–1324.

Hussain T., Llácer J.L., Wimberly B.T., Kieft J.S., Ramakrishnan V. (2016). Large-Scale Movements of IF3 and tRNA during Bacterial Translation Initiation. *Cell* 167, 133-144.

Ieong, K.-W., Uzun, Ü., Selmer, M., and Ehrenberg, M. (2016). Two proofreading steps amplify the accuracy of genetic code translation. *Proceedings of the National Academy of Sciences* 113, 13744.

Ishii, E., Chiba, S., Hashimoto, N., Kojima, S., Homma, M., Ito, K., Akiyama, Y., Mori, H. (2015). Nascent chain-monitored remodeling of the Sec machinery for salinity adaptation of marine bacteria. *Proc Natl Acad Sci U S A* 112, 5513-5522.

Ismail, N., Hedman, R., Schiller, N. & von Heijne, G. (2012). A biphasic pulling force acts on transmembrane helices during translocon-mediated membrane integration. *Nat Struct Mol Biol* 19, 1018–1022.

Ito, K., Uno, M., and Nakamura, Y. (2000). A tripeptide ‘anticodon’ deciphers stop codons in messenger RNA. *Nature* 403, 680-684.

Ito, K., Chiba, S. (2013). Arrest peptides: cis-acting modulators of translation. *Annu Rev Biochem* 82, 171-202.

Jain, A., and Dixit, P. (2008). Multidrug-resistant to extensively drug resistant tuberculosis: what is next? *J. Biosci* 33, 605–616.

Janosi, L., Shimizu, I., and Kaji, A. (1994). Ribosome recycling factor (ribosome releasing factor) is essential for bacterial growth. *Proceedings of the National Academy of Sciences* 91, 4249.

Javed A., Christodoulou J., Cabrita L.D., Orlova E.V. (2017). The ribosome and its role in protein folding: looking through a magnifying glass. *Acta Crystallogr D Struct Biol* 73, 509-521.

Jensen, M.K., Samelson, A.J., Steward, A., Clarke, J. & Marqusee, S. (2020). The folding and unfolding behavior of ribonuclease H on the ribosome. *J Biol Chem* 295, 11410–11417.

Jha, S.S. & Komar, A.A. (2012). Using SecM arrest sequence as a tool to isolate ribosome bound polypeptides. *J Vis Exp* 19, 4027.

Jin, H., Kelley, A.C., and Ramakrishnan, V. (2011). Crystal structure of the hybrid state of ribosome in complex with the guanosine triphosphatase release factor 3. *Proc Natl Acad Sci U S A*, Epub.

Johansson, M., Jeong, K.W., Trobro, S., Strazewski, P., Åqvist, J., Pavlov, M.Y., Ehrenberg, M. (2011). pH-sensitivity of the ribosomal peptidyl transfer reaction dependent on the identity of the A-site aminoacyl-tRNA. *Proc Natl Acad Sci U S A* *108*, 79-84.

Jomaa, A., Boehringer, D., Leibundgut, M. & Ban, N. (2016). Structures of the *E. coli* translating ribosome with SRP and its receptor and with the translocon. *Nat Commun* *7*, 10471.

Julian, P., Konevega, A.L., Scheres, S.H., Lazaro, M., Gil, D., Wintermeyer, W., Rodnina, M.V., and Valle, M. (2008). Structure of ratcheted ribosomes with tRNAs in hybrid states. *Proc Natl Acad Sci U S A* *105*, 16924-16927.

Kaiser C.M., Goldman, D.H., Chodera, J.D., Tinoco, I.Jr., Bustamante C. (2011). The ribosome modulates nascent protein folding. *Science* *334*, 1723-1727.

Kaledhonkar, S., Fu, Z., Caban, K., Li, W., Chen, B., Sun, M., Gonzalez, R.L., and Frank, J. (2019). Late steps in bacterial translation initiation visualized using time-resolved cryo-EM. *Nature* *570*, 400-404.

Kannan, K., Mankin, A.S. (2012a). Macrolide antibiotics in the ribosome exit tunnel: Species-specific binding and action. *Ann NY Acad Sci* *1241*, 33–47.

Kannan, K., Vazquez-Laslop, N., Mankin, A.S. (2012b). Selective protein synthesis by ribosomes with a drug-obstructed exit tunnel. *Cell* *151*, 508–520.

Kannan, K., Kanabar, P., Schryer, D., Florin, T., Oh, E., Bahroos, N., Tenson, T., Weissman, J.S., Mankin, A.S. (2014). The general mode of translation inhibition by macrolide antibiotics. *Proc Natl Acad Sci* *111*, 15958–15963.

Karimi, R., Pavlov, M.Y., Buckingham, R.H., and Ehrenberg, M. (1999). Novel roles for classical factors at the interface between translation termination and initiation. *Mol Cell* *3*, 601-609.

Kihira, K., Shimizu, Y., Shomura, Y., Shibata, N., Kitamura, M., Nakagawa, A., Ueda, T., Ochi, K., and Higuchi, Y. (2012). Crystal structure analysis of the translation factor RF3 (release factor 3). *FEBS Letters* *586*, 3705-3709.

- Kim, D., and Green, R. (1999). Base-pairing between 23S rRNA and tRNA in the ribosomal A site. *Mol Cell* 4, 859-864.
- Kim, K.K., Min, K., and Suh, S.W. (2000). Crystal structure of the ribosome recycling factor from *Escherichia coli*. *EMBO J* 19, 2362-2370.
- Kim, S.H., Quigley, G.J., Suddath, F.L., McPherson, A., Sneden, D., Kim, J.J., Weinzierl, J., and Rich, A. (1973). Three-dimensional structure of yeast phenylalanine transfer RNA: folding of the polynucleotide chain. *Science* 179, 285-288.
- Klein D.J., Moore P.B., Steitz T.A. (2004). The roles of ribosomal proteins in the structure assembly, and evolution of the large ribosomal subunit. *J Mol Biol.* 340, 141-177.
- Knappe, D., Zahn, M., Sauer, U., Schiffer, G., Sträter, N., Hoffmann, R. (2011). Rational design of oncocin derivatives with superior protease stabilities and antibacterial activities based on the high-resolution structure of the oncocin-DnaK complex. *Chembiochem* 12, 874-876.
- Komarova A.V., Tchufistova L.S., Dreyfus M., Boni I.V. (2005). AU-rich sequences within 5' untranslated leaders enhance translation and stabilize mRNA in *Escherichia coli*. *J Bacteriol* 187, 1344-1349.
- Komarova E.S., Chervontseva Z.S., Osterman I.A., Evfratov S.A., Rubtsova M.P., Zatsepin T.S., Semashko T.A., Kostryukova E.S., Bogdanov A.A., Gelfand M.S., Dontsova O.A., Sergiev P.V. (2020). Influence of the spacer region between the Shine-Dalgarno box and the start codon for fine-tuning of the translation efficiency in *Escherichia coli*. *Microb Biotechnol* 13, 1254-1261.
- Korostelev, A., Asahara, H., Lancaster, L., Laurberg, M., Hirschi, A., Zhu, J., Trakhanov, S., Scott, W.G., and Noller, H.F. (2008). Crystal structure of a translation termination complex formed with release factor RF2. *Proc Natl Acad Sci U S A* 105, 19684-19689.
- Korostelev, A., Zhu, J., Asahara, H., and Noller, H.F. (2010). Recognition of the amber UAG stop codon by release factor RF1. *EMBO J* 29, 2577-2585.
- Korostelev A. (2011). Structural aspects of translation termination on the ribosome. *RNA* 17, 1409-1421.
- Kothe, U., Wieden, H.J., Mohr, D., and Rodnina, M.V. (2004). Interaction of helix D of elongation factor Tu with helices 4 and 5 of protein L7/12 on the ribosome. *J Mol Biol* 336, 1011-1021.

Kothe, U., and Rodnina, M.V. (2006). Delayed Release of Inorganic Phosphate from Elongation Factor Tu Following GTP Hydrolysis on the Ribosome. *Biochemistry* *45*, 12767-12774.

Koutmou, K.S., McDonald, M.E., Brunelle, J.L., and Green, R. (2014). RF3:GTP promotes rapid dissociation of the class 1 termination factor. *RNA* *20*, 609-620.

Peske, F., Kuhlenkoetter, S., Rodnina, M.V., and Wintermeyer, W. (2014). Timing of GTP binding and hydrolysis by translation termination factor RF3. *Nucleic Acids Res* *42*, 1812-1820.

Kozak M. (1983). Comparison of initiation of protein synthesis in procaryotes, eucaryotes, and organelles. *Microbiol Rev.* *47*, 1-45.

Krizsan, A., Prahl, C., Goldbach, T., Knappe, D. & Hoffmann, R. (2015). Short proline-rich antimicrobial peptides inhibit either the bacterial 70S ribosome or the assembly of its large 50S subunit. *ChemBioChem* *16*, 2304–2308.

Kudla, G., Murray, A.W., Tollervey, D., and Plotkin, J.B. (2009). Coding-sequence determinants of gene expression in *Escherichia coli*. *Science* *324*, 255-258.

Kuhlenkoetter, S., Wintermeyer, W., and Rodnina, M.V. (2011). Different substrate-dependent transition states in the active site of the ribosome. *Nature* *476*, 351-354.

Kunst F., Ogasawara N., Moszer I., Albertini A.M., Alloni G., Azevedo V., Bertero M.G., Bessières P., Bolotin A., Borchert S., Borriss R., Boursier L., Brans A., Braun M., Brignell S.C., Bron S., Brouillet S., Bruschi C.V., Caldwell B., Capuano V., Carter N.M., Choi S.K., Cordani J.J., Connerton I.F., Cummings N.J., Daniel R.A., Denziot F., Devine K.M., Düsterhöft A., Ehrlich S.D., Emmerson P.T., Entian K.D., Errington J., Fabret C., Ferrari E., Foulger D., Fritz C., Fujita M., Fujita Y., Fuma S., Galizzi A., Galleron N., Ghim S.Y., Glaser P., Goffeau A., Golightly E.J., Grandi G., Guiseppi G., Guy B.J., Haga K., Haiech J., Harwood C.R., Hènaut A., Hilbert H., Holsappel S., Hosono S., Hullo M.F., Itaya M., Jones L., Joris B., Karamata D., Kasahara Y., Klaerr-Blanchard M., Klein C., Kobayashi Y., Koetter P., Koningstein G., Krogh S., Kumano M., Kurita K., Lapidus A., Lardinois S., Lauber J., Lazarevic V., Lee S.M., Levine A., Liu H., Masuda S, Mauël C., Médigue C., Medina N., Mellado R.P., Mizuno M., Moestl D., Nakai S., Noback M., Noone D., O'Reilly M., Ogawa K., Ogiwara A., Oudega B., Park S.H., Parro V., Pohl T.M., Portelle D., Porwollik S., Prescott A.M., Presecan E., Pujic P., Purnelle B., Rapoport G., Rey M., Reynolds S., Rieger M., Rivolta C., Rocha E., Roche B., Rose M., Sadaie Y., Sato T., Scanlan E., Schleich S., Schroeter R., Scoffone F., Sekiguchi J., Sekowska A., Seror S.J., Serror P., Shin B.S., Soldo B., Sorokin A., Tacconi E., Takagi T., Takahashi H., Takemaru K., Takeuchi M., Tamakoshi A., Tanaka T., Terpstra P., Togoni A., Tosato V., Uchiyama S.,

Vandebol M., Vannier F., Vassarotti A., Viari A., Wambutt R., Wedler H., Weitzenegger T., Winters P., Wipat A., Yamamoto H., Yamane K., Yasumoto K., Yata K., Yoshida K., Yoshikawa H.F., Zumstein E., Yoshikawa H., Danchin A. (1997) The complete genome sequence of the gram-positive bacterium *Bacillus subtilis*. *Nature* 390, 249-256.

La Teana, A., Pon, C.L., and Gualerzi, C.O. (1996). Late events in translation initiation. Adjustment of fMet-tRNA in the ribosomal P-site. *J Mol Biol* 256, 667-675.

La Teana, A., Gualerzi, C.O., and Dahlberg, A.E. (2001). Initiation factor IF 2 binds to the alpha-sarcin loop and helix 89 of *Escherichia coli* 23S ribosomal RNA. *RNA* 7, 1173-1179.

Laurberg, M., Asahara, H., Korostelev, A., Zhu, J., Trakhanov, S., and Noller, H.F. (2008). Structural basis for translation termination on the 70S ribosome. *Nature* 454, 852-857.

Laursen, B.S., Sorensen, H.P., Mortensen, K.K., and Sperling-Petersen, H.U. (2005). Initiation of protein synthesis in bacteria. *Microbiol Mol Biol Rev* 69, 101-123.

Lawrence, M.G., Lindahl, L., Zengel, J.M. (2008). Effects on translation pausing of alterations in protein and mRNA components of the ribosome exit tunnel. *J Bacteriol* 190, 5862-5869.

Lee, C.P., Seong, B.L., and RajBhandary, U.L. (1991). Structural and sequence elements important for recognition of *Escherichia coli* formylmethionine tRNA by methionyl-tRNA transformylase are clustered in the acceptor stem. *Journal of Biological Chemistry* 266, 18012-18017.

Lee, C.P., Dyson, M.R., Mandal, N., Varshney, U., Bahramian, B., and RajBhandary, U.L. (1992). Striking effects of coupling mutations in the acceptor stem on recognition of tRNAs by *Escherichia coli* Met-tRNA synthetase and Met-tRNA transformylase. *Proceedings of the National Academy of Sciences* 89, 9262.

Lele, D.S., Dwivedi, R., Kumari, S. & Kaur, K.J. (2015a). Effect of distalsugar and interglycosidic linkage of disaccharides on the activity of proline rich antimicrobial glycopeptides. *J Pept Sci* 21, 833–844.

Lele, D.S., Talat, S., Kumari, S., Srivastava, N. & Kaur, K.J. (2015b) Understanding the importance of glycosylated threonine and stereospecific action of drosocin, a proline rich antimicrobial peptide. *Eur J Med Chem* 92, 637–647.

- Li, L., Rybak, M.Y., Lin, J., Gagnon, M.G. (2024). The ribosome termination complex remodels release factor RF3 and ejects GDP. *Nat Struct Mol Biol*.
- Li, Q., and Seiple, I.B. (2017). Modular, scalable synthesis of group A streptogramin antibiotics. *J Am Chem Soc* *139*, 13304–13307.
- Lin, J., Gagnon, Matthieu G., Bulkley, D., and Steitz, Thomas A. (2015). Conformational Changes of Elongation Factor G on the Ribosome during tRNA Translocation. *Cell* *160*, 219-227.
- Liutkute M., Samatova E., Rodnina M.V. (2020). Cotranslational Folding of Proteins on the Ribosome. *Biomolecules* *10*, 97.
- Loveland, A.B., Demo, G., Grigorieff, N., and Korostelev, A.A. (2017). Ensemble cryo-EM elucidates the mechanism of translation fidelity. *Nature* *546*, 113-117.
- Ludwig, T., Krizsan, A., Mohammed, G.K. & Hoffmann, R. (2022). Antimicrobial activity and 70S ribosome binding of apidaecin-derived Api805 with increased bacterial uptake rate. *Antibiotics (Basel)* *11*, 430.
- Ly, C.T., Altuntop, M.E., and Wang, Y. (2010). Single-molecule study of viomycin's inhibition mechanism on ribosome translocation. *Biochemistry* *49*, 9732–9738.
- Maden, B.E.H., and Monro, R.E. (1968). Ribosome-Catalyzed Peptidyl Transfer. *European Journal of Biochemistry* *6*, 309-316.
- Maguire, B.A., Beniaminov, A.D., Ramu, H., Mankin, A.S., and Zimmermann, R.A. (2005). A protein component at the heart of an RNA machine: the importance of protein L27 for the function of the bacterial ribosome. *Mol Cell* *20*, 427-435.
- Malkin L.I., Rich A. (1967). Partial resistance of nascent polypeptide chains to proteolytic digestion due to ribosomal shielding. *J Mol Biol* *26*, 329-346.
- Manickam, N., Nag, N., Abbasi, A., Patel, K., and Farabaugh, P.J. (2014). Studies of translational misreading in vivo show that the ribosome very efficiently discriminates against most potential errors. *RNA* *20*, 9-15.
- Manzella, J.P. (2001). Quinupristin-dalfopristin: a new antibiotic for severe gram-positive infections. *Am Fam Phys* *64*, 1863–1866.
- Maracci, C., Wohlgemuth, I., and Rodnina, M.V. (2015). Activities of the peptidyl transferase center of ribosomes lacking protein L27. *RNA* *21*, 2047-2052.

- Maracci, C., and Rodnina, M.V. (2016). Review: Translational GTPases. *Biopolymers* *105*, 463-475.
- Marcaurrelle, L.A., Rodriguez, E.C. & Bertozzi, C. (1998). Synthesis of an oxime-linked neoglycopeptide with glycosylation-dependent activity similar to its native counterpart. *Tetrahedron Lett.* *39*, 8417–8420.
- Mardirossian, M., Pérébasquine, N., Benincasa, M., Gambato, S., Hofmann, S., Huter, P., Müller, C., Hilpert, K., Innis, C.A., Tossi, A., Wilson, D.N. (2018). The dolphin Proline-Rich Antimicrobial Peptide Tur1A inhibits protein synthesis by targeting the bacterial ribosome. *Cell Chem Biol* *25*, 530-539.
- Marino, J., von Heijne, G. & Beckmann, R. (2016). Small protein domains fold inside the ribosome exit tunnel. *FEBS Lett* *590*, 655–660.
- Marsden, A.P., Hollins, J.J., O'Neill, C., Ryzhov, P., Higson, S., Mendonça, C.A.T.F., Kwan, T.O., Kwa, L.G., Steward, A., Clarke, J. (2018). Investigating the effect of chain connectivity on the folding of a beta-sheet protein on and off the ribosome. *J Mol Biol* *430*, 5207-5216.
- McCutcheon, J.P., Agrawal, R.K., Philips, S.M., Grassucci, R.A., Gerchman, S.E., Clemons, W.M., Ramakrishnan, V., and Frank, J. (1999). Location of translational initiation factor IF3 on the small ribosomal subunit. *Proc Natl Acad Sci USA* *96*, 4301-4306.
- Meteliev, M., Osterman, I.A., Ghilarov, D., Khabibullina, N.F., Komarova, E.S., Travin, D.Y., Komarova, E.S., Serebryakova, M., Artamonova, T., Khodorkovskii, M., Konevega, A.L., Sergiev, P.V., Severinov, K., Polikanov, Y.S. (2017). Klebsazolicin inhibits 70S ribosome by obstructing the peptide exit tunnel. *Nat Chem Biol* *13*, 1129–1136.
- Meydan, S., Marks, J., Klepacki, D., Sharma, V., Baranov, P.V., Firth, A.E., Margus, T., Kefi, A., Vázquez-Laslop, N., Mankin, A.S. (2019). Retapamulin-Assisted Ribosome Profiling Reveals the Alternative Bacterial Proteome. *Mol Cell* *74*, 481-493.
- Milon, P., Konevega, A.L., Gualerzi, C.O., and Rodnina, M.V. (2008). Kinetic checkpoint at a late step in translation initiation. *Mol Cell* *30*, 712-720.
- Milon, P., Carotti, M., Konevega, A.L., Wintermeyer, W., Rodnina, M.V., and Gualerzi, C.O. (2010). The ribosome-bound initiation factor 2 recruits initiator tRNA to the 30S initiation complex. *EMBO Rep* *11*, 312-316.

Milon, P., and Rodnina, M.V. (2012a). Kinetic control of translation initiation in bacteria. *Crit Rev Biochem Mol Biol* 47, 334-348.

Milon, P., Maracci, C., Filonava, L., Gualerzi, C.O., and Rodnina, M.V. (2012b). Real-time assembly landscape of bacterial 30S translation initiation complex. *Nat Struct Mol Biol* 19, 609-615.

Mironova R.S., Xu J., AbouHaidar M.G., Ivanov I.G. (1999). Efficiency of a novel non-Shine-Dalgarno and a Shine-Dalgarno consensus sequence to initiate translation in *Escherichia coli* of genes with different downstream box composition. *Microbiol Res* 154, 35-41.

Moazed, D., Robertson, J.M., and Noller, H.F. (1988). Interaction of elongation factors EF-G and EF-Tu with a conserved loop in 23S RNA. *Nature* 334, 362-364.

Moazed, D., and Noller, H.F. (1989). Intermediate states in the movement of transfer RNA in the ribosome. *Nature* 342, 142-148.

Monro, R.E. (1967). Catalysis of peptide bond formation by 50 s ribosomal subunits from *Escherichia coli*. *Journal of Molecular Biology* 26, 147-151.

Mora, L., Heurgue-Hamard, V., Champ, S., Ehrenberg, M., Kisselev, L.L., and Buckingham, R.H. (2003). The essential role of the invariant GGQ motif in the function and stability in vivo of bacterial release factors RF1 and RF2. *Mol Microbiol* 47, 267-275.

Morse, J.C., Girodat, D., Burnett, B.J., Holm, M., Altman, R.B., Sanbonmatsu, K.Y., Wieden, H.-J., and Blanchard, S.C. (2020). Elongation factor-Tu can repetitively engage. *Proc Natl Acad Sci U S A* 117, 3610-3620.

Mortensen, K.K., Kildsgaard, J., Moreno, J.M., Steffensen, S.A., Egebjerg, J., and Sperling-Petersen, H.U. (1998). A six-domain structural model for *Escherichia coli* translation initiation factor IF2. Characterisation of twelve surface epitopes. *Biochem Mol Biol Int* 46, 1027-1041.

Munro, J.B., Wasserman, M.R., Altman, R.B., Wang, L., and Blanchard, S.C. (2010). Correlated conformational events in EF-G and the ribosome regulate translocation. *Nat Struct Mol Biol* 17, 1470-1477.

Murzin A.G. (1993). OB (oligonucleotide/oligosaccharide binding)-fold: common structural and functional solution for non-homologous sequences. *EMBO J.* 12, 861-867.

- Mustafi, M., and Weisshaar, J.C. (2018). Simultaneous Binding of Multiple EF-Tu Copies to Translating Ribosomes in Live *Escherichia coli*. *mBio* 9, e02143-02117.
- Mustoe, A.M., Busan, S., Rice, G.M., Hajdin, C.E., Peterson, B.K., Ruda, V.M., Kubica, N., Nutiu, R., Baryza, J.L., and Weeks, K.M. (2018). Pervasive Regulatory Functions of mRNA Structure Revealed by High-Resolution SHAPE Probing. *Cell* 173, 181-195.
- Muta, M., Iizuka, R., Niwa, T., Guo, Y., Taguchi, H., Funatsu, T. (2020). Nascent SecM chain interacts with outer ribosomal surface to stabilize translation arrest. *Biochem J* 477, 557-566.
- Muto, H., Nakatogawa, H. & Ito, K. (2006). Genetically encoded but nonpolypeptide prolyl-tRNA functions in the A site for SecM-mediated ribosomal stall. *Mol Cell* 22, 545–552.
- Myasnikov, A., Marzi, S., Simonetti, A., Giuliadori, A., Gualerzi, C., Yusupova, G., Yusupov, M., and Klaholz, B. (2005). Conformational transition of initiation factor 2 from the GTP- to GDP-bound state visualized on the ribosome. *Nat Struct Mol Biol* 12, 1145-1149.
- Nakano, H., Yoshida, T., Uchiyama, S., Kawachi, M., Matsuo, H., Kato, T., Ohshima, A., Yamaichi, Y., Honda, T., Kato, H., *et al.* (2003). Structure and binding mode of a ribosome recycling factor (RRF) from mesophilic bacterium. *J Biol Chem* 278, 3427-3436.
- Nakatogawa, H. & Ito, K. (2001). Secretionmonmr, SecM, undergoes selftranslation arrest in the cytosol. *Mol Cell* 7, 185–192.
- Nakatogawa H., Ito, K. (2002). The ribosomal exit tunnel functions as a discriminating gate., *Cell* 108, 629-636.
- Nakatogawa, H., Murakami, A. & Ito, K. (2004). Control of SecA and SecM translation by protein secretion. *Curr Opin Microbiol* 7, 145–150.
- Nguyen, F., Starosta, A.L., Arenz, S., Sohmen, D., Dönhöfer, A., Wilson, D.N. (2014). Tetracycline antibiotics and resistance mechanisms. *Biol Chem* 395, 559–575.
- Nicolaou, K.C., Chen, J.S., Edmonds, D.J., and Estrada, A.A. (2009). Recent advances in the chemistry and biology of naturally occurring antibiotics. *Angew Chem Int Ed Engl* 48, 660–719.

Nierhaus, K.H. (1991). The assembly of prokaryotic ribosomes. *Biochimie* 73, 739-755.

Nilsson, O.B., Hedman, R., Marino, J., Wickles, S., Bischoff, L., Johansson, M., Müller-Lucks, A., Trovato, F., Puglisi, J.D., O'Brien, E.P., Beckmann, R., von Heijne, G. (2015). Cotranslational protein folding inside the ribosome exit tunnel. *Cell Rep* 12, 1533-1540.

Nilsson, O.B., Muller-Lucks, A., Kramer, G., Bukau, B. & von Heijne, G. (2016). Trigger factor reduces the force exerted on the nascent chain by a cotranslationally folding protein. *J Mol Biol* 428, 1356–1364.

Nilsson, O.B., Nickson, A.A., Hollins, J.J., Wickles, S., Steward, A., Beckmann, R., von Heijne, G., Clarke, J. (2017). Cotranslational folding of spectrin domains via partially structured states. *Nat Struct Mol Biol* 24, 221-225.

Nishizuka, Y., and Lipmann, F. (1966). The interrelationship between guanosine triphosphatase and amino acid polymerization. *Archives of Biochemistry and Biophysics* 116, 344-351.

Nissen, P., Kjeldgaard, M., Thirup, S., Polekhina, G., Reshetnikova, L., Clark, B.F., and Nyborg, J. (1995). Crystal structure of the ternary complex of Phe-tRNA^{Phe}, EF-Tu, and a GTP analog. *Science* 270, 1464-1472.

Nissen, P., Thirup, S., Kjeldgaard, M., and Nyborg, J. (1999). The crystal structure of Cys-tRNA^{Cys}-EF-Tu-GDPNP reveals general and specific features in the ternary complex and in tRNA. *Structure* 7, 143-156.

Nissen, P., Hansen, J., Ban, N., Moore, P.B., and Steitz, T.A. (2000). The structural basis of ribosome activity in peptide bond synthesis. *Science* 289, 920-930.

Noeske, J., Huang, J., Olivier, N.B., Giacobbe, R.A., Zambrowski, M., and Cate, J.H. (2014). Synergy of streptogramin antibiotics occurs independently of their effects on translation. *Antimicrob. Agents Chemother.* 58, 5269–5279.

Noller, H.F. (2012). Evolution of protein synthesis from an RNA world. *Cold Spring Harb Perspect Biol* 4, a003681.

Notari, L., Martinez-Carranza, M., Farias-Rico, J.A., Stenmark, P. & von Heijne, G. (2018). Cotranslational folding of a pentarepeat beta-helix protein. *J Mol Biol* 430, 5196–5206.

O'Connor, M., Gregory, S.T., Rajbhandary, U.L., and Dahlberg, A.E. (2001). Altered discrimination of start codons and initiator tRNAs by mutant initiation factor 3. *Rna A Publication of the Rna Society* 7, 969-978.

Ogle, J.M., Brodersen, D.E., Clemons, W.M., Jr., Tarry, M.J., Carter, A.P., and Ramakrishnan, V. (2001). Recognition of cognate transfer RNA by the 30S ribosomal subunit. *Science* 292, 897-902.

Ogle, J.M., Brodersen, D.E., Clemons Jr, W.M., Tarry, M.J., Carter, A.P., and Ogle, J.M., Murphy, F.V., Tarry, M.J., and Ramakrishnan, V. (2002). Selection of tRNA by the ribosome requires a transition from an open to a closed form. *Cell* 111, 721-732.

Olivier, N.B., Altman, R.B., Noeske, J., Basarab, G.S., Code, E., Ferguson, A.D., Gao, N., Huang, J., Juette, M.F., Livchak, S., Miller, M.D., Prince, D.B., Cate, J.H., Buurman, E.T., Blanchard, S.C. (2014). Negamycin induces translational stalling and miscoding by binding to the small subunit head domain of the *Escherichia coli* ribosome. *Proc Natl Acad Sci U S A* 111, 16274-16279.

Ortiz-Meoz R.F., Green R. (2011). Helix 69 is key for uniformity during substrate selection on the ribosome. *J Biol Chem* 286, 25604-25610.

Osterman, I.A., Khabibullina, N. F., Komarova, E. S., Kasatsky, P., Kartsev, V. G., Bogdanov, A. A., Dontsova O.A., Konevega A.L., Sergiev P.V., Polikanov Y.S. (2017). Madumycin II inhibits peptide bond formation by forcing the peptidyl transferase center into an inactive state. *Nucleic Acids Res.* 45, 7507–7514.

Otvos, L. Jr. O.I., Rogers, M.E., Consolvo, P.J., Condie, B.A., Lovas, S., Bulet, P., Blaszczyk-Thurin, M. (2000). Interaction between heat shock proteins and antimicrobial peptides. *Biochemistry* 39, 14150-14149.

Pallesen, J., Hashem, Y., Korkmaz, G., Koripella, R.K., Huang, C., Ehrenberg, M., Sanyal, S., and Frank, J. (2013). Cryo-EM visualization of the ribosome in termination complex with apo-RF3 and RF1. *Elife* 2, e00411.

Pan, D., Kirillov, S.V., Cooperman, B.S. (2007). Kinetically competent intermediates in the translocation step of protein synthesis. *Mol Cell* 25, 519–529.

Pantel, L., Florin, T., Dobosz-Bartoszek, M., Racine, E., Sarciaux, M., Serri, M., Houard, J., Campagne, J.M., de Figueiredo, R.M., Midrier, C., Gaudriault, S., Givaudan, A., Lanois, A., Forst, S., Aumelas, A., Cotteaux-Lautard, C., Bolla, J.M., Vingsbo Lundberg, C., Huseby, D.L., Hughes, D., Villain-Guillot, P., Mankin, A.S., Polikanov, Y.S., Gualtieri, M. (2018). Odilorhabdins, antibacterial agents that cause miscoding by binding at a new ribosomal site. *Mol Cell* 70, 83–94.

Pape, T., Wintermeyer, W., and Rodnina, M.V. (1998). Complete kinetic mechanism of elongation factor Tu-dependent binding of aminoacyl-tRNA to the A site of the E.coli ribosome. *EMBO J* 17, 7490-7497.

Pape, T., Wintermeyer, W., and Rodnina, M. (1999). Induced fit in initial selection and proofreading of aminoacyl-tRNA on the ribosome. *EMBO J* 18, 3800-3807.

Pavlov, M.Y., Freistroffer, D.V., Heurgue-Hamard, V., Buckingham, R.H., and Ehrenberg, M. (1997). Release factor RF3 abolishes competition between release factor RF1 and ribosome recycling factor (RRF) for a ribosome binding site. *J Mol Biol* 273, 389-401.

Pellowe, G.A., Findlay, H.E., Lee, K., Gemeinhardt, T.M., Blackholly, L.R., Reading, E., Booth, P.J. (2020). Capturing Membrane Protein Ribosome Nascent Chain Complexes in a Native-like Environment for Co-translational Studies. *Biochemistry* 59, 2764-2775.

Peske, F., Savelsbergh, A., Katunin, V.I., Rodnina, M.V., and Wintermeyer, W. (2004). Conformational changes of the small ribosomal subunit during elongation factor G-dependent tRNA-mRNA translocation. *J Mol Biol* 343, 1183–1194.

Peske, F., Rodnina, M., and Wintermeyer, W. (2005). Sequence of steps in ribosome recycling as defined by kinetic analysis. *Mol Cell* 18, 403-412.

Petry, S., Brodersen, D.E., Murphy, F.V.t., Dunham, C.M., Selmer, M., Tarry, M.J., Kelley, A.C., and Ramakrishnan, V. (2005). Crystal structures of the ribosome in complex with release factors RF1 and RF2 bound to a cognate stop codon. *Cell* 123, 1255-1266.

Petrychenko V., Peng B.Z., de A. P. Schwarzer A.C., Peske F., Rodnina M.V., Fischer N. (2021). Structural mechanism of GTPase-powered ribosome-tRNA movement. *Nat Commun* 12, 5933.

Pierson, W.E., Hoffer, E.D., Keedy, H.E., Simms, C.L., Dunham, C.M., and Zaher, H.S. (2016). Uniformity of Peptide Release Is Maintained by Methylation of Release Factors. *Cell Reports* 17, 11-18.

Pioletti, M., Schlunzen, F., Harms, J., Zarivach, R., Gluhmann, M., Avila, H., Bashan, A., Bartels, H., Auerbach, T., Jacobi, C., Hartsch, T., Yonath, A., Franceschi, F. (2001). Crystal structures of complexes of the small ribosomal subunit with tetracycline, edeine and IF3. *EMBO J* 20, 1829–1839.

Polacek, N., Gaynor, M., Yassin, A., and Mankin, A.S. (2001). Ribosomal peptidyl transferase can withstand mutations at the putative catalytic nucleotide. *Nature* *411*, 498-501.

Polikanov, Y.S., Steitz T.A., Innis C.A. (2014a). A proton wire to couple aminoacyl-tRNA accommodation and peptide-bond formation on the ribosome. *Nat Struct Mol Biol* *21*, 787-793.

Polikanov, Y.S., Szal, T., Jiang, F., Gupta, P., Matsuda, R., Shiozuka, M., Steitz, T.A., Vazquez-Laslop, N., Mankin, A.S. (2014b). Negamycin interferes with decoding and translocation by simultaneous interaction with rRNA and tRNA. *Mol Cell* *56*, 541–550.

Polikanov, Y.S., Osterman, I.A., Szal, T., Tashlitsky, V.N., Serebryakova, M.V., Kusochek, P., Bulkley, D., Malanicheva, I.A., Efimenko, T.A., Efremenkova, O.V., Konevega, A.L., Shaw, K.J., Bogdanov, A.A., Rodnina, M.V., Dontsova, O.A., Mankin, A.S., Steitz, T.A., Sergiev, P.V. (2014c). Amicoumacin A inhibits translation by stabilizing mRNA interaction with the ribosome. *Mol Cell* *56*, 531–540.

Polikanov, Y.S., Starosta, A.L., Juette, M.F., Altman, R.B., Terry, D.S., Lu, W., Burnett, B.J., Dinos, G., Reynolds, K.A., Blanchard, S.C., Steitz, T.A., Wilson, D.N. (2015). Distinct tRNA accommodation intermediates observed on the ribosome with the antibiotics Hygromycin A and A201A. *Mol Cell* *58*, 832–844.

Polikanov, Y.S. Nikolay A. Aleksashin, Beckert B. and Wilson, D. N. (2018). The mechanisms of action of ribosome-targeting peptide antibiotics. *Front Mol Biosci* *5*, 48.

Prabhakar, A., Capece, M.C., Petrov, A., Choi, J., and Puglisi, J.D. (2017). Posttermination Ribosome Intermediate Acts as the Gateway to Ribosome Recycling. *Cell Rep* *20*, 161-172.

Pulk, A., and Cate, J.H.D. (2013). Control of Ribosomal Subunit Rotation by Elongation Factor G. *Science* *340*, 1235970.

Qin, H., Grigoriadou, C., and Cooperman, B.S. (2009). Interaction of IF2 with the ribosomal GTPase-associated center during 70S initiation complex formation. *Biochemistry* *48*, 4699-4706.

Rabel, D., Charlet, M., Ehret-Sabatier, L., Cavicchioli, L., Cudic, M., Otvos, L. Jr, Bulet, P. (2004). Primary structure and in vitro antibacterial properties of the *Drosophila melanogaster* attacin C Pro-domain. *J Biol Chem* *279*, 14853-14859.

- RajBhandary U.L. (1994). Initiator transfer RNAs. *J Bacteriol* 176, 547-552.
- Ramakrishnan V.(2002). Ribosome structure and the mechanism of translation. *Cell* 108, 557-572.
- Ramu, H., Mankin, A., Vazquez-Laslop, N. (2009). Programmed drug-dependent ribosome stalling. *Mol Microbiol* 71, 811-824.
- Risuleo, G., Gualerzi, C., and Pon, C. (1976). Specificity and properties of the destabilization, induced by initiation factor IF-3, of ternary complexes of the 30S ribosomal subunit. *Eur J Biochem* 67, 603-613.
- Rodnina, M.V., Savelsbergh, A., Katunin, V.I., and Wintermeyer, W. (1997). Hydrolysis of GTP by elongation factor G drives tRNA movement on the ribosome. *Nature* 385, 37-41.
- Rodriguez, E.C., Winans, K.A., King, D.S. & Bertozzi, C.R. (1997). A strategy for the chemoselective synthesis of O-linked glycopeptides with native sugar-peptide linkages. *J Am Chem Soc* 113, 9905-9906.
- Roy, R.N., Lomakin, I.B., Gagnon, M.G., Steitz, T.A. (2015). The mechanism of inhibition of protein synthesis by the proline-rich peptide oncocin. *Nat Struct Mol Biol* 22, 466-469.
- Rozov, A., Demeshkina, N., Westhof, E., Yusupov, M., and Yusupova, G. (2015). Structural insights into the translational infidelity mechanism. *Nat Commun* 6, 7251.
- Rozov, A., Demeshkina, N., Khusainov, I., Westhof, E., Yusupov, M., and Yusupova, G. (2016a). Novel base-pairing interactions at the tRNA wobble position crucial for accurate reading of the genetic code. *Nat Commun* 7, 10457.
- Rozov, A., Westhof, E., Yusupov, M., and Yusupova, G. (2016b). The ribosome prohibits the G*U wobble geometry at the first position of the codon-anticodon helix. *Nucleic Acids Res* 44, 6434-6441.
- Rozov, A., Wolff, P., Grosjean, H., Yusupov, M., Yusupova, G., and Westhof, E. (2018). Tautomeric G*U pairs within the molecular ribosomal grip and fidelity of decoding in bacteria. *Nucleic Acids Res* 46, 7425-7435.
- Rundlet E.J., Holm M., Schacherl M., Natchiar S.K., Altman R.B., Spahn C.M.T., Myasnikov A.G., Blanchard S.C. (2021). Structural basis of early translocation events on the ribosome. *Nature* 595, 741-745.

Rychkova, A., Mukherjee, S., Bora, R.P. & Warshel, A. (2013). Simulating the pulling of stalled elongated peptide from the ribosome by the translocon. *Proc Natl Acad Sci USA* *110*, 10195–10200.

Saikrishnan, K., Kalapala, S., Varshney, U., and Vijayan, M. (2005). X-ray structural studies of *Mycobacterium tuberculosis* RRF and a comparative study of RRFs of known structure. Molecular plasticity and biological implications. *J Mol Biol* *345*, 29–38.

Sakiyama, K., Shimokawa-Chiba, N., Fujiwara, K., Chiba, S. (2021). Search for translation arrest peptides encoded upstream of genes for components of protein localization pathways. *Nucleic Acids Res* *49*, 1550-1566.

Salsi, E., Farah, E., Netter, Z., Dann, J., and Ermolenko, D.N. (2015). Movement of Elongation Factor G between Compact and Extended Conformations. *Journal of Molecular Biology* *427*, 454-467.

Samaha, R.R., Green, R., and Noller, H.F. (1995). A base pair between tRNA and 23S rRNA in the peptidyl transferase center of the ribosome. *Nature* *377*, 309-314.

Sanbonmatsu, K.Y., Joseph, S., and Tung, C.S. (2005). Simulating movement of tRNA into the ribosome during decoding. *Proc Natl Acad Sci U S A* *102*, 15854-15859.

Sauna, Z. and Kimchi-Sarfaty, C. (2011). Understanding the contribution of synonymous mutations to human disease. *Nat Rev Genet* *12*, 683–691.

Savelsbergh, A., Rodnina, M.V., Wintermeyer, W. (2009). Distinct functions of elongation factor G in ribosome recycling and translocation. *RNA* *15*, 772–780.

Schaffitzel, C. & Ban, N. (2007). Generation of ribosome nascent chain complexes for structural and functional studies. *J Struct Biol* *158*, 463–471.

Schlunzen, F., Takemoto, C., Wilson, D.N., Kaminishi, T., Harms, J.M., Hanawa-Suetsugu, K., Szaflarski, W., Kawazoe, M., Shirouzu, M., Nierhaus KH, Yokoyama, S., Fucini, P. (2006). The antibiotic kasugamycin mimics mRNA nucleotides to destabilize tRNA binding and inhibit canonical translation initiation. *Nat Struct Mol Biol* *13*, 871–878.

Schlünzen F., Zarivach R., Harms J., Bashan A., Tocilj A., Albrecht R., Yonath A., Franceschi F. (2001). Structural basis for the interaction of antibiotics with the peptidyl transferase centre in eubacteria. *Nature* *413*, 814-821.

Schmeing, T.M., Seila, A.C., Hansen, J.L., Freeborn, B., Soukup, J.K., Scaringe, S.A., Strobel, S.A., Moore, P.B., and Steitz, T.A. (2002). A pre-translocational intermediate in protein synthesis observed in crystals of enzymatically active 50S subunits. *Nature Structural Biology* 9, 225-230.

Schmeing, T.M., Huang, K.S., Kitchen, D.E., Strobel, S.A., and Steitz, T.A. (2005a). Structural insights into the roles of water and the 2' hydroxyl of the P site tRNA in the peptidyl transferase reaction. *Mol Cell* 20, 437-448.

Schmeing, T.M., Huang, K.S., Strobel, S.A., and Steitz, T.A. (2005b). An induced-fit mechanism to promote peptide bond formation and exclude hydrolysis of peptidyltRNA. *Nature* 438, 520-524.

Schmeing, T.M., and Ramakrishnan, V. (2009). What recent ribosome structures have revealed about the mechanism of translation. *Nature* 461, 1234.

Schmitt, E., Panvert, M., Blanquet, S., and Mechulam, Y. (1998). Crystal structure of methionyl-tRNA^{fMet} transformylase complexed with the initiator formyl-methionyl-tRNA^{fMet}. *EMBO J* 17, 6819-6826.

Schuwirth, B.S., Borovinskaya, M.A., Hau, C.W., Zhang, W., Vila-Sanjurjo, A., Holton, J.M., and Cate, J.H. (2005). Structures of the bacterial ribosome at 3.5 Å resolution. *Science* 310, 827-834.

Schuwirth, B.S., Day, J.M., Hau, C.W., Janssen, G.R., Dahlberg, A.E., Cate, J.H., Vila-Sanjurjo, A. (2006). Structural analysis of kasugamycin inhibition of translation. *Nat Struct Mol Biol* 13, 879–886.

Scocchi, M., Tossi, A., Gennaro, R. 2011. Proline-rich antimicrobial peptides: converging to a non-lytic mechanism of action. *Cell Mol Life Sci* 68, 2317-2330.

Seefeldt, A.C., Nguyen, F., Antunes, S., Perebaskine, N., Graf, M., Arenz, S., Inampudi, K.K., Douat, C., Guichard, G., Wilson, D.N., Innis, C.A. (2015). The proline-rich antimicrobial peptide Oncl12 inhibits translation by blocking and destabilizing the initiation complex. *Nat Struct Mol Biol* 22, 470-475.

Seefeldt, A.C., Graf, M., Pérébaskine, N., Nguyen, F., Arenz, S., Mardirossian, M., Scocchi, M., Wilson, D.N., Innis, C.A. (2016). Structure of the mammalian antimicrobial peptide Bac7(1-16) bound within the exit tunnel of a bacterial ribosome. *Nucleic Acids Res* 44, 2429-2438.

Seidelt, B., Innis, C.A., Wilson, D.N., Gartmann, M., Armache, J.-P., Villa, E., Trabuco, L.G., Becker, T., Mielke, T., Schulten, K., Steitz T.A., Beckmann R. (2009).

Structural insight into nascent polypeptide chain-mediated translational stalling. *Science* 326, 1412.

Seit-Nebi, A., Frolova, L., Justesen, J., and Kisselev, L. (2001). Class-1 translation termination factors: invariant GGQ minidomain is essential for release activity and ribosome binding but not for stop codon recognition. *Nucleic Acids Research* 29, 3982-3987.

Selmer, M., Al-Karadaghi, S., Hirakawa, G., Kaji, A., and Liljas, A. (1999). Crystal structure of *Thermotoga maritima* ribosome recycling factor: A tRNA mimic. *Science* 286, 2349-2352.

Selmer, M., Dunham, C.M., Murphy, F.V.t., Weixlbaumer, A., Petry, S., Kelley, A.C., Weir, J.R., and Ramakrishnan, V. (2006). Structure of the 70S ribosome complexed with mRNA and tRNA. *Science* 313, 1935-1942.

Seong, B.L., and RajBhandary, U.L. (1987a). *Escherichia coli* formylmethionine tRNA: mutations in GGGCCC sequence conserved in anticodon stem of initiator tRNAs affect initiation of protein synthesis and conformation of anticodon loop. *Proceedings of the National Academy of Sciences* 84, 334.

Seong, B.L., and RajBhandary, U.L. (1987b). Mutants of *Escherichia coli* formylmethionine tRNA: a single base change enables initiator tRNA to act as an elongator in vitro. *Proceedings of the National Academy of Sciences* 84, 8859.

Sette, M., van Tilborg, P., Spurio, R., Kaptein, R., Paci, M., Gualerzi, C.O., and Boelens, R. (1997). The structure of the translational initiation factor IF1 from *E.coli* contains an oligomer-binding motif. *EMBO J* 16, 1436-1443.

Sharma, P.K., Xiang, Y., Kato, M. and Warshel, A. 2005. What are the roles of substrate-assisted catalysis and proximity effects in peptide bond formation by the ribosome? *Biochemistry* 44, 11307-11314.

Sharma, H., Adio, S., Senyushkina, T., Belardinelli, R., Peske, F., and Rodnina, M.V. (2016). Kinetics of Spontaneous and EF-G-Accelerated Rotation of Ribosomal Subunits. *Cell Rep* 16, 2187-2196.

Shaw, J.J., and Green, R. (2007). Two distinct components of release factor function uncovered by nucleophile partitioning analysis. *Mol Cell* 28, 458-467.

Shin, D.H., Brandsen, J., Jancarik, J., Yokota, H., Kim, R., and Kim, S.H. (2004). Structural analyses of peptide release factor 1 from *Thermotoga maritima* reveal

domain flexibility required for its interaction with the ribosome. *J Mol Biol* 341, 227-239.

Shine J., Dalgarno L. (1974). The 3'-terminal sequence of *Escherichia coli* 16S ribosomal RNA: complementarity to nonsense triplets and ribosome binding sites. *Proc Natl Acad Sci U S A*. 71,1342-1346.

Shoji, S., Walker, S.E., and Fredrick, K. (2006). Reverse translocation of tRNA in the ribosome. *Mol Cell* 24, 931-942.

Sievers, A., Beringer, M., Rodnina, M.V., and Wolfenden, R. (2004). The ribosome as an entropy trap. *Proc Natl Acad Sci U S A* 101, 7897.

Simonetti, A., Marzi, S., Myasnikov, A.G., Fabbretti, A., Yusupov, M., Gualerzi, C.O., and Klaholz, B.P. (2008). Structure of the 30S translation initiation complex. *Nature* 455, 416-420.

Simonetti, A., Marzi, S., Billas, I.M.L., Tsai, A., Fabbretti, A., Myasnikov, A.G., Roblin, P., Vaiana, A.C., Hazemann, I., Eiler, D., *et al.* (2013). Involvement of protein IF2 N domain in ribosomal subunit joining revealed from architecture and function of the fulllength initiation factor. *Proceedings of the National Academy of Sciences* 110, 15656.

Sohmen, D., Harms, J.M., Schlünzen, F., Wilson, D.N. (2009). Enhanced SnapShot: Antibiotic inhibition of protein synthesis II. *Cell* 139, 212-212.

Sohmen, D., Chiba, S., Shimokawa-Chiba, N., Innis, C.A., Berninghausen, O., Beckmann, R., Ito, K., Wilson, D.N. (2015). Structure of the *Bacillus subtilis* 70S ribosome reveals the basis for species-specific stalling. *Nat Commun* 6, 6941.

Sørensen H.P., Hedegaard J., Sperling-Petersen H.U., Mortensen K.K. (2001). Remarkable conservation of translation initiation factors: IF1/eIF1A and IF2/eIF5B are universally distributed phylogenetic markers. *IUBMB Life* 51, 321-327.

Spevak, C.C., Ivanov, I.P., Sachs, M.S. (2010). Sequence requirements for ribosome stalling by the arginine attenuator peptide. *J Biol Chem* 285, 40933-40942.

Spiegel, P.C., Ermolenko, D.N., and Noller, H.F. (2007). Elongation factor G stabilizes the hybrid-state conformation of the 70S ribosome. *RNA* 13, 1473-1482.

Sprink T., Ramrath D.J., Yamamoto H., Yamamoto K., Loerke J., Ismer J., Hildebrand P.W., Scheerer P., Bürger J., Mielke T., Spahn C.M. (2016). Structures of ribosome-

bound initiation factor 2 reveal the mechanism of subunit association. *Sci Adv* *2*,e1501502

Stanley, R.E., Blaha, G., Grodzicki, R.L., Strickler, M.D., Steitz, T.A. (2010). The structures of the anti-tuberculosis antibiotics viomycin and capreomycin bound to the 70S ribosome. *Nat Struct Mol Biol* *17*, 289–293.

Stark, H., Rodnina, M.V., Rinkeappell, J., Brimacombe, R., Wintermeyer, W., and Vanheer, M. (1997). Visualization of Elongation Factor Tu On the *Escherichia coli* Ribosome. *Nature* *389*, 403-406.

Su, T., Cheng, J., Sohmen, D., Hedman, R., Berninghausen, O., von Heijne, G., Wilson, D.N., Beckmann, R. (2017). The force-sensing peptide VemP employs extreme compaction and secondary structure formation to induce ribosomal stalling. *Elife* *6*, e25642.

Sundari, R.M., Stringer, E.A., Schulman, L.H., and Maitra, U. (1976). Interaction of bacterial initiation factor 2 with initiator tRNA. *Journal of Biological Chemistry* *251*, 3338-3345.

Sussman, J.K., Simons, E.L., and Simons, R.W. (1996). *Escherichia coli* translation initiation factor 3 discriminates the initiation codon *in vivo*. *Mol Microbiol* *21*, 347-360.

Svetlov, M.S., Cohen, S., Alsuhebany, N., Vazquez-Laslop, N. & Mankin, A.S. (2020). A long-distance rRNA base pair impacts the ability of macrolide antibiotics to kill bacteria. *Proc Natl Acad Sci USA* *117*, 1971–1975.

Svidritskiy, E., Ling, C., Ermolenko, D.N., Korostelev, A.A. (2013). Blastocidin S inhibits translation by trapping deformed tRNA on the ribosome. *Proc Natl Acad Sci* *110*, 12283–12288.

Syroegin, E.A., Flemmich, L., Klepacki, D., Vazquez-Laslop, N., Micura, R., Polikanov, Y.S. (2022). Structural basis for the context-specific action of the classic peptidyl transferase inhibitor chloramphenicol. *Nat Struct Mol Biol* *29*, 152-161.

Syroegin, E.A., Aleksandrova, E.V., Polikanov, Y.S. (2023). Insights into the ribosome function from the structures of non-arrested ribosome-nascent chain complexes. *Nat Chem* *15*, 143-153.

Takahashi, S., Iida, M., Furusawa, H., Shimizu, Y., Ueda, T., Okahata, Y. (2009). Real-time monitoring of cell-free translation on a quartz-crystal microbalance. *J Am Chem Soc* *131*, 9326-9332.

Talat, S., Thiruvikraman, M., Kumari, S. & Kaur, K. J. (2011). Glycosylated analogs of formaecin I and drosocin exhibit differential pattern of antibacterial activity. *Glycoconj. J.* 28, 537–555.

Tate, W.P., and Brown, C.M. (1992). Translational termination: "stop" for protein synthesis or "pause" for regulation of gene expression. *Biochemistry* 31, 2443-2450.

Thomas, M. G., Chan, Y. A., and Ozanick, S. G. (2003). Deciphering tuberactinomycin biosynthesis: isolation, sequencing, and annotation of the viomycin biosynthetic gene cluster. *Antimicrob. Agents Chemother* 47, 2823–2830

Thompson, R.C., and Stone, P.J. (1977). Proofreading of the codon-anticodon interaction on ribosomes. *Proceedings of the National Academy of Sciences* 74, 198.

Tourigny, D.S., Fernandez, I.S., Kelley, A.C., and Ramakrishnan, V. (2013). Elongation factor G bound to the ribosome in an intermediate state of translocation. *Science* 340, 1235490.

Toyoda, T., Tin, O.F., Ito, K., Fujiwara, T., Kumasaka, T., Yamamoto, M., Garber, M.B., and Nakamura, Y. (2000). Crystal structure combined with genetic analysis of the *Thermus thermophilus* ribosome recycling factor shows that a flexible hinge may act as a functional switch. *RNA* 6, 1432-1444.

Trobro S., Aqvist J. (2009). Mechanism of the translation termination reaction on the ribosome. *Biochemistry* 48, 11296-11303.

Tsai, A., Kornberg, G., Johansson, M., Chen, J. & Puglisi, J.D. (2014). The dynamics of SecM-induced translational stalling. *Cell Rep* 7, 1521–1533.

Tu, D., Blaha, G., Moore, P.B., and Steitz, T.A. (2005). Structures of MLSBK antibiotics bound to mutated large ribosomal subunits provide a structural explanation for resistance. *Cell* 121, 257–270.

Uemura, S., Iizuka, R., Ueno, T., Shimizu, Y., Taguchi, H., Ueda, T., Puglisi, J.D., Funatsu, T. (2008). Single-molecule imaging of full protein synthesis by immobilized ribosomes. *Nucleic Acids Res* 36, e70.

Uttenweiler-Joseph, S., Moniatte, M., Lagueux, M., Van Dorsselaer, A., Hoffmann, J.A., Bulet, P. (1998). Differential display of peptides induced during the immune response of *Drosophila*: a matrix-assisted laser desorption ionization time-of-flight mass spectrometry study. *Proc Natl Acad Sci U S A* 95, 11342-11347.

- VanLoock, M.S., Agrawal, R.K., Gabashvili, I.S., Qi, L., Frank, J., and Harvey, S.C. (2000). Movement of the decoding region of the 16 S ribosomal RNA accompanies tRNA translocation. *J Mol Biol* 304, 507-515.
- Vannuffel, P., and Cocito, C. (1996). Mechanism of action of streptogramins and macrolides. *Drugs* 51(Suppl. 1), 20–30.
- Vazquez-Laslop, N., Thum, C., Mankin, A.S. (2008). Molecular mechanism of drug-dependent ribosome stalling. *Mol Cell* 30, 190-202.
- Vazquez-Laslop, N., Mankin, A.S. (2014). Triggering peptide-dependent translation arrest by small molecules: ribosome stalling modulated by antibiotics. In *Regulatory Nascent Polypeptides*. Edited by Ito K. Springer; 2014, 165-186.
- Vestergaard, B., Van, L.B., Andersen, G.R., Nyborg, J., Buckingham, R.H., and Kjeldgaard, M. (2001). Bacterial Polypeptide Release Factor RF2 Is Structurally Distinct from Eukaryotic eRF1. *Molecular Cell* 8, 1375-1382.
- Voorhees, R.M., Weixlbaumer, A., Loakes, D., Kelley, A.C., and Ramakrishnan, V. (2009). Insights into substrate stabilization from snapshots of the peptidyl transferase center of the intact 70S ribosome. *Nat Struct Mol Biol* 16, 528-533.
- Voorhees, R.M., Schmeing, T.M., Kelley, A.C., and Ramakrishnan, V. (2010). The mechanism for activation of GTP hydrolysis on the ribosome. *Science* 330, 835-838.
- Voss N.R., Gerstein M., Steitz T.A., Moore P.B. (2006). The geometry of the ribosomal polypeptide exit tunnel. *J Mol Biol* 360, 893-906.
- Wang, Z., Fang, P., Sachs, M.S. (1998). The evolutionarily conserved eukaryotic arginine attenuator peptide regulates the movement of ribosomes that have translated it. *Mol Cell Biol* 18, 7528-7536.
- Wang, L., Pulk, A., Wasserman, M.R., Feldman, M.B., Altman, R.B., Cate, J.H., Blanchard, S.C. (2012). Allosteric control of the ribosome by small-molecule antibiotics. *Nat Struct Mol Biol* 19, 957–963.
- Weigert, M.G., and Garen, A. (1965). Base composition of non-sense codons in *E.coli*. *Nature* 206, 992.
- Weinger, J.S., Parnell, K.M., Dorner, S., Green, R. and Strobel, S.A. 2004. Substrate-assisted catalysis of peptide bond formation by the ribosome. *Nat Struct Mol Biol* 11, 1101–1106.

Weixlbaumer, A., Petry, S., Dunham, C.M., Selmer, M., Kelley, A.C., and Ramakrishnan, V. (2007). Crystal structure of the ribosome recycling factor bound to the ribosome. *Nat Struct Mol Biol* 14, 733-737.

Weixlbaumer, A., Jin, H., Neubauer, C., Voorhees, R.M., Petry, S., Kelley, A.C., and Ramakrishnan, V. (2008). Insights into translational termination from the structure of RF2 bound to the ribosome. *Science* 322, 953-956.

Wieden H.J., Wintermeyer W., Rodnina M.V. (2001). A common structural motif in elongation factor Ts and ribosomal protein L7/12 may be involved in the interaction with elongation factor Tu. *J Mol Evol* 52, 129-136.

Wilson, D.N., and Nierhaus, K.H. (2005). Ribosomal Proteins in the Spotlight. *Crit Rev Biochem Mol Biol* 40, 243-267.

Wilson, D.N. (2009). The A–Z of bacterial translation inhibitors. *Crit Rev Biochem Mol Biol* 44, 393–433.

Wilson, D.N., Beckmann, R. (2011). The ribosomal tunnel as a functional environment for nascent polypeptide folding and translational stalling. *Curr Opin Struct Biol* 21, 274-282

Wilson, D.N. (2014). Ribosome-targeting antibiotics and bacterial resistance mechanisms. *Nat Rev Microbiol* 12, 35–48.

Wilson, D.N., Arenz, S., Beckmann, R. (2016). Translation regulation via nascent polypeptide-mediated ribosome stalling. *Curr Opin Struct Biol* 37, 123-133.

Wohlgemuth, I., Beringer, M., and Rodnina, M.V. (2006). Rapid peptide bond formation on isolated 50S ribosomal subunits. *EMBO reports* 7, 699-703.

Wohlgemuth, I., Pohl, C., and Rodnina, M.V. (2010). Optimization of speed and accuracy of decoding in translation. *EMBO J* 29, 3701-3709.

Woo, N.H., Roe, B.A., and Rich, A. (1980). Three-dimensional structure of *Escherichia coli* initiator tRNA^{fMet}. *Nature* 286, 346-351.

Wood, E., Schulenburg, H., Rosenstiel, P., Bergmiller, T., Ankrett, D., Gudelj, I., Beardmore, R. (2023). Ribosome-binding antibiotics increase bacterial longevity and growth efficiency. *Proc Natl Acad Sci U S A* 120, e2221507120.

Woolhead, C.A., Johnson, A.E. & Bernstein, H.D. (2006). Translation arrest requires two-way communication between a nascent polypeptide and the ribosome. *Mol Cell* 22, 587–598.

Woolstenhulme, C.J., Parajuli, S., Healey, D.W., Valverde, D.P., Petersen, E.N., Starosta, A.L., Guydosh, N.R., Johnson, W.E., Wilson, D.N., Buskirk, A.R. (2013). Nascent peptides that block protein synthesis in bacteria. *Proc Natl Acad Sci U S A* *110*, 878-887.

Wrede P., Woo N.H., Rich A. (1979). Initiator tRNAs have a unique anticodon loop conformation. *Proc Natl Acad Sci U S A*. *76*, 3289-3293.

Wu, X.-Q., and RajBhandary, U.L. (1997). Effect of the Amino Acid Attached to Escherichia coli Initiator tRNA on Its Affinity for the Initiation Factor IF2 and on the IF2 Dependence of Its Binding to the Ribosome. *Journal of Biological Chemistry* *272*, 1891-1895.

Yang, Z., Iizuka, R. & Funatsu, T. (2015). Nascent SecM chain outside the ribosome reinforces translation arrest. *PLoS ONE* *10*, e0122017.

Yang, K., Chang, J.Y., Cui, Z., Li, X., Meng, R., Duan, L., Thongchol, J., Jakana, J., Huwe, C.M., Sacchettini, J.C., Zhang, J. (2017). Structural insights into species-specific features of the ribosome from the human pathogen *Mycobacterium tuberculosis*. *Nucleic Acids Res* *45*, 10884-10894.

Yap, M.N. & Bernstein, H.D. (2009). The plasticity of a translation arrestmotif yields insights into nascent polypeptide recognition inside the ribosome tunnel. *Mol Cell* *34*, 201–211 (2009).

Yokoyama, T., Shaikh, T.R., Iwakura, N., Kaji, H., Kaji, A., and Agrawal, R.K. (2012). Structural insights into initial and intermediate steps of the ribosome-recycling process. *EMBO J* *31*, 1836-1846.

Yoshida, T., Uchiyama, S., Nakano, H., Kashimori, H., Kijima, H., Ohshima, T., Saihara, Y., Ishino, T., Shimahara, H., Yoshida, T., *et al.* (2001). Solution Structure of the Ribosome Recycling Factor from *Aquifex aeolicus*. *Biochemistry* *40*, 2387-2396.

Youngman E.M., Brunelle J.L., Kochaniak A.B., Green R. (2004). The active site of the ribosome is composed of two layers of conserved nucleotides with distinct roles in peptide bond formation and peptide release. *Cell* *117*, 589-599.

Youngman, E.M., McDonald, M.E., and Green, R. (2008). Peptide release on the ribosome: mechanism and implications for translational control. *Annu Rev Microbiol* *62*, 353-373.

Yusupov, M.M., Yusupova, G.Z., Baucom, A., Lieberman, K., Earnest, T.N., Cate, J.H., and Noller, H.F. (2001). Crystal structure of the ribosome at 5.5 Å resolution. *Science* 292, 883-896.

Yusupova, G.Z., Yusupov, M.M., Cate, J.H., and Noller, H.F. (2001). The path of messenger RNA through the ribosome. *Cell* 106, 233-241.

Zavialov, A.V., Hauryliuk, V.V., and Ehrenberg, M. (2005). Splitting of the posttermination ribosome into subunits by the concerted action of RRF and EF-G. *Mol Cell* 18, 675-686.

Zeng, F., and Jin, H. (2018). Conformation of methylated GGQ in the Peptidyl Transferase Center during Translation Termination. *Scientific Reports* 8, 2349.

Zhang, J., Jeong, K.-W., Johansson, M., and Ehrenberg, M. (2015a). Accuracy of initial codon selection by aminoacyl-tRNAs on the mRNA-programmed bacterial ribosome. *Proceedings of the National Academy of Sciences* 112, 9602.

Zhang, J., Pan, X., Yan, K., Sun, S., Gao, N., Sui, S.F. (2015b). Mechanisms of ribosome stalling by SecM at multiple elongation steps. *Elife* 4, e09684.

Zhou, J., Korostelev, A., Lancaster, L., and Noller, H.F. (2012a). Crystal structures of 70S ribosomes bound to release factors RF1, RF2 and RF3. *Curr Opin Struct Biol* 22, 733-742.











Zhou, J., Lancaster, L., Trakhanov, S., and Noller, H.F. (2012b). Crystal structure of release factor RF3 trapped in the GTP state on a rotated conformation of the ribosome. *RNA* 18, 230-240.












Zhou D., Tanzawa T., Lin J., Gagnon, M.G. (2020). Structural basis for ribosome recycling by RRF and tRNA. *Nat Struct Mol Biol* 27, 25-32.

Zimmer, M.H., Niesen, M.J.M. & Miller, T.F. (2021). 3rd Force transduction creates long-ranged coupling in ribosomes stalled by arrest peptides. *Biophys J* 120, 2425–2435.

Zoldak, G., Redecke, L., Svergun, D.I., Konarev, P.V., Voertler, C.S., Dobbek, H., Sedlak, E., and Sprinzl, M. (2007). Release factors 2 from *Escherichia coli* and *Thermus thermophilus*: structural, spectroscopic and microcalorimetric studies. *Nucleic Acids Res* 35, 1343-1353.

Auflistung der Gefahrstoffe nach GHS

Chemikalie	GHS-Symbol	H-Sätze	P-Sätze
Ammoniumacetat	-	-	-
Ammoniumchlorid		302, 319	305+351+338
Chloramphenicol		318, 351, 361fd	202, 280, 305+351+338, 310, 405, 501
Dinatriumhydrogenphosphat	-	-	-
Dithiothreitol		302, 315, 318	264, 270, 280, 301+312, 302+352, 305+351+338
Dodecyl-beta-D-maltoside		315, 319, 335	261, 264, 303+361+353, 305+351+338+310
EDTA		319, 332, 373	280, 304+340, 312, 305+351+338, 337+313,
Ethan		220, 280	210, 377, 381, 403
Ethanol		225, 319	210, 240, 305+351+338, 403+233
HEPES-Puffer	-	-	-
Kaliumacetat	-	-	-
Kaliumchlorid	-	-	-
Kaliumhydroxid		290, 302, 315	280, 301+330+331, 305+351+338, 308+310
Kanamycin		360	201, 202, 280, 308+313
Lithiumchlorid		302, 315, 319	302+352, 305+351+338

Luciferase-Substrat		373	314, 501
Magnesiumacetat	-	-	-
Magnesiumchlorid	-	-	-
Natriumchlorid	-	-	-
Natriumdihydrogenphosphat	-	-	-
Natriumhypochlorit	  , 9	290, 314, 335, 410	260, 273, 280, 303+361+353, 305+351,338, 310, 390, 403+233
NTP-mix	-	-	-
Putrescine	  6	226, 302, 311, 314, 330	210, 280, 303+361+353, 304+340+310, 305+351+338
Rnase inhibitor	-	-	-
Saccharose	-	-	-
Salzsäure	 	290, 314, 335	280, 303+361+353, 305+351+338+310
Spermidine		314	260, 280, 303+361+353, 305+351+338, 321, 501
Stickstoff, flüssig		281	282, 336+315, 403
Telithromycin		302, 315, 319, 335	261, 305+351+338
Viomycin		302	264, 270, 301+317, 330, 501

Declaration on Oath

I hereby declare and affirm that this doctoral dissertation is my own work and that I have not used any aids and sources other than those indicated. If electronic resources based on generative artificial intelligence (gAI) were used in the course of writing this dissertation, I confirm that my own work was the main and value-adding contribution and that complete documentation of all resources used is available in accordance with good scientific practice. I am responsible for any erroneous or distorted content, incorrect references, violations of data protection and copyright law or plagiarism that may have been generated by the gAI.

Date: 04/08/2024

Signature:

Publications

Given the cumulative nature of this dissertation, the publications included in the thesis (Publication n. 1, 2 and 3) are attached.


These are open access articles, with their supplementary material available and accessible online.

RAPP-containing arrest peptides induce translational stalling by short circuiting the ribosomal peptidyltransferase activity

Received: 30 August 2023

Accepted: 24 January 2024

Published online: 19 March 2024

 Check for updatesMartino Morici¹, Sara Gabrielli², Keigo Fujiwara³, Helge Paternoga¹, Bertrand Beckert¹, Lars V. Bock², Shinobu Chiba³✉ & Daniel N. Wilson¹✉

Arrest peptides containing RAPP (ArgAlaProPro) motifs have been discovered in both Gram-positive and Gram-negative bacteria, where they are thought to regulate expression of important protein localization machinery components. Here we determine cryo-EM structures of ribosomes stalled on RAPP arrest motifs in both *Bacillus subtilis* and *Escherichia coli*. Together with molecular dynamics simulations, our structures reveal that the RAPP motifs allow full accommodation of the A-site tRNA, but prevent the subsequent peptide bond from forming. Our data support a model where the RAP in the P-site interacts and stabilizes a single hydrogen atom on the Pro-tRNA in the A-site, thereby preventing an optimal geometry for the nucleophilic attack required for peptide bond formation to occur. This mechanism to short circuit the ribosomal peptidyltransferase activity is likely to operate for the majority of other RAPP-like arrest peptides found across diverse bacterial phylogenies.

As the nascent polypeptide chain (NC) is synthesized by the ribosome, it passes through a tunnel in the large subunit. While the ribosomal tunnel is considered a passive conduit for many NCs, in certain cases, specific interactions between the growing NC and components of the tunnel can modulate the rate of translation and even induce translational arrest^{1–4}. In the past years, a number of NC-mediated translational stalling events have been shown to be part of sophisticated regulatory feedback pathways in both prokaryotes and eukaryotes^{2–6}. One of the best-characterized examples is the secretion monitor (SecM) arrest peptide that regulates SecA protein expression in Gram-negative bacteria, such as *Escherichia coli*^{2,7,8} (Fig. 1a). Specifically, translation arrest by SecM is thought to prevent formation of an RNA helix that normally blocks *secA* translational initiation. SecA is a motor protein that facilitates the movement of secretory proteins into and through the SecYEG protein-conducting channel^{9–11}. Since the *secM* gene encodes an N-terminal signal sequence, the SecM NC is itself a substrate for SecA action. Importantly, the pulling force of SecA on the SecM NC relieves the SecM-mediated translation arrest, thereby

creating an autoregulatory feedback loop: When SecA levels are low, SecM stalling persists, leading to upregulation of *secA* expression, however, as SecA levels rise, SecM stalling is relieved, resulting in a reduction in *secA* expression^{2,8} (Fig. 1a). Analogous regulatory systems have also been discovered in other bacteria, including *Bacillus subtilis* and *Vibrio alginolyticus* where the MifM and VemP arrest peptides regulate other components of the protein localization machinery, YidC2 and SecDF, respectively^{12–15}.

A recent bioinformatic analysis of sequenced bacterial genomes identified three additional classes of arrest peptides encoded by genes located upstream of protein localization machinery components¹⁶ (Fig. 1b). The first two arrest peptides, termed ApcA and ApdA, were found in a subset of actinobacteria located upstream of YidC2 and SecDF, respectively, whereas the third arrest peptide, termed ApdP, was found upstream of SecDF in a subset of α -proteobacteria¹⁶ (Fig. 1b). While ApcA and ApdA selectively arrested translation elongation on *B. subtilis* but not *E. coli* ribosomes, ApdP induced translational arrest on both *B. subtilis* and *E. coli* ribosomes¹⁶.

¹Institute for Biochemistry and Molecular Biology, University of Hamburg, Martin-Luther-King-Platz 6, 20146 Hamburg, Germany. ²Theoretical and Computational Biophysics Department, Max Planck Institute for Multidisciplinary Sciences, Göttingen, Germany. ³Faculty of Life Sciences and Institute for Protein Dynamics, Kyoto Sangyo University, Kamigamo, Motoyama, Kita-ku, Kyoto 603-8555, Japan. ✉e-mail: schiba@cc.kyoto-su.ac.jp; Daniel.Wilson@chemie.uni-hamburg.de

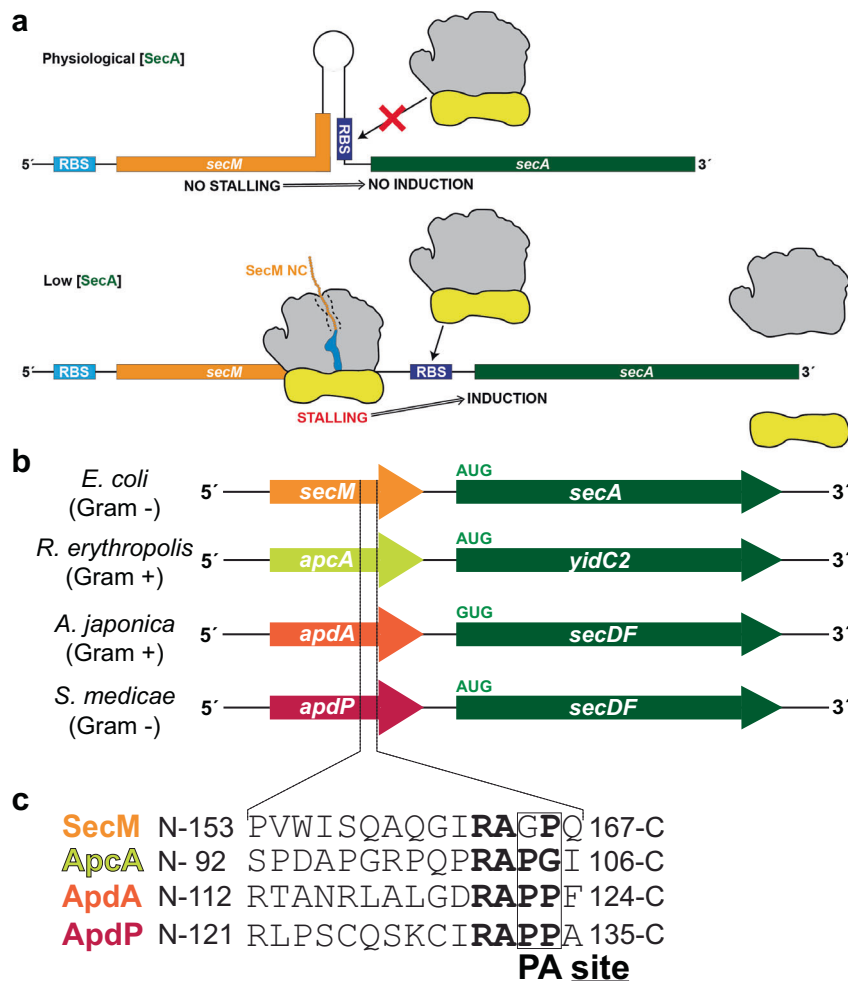


Fig. 1 | Arrangement of bacterial regulatory operons. a Schematic representation for the regulation of SecA by SecM. Upper panel: When SecA levels are high, the pulling force of SecA on the SecM nascent chain prevents stalling, and therefore the ribosome binding site (RBS) of the downstream *secA* gene is sequestered in a stem-loop structure, preventing SecA expression. Lower panel: When SecA levels are low, ribosomes stall during translation of SecM, leading to mRNA rearrangements that expose the RBS of the *secA* gene, leading to the expression of SecA. **b** Examples of bacterial operons containing regulatory upstream open reading frames (uORFs),

including *secM-secA* in Gram-negative γ -proteobacteria, such as *Escherichia coli*, *apcA-yidC2* from Gram-positive actinomycetes, such as *Rhodococcus erythropolis*, *apdA-secDF* from Gram-positive actinomycetes, such as *Amycolatopsis japonica*, and *apdP-secDF* from Gram-negative α -proteobacteria, such as *Sinorhizobium medicae*. **c** Amino acid sequences for the SecM, ApcA, ApdA, and ApdP arrest peptides, aligned based on stalling site during translation, with A- and P-site positions indicated. Conserved residues around the stalling sites are highlighted in bold.

Biochemical analysis revealed that all three arrest peptides caused translation arrest at a conserved RAP(P/G)¹⁶, reminiscent of the stalling at the conserved RAG/P-site reported previously for SecM^{2,8,17,18} (Fig. 1c). The ApdA, ApdP and ApcA arrest peptides stall the ribosome with a peptidyl-RAP-tRNA located in the P-site and a Pro-tRNA (for ApdA and ApdP) or Gly-tRNA (for ApcA) in the A-site¹⁶ (Fig. 1c). This indicates that, similar to SecM^{2,17,19}, these three arrest peptides prevent translation elongation by interfering with A-site tRNA accommodation and/or peptide bond formation¹⁶. A previous structural study on SecM-stalled ribosomes reported that SecM blocks the accommodation of Pro-tRNA in the A-site by inducing conformational changes within the peptidyltransferase center (PTC) that lead to an inactive state of the ribosome²⁰. Moreover, the sidechain of the critically important Arg of the conserved RAG of SecM^{17,18} was proposed to extend into the A-site cavity at the PTC in a manner that would sterically interfere with the placement of the Pro moiety linked to the A-site tRNA²⁰. While mutagenesis studies have revealed that the Arg of the RAP motif is also critical for stalling of ApcA, ApdA, and ApdP¹⁶, a molecular basis for the arrest mechanism used by these

arrest peptides and whether it is analogous to that reported for SecM remains to be determined.

Here we report cryo-electron microscopy (cryo-EM) structures of *B. subtilis* ApdA- and *E. coli* ApdP-stalled-ribosomal complexes (SRC) at 2.3 and 2.2 Å resolution, respectively. The structures reveal that while paths of the NCs within the ribosomal tunnel diverge for the N-terminal region, a highly conserved conformation is acquired for the C-terminal RAP/P motif at the PTC. The RAP motif of the ApdA and ApdP NCs in the P-site adopts a defined conformation that allows the PTC to acquire the induced conformation required for A-site tRNA accommodation. However, the Pro moiety on the A-site tRNA is prevented from initiating the nucleophilic attack on the P-site tRNA that would lead to peptide bond formation. Molecular dynamics (MD) simulations support a model where nucleophilic attack is prevented because a hydrogen bond between the nitrogen group of the Pro moiety in the A-site and the carbonyl-oxygen of the Ala within the RAP motif in the P-site restrains the dynamics of the Pro moiety. Although the mechanism for ApdA and ApdP is different from that reported previously for SecM²⁰, it is consistent with the mechanism based on a

more recent SecM structure²¹. In conclusion, our study illustrates that ApdA and ApdP arrest peptides utilize an analogous mechanism to SecM²¹ to stall translation by trapping a pre-peptide bond formation (pre-attack) state of the PTC on the ribosome, and that this mechanism can operate in both Gram-positive and Gram-negative bacteria.

Results

Structures of *B. subtilis* ApdA-SRC and *E. coli* ApdP-SRC

Since ApdA was shown to stall efficiently on *B. subtilis*, but not *E. coli*, 70S ribosomes¹⁶, we employed a *B. subtilis* cell-free in vitro translation system to generate ApdA-stalled-ribosomal complexes (ApdA-SRC), as used previously to generate *B. subtilis* MifM-SRCs²². In contrast to the MifM-SRC²², the ApdA-SRC was purified using an N-terminal FLAG-tag exposed at the exit tunnel and was formed with full-length, rather than truncated, mRNA (see Methods). The ApdA-SRC was applied to cryo-

EM grids and analyzed using single-particle cryo-EM. A total of 9930 micrographs were collected on a Titan Krios transmission electron microscope (TEM) equipped with a K3 direct electron detector (DED), which yielded 334,479 ribosomal particles after 2D classification (Supplementary Fig. 1). Focused 3D classification revealed two major subpopulations of 70S ribosomes, one bearing A- and P-site tRNAs (43%; 142,978 particles) and one with only P-site tRNA (46%; 152,257 particles), collectively representing a total of 89% of the initial ribosomal particles (Supplementary Fig. 1). The 70S ribosome with A- and P-site tRNAs was further refined, yielding a cryo-EM map of the ApdA-stalled-ribosomal complex (ApdA-SRC) with an average resolution of 2.3 Å (Fig. 2a, Supplementary Figs. 1, 2, and Table 1). In the ApdA-SRC, the ApdA nascent polypeptide chain (NC) was well-resolved near the PTC (Supplementary Fig. 2 and Supplementary Movie 1), such that nine amino acids, including sidechains, could be modeled unambiguously,

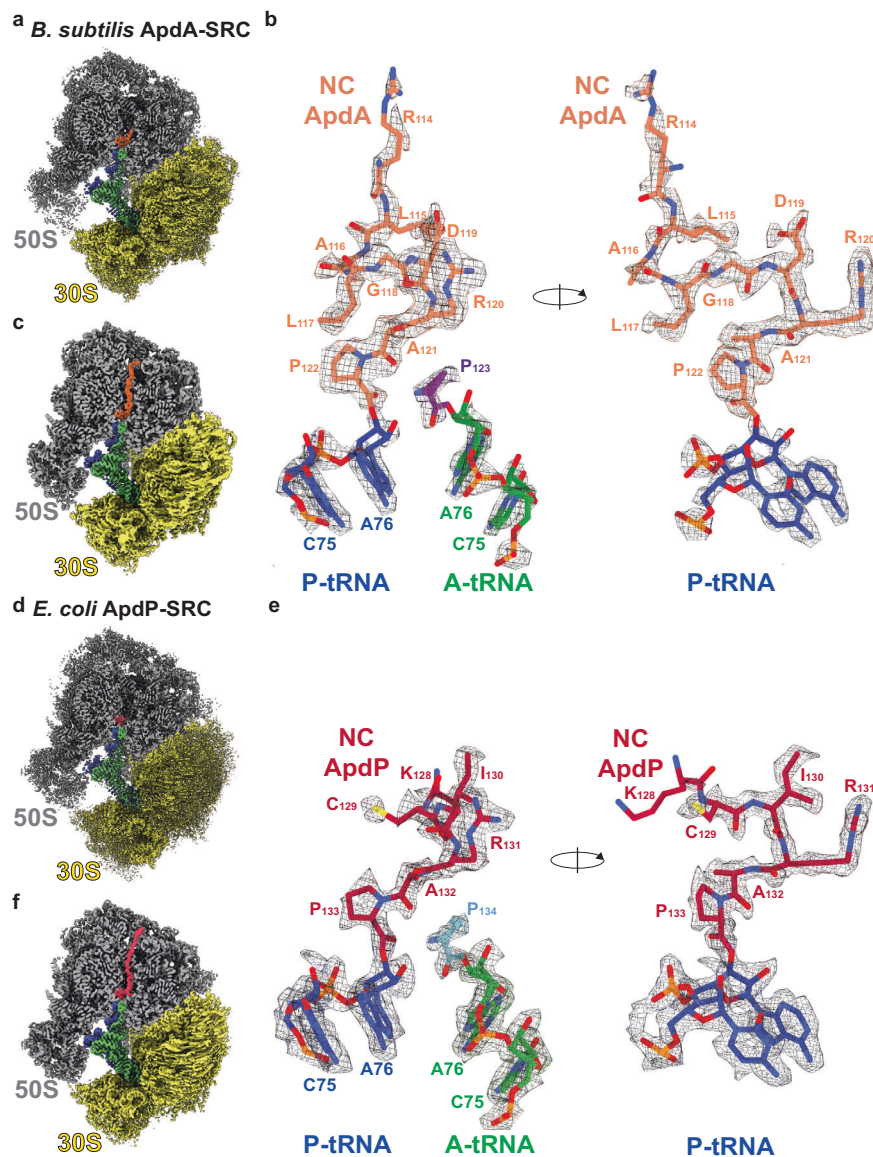


Fig. 2 | Cryo-EM structures of ApdA- and ApdP-SRCs. **a** Cryo-EM map of the post-processed *B. subtilis* ApdA-SRC with a transverse section of the 50S (gray) to reveal density for the nascent chain (orange), P-tRNA (blue), A-tRNA (green); 30S (yellow). **b** Two views showing the cryo-EM map density for A- and P-site tRNAs of the post-processed *B. subtilis* ApdA-SRC. The P-site tRNA (blue) bears the ApdA nascent chain (orange), whereas the A-site tRNA (green) carries proline (purple). **c** as **(a)**, but cryo-EM map of 3D-refined *B. subtilis* ApdA-SRC. **d** Cryo-EM map of the post-

processed *E. coli* ApdP-SRC with a transverse section of the 50S (gray) to reveal density for the nascent chain (red), P-tRNA (blue), A-tRNA (green); 30S (yellow). **e** Two views showing cryo-EM map density for A- and P-site tRNAs of the post-processed *E. coli* ApdP-SRC. The P-site tRNA (blue) bears the ApdP nascent chain (red), whereas the A-site tRNA (green) carries proline (cyan). **f** as **(d)**, but cryo-EM map of 3D-refined *E. coli* ApdP-SRC.

Table 1 | Cryo-EM data collection, refinement and validation statistics

Complex	<i>B. subtilis</i> ApdA-SRC	<i>E. coli</i> ApdP-SRC
EMDB ID	18332	18320
PDB ID	8QCQ	8QBT
Data collection and processing		
Magnification (×)	105,000	105,000
Acceleration voltage (kV)	300	300
Electron fluence (e ⁻ /Å ²)	42	42
Defocus range (μm)	-0.6 to -1.8	-0.6 to -1.8
Pixel size (Å)	0.82	0.82
Symmetry imposed	C1	C1
Initial particles	334,479	263,503
Final particles	142,978	205,838
Average resolution (Å) (FSC threshold 0.143)	2.3	2.2
Model composition		
Initial model used (PDB code)	6HA1	5JTE
Atoms	136,962	141,132
Protein residues	4822	4848
RNA bases	4564	4738
Refinement		
Map CC around atoms	0.76	0.69
Map CC whole unit cell	0.74	0.67
Map sharpening B factor (Å ²)	-45.24	-46.75
R.M.S. deviations		
Bond lengths (Å)	0.009	0.010
Bond angles (°)	1.717	1.727
Validation		
MolProbity score	1.08	1.16
Clash score	0.78	0.91
Poor rotamers (%)	0.94	0.78
Ramachandran statistics		
Favored (%)	95.22	94.39
Allowed (%)	4.54	5.42
Outlier (%)	0.23	0.19
Ramachandran Z-score	-2.30	-2.04

covering the C-terminal conserved ¹²⁰RAP¹²² motif that is directly linked to the CCA-end of the P-site tRNA (Fig. 2b and Supplementary Fig. 2). In addition, the high quality of the cryo-EM map density allowed the Pro¹²³ moiety attached to the CCA-end of the A-site tRNA to be unambiguously identified and modeled (Fig. 2b). Although additional density for the ApdA NC could also be observed throughout the entirety of the ribosomal exit tunnel in some pre-processed maps (Fig. 2c), it was poorly resolved, indicating flexibility, and precluded a molecular model to be generated for these regions.

Unlike ApdA, ApdP was shown to stall efficiently on both *B. subtilis* and *E. coli* 70S ribosomes¹⁶; therefore, we generated ApdP-stalled-ribosomal complexes (ApdP-SRC), as used previously to generate *E. coli* SecM-SRC²³ and Vemp-SRC²⁴. As for ApdA-SRC, the ApdP-SRC was purified using an N-terminal FLAG-tag and full-length mRNA, and analyzed by single-particle cryo-EM using a Titan Krios TEM equipped with a K3 DED (see Methods). A total of 4921 micrographs were collected, which yielded 263,503 ribosomal particles after 2D classification (Supplementary Fig. 3 and Table 1). Focused 3D classification revealed one major subpopulation of 70S ribosomes bearing A- and P-site tRNAs (78%; 205,838 particles), as well as one minor population with P-site tRNA only (7%; 17,657 particles), collectively representing a

total of 85% of the initial ribosomal particles (Supplementary Fig. 3). The 70S ribosome with A- and P-site tRNAs were further refined, yielding a cryo-EM map of the ApdP-stalled-ribosomal complex (ApdP-SRC) with an average resolution of 2.2 Å (Fig. 2d and Supplementary Fig. 4). In the ApdP-SRC, the ApdP NC was well-resolved near the PTC (Supplementary Fig. 4 and Supplementary Movie 2), such that six amino acids, including sidechains, could be modeled, including the C-terminally conserved ¹³¹RAP¹³³ motif that is directly linked to the CCA-end of the P-site tRNA (Fig. 2e and Supplementary Fig. 4). As for the ApdA-SRC, the cryo-EM map density of the ApdP-SRC allowed the unambiguous modeling of Pro¹³⁴ attached to the CCA-end of the A-site tRNA (Fig. 2e), whereas the additional density for the ApdP NC observed in the deeper regions of the ribosomal exit tunnel in some pre-processed maps was poorly resolved (Fig. 2f), precluding a molecular model to be built.

We also refined the ApdA- and ApdP-ribosome populations lacking A-site tRNA, yielding cryo-EM maps of the ApdA-(ΔA-tRNA)-SRC and ApdP-(ΔA-tRNA)-SRC with average resolutions of 2.3 and 2.9 Å, respectively (Supplementary Fig. 5). Although the ribosome and P-site tRNA were well-resolved, in both cases the density for the NC, even directly at the PTC, was poorly defined, preventing molecular models to be generated. Alignment with the ApdA- and ApdP-SRCs indicated that some density is observed for the RAP motif attached to the P-site tRNA and that the overall conformation appears to be similar to that observed for ApdA/ApdP from the ApdA/ApdP-SRCs, but with higher flexibility (Supplementary Fig. 5). Thus, we conclude that the presence of the A-site tRNA in the ApdA- and ApdP-SRC stabilizes the conformation of the NC on the peptidyl-tRNA in the P-site. Collectively, the cryo-EM structures of the ApdA- and ApdP-SRC revealed that the peptidyl-tRNA is present in the P-site, consistent with previous biochemical analysis¹⁶, supporting the suggestion that the ApdA and ApdP arrest peptides interfere with peptide bond formation between the peptidyl-RAP-tRNA in the P-site and the incoming A-site Pro-tRNA¹⁶.

Interaction of ApdA and ApdP at the ribosomal PTC

Superimposition of the ApdA- and ApdP-SRCs reveals that the RAP motif attached to the P-site tRNA is positioned identically (within the limits of the resolution) between the two structures (Fig. 3a). Similarly, the interactions of the RAP motif of ApdP with the 23S rRNA nucleotides located at the PTC of the *E. coli* ribosome (Fig. 3b) are indistinguishable from that observed between the RAP motif of the ApdA and the *B. subtilis* ribosome (Fig. 3c). This finding is consistent with the high sequence and structural conservation of these nucleotides (Fig. 3b, c). With the exception of a potential hydrogen bond between the backbone nitrogen of Ala132 of ApdP (Ala121 in ApdA) and U2506 (BsU2535), the RAP motif interactions with the surrounding 23 S rRNA involve exclusively the Arg131 of ApdP (Arg120 in ApdA) (Fig. 3b, c). Specifically, the Arg of the RAP motif inserts into a pocket formed by 23S rRNA nucleotides of the PTC, where the sidechain stacks upon Ψ2504 (BsU2533) (Fig. 3b–d) and can form five direct hydrogen bonds to rRNA, three with the nucleobases of Ψ2504 (BsU2533) and G2061 (BsG2090) as well as two with the phosphate-oxygen backbone of G2505 (BsG2534) (Fig. 3b, c). In addition, we observe density for two water molecules that mediate interactions between the Arg of the RAP motif and 23S rRNA nucleotides G2505 (BsG2534), m²A2503 (Bs m²A2532), and G2061 (BsG2090) (Fig. 3b, c). The importance of these interactions is supported by the observation that mutation of Arg120 to Ala in ApdA abolishes stalling in *B. subtilis*, and mutation of Arg131 to Ala in ApdP abolishes stalling in both *B. subtilis* and *E. coli*¹⁶. By contrast, mutation of Ala121 in ApdA, and Ala132 in ApdP, to Ser had a less dramatic effect on the stalling efficiency¹⁶, consistent with the backbone interaction of the Ala of the RAP motif observed in the respective structures (Fig. 3b, c).

Given the ability of the RAPP motif to stall translation in both Gram-positive and Gram-negative bacteria, we also tested whether the

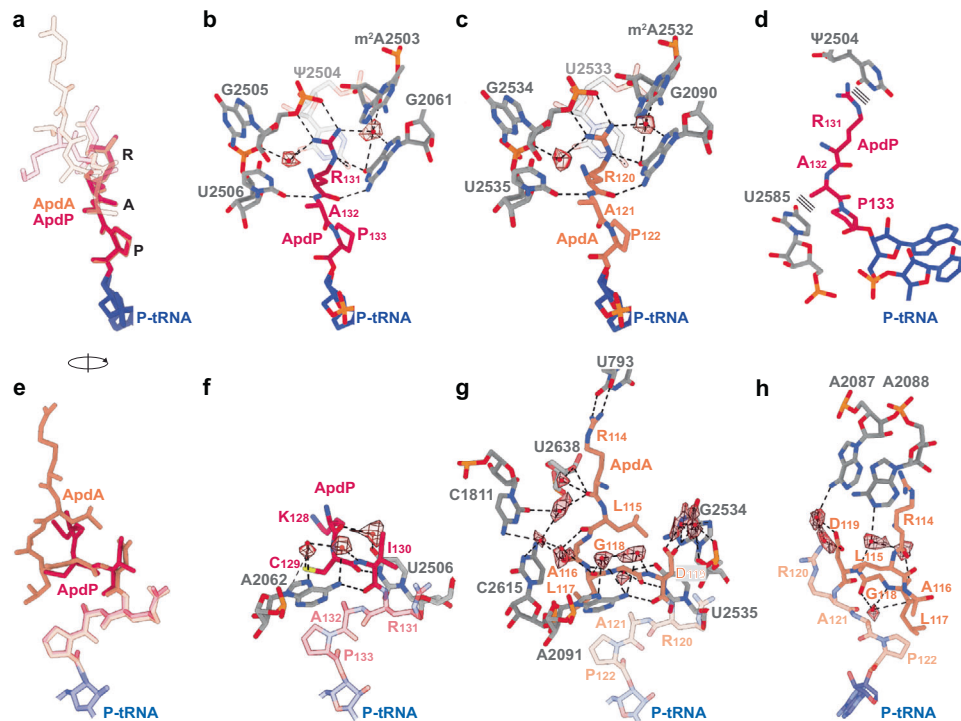


Fig. 3 | Interaction of ApdA and ApdP NCs within the ribosomal tunnel.

a Overlay (aligned on the basis of the 23S rRNA) of the molecular models for ApdA (orange), ApdP (red), and P-tRNA (blue) with a focus on the RAP motif. **b, c** Interactions of RAP motif of the **b** ApdP (red) and **c** ApdA (orange) nascent chains with the exit tunnel nucleotides (gray) of the **b** *E. coli* and **c** *B. subtilis* 23S rRNA, respectively. Potential hydrogen bonds are shown as dashed lines and water molecules as red spheres (with meshed density). **d** Rotated view of (**b**) showing the

stacking interactions (depicted as three parallel lines) between the conserved RAP motif of ApdP (red) and 23S rRNA nucleotides (gray). In (**b**) and (**d**), ψ indicates the presence of pseudouridine at position 2504 in *E. coli*. **e** Rotated view of (**a**) with a focus on residues N-terminal to the RAP motif. **f–h** Interactions (**f**) ApdP (red) and (**g, h**) ApdA (orange) nascent chains with the exit tunnel nucleotides (gray) of the **f** *E. coli* and **g, h** *B. subtilis* 23S rRNA, respectively. Potential hydrogen bonds are shown as dashed lines and water molecules as red spheres (with meshed density).

RAPP motif could induce translational stalling in a eukaryotic system. To do this, we introduced the C-terminal soluble domains of wildtype ApdA and ApdP, as well as their variants where the RAPP motif was mutated to AAPP, into a GFP-LacZ reporter and monitored for presence of peptidyl-tRNA and full-length protein after incubation in a rabbit reticulocyte in vitro translation system (Supplementary Fig. 6). As a positive control, we employed the XBP1u arrest peptide, where we observed stalling, as expected²⁵, indicated by the accumulation of peptidyl-tRNA that is resolved upon addition of RNase (Supplementary Fig. 6a). By contrast, we observed no accumulation of peptidyl-tRNA caused by elongation arrest using the ApdA or ApdP sequences, suggesting that the RxPP motif does not stall eukaryotic translation efficiently. One explanation is that in ApdA and ApdP, the critically important Arg of the RxPP motif stacks upon Ψ 2504 (BsU2533) (Fig. 3b–d), however, in eukaryotic ribosomes, the equivalent rRNA nucleotide, U4412, adopts a different conformation that precludes this stacking interaction (Supplementary Fig. 6b).

In contrast to the RAPP motif, the conformation of the modeled residues located N-terminally is distinct when comparing ApdA and ApdP (Fig. 3e), which is not unexpected given the lack of sequence homology in this region (Fig. 1c). The three N-terminal residues (Lys128–Ile130) observed for ApdP form a network of direct and water-mediated interactions with A2062 and U2506 of the 23S rRNA (Fig. 3f). Similar interactions are observed for the corresponding region of ApdA (Leu117–Asp119) with direct and water-mediated interactions observed to A2091 (EcA2062) and G2534 (EcU2505) (Fig. 3g). Unlike for ApdP, we observe an additional three residues (Arg114–Ala116) of ApdA that establish direct and water-mediated interactions with U793

(Ec Ψ 746), C1811 (EcU1782), C2615 (EcU2586), U2638 (EcU2609) (Fig. 3g), and A2087/A2088 (EcA2058/A2059) (Fig. 3h). While single point mutation of these residues to alanine had no influence on translational stalling¹⁶, frameshifted constructs indicate that residues within this N-terminal region, namely, residues 125–130 for ApdP and 108–119 for ApdA, do contribute to the efficiency of translational stalling¹⁶. These observations suggest that while individual interactions are unlikely to be important, collectively, this N-terminal region also plays a role in facilitating translational stalling of both ApdA and ApdP.

The species-specificity determining region of ApdA and ApdP

Since previous studies demonstrated that ApdP induces efficient translational stalling in both *E. coli* and *B. subtilis*, whereas ApdA exhibits efficient stalling only in *B. subtilis*¹⁶, we generated a series of ApdA–ApdP chimeric constructs (Fig. 4a) and monitored whether stalling is observed using *B. subtilis* and *E. coli* in vitro translation systems (Fig. 4b, c). As expected, all ApdA–ApdP chimeric constructs induced efficient stalling on *B. subtilis* ribosomes (Fig. 4b, lanes 1–20), whereas different efficiencies of translational stalling were observed on *E. coli* ribosomes (Fig. 4c, lanes 1–20). Compared to the wildtype ApdP sequence (Fig. 4c, lanes 1–2), the substitution of ApdP residues N-terminal to the RAPP motif with the corresponding ApdA sequence led to reduced stalling, as observed by the reduction of peptidyl-tRNA and the appearance of full-length (FL) protein (Fig. 4c, lanes 3–8). Loss of ApdP stalling on *E. coli* ribosomes was observed with the ApdP125–A115 construct (Fig. 4c, lanes 7–8) when only five residues of ApdP (126QSKC130) were replaced with the corresponding residues from ApdA (115LALGD119) (Fig. 4a). Conversely, compared to the wildtype

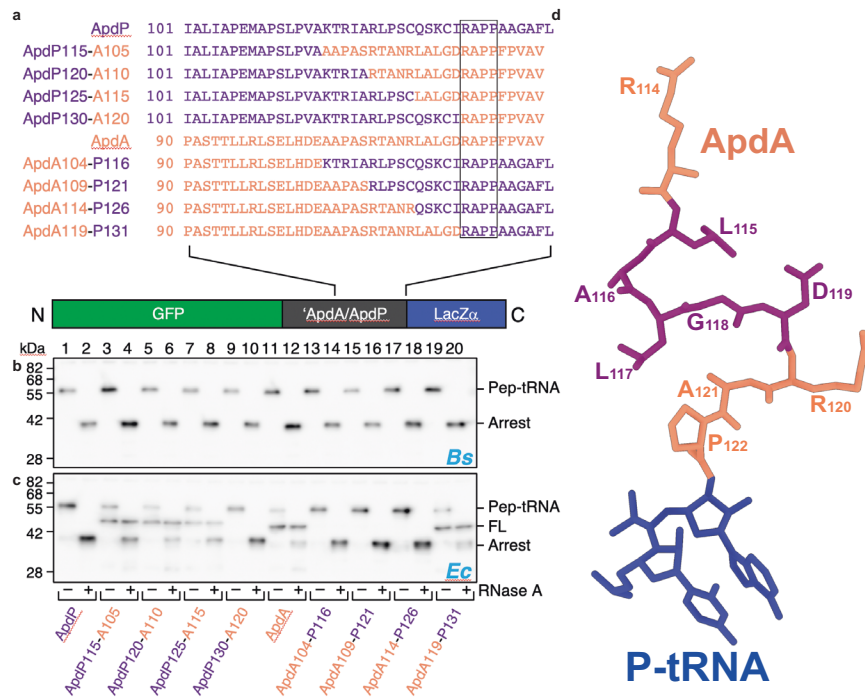


Fig. 4 | Species-specific stalling of chimeric ApdA-ApdP constructs. **a** Sequences of different chimeras between ApdA (orange) and ApdP (purple) (with the common RAPP motif boxed) cloned in the GFP-LacZ α construct shown at the bottom.

b, c Western blot against GFP showing the outcome of the stalling assay in **b** *B. subtilis* and **c** *E. coli* in vitro translation system for the chimeras listed in **(a)**; each reaction was loaded before (–) and after (+) RNase A treatment. Bands

corresponding to peptidyl-tRNA (Pep-tRNA), full-length peptide (FL), and truncated peptide arising due to the stalling (Arrest) are indicated. Experiments were performed in two independent experiments with similar results. Source data are provided as a Source Data file. **d** Structure of ApdA (orange) with residues colored purple that enhanced stalling on *E. coli* ribosomes when substituted with the corresponding ApdP residues.

ApdA sequence (Fig. 4c, lanes 11–12), substitution of ApdA residues N-terminal to the RAPP motif with the corresponding ApdP sequence led to increased stalling, as observed by the increase in peptidyl-tRNA and the loss of full-length (FL) protein (Fig. 4c, lanes 13–18). Here, the gain of ApdA stalling on *E. coli* ribosomes was observed with the ApdA114-P126 construct (Fig. 4c, lanes 17–18) when only five residues of ApdA (₁₁₅LALGD₁₁₉) were replaced with the corresponding residues from ApdP (₁₂₆QSKCI₁₃₀) (Fig. 4a). Collectively, this suggested that one or more of the five residues located within the region directly N-terminal to the RAPP motif (Fig. 4d) play(s) a critical role in the species-specificity of ApdA translational stalling.

A comparison of the 23S rRNA nucleotides that surround and interact with these five ApdA residues (₁₁₅LALGD₁₁₉) in the ApdA-SRC with the equivalent 23S rRNA nucleotides in the *E. coli* ribosome revealed no discernable conformational differences that would provide an explanation for the species-specific stalling (Supplementary Fig. 7a, b). We note that while there is one sequence difference between *B. subtilis* and *E. coli* ribosomes within this region, namely, the equivalent nucleotide to C2615 in the *B. subtilis* ribosome is U2586 in the *E. coli* ribosome, we do not believe that it is responsible for the species-specificity of ApdA since the 23S rRNA of *A. japonica*, where ApdA was discovered¹⁶, contains a U rather than a C at the equivalent position. Collectively, this suggests that more distal regions must cooperate with the proximal five residues to influence species-specificity. Indeed, the ability of MifM to stall on *B. subtilis* ribosomes, but not *E. coli* ribosomes, was shown to arise due to sequence differences between ribosomal protein uL22, with one residue (Met90) of uL22 playing a critical role²². Although the ApdA and ApdP NCs were not resolved sufficiently in the distal regions of the tunnel to generate a molecular model, a comparison of the cryo-EM densities for the ApdA and ApdP NCs indicates that their paths may deviate in proximity to the loops of ribosomal proteins uL4, uL22, and uL23 (Supplementary

Fig. 7c, d). Therefore, to assess whether these ribosomal proteins contribute to the stalling efficiency of ApdA and ApdP in *B. subtilis*, we monitored stalling in vivo using wildtype *B. subtilis* as well as *B. subtilis* with alterations in ribosomal proteins uL4, uL22, and uL23 (Supplementary Fig. 7e–h). As a control, we employed a reporter with the MifM stalling sequence, where stalling was observed in the wildtype *B. subtilis* strain as well as a *B. subtilis* strain with a loop deletion (Δ 65–69) in uL23, but was impaired in *B. subtilis* strains with loop deletions in uL4 (Δ 66–70) or uL22 (Δ 86–90), or when the *B. subtilis* uL22 loop was substituted with the *E. coli* sequence (Ec-loop), as reported previously²². In contrast to MifM, stalling due to ApdA and ApdP remained completely unaffected in all strains regardless of deletions or substitutions in the loops of uL4, uL22, and uL23 (Supplementary Fig. 7e–h). This suggests that, unlike MifM, the interaction of ApdA and ApdP with the loops of uL4, uL22, and uL23 does not appear to be critical for their mechanism of translational stalling or species-specificity. However, we cannot rule out that interactions of other regions of uL4, uL22, and uL23 with the ApdA NC may contribute to the species-specificity of stalling of ApdA.

Interaction of ApdA and ApdP NCs with the A-site proline

To understand how the ApdA and ApdP arrest peptides interfere with peptide bond formation, we compared the conformation of the A- and P-site tRNAs and surrounding 23S rRNA at the PTCs of the ApdA- and ApdP-SRC with the previous structures of pre-attack state ribosomes at 2.5–2.6 Å^{26,27} (Fig. 5a–f and Supplementary Figs. 8, 9). We note that the conformation of the 23S rRNA at the PTC of the pre-attack state appears to be identical (within the limits of the resolution) with the 23S rRNA of the ApdA- and ApdP-SRC (Supplementary Fig. 9), indicating that the PTC of the ApdA- and ApdP-SRC have adopted the induced state that is necessary for full accommodation of the A-site tRNA^{26,28}. During peptide bond formation, the α -amino group of the aminoacyl

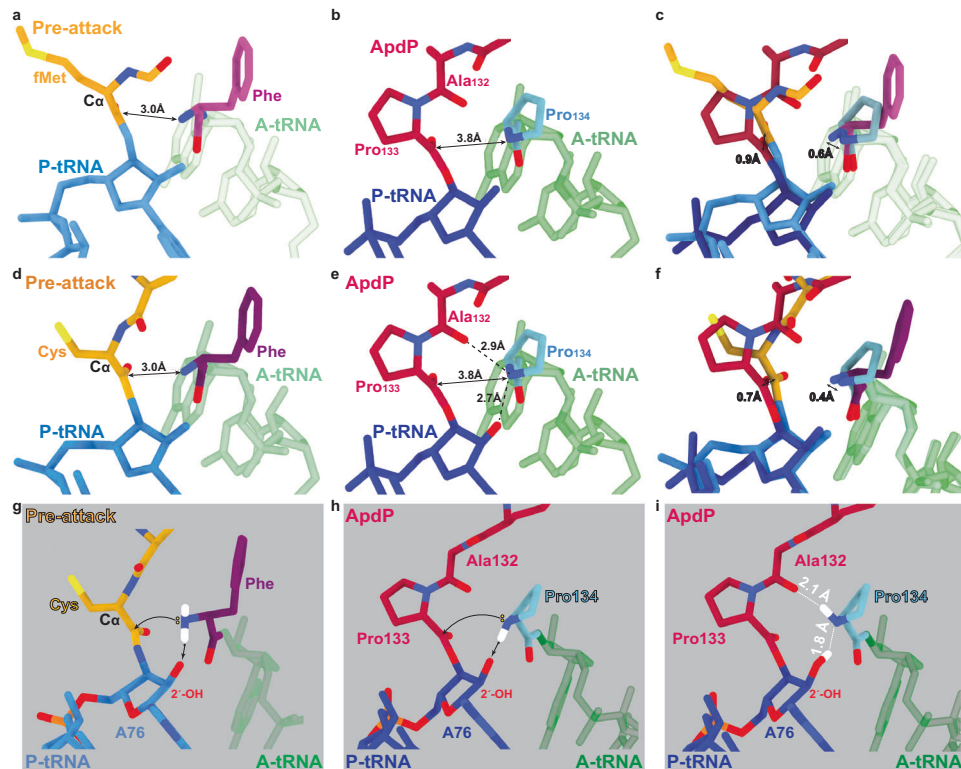


Fig. 5 | ApdA/ApdP stabilize the pre-attack state at the PTC. **a** View of the PTC of a pre-attack state (PDB ID 1VY4)²⁶, showing a fMet-NH-tRNA (gold/blue) at the P-site and a phenyl-NH-tRNA (purple/green) at the A-site. The distance (3.0 Å) between the attacking amine of the A-tRNA and the carbonyl-carbon of the P-tRNA is arrowed. **b** Same view as (a), but for the ApdP-SRC with ApdP-tRNA (red/dark blue) in the P-site and Pro-tRNA (cyan/green) in the A-site. **c** Overlay of (a, b) (aligned on the basis of the 23S rRNA) highlighting the difference in the distance between the attacking nitrogen groups of A-site aminoacyl moiety and the carbonyl carbons at the P-site. **d** View of the PTC of a pre-attack state (PDB ID 8CVK)²⁷, showing a tripeptidyl-NH-tRNA (gold/blue) at the P-site and a phenyl-NH-tRNA (purple/green) at the A-site. The distance (3.0 Å) between the attacking nitrogen of the A-tRNA and the carbonyl-carbon of the P-tRNA is arrowed. **e** Same view as (d), but for the ApdP-SRC with ApdP-tRNA (red/dark blue) in the P-site and Pro-tRNA (cyan/green) in the

A-site. **f** Overlay of (d, e) (aligned on the basis of the 23S rRNA) highlighting the difference in the distance between the attacking nitrogen groups at the A-site and the carbonyl carbons at the P-site. **g** Schematic view of the PTC of a pre-attack from (d), but with hydrogen atoms (white) modeled in silico for the α -amino group of the Phe moiety in the A-site. The yellow spheres indicate the lone pair electrons that make the nucleophilic attack (arrowed) on the carbonyl-carbon of the fMet moiety on the P-site tRNA. **h** Same schematic as (b), but with the hydrogen atom (white) modeled in silico towards the 2'-OH of A76 of the P-site tRNA, which would allow a nucleophilic attack (arrowed) on the carbonyl-carbon of the Pro133 moiety attached to the P-site tRNA. **i** Same schematic as (h) but with the hydrogen atom (white) modeled toward the carbonyl of Ala132, a conformation that would prohibit any nucleophilic attack.

moiety of the A-site tRNA makes a nucleophilic attack on the carbonyl-carbon of the peptidyl-tRNA in the P-site^{29–31}. In the pre-attack state structures, the α -amino group of Phe-tRNA in the A-site is located 3.0 Å from the carbonyl-carbon of the fMet-tRNA in the P-site; however, no peptide bond formation can occur because the fMet moiety is linked to the P-site tRNA via an amide, rather than an ester, linkage^{26,27} (Fig. 5a, c). In the ApdA- and ApdP-SRC, the α -amino group of Pro-tRNA in the A-site is located 3.7 and 3.8 Å, respectively, from the carbonyl-carbon of the peptidyl-RAP-tRNA in the P-site (Fig. 5b and Supplementary Fig. 8), however, peptide bond formation has not occurred, despite the existence of an ester linkage between the NC and the P-site tRNA. Superimposition of the pre-attack states with the ApdA- or ApdP-SRC suggests that the enlarged distance between the α -amino group and the carbonyl-carbon results from a slightly shifted position in both the A- and P-site moieties, but not in the A- and P-site tRNAs themselves (Fig. 5c, f and Supplementary Fig. 8), however, exact quantification is not possible, even at this resolution. Collectively, these observations indicate that the translation of ApdA and ApdP becomes stalled even though the PTC is in the canonical induced state, suggesting that the process of peptide bond formation itself is directly affected.

In the current models for peptide bond formation^{26,32–34}, a proton is extracted from the attacking α -amino group by the 2'-O of the A76 of

the P-site tRNA, which increases the nucleophilicity of the α -amino group and thereby facilitates the nucleophilic attack (Fig. 5g). For stalling of ApdA and ApdP, proline (Pro134 for ApdP and Pro123 for ApdA) in the A site is required. In contrast to all other proteinogenic amino acids, Pro does not have a primary amino group, but rather is a secondary amine, such that the nitrogen carries only one hydrogen in the uncharged state (Fig. 5h). The rate of peptidyl transfer when the Pro-tRNA is in the A-site is low³⁵ and it has been suggested that the elevated pKa of Pro might contribute to the reduced cumulative rate of steps leading to peptidyl transfer after GTP hydrolysis on EF-Tu³⁶. However, the exact protonation state of Pro prior to peptidyl transfer is unclear. While the protonation state cannot be directly inferred from our cryo-EM structures because hydrogens are not resolved, the position of hydrogens can be predicted based on hydrogen-bonding distances. For example, in the ApdA- and ApdP-SRC structures, the N of the A-site Pro is in close proximity to both the carbonyl-oxygen of Ala132 of ApdP (2.7–2.9 Å) as well as the 2'-O of the P-site tRNA A76 ribose (2.6–2.7 Å) (Fig. 5e and Supplementary Fig. 8). In the case of an uncharged Pro, it is only possible to form these two strong hydrogen bond interactions when the single hydrogen of the nitrogen of Pro acts as a donor with the carbonyl-oxygen of Ala132, and the nitrogen as an acceptor for the hydrogen from the 2'-O of A76 (Fig. 5i)—a scenario that is not compatible with peptide bond formation because the 2'-O cannot

extract a proton from the Pro. An alternative scenario is that the Pro is protonated, i.e., presenting two hydrogens, and therefore could act as a donor for both the carbonyl-oxygen of Ala132 as well as the 2'O of A76 (Supplementary Fig. 10). However, also in this scenario where a proton could be extracted by the ribose 2'O, the hydrogen bond remaining with the carbonyl-oxygen of Ala132 maintains a geometry that is incompatible with nucleophilic attack by the lone pair electrons (Supplementary Fig. 10). Taken together, this suggests that translation of ApdA and ApdP becomes stalled because the nucleophilic attack of the A-site Pro moiety on the carbonyl-carbon of the P-site peptidyl-tRNA is blocked, and thus peptide bond formation cannot ensue.

MD simulations of the ApdP-SRC

To test our predictions, we initiated MD simulations from the ApdP-SRC cryo-EM model with different Pro134 protonation states and compared the resulting ensemble with the cryo-EM model. Three protonation states were simulated, (i) \searrow Pro134, where the N-H of the uncharged Pro is oriented towards the carbonyl-O (Ala132), (ii) \swarrow Pro134, where the N-H points towards the ribose O2' (A76), and (iii) \nearrow Pro⁺134, where the charged state of Pro has two N-H forming interactions with both the carbonyl-O (Ala132) and the ribose O2' (A76). For the correct scenario, the structural ensemble generated by the MD simulations is expected to remain close to the cryo-EM model, while for the other scenarios, the protonation state could lead to conformational changes and, therefore, larger structural deviations. To quantify the deviation from the cryo-EM model, we calculated the root mean square deviation (rmsd) of the P-site tRNA A76 and of the two C-terminal amino acids of ApdP (Pro133 and Pro134) from their cryo-EM conformation (Fig. 6a). While the distribution of rmsd values of Pro133 is similar for all three scenarios, a clear shift towards larger rmsd values was observed for Pro134 and A76 in the \nearrow Pro⁺134 state.

These results suggested that a protonated Pro134 causes Pro133 and A76 to undergo conformational changes that are incompatible with the cryo-EM model, rendering this scenario highly unlikely. While the distribution of rmsd values of Pro133, Pro134, and A76 are similar for the two uncharged protonation states of Pro134, the N(Pro134)-C(Pro133) distance between the α -amino group of Pro134 and the carbonyl-carbon of Pro133 sampled by the \swarrow Pro134 protonation state largely deviates from the one observed in the cryo-EM structure (Fig. 6b). Hence, in agreement with our predictions, the structural ensemble that is closest to the cryo-EM model is the one obtained for the \searrow Pro134 protonation state (Fig. 6c).

For a peptide bond to form, two conditions must be met: Firstly, a short distance between the N and C atoms involved in the peptide bond must arise, presumably shifting towards the distance (3.0 Å) observed in the pre-attack structures^{26,27}, and, secondly, the α -amino N must lose one hydrogen (proton), which, as mentioned before, is mediated by the 2'O of A76^{26,32-34}. We propose that the reason for ApdP stalling is that even if the N-C distance is small, the A-site amino acid and the P-site peptide are hindered from reaching conformations that allow the proton transfer from the N-H (Pro134) to the 2'O of A76. It has been shown that mutations in the RAPP motif of ApdP can alleviate stalling¹⁶, presumably because the dynamics for non-stalling mutants change, enabling productive conformations to be visited that allow peptide bond formation. To test this, we performed additional MD simulations with non-stalling ApdP variants R131A, A132S, P133A, and P134A. As a negative control, we performed MD of the K128A variant that did not affect the ApdP stalling efficiency¹⁶. To check if productive conformations were reached for the ApdP variants, we identified the conformations that satisfy all the conditions required for peptide bond formation. Firstly, to check for the proximity requirement, we counted how often conformations with N(Pro134)-C(Pro133) distance lower than 3.8 Å were sampled. The threshold of 3.8 Å was chosen as it is the

distance observed in the cryo-EM structure. As shown in Fig. 6d (magenta bars), conformations meeting the first requirement are sampled in all variants with frequencies in the same order of magnitude. However, marked differences between stalling and non-stalling variants arise when, in addition to the proximity condition, also the second condition for peptide bond formation, i.e., the N-H(Pro134)-2'O(A76) hydrogen bond, is met (Fig. 6d, blue bars). The differences are even more pronounced when considering also the 2'OH(A76)-2'O(A2451) hydrogen bond (Fig. 6d, yellow bars), which constitutes the second step in the proton wire mechanism²⁶. Interestingly, while in the wildtype and control, the three conditions are rarely met simultaneously, the non-stalling variants meet all requirements 100- to 1000-fold more often. This confirms our prediction that, despite reaching short N(Pro134)-C(Pro133) distances, stalling of the wildtype and control takes place due to the inability of the ApdP peptide to efficiently assume the conformations required for activating the proton transfer. By contrast, the increase in flexibility of the non-stalling mutants compared to wildtype and NC control, allows productive conformations for peptide bond formation to be attained (Supplementary Fig. 11a-c). We also performed additional simulations without the tRNA present in the A-site, where it was observed that the presence of the A-tRNA restricts the movement of the P-site NC (Supplementary Fig. 11d), consistent with the cryo-EM structures when comparing the NC densities in the presence and absence of A-tRNA (Fig. 2 and Supplementary Fig. 5). Taken together, these observations suggest that peptide bond formation is indeed prevented because the Pro-tRNA in the A-site interacts with the P-site nascent chain, together adopting a conformation that is prohibitive for proton transfer in the A-site as well as the subsequent nucleophilic attack onto the P-site peptidyl-tRNA.

Discussion

In this study, we have determined structures of ribosomes stalled during translation by the RAPP-containing arrest peptides ApdA and ApdP at resolutions of 2.3 and 2.2 Å, respectively. The structures, together with complementary MD simulations and previous biochemistry¹⁶, allow a molecular model to be presented for the mechanism by which the RAPP arrest peptides stall translation by interfering with the process of peptide bond formation. During normal translation, peptide bond formation ensues because the α -amino group of the aminoacyl moiety attached to the A-site tRNA makes a nucleophilic attack on the carbonyl-carbon of the amino acid in the O position (the amino acid linked to A76) of the peptidyl-tRNA (Fig. 7a). For the nucleophilic attack to occur, a proton needs to be extracted from the α -amino of the aminoacyl moiety in the A-site, which is thought to be mediated by the 2'O of the ribose of A76 (Fig. 7a). By contrast, during translation of the ApdA and ApdP arrest peptides, the ribosome becomes trapped with the peptidyl-RAP-tRNA in the P-site and the Pro-tRNA in the A-site (Fig. 7b). The PTC of the ribosome is in an induced state with a fully accommodated Pro-tRNA, thus, the stage is set for peptide bond formation to occur, yet, the nucleophilic attack does not take place (Fig. 7b). Our structures and MD simulations indicate that the nucleophilic attack cannot occur because the nitrogen of the Pro in the A-site forms a hydrogen bond with the carbonyl-oxygen of the Ala of the RAP motif in the P-site (Fig. 7b). In this scenario, the 2'O of the ribose of A76 is actually donating, rather than extracting, a proton to the nitrogen of Pro, thereby, also forming a second hydrogen bond, and nullifying any possibility of nucleophilic attack on the peptidyl-tRNA in the P-site (Fig. 7b). Thus, a critical player in our model is the carbonyl-oxygen of the Ala of the RAP motif, which we propose is positioned to interact with the A-site Pro due to structural restraints imposed by the preceding Pro and the following Arg of the RAP motif of the NC (Fig. 7b), explaining why mutations at either Pro or Arg of the RAP motif alleviate stalling¹⁶. The RAP motifs of ApdA and ApdP do not adopt the β -strand geometry observed for non-stalling peptides where the carbonyl-oxygen of the amino acid in the -1

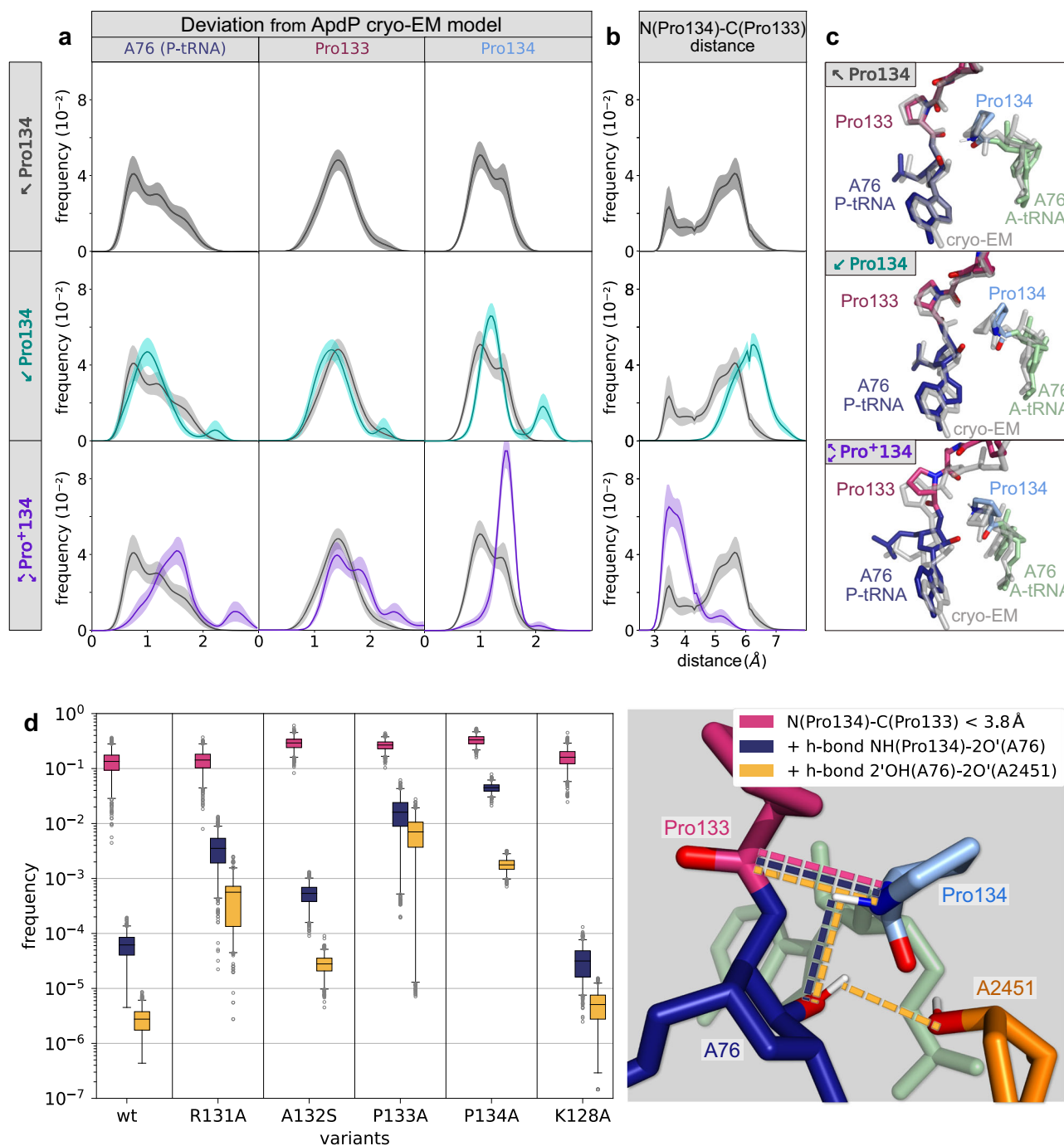


Fig. 6 | MD simulations of ApdP in the ribosome. a, b For different protonation states (\backslash Pro134, \checkmark Pro134, \searrow Pro⁺134), histograms of deviations (rmsd) from the cryo-EM model (ribose ring of A76, Pro134, and Pro133) (a) and of the distances between the α -amino N of Pro134 and the carbonyl C of Pro133 (b) are shown. Uncharged protonation states with the N-H pointing either towards the O (Ala132) or towards O2' (A76) are denoted by \backslash Pro134 and \checkmark Pro134, respectively. \searrow Pro134 denotes the charged state with both hydrogens. Lines and error bars in (a) and (b) were obtained from the mean and standard deviations of 10,000 bootstraps of 20 independent simulations. c From the MD simulations of each protonation state, structures corresponding to the most probable rmsd values are shown (colored) and

compared with the stalled cryo-EM structure (grey). d Frequencies of the conformations fulfilling three conditions required for peptide bond formation. Frequencies of N(Pro134)-C(Pro133) distances lower than 3.8 Å (proximity requirement, magenta). Frequency of conformations which, in addition to the first condition, contain an N-H(Pro134)-2'O(A76) hydrogen bond (blue). Frequency of the conformations that additionally contain the 2'OH(A76)-2'O(A2451) hydrogen bond (yellow). The box plots were obtained by bootstrapping 10,000 samples of 20 independent simulations for each variant. The boxes extend from the first to third quartiles. Whiskers display a 95% confidence interval. Points out of the confidence interval are shown (grey circles). Source data can be obtained from Zenodo (10.5281/zenodo.10426362).

position cannot form a hydrogen bond with the N of the aminoacyl moiety of the A-site tRNA^{26,27}. This suggests that the formation of a β -strand geometry by the NC at the PTC may contribute to the efficiency of translation by preventing non-productive NC conformations that

interfere with peptide bond formation, as observed here for ApdA and ApdP. We also note that in the absence of the A-site tRNA, we observe that the RAP motif in the ApdA and ApdP NC is relatively flexible (Supplementary Figs. 5, 11), suggesting that the accommodation of the

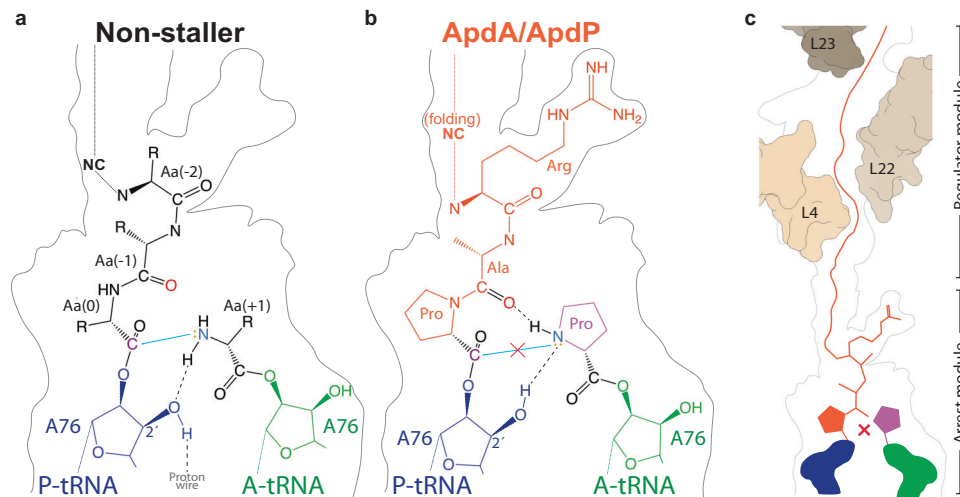


Fig. 7 | Model for ApdA/ApdP-mediated translational stalling. **a, b** Schematic representations of the PTC for **a** canonical non-stalling nascent polypeptide chains, where the lone pair electrons on the α -amino group of the aminoacyl moiety attached to the A-site tRNA makes a nucleophilic attack (blue arrow) on the carbonyl-carbon of the peptidyl-tRNA in the P-site. The nucleophilicity of the α -amino group is increased by the extraction of a proton by the 2' OH of ribose of A76 of the P-tRNA. **b** RAPP-mediated translation stalling by ApdA or ApdP, where the nucleophilic attack of the nitrogen of the A-site Pro on the carbonyl-carbon of the

peptidyl-tRNA cannot occur because (i) the hydrogen of the nitrogen of Pro is involved in a hydrogen bond with the carbonyl-oxygen of Ala of the RAP motif in the P-site, and (ii) the 2' O of the ribose of A76 donates hydrogen to form a hydrogen bond with the lone pair electron, rather than extracting the proton as required for peptide bond formation. **c** ApdA and ApdP stalling is strongly driven by the RAPP arrest module; however, the N-terminal regulator module also contributes by fine-tuning the stalling efficiency.

Pro-tRNA in the A-site contributes to stabilizing the observed conformation. Mutation of the A-site Pro alleviates stalling¹⁶, presumably because, unlike Pro, other amino acids have rotational freedom around the α -amino group, allowing them to more easily adopt optimal geometries for nucleophilic attack and undergo more rapid peptide bond formation (Supplementary Fig. 10).

Despite the similarity of the RAP/P motif present in the ApdA and ApdP with the RAG/P motif present in the SecM, we observe completely different NC conformations and a distinct mechanism of translational inhibition for ApdA and ApdP compared to that reported previously for SecM²⁰. Unlike SecM where the Arg of the RAG motif in the P-site is reported to sterically block accommodation of the Pro-tRNA in the A-site²⁰, we observe that the conformation of the RAP motif in ApdA/ApdP is not only compatible with, but even stabilizes, Pro-tRNA binding at the A-site (Supplementary Fig. 12a–c). These findings were surprising and prompted us to re-determine the structure of a SecM-SRC, where in contrast to ref. 20, we observed that the RAG/P motif of SecM does, in fact, utilize an identical mechanism to stall translation as reported here for ApdA and ApdP²¹. This mechanism is distinct from most other elongation stalling, since they have been shown to generally interfere with the accommodation of the A-site tRNA by promoting an inactive uninduced conformation of the PTC, as exemplified by MifM²² and VemP²⁴. In contrast to VemP, for example, the PTC for ApdA/ApdP is observed in the active induced state with an accommodated A-tRNA (Supplementary Fig. 12d–f). In terms of functional state, the most similar arrest peptide to ApdA/ApdP (with the exception of SecM²¹) is the macrolide-dependent ErmBL arrest peptide, which also traps a pre-attack state of the ribosome with an accommodated A-site tRNA³⁷. However, the stalling mechanism differs from ErmBL since peptide bond formation is inhibited because the macrolide induces a rotation of the ErmBL NC that causes displacement of the A76 ribose of the peptidyl-tRNA (Supplementary Fig. 12g–i). Moreover, no interaction is observed between the NC and aminoacyl moiety in the A-site, as observed for ApdA/ApdP (Supplementary Fig. 12g–i).

Despite both containing conserved RAPP motifs, ApdP stalls translation on *B. subtilis* and *E. coli* ribosomes, whereas ApdA stalls

translation efficiently only on *B. subtilis* ribosomes¹⁶. By generating chimeras between ApdA and ApdP, we could localize a region in ApdP that confers this specificity, namely, five residues directly adjacent (N-terminal) to the RAPP motif (Fig. 4). While the conformation of the NC in this region of ApdP adopts a distinct conformation compared to the equivalent region in ApdA (Fig. 3e), the surrounding region of the tunnel encompassing these residues is conserved between *B. subtilis* and *E. coli*. Thus, it remains unclear exactly how these residues contribute to the species-specificity. One possibility is that they are influenced by NC regions deeper in the tunnel where species-specific differences are evident between *B. subtilis* and *E. coli* ribosomes, particularly, the regions involving ribosomal proteins uL4, uL22, and uL23²². However, so far, our attempts investigating alterations in these r-proteins, some of which have been documented to alter the species-specificity of MifM stalling²², were unsuccessful in identifying tunnel components that influence the specificity of ApdA and ApdP stalling (Supplementary Fig. 7).

While the influence of the N-terminal region of the NC on species-specificity of RAPP stalling remains unclear, there is strong evidence that the N-terminal region is important for RAPP stalling. An elegant study by Buskirk and coworkers used a genetic selection for stalling sequences, leading to the identification of RxPP and R/HxPP (amongst others) as strong stalling motifs³⁸. Interestingly, when the N-terminal seven residues upstream of RxPP were replaced with the seven residues in front of the HGPP stalling motif (or vice versa), stalling was abolished, illustrating how the N-terminal region can influence, or in this case, alleviate, stalling at these motifs³⁸. This study also illustrated that the minimal RxPP motif was sufficient to induce translational arrest, presumably using the mechanism revealed here for ApdA and ApdP, and likely explaining why RxPP motifs are selected against and therefore underrepresented in bacterial proteomes³⁸. Collectively, this suggests that RAPP arrest peptides are comprised of two modules, the RAPP “arrest module” that is attached to the P-tRNA and directly involved in preventing peptide bond formation together with a Pro-tRNA in the A-site, as well as a second N-terminal “regulator module” that can modulate the strength (and sometimes even the specificity) of stalling (Fig. 7c).

Recent evidence points to broader implications of the use of the RXP in bacterial translation regulation beyond proteins involved in the protein localization machinery. For example, in *Bordetella pertussis*, the Gram-negative bacteria responsible for whooping cough, a three gene-operon involved in copper import has been shown to be regulated by an upstream open reading frame containing a conserved RAPP motif³⁹. Mutations within the RAPP motif abolished expression of the downstream genes, leading to the suggestion that ribosome stalling occurs at the RAPP motif³⁹, which we would propose utilizes an analogous mechanism to inhibit peptide bond formation as determined here for ApdA and ApdP. Thus, it seems quite likely that RAPP-like sequences are utilized to regulate the translation of a wide variety of proteins across diverse bacterial phylogenies⁴⁰, the full impact of which has yet to be elucidated.

Methods

Bacterial strains and plasmids

B. subtilis strains (Supplementary Table 1) used for the genetic analysis were constructed by transformation of plasmids (Supplementary Table 2), which were constructed by fusing PCR fragments amplified with PrimeSTAR GXL DNA polymerase (Takara), the template DNAs, and primers (Supplementary Table 3) by Gibson Assembly⁴¹. Cell extracts for in vitro translation on *B. subtilis* ribosomes were generated as described previously²² but using the *B. subtilis* strain 168 $\Delta yvyD \Delta ssaA \Delta smpB$ (see below). The protein-coding sequence of ApdA from *Amycolatopsis japonica* and ApdP from *Sinorhizobium medicae*¹⁶ were individually cloned into pDG1662 downstream of a T7 promoter, a ribosome binding site, a His-tag and a Flag-tag using restriction enzymes SphI and HindIII (NEB). The insert of ApdA was amplified by PCR using Q5 High-Fidelity DNA polymerase (NEB) from plasmid pCH2125¹⁶ using primers ApdA-FOR (5'-TACGCTGCATGCCGGAC-GAGTCGCGCGGGGCGAACGCGACG-3') and ApdA-REV (5'-AAGCTTTCAGACGGCTACCGGAAAGGAGGAGCG-3'), whereas the insert of ApdP was amplified by PCR using Q5 High-Fidelity DNA polymerase (NEB) from pCH2126¹⁶ using primers ApdP-FOR (5'-AAAGCATGCAT-CATCGCCAGAGTGCCGCGTCCCCTG-3') and ApdP-REV (5'-TTT AAGCTTCGCGAAAGACTGCCGAAGCT-3'). All DNA oligonucleotide primers were purchased from Metabion.

PCR and in vitro transcription

PCR reaction (Q5 High-Fidelity DNA Polymerase (NEB), Q5 Reaction buffer (NEB) and Q5 High GC Enhancer (NEB)) was used with primers T7FOR (5'-AAATTTTAAATACGACTCACTATAGG-3') and ApdA-REV on the vector harboring the *apdA* gene to generate the amplified DNA sequence (5'-TAATACGACTCACTATAGGGGAATTGTGAGCGGATAAC AATCCCCACTAGTAATAATTTTGTAACTTTAAGAAGGAGATATA CCATGGGCAGCAGCCATCATCATCATCACGATTACAAGGATGAC GACGATAAGGCTAGCAGCAGCGGTACCGGCAGCGCGAAACCTCTA TTTTCAGGGTAGTGCGCAAGCATGCGCGGACGAGTCGCGCGGGGGC AACCGCAGCGGTGCAATCCTCGGTCTCAAGGCCGTCGCGCCGGT GCGCGCGCGGGCAGGCTCGCCGCCGAACCCGCGCTCCTGGGTGTGC ACGGTACCGGTGACTGCCTCTCTTCGGCACCGTCCCAGCAGGACC GGCTCCAGCAGCTGCTCCGCTCAGCGAGCTCCACGACGACGA GCTCCCGCTCGCGCAGCGCAACCCCTCGCGCTGGGTGATCGCG CTCCTCTTTCCCGGTAGCCGTCTGAAAGCTT-3'; underlined are the T7 promoter region, ribosomal binding site, start codon, FLAG-tag and stop codon, respectively); primers T7FOR and ApdP-REV were used to perform the same PCR protocol on the vector harboring the *apdP* gene to generate the amplified DNA sequence (5'-TAATACGACTCACTA-TAGGGGAATTGTGAGCGGATAACAATCCCCACTAGTAATAATTTTGT TAACTTTAAGAAGGAGATATACCATGGGCAGCAGCCATCATCAT CATCACGATTACAAGGATGACGACGATAAGGCTAGCAGCAGCGGTA CCGCAGCGCGCGAAACCTCTATTTTCAGGGTAGTGCGCAAGCATGC ATCGCCAGAGTGCCGCGTCCCGTTCGCGCGGGGGCGCGCCGGC AATGTGCTCAGCCGATACAGGCTCCTCCGACCGCCGGTTCGCTC

GCCAGATATGACGGGCGGTTGCGCTGCCGATCTTCGTTTCATCGG CGAGCGGGCCGATGGCAAGTCATGCTCCGGCGCAGATCCTGCAGCG TTCGTTTCCTTCCAGGCCATTGCCCTGATTGCGCCAGAGATGGCTCC TTCCCTGCCGGTGGCGAAAACCAGAATTGCGCGTCTCCCATCCTGTC AGAGCAAGTGCATTGCGCGCGCCAGCGCGGGAGCCTTCCTTTGA GAGTTCGCGAGGTCTTTTCGCGAAGCTT-3'; underlined are the T7 promoter region, ribosomal binding site, start codon, FLAG-tag and stop codon, respectively). PCR conditions applied were as suggested by the manufacturer and PCR products were purified via spin columns, and in vitro transcription reaction was set up using 1 μ g PCR product per 50 μ l reaction volume and T7 RNA polymerase (Thermo Fischer ScientificTM). RNA was purified by LiCl/ethanol precipitation.

Bacillus subtilis S12 translation extract

The *B. subtilis* S12 translation extract was prepared following a procedure described²², with some modifications. Briefly, cells (*B. subtilis* strain 168 $\Delta yvyD \Delta ssaA \Delta smpB$) were grown to OD₆₀₀ 0.8 in 2 \times YPTG medium (16 g L⁻¹ peptone, 10 g L⁻¹ yeast extract, 5 g L⁻¹ NaCl, 22 mM NaH₂PO₄, 40 mM Na₂HPO₄, 19.8 g L⁻¹ glucose, sterile-filtered) at 37 °C. Cells were collected by centrifugation at 5000 rpm at room temperature for 15 min and subsequently washed 3 \times in room temperature Buffer A (10 mM Tris-acetate (pH 8.2, 4 °C), 14 mM magnesium acetate, 60 mM potassium glutamate, 1 mM dithiothreitol, and 6 mM 2-mercaptoethanol, sterile-filtered). After the third wash, cells were resuspended in a minimal volume (0.7 mL g⁻¹) of room temperature Buffer B (Buffer A without 2-mercaptoethanol). Cells were snap-frozen in liquid nitrogen and stored at -80 °C. Cells were subsequently thawed on ice and then lysed using FastPrep-24TM MP (4 \times 30 min, shaking 4.5 m s⁻¹ intercalated by 1 min rest on ice), the lysate was collected by centrifugation (1000 \times g, 4 °C, 1 min) and further cleared by centrifugation at 12,000 \times g, 4 °C, 10 min. The lysate was used immediately, or aliquoted, snap-frozen, and stored at -80 °C.

Generation of stalled-ribosomal complexes

To generate the ApdA-SRC, the ApdA mRNA template (500 ng μ L⁻¹) was translated by incubation in a *B. subtilis* in vitro translation system. Briefly, a total reaction volume of 450 μ L was prepared by mixing 5.85 μ L reconstitution buffer, 7.65 μ L of methionine, 90 μ L amino acid mix, 76.5 μ L reaction mix (from RTS 100 HY Kit from Biotechrabbit GmbH) with 90 μ L *B. subtilis* S12 translation extract, 135 μ L ApdA mRNA, 45 μ L 100 mM magnesium acetate, and then incubated for 40 min at 30 °C shaking in a thermomixer (500 rpm).

To generate the ApdP-SRC, the ApdP mRNA template (250 ng μ L⁻¹) was translated by incubation in a fully reconstituted *E. coli* in vitro PURExpress (NEB) translation system. Briefly, a total reaction volume of 100 μ L was prepared by mixing 18 μ L water, 40 μ L solution A, 12 μ L factor mix, 15 μ L *E. coli* ribosome (PURExpress[®] Δ Ribosome Kit, NEB) with 15 μ L ApdP mRNA, and then incubated for 40 min at 30 °C shaking in a thermomixer (500 rpm).

Purification of the stalled-ribosomal complexes

The ApdA-SRC and ApdP-SRC were purified by incubating the respective in vitro translation reactions with 50 μ L anti-FLAG[®] M2 affinity gel (Merck) (previously equilibrated with Hico buffer (50 mM HEPES-KOH (pH 7.4, 4 °C), 100 mM potassium acetate, 15 mM magnesium acetate, 1 mM dithiothreitol, 0.01 % (w/v) *n*-dodecyl-beta-maltoside, sterile-filtered)) inside a Mobicol column fitted with a 35- μ m filter (MoBiTec) at 4 °C overnight with rolling. After removal of the flow-through, the beads were washed with a total of 4 mL Hico buffer, and then the bound complex was eventually eluted by incubation with 15 μ L Hico buffer containing 0.6 mg mL⁻¹ 3xFLAG peptide for 40 min at 4 °C while rolling, followed by centrifugation (2000 \times g, 4 °C, 2 min). Aliquots from each fraction were checked by Western blotting.

Preparation of cryo-EM grids and data collection

About 3.5 μl of sample (8 OD₂₆₀/ml) were applied to grids (Quantifoil, Cu, 300 mesh, R3/3 with 3 nm carbon) which had been freshly glow discharged using a GloQube (Quorum Technologies) in negative charge mode at 25 mA for 90 s. Sample vitrification was performed using ethane/propane mix in a Vitrobot Mark IV (Thermo Scientific), with the chamber set to 4 °C and 100% relative humidity, and blotting was performed for 3 s with no drain or wait time. The grids were subsequently mounted into the Autogrid cartridges and loaded onto Talos Arctica (Thermo Fischer Scientific) TEM for screening. Grids were stored in liquid nitrogen until high-resolution data collection. High-resolution data was collected on a Titan Krios microscope aligned for fringe-free imaging and equipped with a Bioquantum K3 (Ametek) direct electron detector. The camera was operated in correlated double sampling (CDS) mode, and the data were collected at the pixel size of 0.82 Å/px. The microscope condenser system was set to produce 42 e/Å²s electron flux on the specimen, and the data from 1.8 s exposure were stored in 40 frames. The energy-selecting slit was set to 10 eV. The data from 3 × 3 neighboring holes were collected using beam/image shifting while compensating for the additional coma aberration. The data was collected with the nominal defocus range of -0.6 to -1.8 μm . For the ApdA- and ApdP-SRC, a total number of 9930 and 4921 movies were collected, respectively.

Single-particle reconstruction of SRC complexes

RELION version 3.1^{42,43} was used for processing, unless otherwise specified. For motion correction, RELION's implementation of MotionCor2 with 4 × 4 patches, and, for initial contrast transfer function (CTF) estimation, CTFFIND version 4.1.14⁴⁴, were employed. To estimate local resolution values, Bsoft⁴⁵ was used on the half-maps of the final reconstructions (bloccres -sampling 0.82 -maxres -box 20 -cutoff 0.143 -verbose 1 -fill 150 -origin 0,0,0 -Mask half_map1 half_map 2) (Supplementary Figs. 2, 4).

ApdA-SRC dataset. From 9930 micrographs, 532,749 particles were picked using crYOLO with a general model⁴⁶. In total, 334,479 ribosome-like particles were selected after two-dimensional (2D) classification and extracted at 3× decimated pixel size (2.46 Å per pixel) (Supplementary Fig. 1). An initial three-dimensional (3D) refinement was done using a mol map of an *E. coli* 70S ribosome (PDB ID 7K00 with mRNA and tRNAs removed) as a reference, then partial signal subtraction was performed on the particles to focus on the tRNAs sites, followed by initial 3D classification without angular sampling with six classes. One class containing 70S ribosomes with P-tRNA and substoichiometric A-tRNA (295,256 particles) was subsorted. A class containing 70S with P- and A-tRNAs (142,978 particles) and a class containing 70S with P-tRNA only (152,257 particles) were further processed (Supplementary Fig. 1). In particular, the subtracted particles from the resulting classes were reverted, and 3D and CTF refined (fourth-order aberrations, beam tilt, anisotropic magnification and per-particle defocus value estimation), then subjected to Bayesian polishing⁴⁷ and another round of CTF refinement. For the ApdA-SRC with P-tRNA and A-tRNA, a final resolution (gold-standard FSC_{0.143}) of masked reconstruction of 2.3 Å was achieved (Supplementary Fig. 2). For the ApdA-SRC with P-tRNA, a final resolution (gold-standard FSC_{0.143}) of the masked reconstruction of 2.3 Å was achieved (Supplementary Fig. 5).

ApdP-SRC dataset. From 4921 micrographs, 404,941 particles were picked using crYOLO with a general model⁴⁶. In total, 263,503 ribosome-like particles were selected after two-dimensional (2D) classification and extracted at 3× decimated pixel size (2.46 Å per pixel) (Supplementary Fig. 3). An initial three-dimensional (3D) refinement was done using a mol map of an *E. coli* 70S ribosome (PDB ID 7K00 with mRNA and tRNAs removed) as a reference, then partial

signal subtraction was performed on the particles to focus on the tRNAs sites, followed by initial 3D classification without angular sampling with eight classes. One class containing 70S ribosomes with P-tRNA and substoichiometric A-tRNA (205,842 particles) was subsorted into five subclasses, two of which were identical and high-resolution, therefore joined (205,838) for further processing; one class containing 70S with P-tRNA only (52,581 particles) was subsorted into five subclasses, one of which (17,657) was selected for further processing (Supplementary Fig. 3). In particular, the subtracted particles of the resulting classes were reverted and 3D and CTF refined (fourth-order aberrations, beam tilt, anisotropic magnification and per-particle defocus value estimation), then subjected to Bayesian polishing⁴⁷ and another round of CTF refinement. For the ApdP-SRC with P-tRNA and A-tRNA, a final resolution (gold-standard FSC_{0.143}) of the masked reconstruction of 2.2 Å was achieved (Supplementary Fig. 4). For the ApdP-SRC with P-tRNA, a final resolution (gold-standard FSC_{0.143}) of the masked reconstruction of 2.9 Å was achieved (Supplementary Fig. 5).

Molecular modeling of the SRC complexes

The molecular models of the 30S and 50S ribosomal subunits were based on the *B. subtilis* 70S ribosome (Protein Data Bank (PDB) ID: 6HA1)⁴⁸ for ApdA-SRC and on the *E. coli* 70S ribosome (Protein Data Bank (PDB) ID: 5JTE)³⁷ for ApdP-SRC. The tRNAs and nascent chains were modeled de novo. Restraint files for modified residues were created using aceDRG⁴⁹, while the restrain file to link the tRNAs to their aminoacyl-/peptidyl- moiety were kindly provided by Keitaro Yamashita (MRC LMB, UK). The starting models were rigid body fitted using ChimeraX⁵⁰ and modeled using Coot 0.9.8.4⁵¹ from the CCP4 software suite version 8.0⁵². The sequence for the tRNAs was adjusted based on the appropriate anticodons corresponding to the mRNA. Final refinements were done in REFMAC 5⁵³ using Servalcat⁵⁴. The molecular models were validated using Phenix comprehensive cryo-EM validation in Phenix 1.20-4487⁵⁵.

Bacterial in vitro translation arrest assay

In vitro translation arrest assay was carried out using *E. coli*-based coupled transcription-translation system (PUREreflex 1.0; Gene-Frontier), and *Bs* hybrid PURE system¹³, in which 1 μM of the *B. subtilis* ribosomes was added instead of *E. coli* ribosome. About 2.5 U/L of T7 RNA polymerase (Takara) was added further to reassure transcription. The DNA templates were prepared by PCR using primers and template DNA listed in Supplementary Table 4. After the translation reaction at 37 °C for 20 min, the reaction was stopped by adding three volumes of 1.3 × SDS-PAGE loading buffer (167 mM Tris-HCl (pH 6.8), 2.7% (wt/vol) SDS, 20% (vol/vol) glycerol, 6.7 mM DTT, a trace amount of bromophenol blue), and, when indicated, samples were further treated with 0.2 mg/ml RNase A (Promega) at 37 °C for 10 min to degrade the tRNA moiety of peptidyl-tRNA immediately before electrophoresis.

Eukaryotic in vitro translation arrest assay

The DNA templates were prepared by PCR using primers and templates listed in Supplementary Table 4. In vitro transcription was carried out using T7 RNA Polymerase ver.2.0 (TaKaRa) and 175 ng of PCR product per 10 μl reaction volume. The mRNA was then purified by RNAClean XP (Beckman Coulter) and used for in vitro translation using the Rabbit Reticulocyte Lysate (RRL) translation system (Promega). A total reaction volume of 4 μl was prepared by mixing 2.8 μl Rabbit Reticulocyte Lysate (Nuclease-Treated), 10 μM Amino Acid Mixture Minus Methionine, and 10 μM Amino Acid Mixture Minus Leucine with the 40 ng/ μl mRNA. After the translation reaction at 30 °C for 20 min, the reaction was stopped by adding seven volumes of 1.1 × SDS-PAGE loading buffer (143 mM Tris-HCl (pH 6.8), 2.3% (wt/vol) SDS, 17% (vol/vol) glycerol, 5.7 mM DTT, a trace amount of bromophenol blue), and, when indicated, samples were further treated with 0.2 mg/ml RNase A

(Promega) at 37 °C for 10 min to degrade the tRNA moiety of peptidyl-tRNA immediately before electrophoresis.

Western blotting

Samples were separated by 10% polyacrylamide gel prepared with WIDE RANGE Gel buffer (Nacalai Tasque), transferred onto a PVDF membrane, and then subjected to immuno-detection using primary antibodies against GFP (mFX75, 012–22541; Wako) or FLAG-tag (M2, F3165; Sigma) at 1/3000 and 1/5000 dilutions, respectively, and the secondary antibody against mouse IgG-HRP (170-6516; Bio-Rad) at 1/5000 dilution. The Images were obtained and analyzed using Amersham Imager 600 (GE Healthcare) luminoimager.

β -galactosidase assay

B. subtilis cells were cultured in LB medium at 37 °C and withdrawn at an optical density at 600 nm (OD_{600}) of 0.5–1.0 for β -galactosidase assay. About 100 μ L portions of the cultures were transferred to individual wells of a 96-well plate, and OD_{600} was recorded. Cells were then lysed with 50 μ L of Y-PER reagent (Thermo Scientific) for 20 min at room temperature. After 30 μ L of o-nitrophenyl- β -D-galactopyranoside (ONPG) in Z-buffer (60 mM Na_2HPO_4 , 40 mM NaH_2PO_4 , 10 mM KCl, 1 mM $MgSO_4$, 38 mM β -mercaptoethanol) was added to each well, OD_{420} and OD_{550} were measured every 5 min over 60 min at 28 °C. Arbitrary units [AU] of β -galactosidase activity were calculated by the formula $[(1000 \times V_{420} - 1.3 \times V_{550})/OD_{600}]$, where V_{420} and V_{550} are the first-order rate constants, OD_{420}/min and OD_{550}/min , respectively.

Molecular dynamics (MD) simulations

From the model of the ApdP-SRC with both A- and P-site tRNAs, we extracted all residues within 35 Å of the ApdP NC and used it as a starting structure for the MD simulations of the wild-type simulation system. In order to test which protonation state of Pro134 is the most compatible with the cryo-EM model, we considered three possible scenarios: (i) \backslash Pro134, where Pro134 is uncharged and the α -amino hydrogen points towards the O (Ala132), (ii) $/$ Pro134, where Pro134 is uncharged and the α -amino hydrogen is oriented towards the O2' (A76), and (iii) \nearrow Pro⁺134, where the proline is charged and the two α -amino hydrogens point towards the O (Ala132) the O2' (A76) respectively. The distinction between the \backslash Pro134 and the $/$ Pro134 states was required since classical MD simulations do not allow nitrogen pyramidal inversion to be observed and, hence, interconversion between the two scenarios.

To obtain the dynamics of ApdP NC variants shown to alleviate stalling¹⁶, we also performed MD simulations with the variants: P134A, P133A, A132S, and R131A. As a negative control, we also included the K128A variant, which does not affect the stalling efficiency¹⁶. The starting structures for the ApdP variants were obtained by mutating single residues in the wild-type model with the mutagenesis tool of PyMOL (Schrödinger). Since we observed that the structural ensemble with the \backslash Pro134 protonation state agreed best with the cryo-EM structure (Fig. 6a), we used this protonation state for the P133A, A132S, R131A, and K128A variants. Ala134 in the P134A variant was modeled as uncharged.

The protonation states of the histidine residues were determined using WHAT IF⁵⁶. Water molecules, K^+ , and Mg^{2+} ions from the cryo-EM structure were included in the starting structure. Each structure was positioned at the center of a dodecahedral box, with a minimum distance of 1.5 nm between the atoms and the box boundaries (Supplementary Table 5). The system was then solvated using the program solvate⁵⁷ and neutralized by using the program GENION to replace water molecules with K^+ ions⁵⁷. GENION was additionally used to add 7 mM $MgCl_2$ and 150 mM KCl. All simulations were performed with GROMACS 2018⁵⁷ using the amber14sb forcefield⁵⁸, the OPC water model⁵⁹, and the microMg parameters from ref. 60 for the Mg^{2+} ions,

and the K^+ and Cl^- parameters from ref. 61. Partial charges of N-terminal residues with a neutral α -amino group are not included by default in the Amber force field. Therefore, we computed the charges of Pro134 and Ala134 in their uncharged states with GaussView 5.0.8⁶², using *N*-methylamide as the capping group for the C-terminus of the two amino acids. Geometry optimization of the molecules and charge calculation were both carried out with the Hartree-Fock method⁶³, using the 6-31G basis set⁶⁴. To obtain charges compatible with the Amber force field, the Restrained Electrostatic Potential (RESP) method was applied to fit the charges obtained from the Hartree-Fock calculation⁶⁵. During the RESP fitting, the partial charges of the *N*-methylamide group were restrained to the ones already provided in the force field. Lennard-Jones and short-range electrostatic interactions were calculated within a distance of 1 nm. For distances beyond 1 nm, long-range electrostatic interactions were computed by particle-mesh Ewald summation⁶⁶ with a 0.12-nm grid spacing. Bond lengths were constrained using the LINCS algorithm⁶⁷. Temperature coupling to a heat bath at $T = 300$ K was performed independently for solute and solvent using velocity rescaling⁶⁸ with a coupling time constant of $\tau_T = 0.1$ ps. Virtual site constraints⁶⁹ were applied for hydrogen atoms allowing for an integration time step of 4 fs. Coordinates were recorded every 5 ps.

Initially, energy minimization by steepest descent was performed on each system by applying harmonic position restraints ($k = 1000$ kJ mol⁻¹ nm⁻¹) to the solute-heavy atoms. After that, for each minimized system, 20 simulations were carried out, each one consisting of two equilibration steps and one production run. In the first equilibration step (0–50 ns), the pressure was coupled to a Berendsen barostat Berendsen, 1984 #17353 ($\tau_p = 1$ ps) and position restraints ($k = 1000$ kJ mol⁻¹ nm⁻¹) were applied on all the heavy atoms of the solute. In the second equilibration step (50–70 ns), the position restraints were linearly decreased to zero for all the heavy atoms of the solute positioned within 25 Å from the P-site peptide. The force constant of the restraining potential applied to the heavy atoms placed in the outer shell (25–35 Å) was decreased to the one obtained from the fluctuations previously observed in full-ribosome simulations⁷⁰. Finally, during the production run (70–2070 ns), the Parrinello-Rahman barostat⁷¹ ($\tau_p = 1$ ps) was used, keeping the position restraints only on the outer-shell heavy atoms. The 20 simulations performed for each system sum up to a total simulation time of 40 μ s of production run per system and 360 μ s in total. The trajectories were analyzed using GROMACS⁵⁷, Python 3.8.5 (<https://www.python.org>), and Pandas 1.1.3 (<https://pandas.pydata.org/>). The results were plotted using Matplotlib 3.3.2 (<https://matplotlib.org/>). The first 200 ns of each production run were excluded from the analyses to allow equilibration of the system.

Structural deviations

To identify the protonation state of Pro134 that is most compatible with the cryo-EM data of the ribosome in complex with ApdP, we quantified, for each protonation state (\backslash Pro134, $/$ Pro134, and \nearrow Pro⁺134), the deviation of the simulated conformational ensemble from the cryo-EM structure. To that aim, the root mean square deviation (rmsd) of the residues and bases directly involved in peptide bond formation (P-site tRNA A76, Pro133, and Pro134) from their cryo-EM conformation was calculated. The rmsd values were computed for each frame after the rigid-body fitting of all the P-atoms of the system. Histograms of the rmsd values were then obtained using 80 bins (Fig. 6a). To identify the two most dominant conformational modes of Ala132, we performed principal component analysis (PCA) of the Ala132 backbone atoms positions. First, all trajectories of wildtype (\backslash Pro134 protonation state) and variants were superimposed by least-square fitting of the positions of the 23S rRNA phosphate atoms. Then the trajectories were concatenated and the atomic displacement

covariance matrix was calculated. Finally, for each system, the trajectories of each replica were projected on the first two eigenvectors of this matrix. Histograms of the projection values were then obtained using 80 bins for each conformational mode (Supplementary Fig. 11c). To obtain statistical uncertainties, 10,000 (for the rmsd values) or 1000 (for the PCA) combinations of 20 replicas were randomly selected for each simulated system and the analysis was repeated on each subset. The mean and standard deviation of all subsets were then computed.

Monitoring distances relevant to peptide bond formation

The distances between the α -amino N of Pro134 and the carbonyl C of Pro133 were calculated for each frame of the \backslash Pro134, \swarrow Pro134, and \searrow Pro⁺134 simulations. The distributions of the N(Pro134)-C(Pro133) distances were used to further evaluate which of the three systems is most similar to the cryo-EM structure (Fig. 6a). To obtain statistical uncertainties, 10,000 combinations of 20 replicas were randomly selected for each state, and the analysis was repeated on each subset. The mean and standard deviation of all subsets were then computed.

To identify the mechanism of ApdP stalling, we monitored distances that are relevant to fulfill the conditions required for peptide bond formation, i.e., the proximity between the α -amino N and the C involved in the peptide bond, and deprotonation of the α -amino group. For identifying conformations that satisfy the first condition, we monitored the N(Pro134)-C(Pro133) distances. To assess conformations meeting the second condition, we computed the distances between the N-H of Pro134 and the 2'O of A76, since a hydrogen bond between these atoms is necessary for the α -amino nitrogen to lose one hydrogen. Additionally, we identified conformations compatible with the proton wire mechanism of deprotonation²⁶ by monitoring the distances between the 2'OH of A76 and 2'O of A2451. In order to compare how frequently stalling and non-stalling variants accessed productive conformations, we counted the number of frames where the proximity and the α -amino group deprotonation were fulfilled. The counts were then divided by the total number of simulation frames. We considered the proximity condition fulfilled for conformations with N(Pro134)-C(Pro133) distances lower than 3.8 Å. To account for hydrogen bonds solely between N-H of Pro134 and 2'O of A76, while excluding bifurcated hydrogen bonds with O(Ala132), we identified conformations as productive when the N-H(Pro134)-2'O(A76) distance was <3 Å and the N-H(Pro134)-O(Ala132) distance >3 Å. We considered the 2'OH(A76)-2'O(A2451) hydrogen bond formed when the distance between the two atoms was lower than 3 Å.

Structural flexibility

In order to assess the structural flexibility of the ApdP peptide variants and of the peptide in the absence of the A-site tRNA, the root mean square fluctuation (rmsf) was computed for the backbone of each residue of the peptide after aligning the MD trajectory frames using the P-atoms of the simulated region of the 23S rRNA.

Figures

UCSF ChimeraX 1.3 was used to isolate density and visualize density images and structural superpositions. Hydrogen bonds were determined using the default settings of ChimeraX 1.3, (distance between donor and acceptor <3.4 Å with an angle of $120^\circ \pm 20^\circ$). Models were aligned using PyMol version 2.4 (Schrödinger). Figures were assembled with Adobe Illustrator (the latest development release, regularly updated).

Reporting summary

Further information on research design is available in the Nature Portfolio Reporting Summary linked to this article.

Data availability

Micrographs have been deposited as uncorrected frames in the Electron Microscopy Public Image Archive (EMPIAR) with the accession codes [EMPIAR-11698](#) (ApdP-SRC) and [EMPIAR-11702](#) (ApdA-SRC). Cryo-EM maps have been deposited in the Electron Microscopy Data Bank (EMDB) with accession codes [EMD-18332](#) (ApdA-SRC with A- and P-site tRNA), [EMD-18341](#) (ApdA-SRC with P-site tRNA only), [EMD-18320](#) (ApdP-SRC with A- and P-site tRNA), [EMD-18340](#) (ApdP-SRC with P-site tRNA only). Molecular models have been deposited in the Protein Data Bank with accession codes [8QCQ](#) (ApdA-SRC with A- and P-site tRNA) and [8QBT](#) (ApdP-SRC with A- and P-site tRNA). Publicly available data used included PDB ID [1VY4](#), [8CVK](#), [6OLG](#), [3JBU](#), [5NWY](#), and [5JTE](#). Initial coordinates, input files and output coordinates of the MD simulations, residue topologies of the uncharged terminal Alanine and Proline (used for modeling Ala134 and Pro134), rmsd, distances, rmsf values obtained from the MD trajectories, and projections on the most dominant conformational modes sampled by the Ala132 backbone atoms are publicly available on Zenodo ([10.5281/zenodo.10426362](#)). Source data are provided with this paper.

References

- Wilson, D. N. & Beckmann, R. The ribosomal tunnel as a functional environment for nascent polypeptide folding and translational stalling. *Curr. Opin. Struct. Biol.* **21**, 1–10 (2011).
- Ito, K. & Chiba, S. Arrest peptides: cis-acting modulators of translation. *Annu. Rev. Biochem.* **82**, 171–202 (2013).
- Wilson, D. N., Arenz, S. & Beckmann, R. Translation regulation via nascent polypeptide-mediated ribosome stalling. *Curr. Opin. Struct. Biol.* **37**, 123–133 (2016).
- Dever, T. E., Ivanov, I. P. & Sachs, M. S. Conserved upstream open reading frame nascent peptides that control translation. *Annu. Rev. Genet.* **54**, 237–264 (2020).
- Ramu, H., Mankin, A. & Vazquez-Laslop, N. Programmed drug-dependent ribosome stalling. *Mol. Microbiol.* **71**, 811–824 (2009).
- Chiba, S., Fujiwara, K., Chadani, Y. & Taguchi, H. Nascent chain-mediated translation regulation in bacteria: translation arrest and intrinsic ribosome destabilization. *J. Biochem.* **173**, 227–236 (2023).
- Nakatogawa, H. & Ito, K. Secretion monitor, SecM, undergoes self-translation arrest in the cytosol. *Mol. Cell* **7**, 185–192 (2001).
- Nakatogawa, H., Murakami, A. & Ito, K. Control of SecA and SecM translation by protein secretion. *Curr. Opin. Microbiol.* **7**, 145–150 (2004).
- Driessen, A. J. & Nouwen, N. Protein translocation across the bacterial cytoplasmic membrane. *Annu. Rev. Biochem.* **77**, 643–667 (2008).
- Rapoport, T. A., Li, L. & Park, E. Structural and mechanistic insights into protein translocation. *Annu. Rev. Cell Dev. Biol.* **33**, 369–390 (2017).
- Komarudin, A. G. & Driessen, A. J. M. SecA-mediated protein translocation through the SecYEG channel. *Microbiol. Spectr.* **7** (2019).
- Chiba, S., Lamsa, A. & Pogliano, K. A ribosome-nascent chain sensor of membrane protein biogenesis in *Bacillus subtilis*. *EMBO J.* **28**, 3461–3475 (2009).
- Chiba, S. et al. Recruitment of a species-specific translational arrest module to monitor different cellular processes. *Proc. Natl Acad. Sci. USA* **108**, 6073–6078 (2011).
- Chiba, S. & Ito, K. MifM monitors total YidC activities of *Bacillus subtilis* including that of YidC2, the target of regulation. *J. Bacteriol.* **197**, 99–107 (2014).
- Ishii, E. et al. Nascent chain-monitored remodeling of the Sec machinery for salinity adaptation of marine bacteria. *Proc. Natl Acad. Sci. USA* **112**, E5513–E5522 (2015).
- Sakiyama, K., Shimokawa-Chiba, N., Fujiwara, K. & Chiba, S. Search for translation arrest peptides encoded upstream of genes for

- components of protein localization pathways. *Nucleic Acids Res.* **49**, 1550–1566 (2021).
17. Nakatogawa, H. & Ito, K. The ribosomal exit tunnel functions as a discriminating gate. *Cell* **108**, 629–636 (2002).
 18. Yap, M. N. & Bernstein, H. D. The plasticity of a translation arrest motif yields insights into nascent polypeptide recognition inside the ribosome tunnel. *Mol. Cell* **34**, 201–211 (2009).
 19. Muto, H., Nakatogawa, H. & Ito, K. Genetically encoded but non-polypeptide prolyl-tRNA functions in the A site for SecM-mediated ribosomal stall. *Mol. Cell* **22**, 545–552 (2006).
 20. Zhang, J. et al. Mechanisms of ribosome stalling by SecM at multiple elongation steps. *eLife* **4**, e09684 (2015).
 21. Gersteuer, F. et al. The SecM arrest peptide traps a pre-peptide bond formation state of the ribosome. *Nat. Commun.* (2024).
 22. Sohmen, D. et al. Structure of the *Bacillus subtilis* 70S ribosome reveals the basis for species-specific stalling. *Nat. Commun.* **6**, 6941 (2015).
 23. Bhushan, S. et al. SecM-stalled ribosomes adopt an altered geometry at the peptidyltransferase center. *PLoS Biol.* **19**, e1000581 (2011).
 24. Su, T. et al. The force-sensing peptide VemP employs extreme compaction and secondary structure formation to induce ribosomal stalling. *eLife* **6**, e25642 (2017).
 25. Yanagitani, K., Kimata, Y., Kadokura, H. & Kohno, K. Translational pausing ensures membrane targeting and cytoplasmic splicing of XBP1u mRNA. *Science* **331**, 586–589 (2011).
 26. Polikanov, Y. S., Steitz, T. A. & Innis, C. A. A proton wire to couple aminoacyl-tRNA accommodation and peptide-bond formation on the ribosome. *Nat. Struct. Mol. Biol.* **21**, 787–793 (2014).
 27. Syroegin, E. A., Aleksandrova, E. V. & Polikanov, Y. S. Insights into the ribosome function from the structures of non-arrested ribosome-nascent chain complexes. *Nat. Chem.* **15**, 143–153 (2023).
 28. Schmeing, T. M., Huang, K. S., Strobel, S. A. & Steitz, T. A. An induced-fit mechanism to promote peptide bond formation and exclude hydrolysis of peptidyl-tRNA. *Nature* **438**, 520–524 (2005).
 29. Polacek, N. & Mankin, A. S. The ribosomal peptidyl transferase center: structure, function, evolution, inhibition. *Crit. Rev. Biochem. Mol. Biol.* **40**, 285–311 (2005).
 30. Rodnina, M. V., Beringer, M. & Wintermeyer, W. How ribosomes make peptide bonds. *Trends Biochem. Sci.* **32**, 20–26 (2007).
 31. Simonovic, M. & Steitz, T. A. A structural view on the mechanism of the ribosome-catalyzed peptide bond formation. *Biochim. Biophys. Acta* **1789**, 612–623 (2009).
 32. Lang, K., Erlacher, M., Wilson, D. N., Micura, R. & Polacek, N. The role of 23S ribosomal RNA residue A2451 in peptide bond synthesis revealed by atomic mutagenesis. *Chem. Biol.* **15**, 485–492 (2008).
 33. Wallin, G. & Aqvist, J. The transition state for peptide bond formation reveals the ribosome as a water trap. *Proc. Natl Acad. Sci. USA* **107**, 1888–1893 (2010).
 34. Rodnina, M. V. Translation in prokaryotes. *Cold Spring Harb. Perspect. Biol.* **10**, a032664 (2018).
 35. Pavlov, M. Y. et al. Slow peptide bond formation by proline and other N-alkylamino acids in translation. *Proc. Natl Acad. Sci. USA* **106**, 50–54 (2009).
 36. Johansson, M. et al. pH-sensitivity of the ribosomal peptidyl transfer reaction dependent on the identity of the A-site aminoacyl-tRNA. *Proc. Natl Acad. Sci. USA* **108**, 79–84 (2011).
 37. Arenz, S. et al. A combined cryo-EM and molecular dynamics approach reveals the mechanism of ErmBL-mediated translation arrest. *Nat. Commun.* **7**, 12026 (2016).
 38. Woolstenhulme, C. J. et al. Nascent peptides that block protein synthesis in bacteria. *Proc. Natl Acad. Sci. USA* **110**, E878–E887 (2013).
 39. Roy, G. et al. Posttranscriptional regulation by copper with a new upstream open reading frame. *mBio* **13**, e0091222 (2022).
 40. Fujiwara, K., Tsuji, N., Yoshida, M., Takada, H. & Chiba, S. Patchy and widespread distribution of bacterial translation arrest peptides associated with the protein localization machinery. *Nat. Commun.* **15**, 2711 (2024).
 41. Gibson, D. G. et al. Enzymatic assembly of DNA molecules up to several hundred kilobases. *Nat. Methods* **6**, 343–345 (2009).
 42. Scheres, S. H. RELION: implementation of a Bayesian approach to cryo-EM structure determination. *J. Struct. Biol.* **180**, 519–530 (2012).
 43. Kimanius, D., Dong, L., Sharov, G., Nakane, T. & Scheres, S. H. W. New tools for automated cryo-EM single-particle analysis in RELION-4.0. *Biochem. J.* **478**, 4169–4185 (2021).
 44. Zheng, S. Q. et al. MotionCor2: anisotropic correction of beam-induced motion for improved cryo-electron microscopy. *Nat. Methods* **14**, 331–332 (2017).
 45. Heymann, J. B. Guidelines for using Bsoft for high resolution reconstruction and validation of biomolecular structures from electron micrographs. *Protein Sci.* **27**, 159–171 (2018).
 46. Wagner, T. et al. SPHIRE-crYOLO is a fast and accurate fully automated particle picker for cryo-EM. *Commun. Biol.* **2**, 218 (2019).
 47. Zivanov, J., Nakane, T. & Scheres, S. H. W. A Bayesian approach to beam-induced motion correction in cryo-EM single-particle analysis. *IUCr J* **6**, 5–17 (2019).
 48. Crowe-McAuliffe, C. et al. Structural basis for antibiotic resistance mediated by the *Bacillus subtilis* ABCF ATPase VmIR. *Proc. Natl Acad. Sci. USA* **115**, 8978–8983 (2018).
 49. Long, F. et al. AceDRG: a stereochemical description generator for ligands. *Acta Crystallogr. D. Struct. Biol.* **73**, 112–122 (2017).
 50. Pettersen, E. F. et al. UCSF ChimeraX: structure visualization for researchers, educators, and developers. *Protein Sci.* **30**, 70–82 (2021).
 51. Emsley, P., Lohkamp, B., Scott, W. G. & Cowtan, K. Features and development of Coot. *Acta Crystallogr. D. Biol. Crystallogr.* **66**, 486–501 (2010).
 52. Winn, M. D. et al. Overview of the CCP4 suite and current developments. *Acta Crystallogr. D. Biol. Crystallogr.* **67**, 235–242 (2011).
 53. Vagin, A. A. et al. REFMAC5 dictionary: organization of prior chemical knowledge and guidelines for its use. *Acta Crystallogr. D. Biol. Crystallogr.* **60**, 2184–2195 (2004).
 54. Yamashita, K., Palmer, C. M., Burnley, T. & Murshudov, G. N. Cryo-EM single-particle structure refinement and map calculation using Servalcat. *Acta Crystallogr. D. Struct. Biol.* **77**, 1282–1291 (2021).
 55. Liebschner, D. et al. Macromolecular structure determination using X-rays, neutrons and electrons: recent developments in Phenix. *Acta Crystallogr. D. Struct. Biol.* **75**, 861–877 (2019).
 56. Vriend, G. WHAT IF: a molecular modeling and drug design program. *J. Mol. Graph.* **8**, 52–56 (1990).
 57. Abraham, M. J. et al. GROMACS: High performance molecular simulations through multi-level parallelism from laptops to supercomputers. *SoftwareX* **1-2**, 19–25 (2015).
 58. Maier, J. A. et al. ff14SB: improving the accuracy of protein side chain and backbone parameters from ff99SB. *J. Chem. Theory Comput.* **11**, 3696–3713 (2015).
 59. Izadi, S., Anandakrishnan, R. & Onufriev, A. V. Building water models: a different approach. *J. Phys. Chem. Lett.* **5**, 3863–3871 (2014).
 60. Grotz, K. K. & Schwierz, N. Magnesium force fields for OPC water with accurate solvation, ion-binding, and water-exchange properties: successful transfer from SPC/E. *J. Chem. Phys.* **156**, 114501 (2022).
 61. Joung, I. S. & Cheatham, T. E. 3rd Determination of alkali and halide monovalent ion parameters for use in explicitly solvated biomolecular simulations. *J. Phys. Chem. B* **112**, 9020–9041 (2008).
 62. Dennington, R. D., Keith, T. A. & Millam, J. M. GaussView 5.0.8 (Gaussian, 2008).
 63. Roothaan, C. C. J. New developments in molecular orbital theory. *Rev. Mod. Phys.* **23**, 69 (1951).

64. Ditchfield, R. H. W. J., Hehre, W. J. & Pople, J. A. Self-consistent molecular-orbital methods. IX. An extended Gaussian-type basis for molecular-orbital studies of organic molecules. *J. Chem. Phys.* **54**, 724–728 (1971).
65. Bayly, C. I., Cieplak, P., Cornell, W. & Kollman, P. A. A well-behaved electrostatic potential based method using charge restraints for deriving atomic charges: the RESP model. *J. Phys. Chem.* **97**, 10269–10280 (1993).
66. Essmann, U. et al. A smooth particle mesh Ewald method. *J. Chem. Phys.* **103**, 8577–8593 (1995).
67. Hess, B. P-LINCS: a parallel linear constraint solver for molecular simulation. *J. Chem. Theory Comput.* **4**, 116–122 (2008).
68. Bussi, G., Donadio, D. & Parrinello, M. Canonical sampling through velocity rescaling. *J. Chem. Phys.* **126**, 014101 (2007).
69. Feenstra, K. A., Hess, B. & Berendsen, H. J. C. Improving efficiency of large time-scale molecular dynamics simulations of hydrogen-rich systems. *J. Comput. Chem.* **20**, 786–798 (1999).
70. Huter, P. et al. Structural basis for polyproline-mediated ribosome stalling and rescue by the translation elongation factor EF-P. *Mol. Cell* **68**, 515–527.e516 (2017).
71. Parrinello, M. & Rahman, A. Polymorphic transitions in single crystals: a new molecular dynamics method. *J. Appl. Phys.* **52**, 7182–7190 (1981).
- figures. B.B. generated strains and helped with sample preparation. H.P. prepared and screened the cryo-EM grids and helped with processing and refinement. K.F. and S.C. performed the biochemical stalling assays. S.G. and L.V.B. performed the MD simulations. D.N.W. and M.M. wrote the manuscript with input from all authors. D.N.W. and S.C. conceived and supervised the project.

Funding

Open Access funding enabled and organized by Projekt DEAL.

Competing interests

The authors declare no competing interests.

Additional information

Supplementary information The online version contains supplementary material available at <https://doi.org/10.1038/s41467-024-46761-3>.

Correspondence and requests for materials should be addressed to Shinobu Chiba or Daniel N. Wilson.

Peer review information *Nature Communications* thanks the anonymous reviewer(s) for their contribution to the peer review of this work. A peer review file is available.

Reprints and permissions information is available at <http://www.nature.com/reprints>

Publisher's note Springer Nature remains neutral with regard to jurisdictional claims in published maps and institutional affiliations.

Open Access This article is licensed under a Creative Commons Attribution 4.0 International License, which permits use, sharing, adaptation, distribution and reproduction in any medium or format, as long as you give appropriate credit to the original author(s) and the source, provide a link to the Creative Commons licence, and indicate if changes were made. The images or other third party material in this article are included in the article's Creative Commons licence, unless indicated otherwise in a credit line to the material. If material is not included in the article's Creative Commons licence and your intended use is not permitted by statutory regulation or exceeds the permitted use, you will need to obtain permission directly from the copyright holder. To view a copy of this licence, visit <http://creativecommons.org/licenses/by/4.0/>.

© The Author(s) 2024, corrected publication 2024

Acknowledgements

We thank Satoshi Naito and Tomoya Imamichi for providing a plasmid for XBP1u, Machiko Murata and Naoko Muraki for their technical support. This work was supported by the Deutsche Forschungsgemeinschaft (DFG) (grant WI3285/11-1 to D.N.W.), JSPS Grant-in-Aid for Scientific Research (Grant No. 16H04788, 26116008, 20H05926, and 21K06053 to S.C and 19K16044 and 21K15020 to K.F), Institute for Fermentation, Osaka (grant G-2021-2-063 to S.C.), and under Germany's Excellence Strategy grant no. EXC 2067/1-390729940 (L.V.B.). We acknowledge financial support from the Open Access Publication Fund of Universität Hamburg. Cryo-EM grid preparation was performed at the Multi-User Cryo-EM Facility at the Centre for Structural Systems Biology, Hamburg, supported by the Universität Hamburg and DFG grant numbers (INST 152/772-1 | 152/774-1 | 152/775-1 | 152/776-1 | 152/777-1 FUGG). We would like to thank Jiří Nováček for data collection via iNEXT-Discovery project number 23828 (funded by the Horizon 2020 program of the European Commission) and acknowledge the cryo-electron microscopy and tomography core facility CEITEC MU of CIISB, Instruct-CZ Centre supported by MEYS CR (LM2018127).

Author contributions

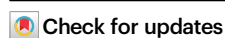
M.M. generated samples and processed the microscopy data, as well as generated and refined the molecular models and made all the structure

The SecM arrest peptide traps a pre-peptide bond formation state of the ribosome

Received: 30 October 2023

Accepted: 7 March 2024

Published online: 19 March 2024



Felix Gersteuer^{1,4}, Martino Morici^{1,4}, Sara Gabrielli², Keigo Fujiwara³, Haaris A. Safdari¹, Helge Paternoga¹, Lars V. Bock², Shinobu Chiba³ & Daniel N. Wilson¹ ✉

Nascent polypeptide chains can induce translational stalling to regulate gene expression. This is exemplified by the *E. coli* secretion monitor (SecM) arrest peptide that induces translational stalling to regulate expression of the downstream encoded SecA, an ATPase that co-operates with the SecYEG translocon to facilitate insertion of proteins into or through the cytoplasmic membrane. Here we present the structure of a ribosome stalled during translation of the full-length *E. coli* SecM arrest peptide at 2.0 Å resolution. The structure reveals that SecM arrests translation by stabilizing the Pro-tRNA in the A-site, but in a manner that prevents peptide bond formation with the SecM-peptidyl-tRNA in the P-site. By employing molecular dynamic simulations, we also provide insight into how a pulling force on the SecM nascent chain can relieve the SecM-mediated translation arrest. Collectively, the mechanisms determined here for SecM arrest and relief are also likely to be applicable for a variety of other arrest peptides that regulate components of the protein localization machinery identified across a wide range of bacteria lineages.

Cells have evolved elaborate post-transcriptional regulatory pathways to monitor and fine-tune expression of particular genes. One such strategy utilizes specific nascent polypeptide chains (NC) to induce translational arrest by inhibiting *in cis* the ribosome that is translating it. These so-called “arrest peptides” are usually encoded in upstream open reading frames (uORFs) where they induce translational stalling to regulate expression of a downstream gene^{1–4}. Perhaps one of the best-characterized examples is the secretion monitor (SecM) arrest peptide that is involved in the regulation of the downstream *secA* gene in Gram-negative bacteria, such as *Escherichia coli*^{2,5,6}. In the absence of SecM-mediated stalling, an intergenic stem-loop structure in the mRNA sequesters the ribosome-binding site (RBS) of the *secA* gene, preventing translation of the SecA protein (Fig. 1a). However, SecM-mediated stalling during translation of the *secM* uORF results in conformational changes

within the mRNA that expose the downstream RBS and thereby promotes translation of the *secA* gene (Fig. 1b). SecA is an ATPase that functions together with the SecYEG protein-conducting channel to facilitate the targeting of secretory proteins into and through the cytoplasmic membrane^{7–9}. Because *secM* encodes an N-terminal signal sequence (Fig. 1c), the SecM arrest peptide is itself a substrate for SecA. Importantly, the interaction of SecA with the N-terminal signal sequence of SecM as it emerges co-translationally from the ribosomal tunnel exerts a pulling force of the SecM NC that relieves the SecM-mediated translational arrest^{2,5,10,11} (Fig. 1a). Thereby, an autoregulatory system is established such that when the intracellular levels of SecA are low, SecM stalling persists, resulting in the upregulation of the expression of *secA* (Fig. 1b). By contrast, as SecA levels are restored, SecM stalling is relieved, leading to repression in the expression of *secA*^{2,6} (Fig. 1a).

¹Institute for Biochemistry and Molecular Biology, University of Hamburg, Martin-Luther-King-Platz 6, 20146 Hamburg, Germany. ²Theoretical and Computational Biophysics Department, Max Planck Institute for Multidisciplinary Sciences, Göttingen, Germany. ³Faculty of Life Sciences and Institute for Protein Dynamics, Kyoto Sangyo University, Kamigamo, Motoyama, Kita-ku, Kyoto 603-8555, Japan. ⁴These authors contributed equally: Felix Gersteuer, Martino Morici. ✉e-mail: Daniel.Wilson@chemie.uni-hamburg.de

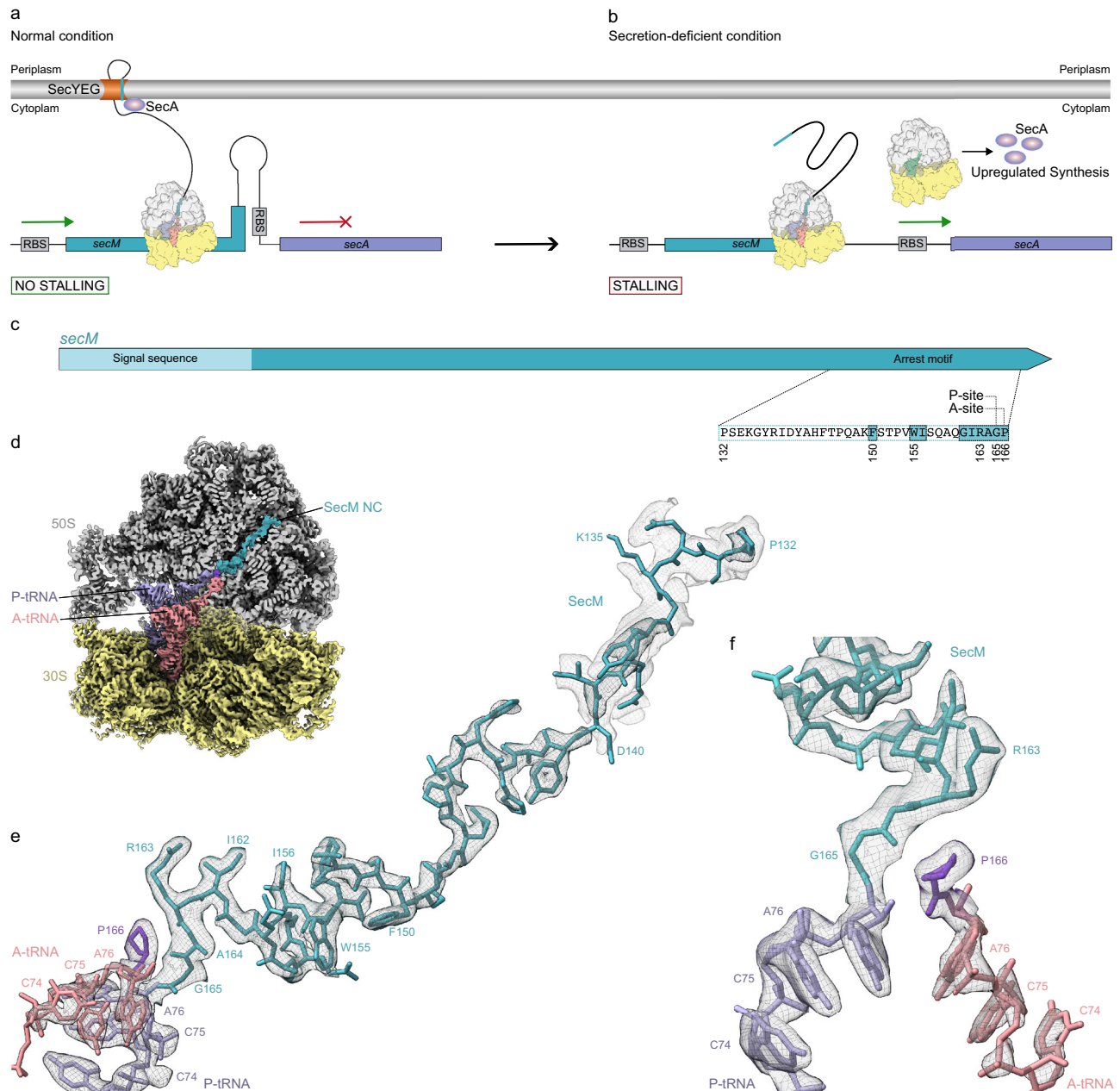


Fig. 1 | Regulation of SecM and cryo-EM structure of SecM-SRC. a Schematic representation of *secM-secA* mRNA illustrating the stem-loop structure at the stalling site of *secM* leader peptide (teal) that sequesters the ribosome-binding site (RBS) of the *secA* gene (lavender) thereby preventing *secA* translation. By SecYEG-mediated SecM translocation, SecM-induced stalling is relieved. **b** Upon stalling of the ribosome at the stalling site of *secM* (teal) the ribosome-binding site of the *secA* gene (lavender) becomes accessible and translation of *secA* starts. **c** Schematic representation of the SecM gene used in the SRC formation with SecM signal sequence and arrest motif as well as functionally relevant amino acids, A- and P-site

of the arrest motif indicated. **d** Cryo-EM map of the 3D-refined *E. coli* SecM-SRC with transverse section of the 50S (grey) to reveal density for the nascent chain (teal), P-tRNA (lavender), proline 166 of SecM (grape), A-tRNA (salmon) and 30S (yellow). **e, f** Two views showing the cryo-EM map density (black mesh) for A- and P-site tRNA as well as the attached nascent chain and proline of the 3D refined *E. coli* SecM-SRC. The P-site tRNA (lavender) bears the SecM nascent chain (teal), whereas the A-site tRNA (salmon) carries proline (grape). Additional density at lower threshold for N-terminal part of nascent chain (grey mesh) in (e).

Biochemical studies have revealed that the SecM arrest peptide stalls the ribosome with the SecM NC attached to tRNA^{Gly165} in the P-site and with Pro¹⁶⁶-tRNA in the A-site^{12,13} (Fig. 1c). Alanine scanning mutagenesis identified residues Arg163 and Pro166 within the *E. coli* SecM sequence as being critical for SecM-mediated stalling, but also other residues that contribute to stalling, leading to designation of a SecM arrest motif₁₅₀FxxxWlxxxGIRAGP₁₆₆¹⁴ (Fig. 1c). Although this small SecM arrest motif is sufficient to induce translational stalling, stronger arrest is observed when using the full-length SecM sequence, indicating that the regions N-terminal to the SecM arrest

motif also contribute to the stalling efficiency^{14–16}. Biophysical studies proposed that SecM adopts a compacted conformation within the exit tunnel, and identified mutations (F150A, W155A and R163A) in SecM where compaction is maintained but stalling is reduced, suggesting that compaction is necessary but not sufficient to induce the translational arrest¹⁷. Mutations within 23S rRNA nucleotides, as well as alterations within ribosomal proteins, such as uL22, comprising the ribosomal tunnel reduce the efficiency of SecM-mediated stalling^{14,18–21}. Specific SecM residues have also been crosslinked to uL22²², collectively, suggesting that interaction between the SecM NC

and the ribosomal tunnel plays an important role in modulating the efficiency of stalling.

The first structures of SecM-stalled ribosomal complexes (SRC) were reported at 6–9 Å, leading to the proposal that SecM causes a shift in the position of the P-site tRNA, which interferes with peptide bond formation with the A-site Pro-tRNA²³. A subsequent structural study²⁴ reported cryo-EM structures of SecM-SRC at higher resolution (3.3–3.7 Å), suggesting that SecM (i) induces conformational changes within the peptidyltransferase centre (PTC) that lead to an inactive state of the ribosome, and (ii) that the sidechain of the critically important Arg163 of the SecM sterically blocks the accommodation of Pro-tRNA in the A-site. The presence of a vacant A-site in the SecM-Gly-SRC structure²⁴ contrasted with previous biochemical studies indicating that the A-site is occupied by Pro-tRNA^{12,13}. Also surprising was that the SecM NC was extended in the tunnel²⁴, rather than adopting a compacted conformation as suggested previously^{17,25}. Of note, was that this SecM-SRC structure was determined using only 17 residues (150–166) of SecM, with the N-terminal residues being replaced by 2xStrep-TEV-tag, the N-terminal 40 residues of OmpA and a Myc-tag²⁴, therefore, the interaction of regions N-terminal of the arrest window could not be ascertained^{15,16,26}. Finally, the SecM-SRC was purified in the presence of chloramphenicol, an antibiotic that inhibits elongation by binding to the PTC²⁷, and may therefore have also affected the final functional state that was visualized²⁴.

In addition to studies addressing the mechanism of SecM-mediated stalling, the SecM arrest peptide has been used extensively for generating ribosome-nascent chain complexes (RNCs) for functional studies^{28–30}, including ribosome display^{31,32}, real-time monitoring in vivo³³ and single molecule imaging^{34,35}, but particularly for investigating co-translational protein folding and targeting events^{36–53}. Furthermore, molecular dynamics simulations based on available structural models for SecM have been performed to investigate how the pulling force could relieve the translational arrest^{38,54–56}. Given the wide usage of SecM for diverse functional studies, it is important to understand the conformation of full-length SecM within the ribosomal tunnel, the number of the residues of SecM that transverse the ribosomal tunnel as well as the exact mechanism of action of SecM to inhibit translation elongation.

Here we report a cryo-electron microscopy (cryo-EM) structure of an *E. coli* SecM-stalled ribosomal complex (SRC) at 2.0 Å resolution. In contrast to the previous SecM-RNC²⁴, we observe one major functional state of the ribosome bearing a SecM-peptidyl-Gly-tRNA in the P-site and Pro-tRNA in the A-site. Our structure reveals that SecM stalls translation by interfering with peptide bond formation, rather than preventing accommodation of the A-site tRNA, as suggested previously²⁴. Specifically, our data support a model whereby interactions between the ₁₆₃RAG₁₆₅ motif in the SecM nascent chain attached to the P-site tRNA with the Pro¹⁶⁶-tRNA in the A-site prevent the proton transfer necessary to allow the nucleophilic attack during peptide bond formation. Additionally, we observe the formation of a short seven amino acid (aa) α -helix encompassing residues Thr152 and Glu158 of SecM. As a consequence, the change in register leads to a completely different set of interactions between the SecM NC and tunnel components compared to previous reports^{23,24}. We believe that the knowledge that 40, rather than 30, residues of SecM are accommodated within the exit tunnel will also be of general importance when using SecM-SRC to investigate co-translational folding and targeting events.

Results

Cryo-EM structure of *E. coli* SecM-SRC at 2.0 Å resolution

E. coli SecM-stalled ribosome complexes (SecM-SRC) were generated using a fully reconstituted *E. coli* in vitro translation system and purified with the N-terminal FLAG affinity tag (see “Methods”). Unlike previous SecM-SRC structures that employed a SecM arrest window of

Table 1 | Cryo-EM data collection, refinement and validation statistics

Model	SecM-SRC (P-tRNA, A-tRNA)
EMDB ID	18534
PDB ID	8QOA
Data collection and processing	
Magnification (×)	105,000
Acceleration voltage (kV)	300
Electron fluence (e ⁻ /Å ²)	40
Defocus range (μm)	−0.3 to −0.9
Pixel size (Å)	0.83
Initial particles	398,692
Final particles	300,107
Average resolution (Å) (FSC threshold 0.143)	2.0
Model composition	
Initial model used (PDB code)	7K00
Atoms	147,754
Protein residues	5607
RNA bases	4549
Refinement	
Map CC around atoms	0.72
Map CC whole unit cell	0.71
Map sharpening B factor (Å ²)	−39.79
R.M.S. deviations	
Bond lengths (Å)	0.008
Bond angles (°)	1.529
Validation	
MolProbity score	0.86
Clash score	0.37
Poor rotamers (%)	0.65
Ramachandran statistics	
Favoured (%)	96.50
Allowed (%)	3.39
Outlier (%)	0.11
Ramachandran Z-score	−1.37

17–27 residues^{23,24}, we utilized the full-length wildtype *E. coli* SecM sequence comprising the full 170 residues (Fig. 1c). Moreover, in contrast to previous structural studies on SecM-SRC^{23,24}, the antibiotic chloramphenicol was not added during any stage of the sample preparation. The purified SecM-SRC was applied to cryo-EM grids and analyzed using single particle cryo-EM. A total of 4388 micrographs were collected on a Titan Krios G3i equipped with a K3 direct electron detector, yielding 398,692 particles after 2D classification (Supplementary Fig. 1 and Table 1). Focused 3D classification on the 377,762 particles containing 70S ribosomes revealed one major class of non-rotated 70S ribosomes bearing A- and P-site tRNAs (75%; 300,107 particles) as well as one minor class with rotated 70S ribosomes with hybrid A/P- and P/E-site tRNAs (9.1%; 36,489 particles), collectively representing a total of 84% of the initial ribosomal particles (Supplementary Fig. 1). The 70S ribosome with A- and P-site tRNAs was further refined, yielding a cryo-EM map of the SecM-SRC with an average resolution of 2.0 Å (Fig. 1d, Table 1 and Supplementary Fig. 1 and 2). In the SecM-SRC, density for the SecM nascent polypeptide chain (NC) was observed throughout the ribosomal exit tunnel (Fig. 1d), enabling 34 amino acids (residues Pro132 to Gly165) of SecM to be modelled (Fig. 1e). With the exception of the four residues (Pro132-Lys135) near the tunnel exit, the density was well-resolved enabling unambiguous placement of almost all the sidechains (Fig. 1e, Supplementary Fig. 2,

Supplementary Movie 1), especially the C-terminally conserved $_{163}\text{RAG}_{165}$ motif that is directly linked to the CCA-end of the P-site tRNA (Fig. 1f). In addition, the high quality of the cryo-EM density map allowed the Pro $_{166}$ moiety attached to the CCA-end of the A-site tRNA to be unambiguously identified and modelled (Fig. 1f, Supplementary Movie 1). We also subrotated and refined the rotated SecM-SRC population with hybrid A/P- and P/E-site tRNAs, yielding a cryo-EM map generated from 36,489 particles with average resolution of 2.6 Å (Supplementary Figs. 1 and 3). Although the ribosome was well-resolved, the density for the tRNAs and the NC were less defined, precluding a molecular model to be generated (Supplementary Fig. 3). Overall the SecM NC path seems similar to that observed in the non-rotated SecM-SRC (Supplementary Fig. 3), therefore, we presume this state represents a small population of SecM-SRC that has undergone peptide bond formation during the long purification process (>4 h at 4 °C, see “Methods”), such that the deacylated tRNA^{Gly} is present in the P/E site and the peptidyl-SecM-Gly-Pro-tRNA^{Pro166} is now shifted into the A/P-site, as observed previously^{23,24}. However, we cannot exclude that this population represents a mixture of states, which coupled with the poor resolution of NC, meant that state was not analyzed further. Taken together, the cryo-EM structure of the SecM-SRC revealed that the majority of ribosomes bear the SecM-Gly-tRNA in the P-site and have Pro-tRNA in the A-site, consistent with previous biochemical analysis^{12,13}. This supports the suggestion that the SecM NC interferes with peptide bond formation between the peptidyl-RAG-tRNA in the P-site and the incoming A-site Pro-tRNA^{12,13}.

The SecM NC adopts a helical structure within the NPET

The path of the SecM NC is observed from the PTC, where the C-terminus is attached to the tRNA^{Gly}, throughout the tunnel to the vestibule where the tunnel widens at the exit (Fig. 2a, b). The SecM NC makes no stable contact with uL4 as it passes through the constriction, whereas multiple interactions with uL22 are observed, not only at the constriction, but also deeper in the tunnel (Fig. 2b). The N-terminal residues Pro132-Lys135 of SecM are within close proximity of uL23 (Fig. 2b), but do not appear to directly make contact. While the majority of the SecM NC adopts an extended conformation, the region located directly between the PTC and the constriction is clearly compacted (Fig. 2a, b). This is consistent with secondary structure predictions of the SecM NC that suggest a high probability of α -helical formation within this region (Fig. 2c). Careful inspection of the molecular model of the SecM NC within this region indeed revealed that for residues Glu158 to Thr152 of SecM adopt a standard [i + 4 \rightarrow i] α -helix where each backbone nitrogen (N-H) forms a hydrogen bond with the backbone carbonyl-oxygen (C=O) of the amino acid four residues earlier (Fig. 2d, e). The seven-residue α -helix forms despite the presence of Pro153, which does not break the helix but its location at the N-terminus may rather facilitate its formation⁵⁷ (Fig. 2d, e). Although reminiscent of the ten residue α -helix that was observed at the PTC of the VemP arrest peptide⁵⁸, the location of the SecM α -helix is shifted by 12 Å deeper into the tunnel (Supplementary Fig. 4a–c), such that, unlike VemP⁵⁸, the SecM α -helix does not perturb the conformation of 23S rRNA nucleotides at the PTC (see later). Rather the location is more similar to the helical regions observed in the exit tunnel of the TnaC and hCMV arrest peptides structures^{59,60} (Supplementary Fig. 4d–g).

The presence of an α -helical conformation for residues Thr152–Glu158 of SecM observed in the SecM-SRC structure determined here (Fig. 2f) is in excellent agreement with compaction observed in a previous study measuring fluorescence resonance energy transfer (FRET) between the acceptor and donor probes at positions 135 and 159 of SecM, respectively¹⁷. Compared to a theoretical fully extended conformation spanning 3.5 Å per residue, the FRET study predicted a compaction of 2.6 Å per residue, which compares well with the 2.0 Å per residue observed here (distance between positions 135 and 159 of 50 Å/25 residues). By contrast, no compaction was observed in the

previous SecM-SRC structure²⁴ and therefore the last NC residue modelled was Glu139 that forms part of the c-Myc tag and was equivalent to Ile139 of SecM (Fig. 2g). Because of the difference in the degree of compaction between the SecM-SRC determined here (Fig. 2f) and the previous SecM-SRC structure (PDB ID 3JBU)²⁴ (Fig. 2g), the register of the SecM residues spanning the ribosomal exit tunnel is completely different (Fig. 2h). This is exemplified by Phe150 of SecM, which in the previous structure²⁴ was located deep in the tunnel past the uL4–uL22 constriction site, whereas in the SecM-SRC structure determined here, Phe150 is located 25 Å away on the PTC side of the constriction site (Fig. 2h). The compacted conformation observed in the SecM-SRC structure determined here is also more consistent with biochemical data reporting crosslinking between Tyr141 of SecM and uL22, as well as the lack of crosslinking between residues 149 and 152 of SecM and uL22 (Fig. 2f)²².

Interaction of SecM with ribosomal proteins of the NPET

As mentioned, a consequence of the compacted conformation of SecM is that the residues (Phe150, Trp155, Ile156, $_{161}\text{GIRAGP}_{166}$) encompassing the SecM motif (FxxxxWlxxxxGIRAGP) are all located before the constriction (Fig. 2f), rather than forming direct interactions with ribosomal proteins uL4 and uL22 located deeper in the tunnel, as proposed previously²⁴. Instead, in the SecM-SRC determined here, we observe that the residues N-terminal to Phe150, specifically, residues 132–149, of SecM form multiple interactions with both ribosomal protein and rRNA components of the exit tunnel. This is in excellent agreement with previous studies indicating that regions N-terminal to the SecM arrest window within the full-length SecM also contribute to the efficiency of stalling^{14–16,26}. Although the N-terminal region of SecM at the exit tunnel site is poorly resolved, the density for the NC clearly passes between the tip of uL23 and 23S rRNA helix 50 (H50), with strong density suggesting that Pro132 of SecM forms stacking interactions with the nucleobase of A1321 within H50 (Fig. 3a). The density for the residues Tyr137 to Lys149 of SecM is well-resolved (Figs. 1e and 2b), presumably due to the multiple interactions observed with tunnel components, in particular, uL22 (Fig. 3a–c). Briefly, the sidechain of Tyr137 of SecM comes within hydrogen bonding distance of the backbone of Ile85 of uL22 and can form stacking interactions with Arg84 of uL22 (Fig. 3a). Direct hydrogen bonds are also possible from the sidechain of Tyr141 of SecM and the backbone of Gly91 of uL22, as well as additional interactions between the backbone of His143 and Gln147 of SecM with the backbone of Lys90 and Ala93 of uL22 (Fig. 3b). The high quality of the map enables a network of water-mediated interactions to be described involving residues (Ala142, Thr145, Pro153) of the SecM NC with residues (Lys90, Arg92 and Ala93) of uL22 as well as 23S rRNA nucleotides A1614 and A751 (Fig. 3c). Interaction with A751 likely explains why the insertion of an adenine within the 5-adenine stretch between A749–A753 reduces SecM-mediated stalling, albeit resulting in a relatively minor effect^{14,19}.

There is good agreement between the interactions observed between SecM and uL22 in the SecM-SRC and previously reported alterations in uL22 that reduce the stalling efficiency of SecM^{14,18}. This includes, for example, substitutions at residues Gly91, Ala93 or Arg84, insertions (+2 and +15 aa at position 99 and 105, respectively) within the loop of uL22, as well as deletion of the $_{82}\text{MKR}_{84}$ motif or the entire loop in uL22^{14,18}. In most cases, the alterations would be predicted to perturb the interactions between SecM and uL22 by either directly introducing steric clashes (substitutions and insertions) and/or inducing conformational changes in the uL22 loop (insertions and deletions) (Supplementary Fig. 5a–f). The later scenario is exemplified by the structures of ribosomal 50S subunits with insertions or deletions in uL22 that lead to dramatic rearrangements in the loop of uL22^{61,62}, which would be incompatible with the observed path of the SecM NC (Supplementary Fig. 5g–j). By contrast, we observe no defined interaction between the SecM NC and uL4, with the closest point of contact

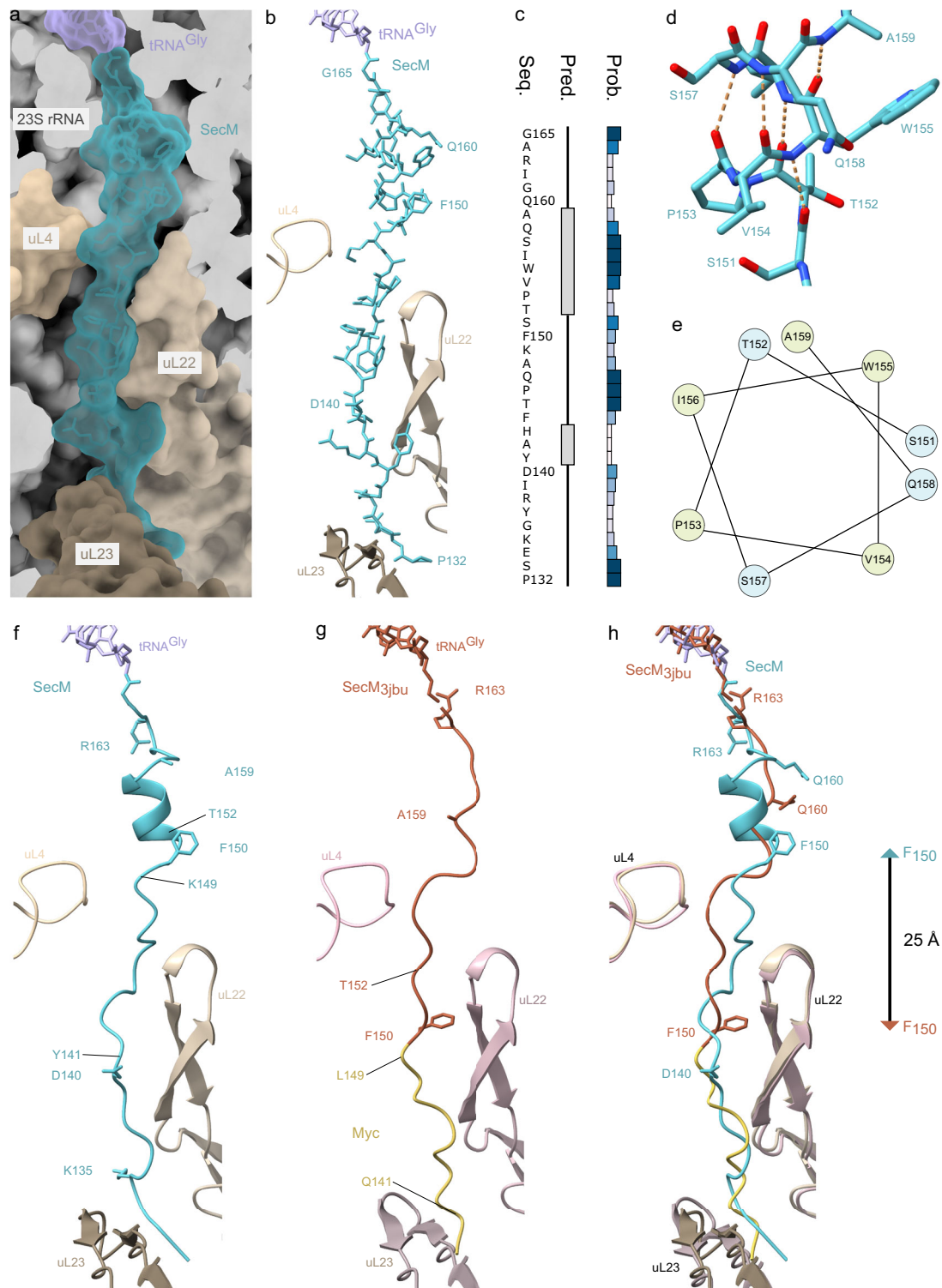


Fig. 2 | Formation of an α -helix inside the NPET by the SecM peptide.

a Transverse section of the NPET shown as surface (grey) with P-tRNA (lavender) and SecM (teal) in relation to uL4 (light gold), uL22 (gold) and uL23 (dark gold) in surface representation. **b** Cryo-EM density (transparent teal, threshold 0.008/ \sim 2.6 σ) and model of SecM (teal) attached to the P-tRNA (lavender) in relation to uL4 (light gold), uL22 (gold) and uL23 (dark gold). **c** Secondary structure prediction (Pred.) and probability (Prob.) of the SecM (Seq.) inside the NPET determined using PSIPRED. **d** Helix region of SecM (teal) inside the NPET and potential hydrogen

bonds shown as dashed orange lines. **e** Downward cross-sectional view of the SecM helix axis with non-polar amino acids coloured in yellow and polar amino acids coloured in blue. **f** Structure of SecM (teal) in ribbon representation attached to the P-tRNA (lavender) in relation to uL4 (light gold), uL22 (gold) and uL23 (dark gold). **g** Myc-SecM (PDB ID 3JBU)²⁴ attached to the P-tRNA (tangerine/yellow) in relation to uL4 (light rose), uL22 (rose) and uL23 (dark rose). **h** Overlay (aligned on basis of 23S rRNA) of (f) SecM and (g) SecM_{3JBU} with distance between F150 position from the two models arrowed.

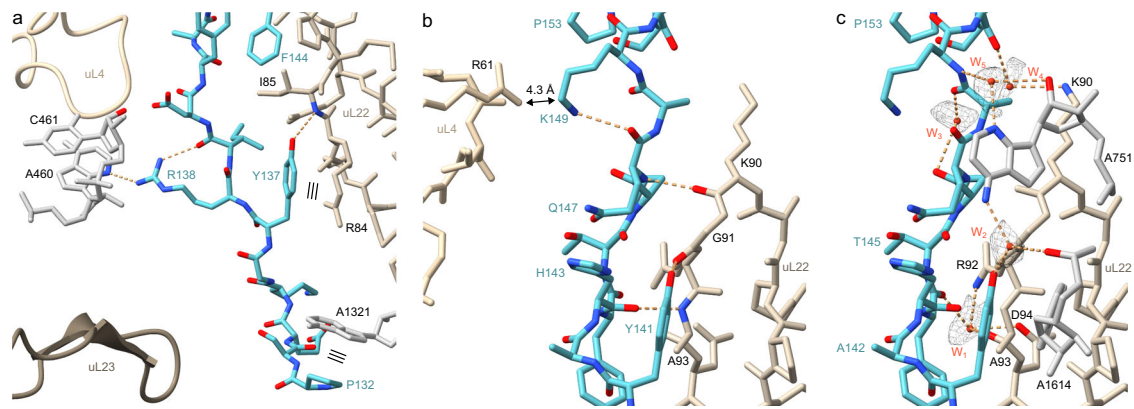


Fig. 3 | Interactions of SecM with components of the NPET. Interactions of a N-terminal and b, c middle part of SecM (teal) inside the NPET with 23S rRNA (grey), uL4 (light gold), uL22 (gold) and uL23 (dark gold). In (a) and (b) direct interactions are shown whereas in (c) water-mediated interactions for the middle

part of SecM (teal) are indicated. Potential hydrogen bonds are shown as dashed orange lines, stacking interactions as three parallel lines and water molecules as red spheres with meshed density.

being 4.3 Å between the sidechains of Lys149 of SecM and Arg61 of uL4 (Fig. 3b). Consistently, selection of mutants that relieve SecM-mediated stalling were identified only in uL22, but not in uL4¹⁴, and engineered uL4 substitutions at positions 62, 63 and 66 had no effect on SecM arrest¹⁸. The exception is an insertion of six amino acids at position 72 of uL4 that was reported to have a minor effect on SecM pausing¹⁸, however, Ser72 of uL4 is located ~20 Å away from the SecM NC and therefore any effects are likely to be indirect via conformational changes in uL4, analogous to the uL22 loop insertions and deletions. We note that the sidechain of Arg138 of SecM can form a hydrogen bond with 23S rRNA nucleotide A460 located in H23 (Fig. 3a), and that H23 also contacts uL4, raising the possibility that this insertion in uL4 indirectly effects SecM stalling via perturbing H23.

A recent study generating deletions in the N-terminus of SecM revealed that residues 58–98 of SecM contribute to the efficiency of SecM-mediated stalling¹⁶. Because this region of SecM was predicted to adopt an α -helical secondary structure and Tyr80 located within this α -helix was shown to crosslink to uL23, the authors proposed that the interaction is likely to occur outside the tunnel exit¹⁶. Since we used the full-length SecM sequence for the SecM-SRC, we carefully analyzed the tunnel exit site and indeed discovered an additional density located in proximity to uL23, albeit only visible at low threshold levels (Supplementary Fig. 6). Although the additional density would be consistent with an α -helical structure, the density is poorly resolved, precluding a molecular model to be generated. Moreover, the lack of density connecting the SecM NC within the tunnel with the helical density at the tunnel exit makes it difficult to assign this region to any specific part of the N-terminus of SecM. In fact, we cannot rule out that the additional density actually represents the N-terminal signal sequence of SecM, which was also included in our construct, although we note that the binding position differs from that reported previously for signal sequences bound to ribosomal complexes^{63,64} (Supplementary Fig. 6).

Interaction of SecM with 23S rRNA nucleotides of the NPET

As mentioned above, a surprise from the SecM-SRC structure determined here was that in contrast to the previous SecM-SRC structure²⁴, the residues of the SecM motif (FxxxxWlxxxxGIRAGP) are not spread out through the exit tunnel, but are rather located in the upper third of the tunnel, at or adjacent to the PTC (Fig. 4a). The α -helical conformation of this region of SecM coupled with the hydrophobic nature of many of the residues suggests that many of the contacts with the ribosome utilize van der Waals interactions (Fig. 4b). This is exemplified by the interaction with A2058, which is surrounded by the sidechains of Thr152, Pro153, Ile156 and Ile162 of SecM (Fig. 4a and

Supplementary Fig. 7a). This intimate interaction explains why the A2058G mutation, which would lead to a clash with the sidechains of Thr152 and Ile156 of SecM (Supplementary Fig. 7b), relieves SecM-mediated stalling^{14,19}. Conversely, dimethylation of A2058 does not affect SecM-mediated stalling¹⁸ and no clash would be predicted based on the structure of the SecM-SRC (Supplementary Fig. 7c). We note that eukaryotic ribosomes contain G3904 in the position equivalent to *E. coli* A2058 (Supplementary Fig. 7d), consistent with our findings that SecM stalling does not work on eukaryotic ribosomes (see below).

Additional direct and water-mediated hydrogen bonds as well as stacking interactions are also observed that are likely to contribute to SecM stalling by stabilizing a defined conformation of the SecM NC. Specifically, the sidechain of Phe150 is observed to stack on the nucleobase of U2609 (Fig. 4a), and mutation of either Phe150¹⁴ or U2609¹⁹ has been reported to reduce the efficiency SecM-stalling. Direct hydrogen bonds are possible between the sidechain of Ser157 of SecM and the ribose of A2062, as well as the backbone carbonyls of Gly161 and Ile162 with the nucleobases of U2506 and A2062, respectively (Fig. 4c). Consistently, mutation of A2062U, which would lead to a loss of interaction with Ile162 (Supplementary Fig. 7e, f), reduces SecM-mediated stalling²⁰. The same study also demonstrated that A2503G mutations reduce SecM-mediated stalling²⁰, although we observe no direct interaction between A2503 and the SecM NC (Supplementary Fig. 7g). Instead, the A2503G mutation may induce an alternative conformation of A2062²⁰ that is incompatible with the modelled path of SecM (Supplementary Fig. 7h).

Additionally, potential water-mediated interactions link Ser157 of SecM with A2062, and Gln160 and Ala159 with U2585 (Fig. 4d), which are likely to contribute to stabilizing the observed conformation of the SecM NC. However, the most intricate network of interactions is observed for Arg163 of SecM, which inserts into a pocket formed by 23S rRNA nucleotides G2061 and A2503-U2506 (Fig. 4e, f). Within the binding pocket, Arg163 stacks upon Ψ 2504 (Fig. 4a) and can potentially establish seven hydrogen bonds with 23S rRNA nucleotides, five direct interactions as well as two mediated via water molecules (Fig. 4f). The interactions are likely to be critical for SecM mediated stalling since Arg163 was reported to be one of only three amino acids positions (together with Ile162 and Pro166) that was invariant in all sequenced SecM homologues²², and mutation of Arg163 (as well as Pro166 in the A-site) produced the strongest relief of SecM-mediated stalling¹⁴.

In eukaryotic ribosomes, U4450, the equivalent nucleotide to *Ec* Ψ 2504, adopts a different conformation that would prevent the stacking interaction with Arg163 (Supplementary Fig. 8a), which may

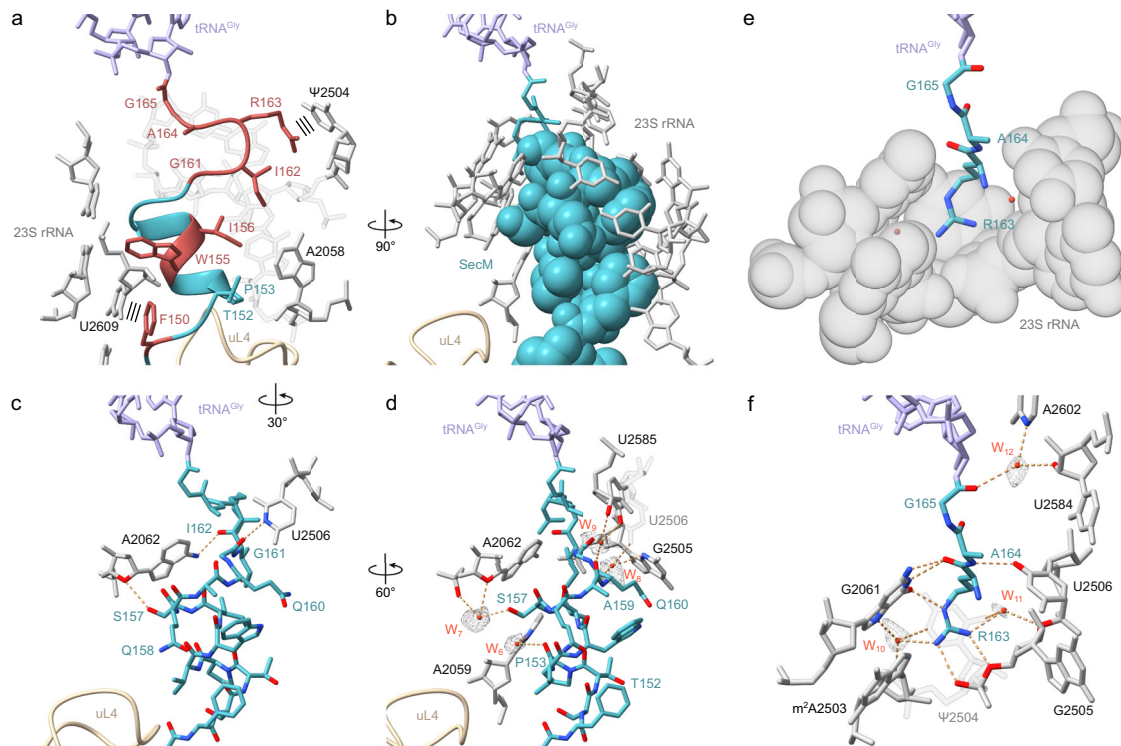


Fig. 4 | Interactions of SecM stalling motif with components of the NPET.

a SecM arrest peptide (teal) with surrounding 23S rRNA (grey) and residues of the SecM stalling motif highlighted in red. Stacking interactions depicted as three parallel lines. **b** Space filling representation of SecM stalling motif (teal) from F₁₅₀ to I₁₆₂ with surrounding 23S rRNA (grey). **c** Direct interactions of SecM stalling motif (teal) from F₁₅₀ to I₁₆₂ with 23S rRNA (grey). **d** Water-mediated interactions of SecM

stalling motif (teal) from F₁₅₀ to I₁₆₂ with 23S rRNA (grey). **e** Space filling representation of a distinct pocket of the NPET formed by 23S rRNA (grey) and entering SecM₁₆₃RAG₁₆₅ (teal). **f** Direct and water-mediated interactions of SecM₁₆₃RAG₁₆₅ (teal) with 23S rRNA (grey). Potential hydrogen bonds are shown as dashed orange lines and water molecules as red spheres (with meshed density).

prevent stalling in eukaryotes, although to our knowledge this is not known. To test this, we introduced the residues of SecM, as well as the Pro166Ala variant, into a GFP-LacZ reporter and monitored for the presence of peptidyl-tRNA and full-length protein after incubation in a rabbit reticulocyte *in vitro* translation system (Supplementary Fig. 8b). As a positive control, we employed an arrest-enhanced variant (S255A) of the XBP1u arrest peptide, where stalling was observed as the accumulation of peptidyl-tRNA that is resolved upon RNase treatment (Supplementary Fig. 8b), as expected⁶⁵. By contrast, we observed no accumulation of SecM-peptidyl-tRNA (Supplementary Fig. 8b), suggesting that SecM does not mediate efficient translation arrest on eukaryotic ribosomes.

SecM stabilizes a pre-attack state of the PTC

In the previous structure of SecM-SRC, Arg163 was modelled with the sidechain extending into the A-site where it would sterically block accommodation of the Pro-tRNA²⁴. However, in the structure presented here, the sidechain of Arg163 of SecM is oriented differently (Fig. 2f, g) such that it would not interfere with Pro-tRNA accommodation at the A-site of the PTC. To understand how SecM allows accommodation of Pro-tRNA at the A-site, but prevents peptide bond formation with the SecM-peptidyl-tRNA, we compared the PTC of the SecM-SRC with that of pre-attack state ribosomal complexes^{66,67} (Fig. 5a–c). In the pre-attack state, the α -amino group of the A-site Phe-tRNA is positioned ~ 3.0 Å from the carbonyl-carbon of the peptidyl-tRNA in the P-site, but peptide bond formation cannot occur because the peptide is linked to the P-site tRNA with an amide, rather than an ester, linkage^{66,67} (Fig. 5a). In the SecM-SRC, the Pro-tRNA is accommodated in the A-site and the nitrogen of the Pro166 moiety on the A-site tRNA is located ~ 4.3 Å from the carbonyl-carbon of the SecM-peptidyl-tRNA in the P-site, yet peptide bond formation has not

occurred, even though the SecM peptide is linked to the P-site tRNA by an ester linkage (Fig. 5b). The Pro-tRNA appears to be fully accommodated in the A-site since the conformation of the 23S rRNA nucleotides at the PTC is indistinguishable from that observed in the pre-attack state structures^{66,67} (Supplementary Fig. 8c, d), indicating that the induced conformation that is concomitant with A-site tRNA accommodation has been attained. Moreover, superimposition of the pre-attack state^{66,67} and the SecM-SRC reveals an identical placement (within the limits of the resolution) of the CCA-end of the A-site tRNA (Fig. 5c). The increased distance between the A-site nitrogen and P-site carbonyl-carbon in the SecM-SRC appears to result from both a shifted path (by -0.9 Å) of the SecM NC in the P-site as well as a different position (by -0.7 Å) of the nitrogen (secondary amine) in the proline moiety, as compared to the nitrogen (primary amine) in other amino acids, such as Phe^{66,67} (Fig. 5c). Although the distance is larger in SecM compared to the pre-attack state, it remains unclear whether this would be sufficient to effectively prevent the nucleophilic attack required for peptide bond formation to occur.

For peptide bond formation to occur, a proton needs to be extracted from the α -amino group of the amino acid linked to the A-site tRNA. In current models for peptide bond formation^{66,68–70}, this is performed by the 2' OH of A76 of the P-site tRNA, which subsequently increases the nucleophilicity of the α -amino group, thereby facilitating the nucleophilic attack of the lone pair electrons onto the carbonyl-carbon of the first amino acid linked to the P-site tRNA (Fig. 5d). In principle, the same pathway should be employed for amino acids such as proline with a secondary amine, with the major difference being the presence of only a single hydrogen on the nitrogen of proline (Fig. 5e), rather than two hydrogens for amino acids with primary amines (Fig. 5d). It is important to emphasize that the resolution of the SecM-SRC (and to date any other ribosomal complexes) is currently

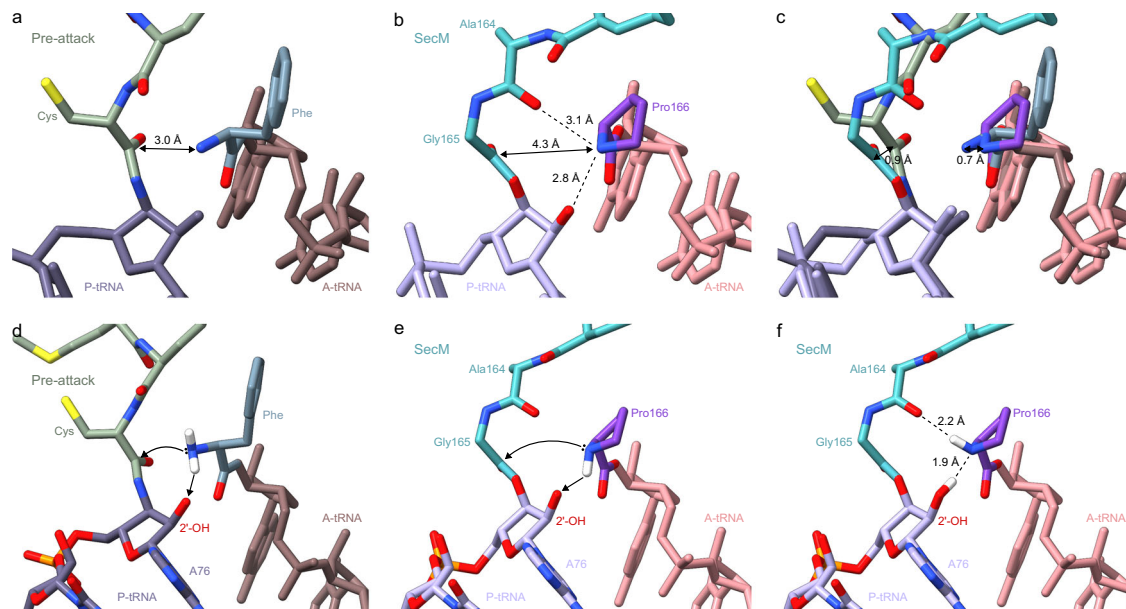


Fig. 5 | Model for SecM-mediated PTC arrangement leading to translational stalling. **a** View of the PTC of a pre-attack state (PDB ID 8CVK)⁹⁷, showing a tripeptidyl-NH-tRNA (green/dark lavender) at the P-site and a phenyl-NH-tRNA (slate blue/brown) at the A-site. The distance between the attacking amine of the A-tRNA and the carbonyl carbon of the P-site is indicated by a double arrow. **b** Same view as **(a)**, but for SecM-SRC with SecM-tRNA (teal/lavender) in the P-site and Pro-tRNA (grape/salmon) in the A-site. **c** Overlay of **(a)** and **(b)** (aligned on the basis of 23S rRNA) highlighting the difference in the distance between the attacking amino groups at the A-site and the carbonyl carbon at the P-site. **d** Schematic view of the

PTC of a pre-attack from **(a)**, but with hydrogen atoms (white) modelled in silico for the amino group of the phenylalanine in the A-site. Black spheres indicate the lone pair electrons that make the nucleophilic attack (arrowed) on the carbonyl carbon of the cysteine attached to the P-site tRNA. **e** Same schematic as **(b)**, but with hydrogen atom (white) modelled in silico towards the 2'-OH of A76 of the P-site tRNA, which would allow a nucleophilic attack (arrowed) on the carbonyl carbon of the Gly165 attached to the P-site tRNA. **f** Same schematic as **(e)** but with the hydrogen atom (white) modelled towards the carbonyl of Ala164, a conformation that would prohibit any nucleophilic attack.

insufficient to observe hydrogens directly, and therefore their position can only be predicted or inferred via hydrogen bonding interactions. Indeed, careful examination of the environment of the nitrogen of the A-site Pro166 in the SecM-SRC reveals that the nitrogen is not only in hydrogen bonding distance to the 2' OH of A76 (2.8 Å in Fig. 5b), as expected, but also to the carbonyl-oxygen of Ala164 (3.1 Å in Fig. 5b), suggesting that these two hydrogen bonds are present simultaneously. Because the carbonyl oxygen of Ala164 can only act as an hydrogen bond acceptor, this suggests that the sole hydrogen of Pro166 must be donated to allow this bond to form (Fig. 5f). A consequence of this is that the 2' OH of A76 must also act as a donor to enable the second hydrogen bond, which would then form with the lone pair electrons on Pro166 (Fig. 5f). Thus, the hydrogen bonding pattern for Pro166 in the SecM-SRC completely disfavours peptide bond formation because (i) the 2' OH of A76 acts as a donor, rather than extracting a proton from Pro166 to increase the nucleophilicity, and (ii) the hydrogen bond with the carbonyl-oxygen of Ala164 creates a geometry where the lone pair electrons cannot make a nucleophilic attack on the carbonyl-carbon of the Gly165 on the P-site tRNA (Fig. 5f). We note that in the pre-attack state, the carbonyl-oxygen of the equivalent amino acid to Ala164 is oriented differently and further away from the A-site nitrogen, but that even if a hydrogen bond could form, the presence of two hydrogens on the primary amine of such an amino acid in the A-site would still allow extraction of a proton by the 2'-OH of A76 while allowing an optimal geometry for peptide bond formation to be attained (Fig. 5d). This is also likely to explain why Pro166, bearing a secondary amine, is critical for SecM-mediated stalling and mutations to any amino acid having a primary amine, such as alanine^{14,22}, but also serine, histidine or arginine⁷¹, lead to relief of stalling.

Relief of stalling by pulling on the N-terminus of SecM

SecM stalling is released in vivo by a mechanical pulling force caused by interaction of the N-terminal signal sequence of SecM with

SecA^{2,5,10,11}. To investigate how this pulling force relieves translational stalling and how this is influenced by the presence of the α -helix in the tunnel, we performed all-atom explicit-solvent molecular dynamics (MD) simulations of the SecM-SRC. Two sets of simulations were carried out: unbiased simulations in the absence of a pulling force and pulling simulations where a harmonic spring potential acts on the N-terminal Pro132 of the SecM NC. During the pulling simulations, the spring position was moved by 56 Å in the direction of the tunnel axis with a constant velocity, exerting a force on Pro132. To check if the observed order of events depends on the pulling velocity, we carried out sets of 8 independent simulations with pulling times τ ranging between 32 ns and 1024 ns. Throughout the unbiased simulations, we observed the SecM α -helix to remain very stable and the fluctuations (rmsf) of the SecM residues to be small (Fig. 6a). In agreement with the cryo-EM structure where N-terminal residues were less well-resolved (Fig. 1e), we observe increased fluctuations for these residues (Fig. 6a). When pulling on the N-terminus, the α -helix could either remain folded and be pulled through the constriction as a whole, or it could unfold before passing through the constriction. The positions of SecM residues along the tunnel during the slower simulations showed that, in the beginning (0–384 ns), the N-terminal part straightens while the C-terminal part remains in place (Fig. 6b and Supplementary Movie 2). When the extension reaches the helix, it unfolds in a step-wise manner starting from the N-terminal side (384–640 ns). The unfolding of the α -helix before reaching the constriction site suggests that the constriction site acts as barrier for α -helices. Only after the helix is completely unfolded (768–1024 ns), can Ala164 of SecM shift away from the positions observed in the unbiased simulations, such that nitrogen of Pro166 cannot form a hydrogen bond with the carbonyl-oxygen of Ala164 anymore (Fig. 6c), thereby providing a rationale for the relief of stalling. This order of events was observed in all simulations and the N-terminus positions at which they occur were very similar (Fig. 6d). These observations were independent of the pulling velocities used in

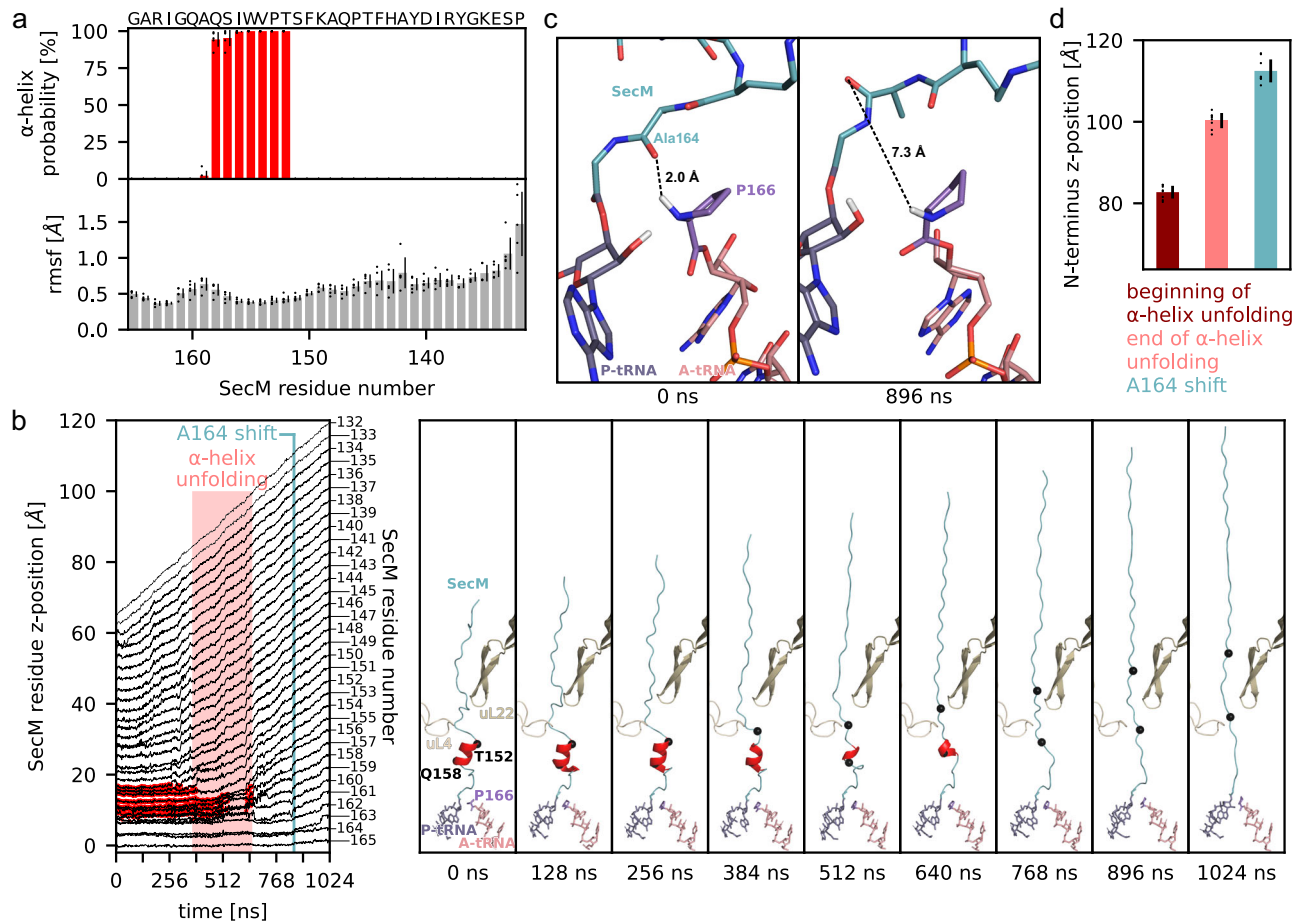


Fig. 6 | MD simulations of the stalling release by pulling on N-terminus.

a Probability of SecM residues being in an α -helix and their root mean square fluctuations in the absence of a pulling force. Mean (bars) and standard deviations (black lines) are shown for 5 independent simulations (circles). **b** Left panel: For one pulling simulation (length 1024 ns), positions of SecM residues along the tunnel axis are shown as a function of time. Initial G165 position is set to zero. Residues in α -helix secondary structure are highlighted in red. Unfolding of α -helix and beginning of A164 shift are indicated by light red rectangle and teal vertical line,

respectively. Right panel: intermediate structures at indicated times.

c Conformation of the PTC before pulling and after the A164 shift. Distance between Pro166 and A164 carbonyl oxygen. **d** Mean and standard deviation of N-terminus position at beginning (dark red) and end of α -helix unfolding (light red) as well as A164 shift (teal) are shown. Mean (bars) and standard deviations (black lines) are shown for 8 independent simulations (circles). DSSP¹⁰⁴ was used to assign α -helices. Source data be obtained from Zenodo (10.5281/zenodo.10492465).

the simulations (Supplementary Fig. 9a), suggesting that the helix also unfolds first in vivo. In the simulations, the maximum force during unfolding was always higher than before unfolding, indicating that helix unfolding represents the first barrier encountered during pulling (Supplementary Fig. 9b). This observation is consistent with the stability of the helix determining the force required to release the stalling, rendering it crucial for the fine-tuning of the stalling relief mechanism.

Discussion

The cryo-EM structure of an *E. coli* ribosome stalled during translation of the full-length *E. coli* SecM sequence at 2.0 Å resolution allows the mechanism by which SecM induces translational arrest to be completely revised (Fig. 7). In our model, the SecM arrest peptide stalls the elongating ribosome in a pre-peptide bond formation state with SecM-peptidyl-Gly-tRNA in the P-site and Pro166-tRNA in the A-site (Fig. 7a). The structure suggests that the accommodation of the Pro-tRNA at the A-site is not affected, but rather that the SecM-peptidyl-tRNA actually stabilizes the Pro-tRNA in the A-site by interacting directly with the Pro moiety (Fig. 7a). Specifically, we observe that the carbonyl-oxygen of Ala164 comes within hydrogen bonding distance and geometry to the nitrogen of the A-site proline. Because Pro is the only natural amino acid with a secondary amine, the hydrogen bond formed between Pro166 and Ala164 sequesters the single hydrogen of Pro166 and

thereby prevents extraction of this proton by the 2' OH of A76 of the P-site tRNA. Instead, we suggest that the 2' OH actually donates a proton to form a hydrogen bond with the lone-pair electrons of the nitrogen on Pro166. Collectively, this creates a chemical environment and geometry that disfavours the nucleophilic attack necessary for a peptide bond formation to occur (Fig. 7a). Importantly, this model rationalizes why Pro166 is critical for SecM stalling¹⁴, whereas all other amino acids have primary amines with two hydrogens that would allow simultaneous hydrogen bonding with Ala164 as well as extraction of a proton by the 2' OH of A76 (Fig. 7b). In our structure, Arg163 establishes a complex network of interactions with the ribosome, which we propose stabilizes the C-terminal end of the SecM NC and, in particular, the carbonyl-oxygen of Ala164 to interact with Pro166, thereby explaining why Arg163 is also critical for SecM-mediated stalling^{14,22}. Lastly, our MD simulations indicate that the pulling force on the N-terminus of the SecM NC relieves stalling by disrupting the interaction between Ala164 and Pro166 (Fig. 6c), but that for this to occur, the α -helix of SecM must be unfolded first (Fig. 6b). Collectively, this suggests that the secondary structures, such as the α -helix observed in SecM, could act to fine-tune the efficiency of stalling by modulating the force required for relief of stalling.

The model presented here differs fundamentally from that based on a previous structure of SecM-SRC where the sidechain of Arg163

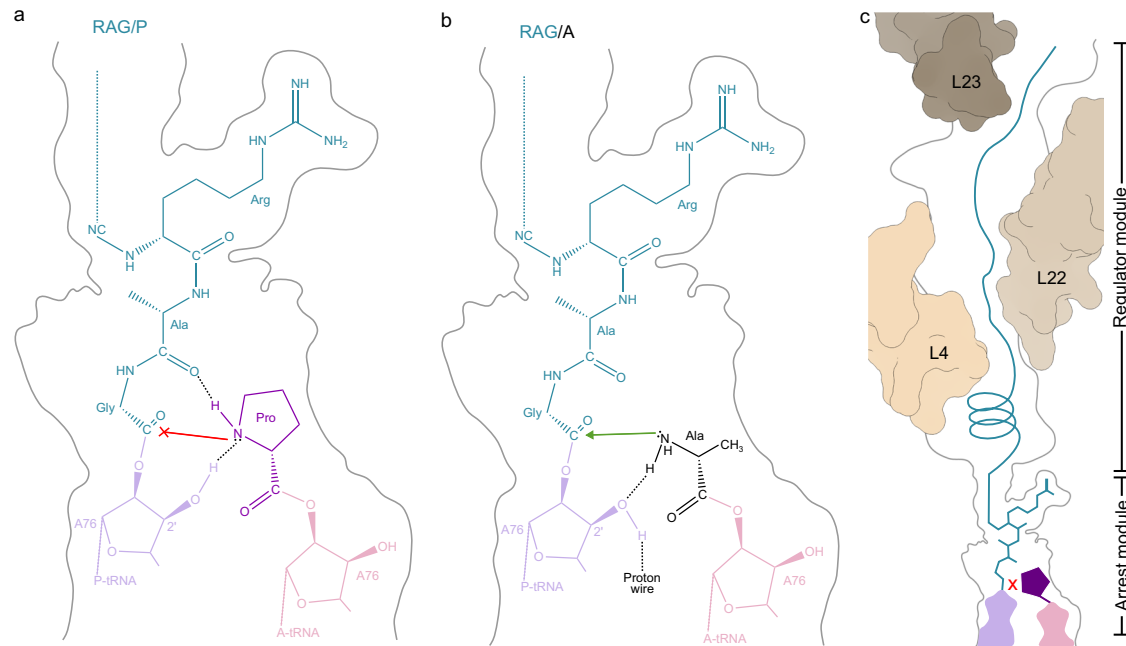


Fig. 7 | Model for SecM-mediated translational arrest. Schematic representation of the (a) RAG/P arrest module from SecM and (b) non-stalling RAG/A motif in the PTC. c SecM stalling is strongly driven by the RAG-P arrest module, however, the N-terminal regulator module also modulates and fine-tunes the stalling efficiency.

was proposed to extend into A-site and sterically block accommodation of the Pro-tRNA²⁴. By contrast, in our SecM-SRC dataset, we observe no functional states with vacant A-sites, which is consistent with previous biochemical data showing that the SecM-stalled ribosome is unreactive to puromycin^{12,13,17} and resilient to tmRNA rescue¹³. One possible explanation for this difference is the addition of chloramphenicol during purification of the previous SecM-SRC²⁴, which could have caused the loss of the A-site tRNA. In this regard, we note that SecM stalls with an alanine in the penultimate position of the SecM-NC attached to the P-site tRNA, which favours binding of chloramphenicol at the A-site^{27,72}. Indeed, the binding site of chloramphenicol in the A-site overlaps with the position of the sidechain of Arg163 (Supplementary Fig. 10a–c). Other differences, such as the extended, rather than compacted, conformation of the SecM NC within the exit tunnel may have arisen due to the lower resolutions (3.7 Å and 6–9 Å) of the previous SecM-SRC structures^{23,24} (Supplementary Fig. 10d–h).

While the structure of SecM-SRC and derived mechanism of stalling determined here differ with that of other ligand-independent arrest peptides, such as Vemp⁵⁸ or MifM⁷³, we note a striking similarity with recently determined structures of phylogenetically-unrelated arrest peptides ApdA and ApdP⁷⁴. Unlike SecM, which stalls at the C-terminal RAG/P motif⁴, the ApdA and ApdP arrest peptides stall at a conserved RAP/P motif⁷⁵. Nevertheless, the superimposition of the ApdA and ApdP with SecM illustrates a remarkable similarity in the conformation of the respective motifs (Supplementary Fig. 11a–f), supporting a common mechanism of peptide bond inhibition⁷⁴. To provide additional support for the commonality in mechanism, we could also demonstrate that the RAG/P motif in SecM could be mutated to RAP/P and retained an equivalent level of stalling both in vivo and in vitro (Supplementary Fig. 11g, h). Collectively, our findings suggest that ApdA, ApdP and a range of other recently identified arrest peptides with RAG/P and RAP/P motifs from a range of diverse bacteria^{75,76} are likely to utilize the same mechanism to induce translational stalling as described here for SecM.

Although the RAG/P motif of SecM plays a critical role in translational stalling, we observed defined interactions between other

residues of the SecM NC and components of the ribosomal tunnel and note that mutations in these regions can also influence the efficiency of translational arrest^{14,18–20}. This leads us to expand our model for SecM-mediated arrest to comprise two modules, the RAG/P or “arrest module” that is attached to the P-tRNA and directly involved in preventing peptide bond formation together with a Pro-tRNA in the A-site, and a second N-terminal “regulator” module that can modulate the strength of stalling (Fig. 7c). We envisage that the regulator module could strengthen stalling by adopting secondary structures and/or establishing additional interactions with the ribosomal tunnel that increase the pulling force requirement to relieve stalling. However, we also envisage that in some cases, the regulator module may weaken or even prevent stalling by perturbing the fine-placement of the RAG/P motif (Fig. 6c), which would explain why RAGP motifs can also be found in non-stalling proteins⁷⁶. Additionally, we believe that the N-terminal regulator module may be responsible for the species-specificity observed for SecM, where stalling is efficient on *E. coli*, but not *B. subtilis*, ribosomes⁷⁷. The basis for this proposal is that the region around the PTC is highly conserved between *E. coli* and *B. subtilis* ribosomes, whereas the largest differences are observed within the tunnel, predominantly, within the ribosomal proteins uL4 and uL22.

Methods

Bacterial strains and plasmids

The protein coding sequence of SecM from *E. coli* was cloned into pDG1662 downstream of a T7 promoter, a ribosome binding site, a His-tag and a Flag-tag using restriction enzyme SphI and HindIII (NEB) and T4 ligase (NEB). The insert of SecM was amplified by PCR using Q5 High-Fidelity DNA polymerase (NEB) from *E. coli* strain K12 genomic DNA using primers Fwd_SphI_SecM (5'-TTTTTGCATGCGTGAGTGGAATACTGACG-3') and Rev_SecM_stop_HindIII (5'-AAAAAAAAGC TTTTAGGTGAGGCGTTGAG-3'). DNA oligo primers used were purchased from Metabion.

PCR and in vitro transcription

PCR reaction (Q5 High-Fidelity DNA Polymerase in Q5 Reaction buffer (NEB)) was used with primers M13 fwd (5'-GTAAACGACGGCCAGT-3')

and M13 rev (5'-CAGGAAACAGCTATGAC-3') on the vector harbouring *secM* ORF to generate the amplified DNA sequence (5'-CAGGAAACAGCTATGACCATGATTACCGAATTCGAGCTCGGTACCCGGGATCCCGCGAAATTAATACGACTCACTATAGGGGAATTGTGAGCGGATAACAAT TCCCCTAGTAATAATTTGTTTAACTTTAAGAAGGAGATATACC ATGGGCAGCAGCCATCATCATCATCATCACGATTACAAGGATGACGACGATAAGGCTAGCAGCAGCGGTACCGGCAGCGCGAAAACCTCTAT TTTCAGGGTAGTGCGCAAGCATGCGTGAGTGGAACTACTGACGCGCTGGCGACAGTTTGGTAAACGCTACTTCTGGCCGCATCTCTTATTAGG GATGGTTGCGGCGAGTTTAGGTTTGCCTGCGCTCAGCAACGCCGCCG AACCAAACGCGCCGCAAAAGCGACAACCCGCAACACGAGCCTTCA GCCAAAGTTAACTTTGGTCAATTGGCCTTGTGGAAGCGAACACACCG CCGCCCGAATTCGAACTATTCGGTTGATTACTGGCATCAACATGCCA TTCGACGGTAATCCGTCATCTTTCTTCGCAATGGCACCGCAAACA CTGCCCGTTGCTGAAGAATCTTTCCTTTCAGGCGCAACATCTTGC ATTACTGGATACGCTCAGCGCGCTGCTGACCCAGGAAGGACCGCG TCTGAAAAGGGTTATCGCATTGATTATGCGCATTTTACCCACAAGC AAAATTCAGCACGCGCTGATAAGCCAGGCGCAAGGCATCCGT GCTGGCCCTCAACGCTCACCTAAAAGCTTGGACTGGCCGTCGTTTT AC-3'; underlined are the T7 promoter region, ribosomal binding site, start codon, FLAG-tag and stop codon, respectively). PCR conditions applied were as suggested by the manufacturer and PCR products were purified via spin columns, and in vitro transcription reaction was set up using 1 µg PCR product per 50 µL reaction volume and T7 RNA polymerase (Thermo Scientific™). RNA was purified by LiCl precipitation and washed with ethanol.

Generation of SecM-SRC

To generate the SecM-SRC, the transcribed template mRNA (250 ng µL⁻¹) was translated by incubation in an *E. coli* cell-free in vitro translation system (PURExpress® In Vitro Protein Synthesis Kit (NEB)). Briefly, a total reaction volume of 80 µL was prepared mixing 15.9 µL DEPC-treated water, 32 µL solution A, 24 µL solution B, 0.1 µL RNase Inhibitor (NEB) and 8 µL mRNA, and then incubated at 30 °C for 40 min with shaking in a thermomixer (500 rpm).

Purification of the stalled-ribosomal complexes

The SecM-SRC was purified by incubating the in vitro translation reaction with 15 µL anti-FLAG® M2 affinity gel (Merck), previously equilibrated with Hico buffer (50 mM HEPES-KOH (pH 7.4, 4 °C), 100 mM potassium acetate, 15 mM magnesium acetate, 1 mM dithiothreitol, 0.01 % (w/v) n-dodecyl-beta-maltoside, sterile-filtered) inside a Mobicol column fitted with 35 µm filter (MoBiTec) at 4 °C for 3.5 h with rolling. After removal of the flow-through, the beads were washed with a total of 4 mL Hico buffer and then the bound complex was eventually eluted by incubation with 5 µL Hico buffer containing 0.6 mg mL⁻¹ 3XFLAG peptide for 45 min at 4 °C with rolling, followed by centrifugation (2000 × *g*, 4 °C, 2 min). Aliquots from each fraction were checked by western blotting or snap frozen and stored at -80 °C until needed.

Cryo-EM sample preparation

3.5 µL of the SecM-SRC sample (8 OD₂₆₀/ml) were applied to grids (Quantifoil, Cu, 300 mesh, R3/3 with 3 nm carbon, Product: C3-C18nCu30-01) which had been freshly glow discharged using a Glo-Qube® Plus (Quorum Technologies) in negative charge at 25 mA for 30 s to make the grids hydrophilic. Sample vitrification was performed using mixture of ethane/propane in 1:2 ratio in a Vitrobot Mark IV (ThermoScientific), with the chamber set to 4 °C and 100% rel. humidity, and blotting performed for 3 sec with zero blot force with Whatman 597 blotting paper. The grids were subsequently clipped into autogrid cartridges and stored in liquid nitrogen until needed.

Cryo-EM data collection

Data collection was performed on 300 kV Titan Krios G3i (Thermo Fisher/FEI) with Fringe-Free Imaging (FFI) setup and equipped with

Gatan K3 direct electron detector using EPU (version 3.2.0.4775REL). Magnification of ×105,000 was used, with data collected using super resolution counted mode at 0.415 pixel size, binned twice on the fly through EPU yielding 0.83 pixel size. Total 40 e⁻/Å² fluence was fractionated into 35 frames resulting in 1.14 e⁻/px/s over an empty area on the camera level). Defocus range of -0.3 µm to -0.9 µm was used with step size of 0.1 µm between holes. C2 aperture of 70 µm was inserted with beam spot size of 7. BioQuantum energy filter set to 20 eV cut-off was used to remove inelastically scattered electrons. Final objective astigmatism correction <1 nm and auto coma free alignment <40 nm was achieved using AutoCTF function of Sherpa (version 2.11.1). A total of 4,388 micrographs were collected for SecM-SRC (12 exposures per hole) and saved as tiff gain corrected files.

Single-particle reconstruction of SRC complexes

RELION v4.0^{78,79} was used for processing, unless otherwise specified. For motion correction, RELION's implementation of MotionCor2 with 4 × 4 patches, and, for initial contrast transfer function (CTF) estimation, CTFFIND version 4.1.14⁸⁰, were employed. From 4,388 micrographs, 499,240 particles were picked using crYOLO with a general model⁸¹. In total, 398,692 ribosome-like particles were selected after two-dimensional (2D) classification and extracted at 2 × decimated pixel size (1.66 Å per pixel) (Supplementary Fig. 1). An initial three-dimensional (3D) consensus refinement was done using a mol map based on *E. coli* 70S ribosome (PDB ID 7K00 with tRNAs and mRNAs removed), then initial 3D classification without angular sampling with five classes was performed. All 70S ribosomal like classes were combined (377,762 particles), followed by partial signal subtraction on the particles with a mask around tRNAs sites to perform focussed classification. One class containing 70S ribosomes with P-tRNA and A-tRNA (300,120 particles) was subsorted into four subclasses, of which one was of high resolution (300,107 particles); one class containing 70S with A/P hybrid state tRNA and P/E hybrid state tRNA (55,259 particles) was subsorted into four subclasses, of which one was of high resolution (36,489 particles). These two major classes were selected for further processing. In particular, the resulting classes' subtracted particles were reverted to their original images and 3D refined and CTF refined (4th order aberrations, beam tilt, anisotropic magnification and per-particle defocus value estimation), then subjected to Bayesian polishing⁸² and another round of CTF refinement. For the SecM-SRC with P-tRNA and A-tRNA a final resolution (gold-standard FSC_{0.143}) of masked reconstructions of 2.0 Å was achieved (Supplementary Fig. 1f, Supplementary Fig. 2a, b, e, f); for the SecM-SRC with A/P hybrid state tRNA and P/E hybrid state tRNA a final resolution (gold-standard FSC_{0.143}) of masked reconstructions of 2.6 Å was achieved (Supplementary Fig. 1g, Supplementary Fig. 3a). To estimate local resolution values, Bsoft⁸³ was used on the half-maps of the final reconstructions (blocres -sampling 0.83 -maxres -box 20 -cutoff 0.143 -verbose 1 -fill 150 -origin 0,0,0 -Mask half_map1 half_map 2) (Supplementary Fig. 2).

Molecular modelling of the SRC complexes

The molecular models of the 30S and 5S ribosomal subunits were based on the *E. coli* 70S ribosome (PDB ID 7K00)⁸⁴. The tRNAs and nascent chains were modelled de novo. The secondary structure of the SecM nascent chain in the NPET was predicted using the PSIPRED 4.0 web service. Restraint files for modified residues were created using aceDRG⁸⁵, while the restraint file to link the tRNAs to their aminoacyl-/peptidyl- moiety was kindly provided by Keitaro Yamashita (MRC LMB, UK). Starting models were rigid body fitted using ChimeraX⁸⁶ and modelled using Coot 0.9.8.5⁸⁷ from the CCP4 software suite version 8.0⁸⁸. The sequence for the tRNAs was adjusted based on the appropriate anticodons corresponding to the mRNA. Final refinements were done in REFMAC 5⁸⁹ using Servalcat⁹⁰. The molecular models were

validated using Phenix comprehensive cryo-EM validation in Phenix 1.20–4487⁹¹.

β-galactosidase assay

E. coli cells (Supplementary Table 1) with plasmids (Supplementary Tables 2 and 3) were cultured in LB medium with 100 μg/mL ampicillin at 37 °C and withdrawn at an optical density at 600 nm (OD₆₀₀) of 0.5–1.0 for β-galactosidase assay. 100 μL portions of the cultures were transferred to individual wells of 96-well plate, and OD₆₀₀ was recorded. To lyse the cells, 50 μL of Y-PER reagent (Thermo Scientific) were added to the 100 μL of 10-fold diluted culture and the samples were frozen at –80 °C for at least 30 min. After thawing the samples, 30 μL of o-nitrophenyl-β-D-galactopyranoside (ONPG) in Z-buffer (60 mM Na₂HPO₄, 40 mM NaH₂PO₄, 10 mM KCl, 1 mM MgSO₄, 38 mM β-mercaptoethanol) was added to each well, OD₄₂₀ and OD₅₅₀ were measured every 5 min over 60 min at 28 °C. Arbitrary units [AU] of β-galactosidase activity were calculated by the formula $[(1000 \times V_{420} - 1.3 \times V_{550})/OD_{600}]$, where V_{420} and V_{550} are the first-order rate constants, OD₄₂₀/min and OD₅₅₀/min, respectively.

Bacterial in vitro translation arrest assay

In vitro translation arrest assay was carried out using *E. coli*-based coupled transcription-translation system (PUREflex 1.0; GeneFrontier). 2.5 U/L of T7 RNA polymerase (Takara) was added further to reassure transcription. The DNA templates were prepared by PCR using primers and template DNA listed in Supplementary Table 4. After the translation reaction at 37 °C for 20 min, the reaction was stopped by adding three volumes of 1.3 × SDS-PAGE loading buffer (167 mM Tris-HCl (pH 6.8), 2.7% (wt/vol) SDS, 20% (vol/vol) glycerol, 6.7 mM DTT, a trace amount of bromophenol blue), and, when indicated, samples were further treated with 0.2 mg/ml RNase A (Promega) at 37 °C for 10 min to degrade the tRNA moiety of peptidyl-tRNA immediately before electrophoresis.

Eukaryotic in vitro translation arrest assay

The DNA templates were prepared by PCR using primers and templates listed in Supplementary Table 4. In vitro transcription was carried out using T7 RNA Polymerase ver.2.0 (TaKaRa) and 150–250 ng of PCR product per 10 μL reaction volume. The mRNA was then purified by RNAClean XP (Beckman Coulter) and used for in vitro translation using the Rabbit Reticulocyte Lysate (RRL) translation system (Promega). A total reaction volume of 4 μL was prepared by mixing 2.8 μL Rabbit Reticulocyte Lysate (Nuclease-Treated), 10 μM Amino Acid Mixture Minus Methionine, and 10 μM Amino Acid Mixture Minus Leucine with the 75 nM mRNA. After the translation reaction at 30 °C for 20 min, the reaction was stopped by adding 24 volumes of SDS-PAGE loading buffer (125 mM Tris-HCl (pH 6.8), 2% (wt/vol) SDS, 15% (vol/vol) glycerol, 5 mM DTT, a trace amount of bromophenol blue), and, when indicated, samples were further treated with 0.1 mg/ml RNase A (Promega) at 37 °C for 20 min to degrade the tRNA moiety of peptidyl-tRNA immediately before electrophoresis.

Western blotting

Samples were separated by 10% polyacrylamide gel prepared with WIDE RANGE Gel buffer (Nacalai Tasque), transferred onto a PVDF membrane, and then subjected to immuno-detection using antibodies against GFP (Wako, mFX75) or FLAG-tag (F3165; Sigma). Images were obtained and analyzed using Amersham Imager 600 (GE Healthcare) luminoimager. The band intensities were quantified using ImageQuant TL (GE Healthcare).

Setup of MD simulations

The starting structure for the MD simulations was obtained by extracting, from the model of the SecM-SRC with A- and P-site tRNAs,

all residues, water molecules, K⁺, and Mg²⁺ ions within 35 Å of the SecM NC. Pro166 was modelled as uncharged and with the α-amino hydrogen pointing towards the carboxylic oxygen of Ala164 as in reference⁷⁴. The protonation states of the histidine residues were determined using the WHATIF software⁹². The structure was then placed in a triclinic orthogonal box, aligning the principal axes of the SecM peptide along the x,y,z coordinate axes. The longest axis of SecM was aligned with the z-axis and the minimum distance between the atoms and the box boundaries was set to 1.5 nm. To accommodate the pulling of the SecM residues out of the exit tunnel, the z-dimension of the box was extended by 2 nm in the pulling direction, resulting in simulation box dimensions of 18.60 nm, 13.25 nm, 12.83 nm. The system was then solvated with OPC water⁹³ using the programme solvate⁹⁴. GENION⁹⁴ was used to add 7 mM MgCl₂ and 150 mM KCl and to neutralize with K⁺ ions⁹⁴. The ions were modelled using the K⁺ and Cl[−] parameters from Joung and Cheatham⁹⁵ and the microMg parameters from Grotz et al.⁹⁶. Partial charges of Pro166 were determined. The simulation system contained 402,745 atoms and 90,783 water molecules. All simulations were performed using GROMACS 2022⁹⁴ with the amber14sb forcefield⁹⁷. Lennard–Jones and short-range electrostatic interactions were computed within a cut-off of 1 nm. Long-range electrostatic interactions were computed for distances larger than 1 nm using the particle-mesh Ewald summation⁹⁸ with a 0.12 nm grid spacing. Bond lengths were constrained using the LINCS algorithm⁹⁹ and virtual sites¹⁰⁰ were used for hydrogen atoms, allowing for an integration time step of 4 fs. The temperature coupling was performed using velocity rescaling¹⁰¹ and solute and solvent were coupled independently to a heat bath at 300 K with a coupling time constant of 0.1 ps. Coordinates were recorded every 5 ps.

Firstly, the system was energy minimized with harmonic position restraints ($k = 1000 \text{ kJ mol}^{-1} \text{ nm}^{-2}$) applied to the solute heavy atoms. After that, 8 replicas of the system were simulated for 70 ns to allow for solvent equilibration. During the first 50 ns, position restraints ($k = 1000 \text{ kJ mol}^{-1} \text{ nm}^{-2}$) were applied on all the heavy atoms of the solute. During the following 20 ns, the position restraints were linearly decreased to zero for all the heavy atoms of the solute placed within 25 Å from the NC. Simultaneously, the force constant of the restraints applied to the heavy atoms positioned further than 25 Å from the NC was decreased to the one obtained from the fluctuations previously observed in full-ribosome simulations as described earlier¹⁰². Production runs (70–270 ns) were then carried out for 5 replica keeping the position restraints only on the outer-shell heavy atoms. During both equilibration steps and production run, the pressure was coupled to a stochastic cell rescaling barostat¹⁰³ with a time constant of 5 ps and scaling the box every 10 steps.

To investigate how stalling is relieved by pulling on the peptide, we carried out pulling MD simulations. To that aim, we added a harmonic potential, representing a spring, which depends on the distance d and has a spring constant of $5000 \text{ kJ mol}^{-1} \text{ nm}^{-1}$. Here, d is the z-component of the difference vector between the centre of mass (COM) of the N-terminal Pro132 backbone atoms and the spring position. The initial spring position was set to the Pro132 COM position in the starting structure. In the pulling simulations, the spring position was moved with constant velocity in the z-direction (along the tunnel axis) by 5.6 nm during the length of the simulation τ . To probe the effect of the velocity, we used different pulling times $\tau = 32 \text{ ns}$, 64 ns, 128 ns, 256 ns, 512, and 1024 ns, resulting in velocities ranging from 0.175 m/s to −0.005 m/s. For each τ , we carried out 8 simulations started from the 8 structures obtained from the solvent equilibration.

Analysis of MD simulations

First, all unbiased and all pulling trajectories were aligned using 23 S rRNA P-atoms. To check if the SecM α-helix remains stable during the unbiased simulations, we extracted peptide coordinates every 10 ns

and used DSSP¹⁰⁴ to obtain the secondary structure. For each simulation and each residue, we calculated the probability of being in an α -helical secondary structure and subsequently the mean values and standard deviations over all simulations. To obtain the mobility of SecM residues, we calculated backbone root mean square fluctuations (rmsf) for each residue and simulation, and calculated mean values and standard deviation over all simulations (Fig. 6a). For the pulling simulations, we extracted 640 structures equally spaced between 0 ns and τ and calculated the z-component of the backbone COM of each SecM residue and subtracted the initial value for G165 (Fig. 6b). For each extracted structure, we obtained the secondary structure using DSSP. For each simulation, we then recorded the time when the α -helix began unfolding, which was defined as the time from which the number of α -helix residues remained below 6, whereas the end of helix unfolding was defined as the earliest time from which no residue was found to be in an α -helical secondary structure. To obtain the time when an A164 shift occurs, we recorded the time from which on the A164 COM z-component is larger than 95% of the z-components obtained from all unbiased simulations. For each τ , the mean and standard deviations of the N-terminus z-positions at the time of the three events were calculated over all pulling simulations (Fig. 6c and Supplementary Fig. 9a). The maximum force from the harmonic potential acting on the N-terminus before helix unfolding, during helix unfolding, and between helix unfolding and the A164 shift were recorded for each simulation to investigate the dependence on the pulling time (Supplementary Fig. 9b).

Figures

UCSF ChimeraX 1.6.1 was used to isolate density and visualize density images and structural superpositions. Models were aligned using PyMol version 2.5.5 (Schrödinger). Figures were assembled with Adobe Illustrator (latest development release, regularly updated) and Inkscape v1.3.

Reporting summary

Further information on research design is available in the Nature Portfolio Reporting Summary linked to this article.

Data availability

Micrographs have been deposited as uncorrected frames in the Electron Microscopy Public Image Archive (EMPIAR) with the accession codes EMPIAR-11758. Cryo-EM maps have been deposited in the Electron Microscopy Data Bank (EMDB) with accession codes [EMD-18534](#) (*SecM-SRC with A- and P-site tRNA*), [EMD-18590](#) (*SecM-SRC with hybrid A/P- and P/E-site tRNAs*). A molecular model has been deposited in the Protein Data Bank with accession code [8QOA](#) (*SecM-SRC with A- and P-site tRNA*). Publicly available data used included PDB ID 1VY4, 1Y9J, 3CC2, 3JBU, 4WFN, 5LZV, 5NCO, 5NWY and 5A8L, 5JTE, 6XHV, 7K00, 7O19, 7RQE, 8CVK, 8QCQ and 8QBT, as well as EMD ID EMD-1829. Source data are provided with this paper.

Code availability

Initial coordinates, input files and output coordinates of the MD simulations, including raw data for the MD figures are publicly available on Zenodo ([10.5281/zenodo.10492465](https://doi.org/10.5281/zenodo.10492465)).

References

- Wilson, D. N. & Beckmann, R. The ribosomal tunnel as a functional environment for nascent polypeptide folding and translational stalling. *Curr. Opin. Struct. Biol.* **21**, 1–10 (2011).
- Ito, K. & Chiba, S. Arrest peptides: cis-acting modulators of translation. *Annu. Rev. Biochem.* **82**, 171–202 (2013).
- Wilson, D. N., Arenz, S. & Beckmann, R. Translation regulation via nascent polypeptide-mediated ribosome stalling. *Curr. Opin. Struct. Biol.* **37**, 123–133 (2016).
- Dever, T. E., Ivanov, I. P. & Sachs, M. S. Conserved upstream open reading frame nascent peptides that control translation. *Annu. Rev. Genet.* **54**, 237–264 (2020).
- Nakatogawa, H. & Ito, K. Secretion monitor, SecM, undergoes self-translation arrest in the cytosol. *Mol. Cell* **7**, 185–192 (2001).
- Nakatogawa, H., Murakami, A. & Ito, K. Control of SecA and SecM translation by protein secretion. *Curr. Opin. Microbiol.* **7**, 145–150 (2004).
- Driessen, A. J. & Nouwen, N. Protein translocation across the bacterial cytoplasmic membrane. *Annu. Rev. Biochem.* **77**, 643–667 (2008).
- Rapoport, T. A., Li, L. & Park, E. Structural and mechanistic insights into protein translocation. *Annu. Rev. Cell Dev. Biol.* **33**, 369–390 (2017).
- Komarudin, A. G. & Driessen, A. J. M. SecA-mediated protein translocation through the SecYEG channel. *Microbiol. Spectr.* **7**, <https://doi.org/10.1128/microbiolspec.PSIB-0028-2019> (2019).
- Butkus, M. E., Prunceanu, L. B. & Oliver, D. B. Translocon “pulling” of nascent SecM controls the duration of its translational pause and secretion-responsive secA regulation. *J. Bacteriol.* **185**, 6719–6722 (2003).
- Goldman, D. H. et al. Ribosome. Mechanical force releases nascent chain-mediated ribosome arrest in vitro and in vivo. *Science* **348**, 457–460 (2015).
- Muto, H., Nakatogawa, H. & Ito, K. Genetically encoded but non-polypeptide prolyl-tRNA functions in the A site for SecM-mediated ribosomal stall. *Mol. Cell* **22**, 545–552 (2006).
- Garza-Sanchez, F., Janssen, B. D. & Hayes, C. S. Prolyl-tRNA(Pro) in the A-site of SecM-arrested ribosomes inhibits the recruitment of transfer-messenger RNA. *J. Biol. Chem.* **281**, 34258–34268 (2006).
- Nakatogawa, H. & Ito, K. The ribosomal exit tunnel functions as a discriminating gate. *Cell* **108**, 629–636 (2002).
- Yang, Z., Iizuka, R. & Funatsu, T. Nascent SecM chain outside the ribosome reinforces translation arrest. *PLoS ONE* **10**, e0122017 (2015).
- Muta, M. et al. Nascent SecM chain interacts with outer ribosomal surface to stabilize translation arrest. *Biochem J.* **477**, 557–566 (2020).
- Woolhead, C. A., Johnson, A. E. & Bernstein, H. D. Translation arrest requires two-way communication between a nascent polypeptide and the ribosome. *Mol. Cell* **22**, 587–598 (2006).
- Lawrence, M. G., Lindahl, L. & Zengel, J. M. Effects on translation pausing of alterations in protein and RNA components of the ribosome exit tunnel. *J. Bacteriol.* **190**, 5862–5869 (2008).
- Tanner, D. R., Cariello, D. A., Woolstenhulme, C. J., Broadbent, M. A. & Buskirk, A. R. Genetic identification of nascent peptides that induce ribosome stalling. *J. Biol. Chem.* **284**, 34809–34818 (2009).
- Vazquez-Laslop, N., Ramu, H., Klepacki, D., Kannan, K. & Mankin, A. S. The key function of a conserved and modified rRNA residue in the ribosomal response to the nascent peptide. *EMBO J.* **29**, 3108–3117 (2010).
- Orelle, C. et al. Protein synthesis by ribosomes with tethered subunits. *Nature* **524**, 119–124 (2015).
- Yap, M. N. & Bernstein, H. D. The plasticity of a translation arrest motif yields insights into nascent polypeptide recognition inside the ribosome tunnel. *Mol. Cell* **34**, 201–211 (2009).
- Bhushan, S. et al. SecM-stalled ribosomes adopt an altered geometry at the peptidyltransferase center. *PLoS Biol.* **19**, e1000581 (2011).
- Zhang, J. et al. Mechanisms of ribosome stalling by SecM at multiple elongation steps. *eLife* **4**, e09684 (2015).
- Bracken, H. A. & Woolhead, C. A. Increased freedom of movement in the nascent chain results in dynamic changes in the structure of the SecM arrest motif. *Biosci. Rep.* **39**, BSR20181246 (2019).

26. Ojima-Kato, T., Nishikawa, Y., Furukawa, Y., Kojima, T. & Nakano, H. Nascent MSKIK peptide cancels ribosomal stalling by arrest peptides in *Escherichia coli*. *J. Biol. Chem.* **299**, 104676 (2023).
27. Syroegin, E. A. et al. Structural basis for the context-specific action of the classic peptidyl transferase inhibitor chloramphenicol. *Nat. Struct. Mol. Biol.* **29**, 152–161 (2022).
28. Evans, M. S., Ugrinov, K. G., Frese, M. A. & Clark, P. L. Homogeneous stalled ribosome nascent chain complexes produced in vivo or in vitro. *Nat. Methods* **2**, 757–762 (2005).
29. Schaffitzel, C. & Ban, N. Generation of ribosome nascent chain complexes for structural and functional studies. *J. Struct. Biol.* **158**, 463–471 (2007).
30. Jha, S. S. & Komar, A. A. Using SecM arrest sequence as a tool to isolate ribosome bound polypeptides. *J. Vis. Exp.* **19**, 4027 (2012).
31. Contreras-Martinez, L. M. & DeLisa, M. P. Intracellular ribosome display via SecM translation arrest as a selection for antibodies with enhanced cytosolic stability. *J. Mol. Biol.* **372**, 513–524 (2007).
32. Chung, S. S. et al. Ribosome stalling of N-linked glycoproteins in cell-free extracts. *ACS Synth. Biol.* **11**, 3892–3899 (2022).
33. Takahashi, S. et al. Real-time monitoring of cell-free translation on a quartz-crystal microbalance. *J. Am. Chem. Soc.* **131**, 9326–9332 (2009).
34. Uemura, S. et al. Single-molecule imaging of full protein synthesis by immobilized ribosomes. *Nucleic Acids Res.* **36**, e70 (2008).
35. Tsai, A., Kornberg, G., Johansson, M., Chen, J. & Puglisi, J. D. The dynamics of SecM-induced translational stalling. *Cell Rep.* **7**, 1521–1533 (2014).
36. Notari, L., Martinez-Carranza, M., Farias-Rico, J. A., Stenmark, P. & von Heijne, G. Cotranslational folding of a pentarepeat beta-helix protein. *J. Mol. Biol.* **430**, 5196–5206 (2018).
37. Marsden, A. P. et al. Investigating the effect of chain connectivity on the folding of a beta-sheet protein on and off the ribosome. *J. Mol. Biol.* **430**, 5207–5216 (2018).
38. Nilsson, O. B. et al. Cotranslational folding of spectrin domains via partially structured states. *Nat. Struct. Mol. Biol.* **24**, 221–225 (2017).
39. Nilsson, O. B., Muller-Lucks, A., Kramer, G., Bukau, B. & von Heijne, G. Trigger factor reduces the force exerted on the nascent chain by a cotranslationally folding protein. *J. Mol. Biol.* **428**, 1356–1364 (2016).
40. Nilsson, O. B. et al. Cotranslational protein folding inside the ribosome exit tunnel. *Cell Rep.* **12**, 1533–1540 (2015).
41. Houwman, J. A., Westphal, A. H., van Berkel, W. J. & van Mierlo, C. P. Stalled flavodoxin binds its cofactor while fully exposed outside the ribosome. *Biochim. Biophys. Acta* **1854**, 1317–1324 (2015).
42. Jomaa, A., Boehringer, D., Leibundgut, M. & Ban, N. Structures of the *E. coli* translating ribosome with SRP and its receptor and with the translocon. *Nat. Commun.* **7**, 10471 (2016).
43. Marino, J., von Heijne, G. & Beckmann, R. Small protein domains fold inside the ribosome exit tunnel. *FEBS Lett.* **590**, 655–660 (2016).
44. Jensen, M. K., Samelson, A. J., Steward, A., Clarke, J. & Marqusee, S. The folding and unfolding behavior of ribonuclease H on the ribosome. *J. Biol. Chem.* **295**, 11410–11417 (2020).
45. Elfageih, R. et al. Cotranslational folding of alkaline phosphatase in the periplasm of *Escherichia coli*. *Protein Sci.* **29**, 2028–2037 (2020).
46. Cymer, F. & von Heijne, G. Cotranslational folding of membrane proteins probed by arrest-peptide-mediated force measurements. *Proc. Natl Acad. Sci. USA* **110**, 14640–14645 (2013).
47. Cabrera, L. D. et al. A structural ensemble of a ribosome-nascent chain complex during cotranslational protein folding. *Nat. Struct. Mol. Biol.* **23**, 278–285 (2016).
48. Deckert, A. et al. Common sequence motifs of nascent chains engage the ribosome surface and trigger factor. *Proc. Natl Acad. Sci. USA* **118**, e2103015118 (2021).
49. Ahn, M. et al. Modulating co-translational protein folding by rational design and ribosome engineering. *Nat. Commun.* **13**, 4243 (2022).
50. Chan, S. H. S. et al. The ribosome stabilizes partially folded intermediates of a nascent multi-domain protein. *Nat. Chem.* **14**, 1165–1173 (2022).
51. Bertolini, M. et al. Interactions between nascent proteins translated by adjacent ribosomes drive homomer assembly. *Science* **371**, 57–64 (2021).
52. Ismail, N., Hedman, R., Schiller, N. & von Heijne, G. A biphasic pulling force acts on transmembrane helices during translocon-mediated membrane integration. *Nat. Struct. Mol. Biol.* **19**, 1018–1022 (2012).
53. Pellowe, G. A. et al. Capturing membrane protein ribosome nascent chain complexes in a native-like environment for co-translational studies. *Biochemistry* **59**, 2764–2775 (2020).
54. Gumbart, J., Schreiner, E., Wilson, D. N., Beckmann, R. & Schulten, K. Mechanisms of SecM-mediated stalling in the ribosome. *Biophys. J.* **103**, 331–341 (2012).
55. Rychkova, A., Mukherjee, S., Bora, R. P. & Warshel, A. Simulating the pulling of stalled elongated peptide from the ribosome by the translocon. *Proc. Natl Acad. Sci. USA* **110**, 10195–10200 (2013).
56. Zimmer, M. H., Niesen, M. J. M. & Miller, T. F. 3rd Force transduction creates long-ranged coupling in ribosomes stalled by arrest peptides. *Biophys. J.* **120**, 2425–2435 (2021).
57. Kim, M. K. & Kang, Y. K. Positional preference of proline in alpha-helices. *Protein Sci.* **8**, 1492–1499 (1999).
58. Su, T. et al. The force-sensing peptide VemP employs extreme compaction and secondary structure formation to induce ribosomal stalling. *eLife* **6**, e25642 (2017).
59. Matheisl, S., Berninghausen, O., Becker, T. & Beckmann, R. Structure of a human translation termination complex. *Nucleic Acids Res.* **43**, 8615–8626 (2015).
60. van der Stel, A. X. et al. Structural basis for the tryptophan sensitivity of TnaC-mediated ribosome stalling. *Nat. Commun.* **12**, 5340 (2021).
61. Tu, D., Blaha, G., Moore, P. & Steitz, T. Structures of MLSBK antibiotics bound to mutated large ribosomal subunits provide a structural explanation for resistance. *Cell* **121**, 257–270 (2005).
62. Wekselman, I. et al. The ribosomal protein uL22 modulates the shape of the protein exit tunnel. *Structure* **25**, 1233–1241 e1233 (2017).
63. Halic, M. et al. Following the signal sequence from ribosomal tunnel exit to signal recognition particle. *Nature* **444**, 507–511 (2006).
64. Jomaa, A. et al. Structure of the quaternary complex between SRP, SR, and translocon bound to the translating ribosome. *Nat. Commun.* **8**, 15470 (2017).
65. Yanagitani, K., Kimata, Y., Kadokura, H. & Kohno, K. Translational pausing ensures membrane targeting and cytoplasmic splicing of XBP1u mRNA. *Science* **331**, 586–589 (2011).
66. Polikanov, Y. S., Steitz, T. A. & Innis, C. A. A proton wire to couple aminoacyl-tRNA accommodation and peptide-bond formation on the ribosome. *Nat. Struct. Mol. Biol.* **21**, 787–793 (2014).
67. Syroegin, E. A., Aleksandrova, E. V. & Polikanov, Y. S. Insights into the ribosome function from the structures of non-arrested ribosome-nascent chain complexes. *Nat. Chem.* **15**, 143–153 (2023).
68. Lang, K., Erlacher, M., Wilson, D. N., Micura, R. & Polacek, N. The role of 23S ribosomal RNA residue A2451 in peptide bond synthesis revealed by atomic mutagenesis. *Chem. Biol.* **15**, 485–492 (2008).

69. Wallin, G. & Aqvist, J. The transition state for peptide bond formation reveals the ribosome as a water trap. *Proc. Natl Acad. Sci. USA* **107**, 1888–1893 (2010).
70. Rodnina, M. V. Translation in prokaryotes. *Cold Spring Harb. Perspect. Biol.* **10**, a032664 (2018).
71. Ha, H. J. et al. Identification of a hyperactive variant of the SecM motif involved in ribosomal arrest. *Curr. Microbiol.* **64**, 17–23 (2012).
72. Marks, J. et al. Context-specific inhibition of translation by ribosomal antibiotics targeting the peptidyl transferase center. *Proc. Natl Acad. Sci. USA* **113**, 12150–12155 (2016).
73. Sohmen, D. et al. Structure of the *Bacillus subtilis* 70S ribosome reveals the basis for species-specific stalling. *Nat. Commun.* **6**, 6941 (2015).
74. Morici, M. et al. RAPP-containing arrest peptides induce translational stalling by short circuiting the ribosomal peptidyltransferase activity. *Nat. Commun.* **15**, 2432 (2024).
75. Sakiyama, K., Shimokawa-Chiba, N., Fujiwara, K. & Chiba, S. Search for translation arrest peptides encoded upstream of genes for components of protein localization pathways. *Nucleic Acids Res.* **49**, 1550–1566 (2021).
76. Fujiwara, K., Tsuji, N., Yoshida, M., Takada, H. & Chiba, S. Patchy and widespread distribution of bacterial translation arrest peptides associated with the protein localization machinery. *Nat. Commun.* **15**, 2711 (2024).
77. Chiba, S. et al. Recruitment of a species-specific translational arrest module to monitor different cellular processes. *Proc. Natl Acad. Sci. USA* **108**, 6073–6078 (2011).
78. Scheres, S. H. RELION: implementation of a Bayesian approach to cryo-EM structure determination. *J. Struct. Biol.* **180**, 519–530 (2012).
79. Kimanius, D., Dong, L., Sharov, G., Nakane, T. & Scheres, S. H. W. New tools for automated cryo-EM single-particle analysis in RELION-4.0. *Biochem. J.* **478**, 4169–4185 (2021).
80. Zheng, S. Q. et al. MotionCor2: anisotropic correction of beam-induced motion for improved cryo-electron microscopy. *Nat. Methods* **14**, 331–332 (2017).
81. Wagner, T. et al. SPHIRE-crYOLO is a fast and accurate fully automated particle picker for cryo-EM. *Commun. Biol.* **2**, 218 (2019).
82. Zivanov, J., Nakane, T. & Scheres, S. H. W. A Bayesian approach to beam-induced motion correction in cryo-EM single-particle analysis. *IUCr J* **6**, 5–17 (2019).
83. Heymann, J. B. Guidelines for using Bsoft for high resolution reconstruction and validation of biomolecular structures from electron micrographs. *Protein Sci.* **27**, 159–171 (2018).
84. Watson, Z. L. et al. Structure of the bacterial ribosome at 2 Å resolution. *eLife* **9**, e60482 (2020).
85. Long, F. et al. AceDRG: a stereochemical description generator for ligands. *Acta Crystallogr. D. Struct. Biol.* **73**, 112–122 (2017).
86. Pettersen, E. F. et al. UCSF ChimeraX: Structure visualization for researchers, educators, and developers. *Protein Sci.* **30**, 70–82 (2021).
87. Emsley, P., Lohkamp, B., Scott, W. G. & Cowtan, K. Features and development of Coot. *Acta Crystallogr. D. Biol. Crystallogr.* **66**, 486–501 (2010).
88. Winn, M. D. et al. Overview of the CCP4 suite and current developments. *Acta Crystallogr. D Biol. Crystallogr.* **67**, 235–242 (2011).
89. Vagin, A. A. et al. REFMAC5 dictionary: organization of prior chemical knowledge and guidelines for its use. *Acta Crystallogr. D. Biol. Crystallogr.* **60**, 2184–2195 (2004).
90. Yamashita, K., Palmer, C. M., Burnley, T. & Murshudov, G. N. Cryo-EM single-particle structure refinement and map calculation using Servalcat. *Acta Crystallogr. D Struct. Biol.* **77**, 1282–1291 (2021).
91. Liebschner, D. et al. Macromolecular structure determination using X-rays, neutrons and electrons: recent developments in Phenix. *Acta Crystallogr. D Struct. Biol.* **75**, 861–877 (2019).
92. Vriend, G. WHAT IF: a molecular modeling and drug design program. *J. Mol. Graph* **8**, 52–56 (1990).
93. Izadi, S., Anandakrishnan, R. & Onufriev, A. V. Building water models: a different approach. *J. Phys. Chem. Lett.* **5**, 3863–3871 (2014).
94. Abraham, M. J. et al. GROMACS: High performance molecular simulations through multi-level parallelism from laptops to supercomputers. *SoftwareX* **1–2**, 19–25 (2015).
95. Joung, I. S. & Cheatham, T. E. 3rd Determination of alkali and halide monovalent ion parameters for use in explicitly solvated biomolecular simulations. *J. Phys. Chem. B* **112**, 9020–9041 (2008).
96. Grotz, K. K. & Schwierz, N. Magnesium force fields for OPC water with accurate solvation, ion-binding, and water-exchange properties: Successful transfer from SPC/E. *The. J. Chem. Phys.* **156**, 114501 (2022).
97. Maier, J. A. et al. ff14SB: improving the accuracy of protein side chain and backbone parameters from ff99SB. *J. Chem. theory Comput.* **11**, 3696–3713 (2015).
98. Essmann, U. et al. A smooth particle mesh Ewald method. *J. Chem. Phys.* **103**, 8577–8593 (1995).
99. Hess, B. P-LINCS: a parallel linear constraint solver for molecular simulation. *J. Chem. Theory Comput.* **4**, 116–122 (2008).
100. Feenstra, K. A., Hess, B. & Berendsen, H. J. C. Improving efficiency of large time-scale molecular dynamics simulations of hydrogen-rich systems. *J. Comput. Chem.* **20**, 786–798 (1999).
101. Bussi, G., Donadio, D. & Parrinello, M. Canonical sampling through velocity rescaling. *J. Chem. Phys.* **126**, 014101 (2007).
102. Huter, P. et al. Structural basis for polyproline-mediated ribosome stalling and rescue by the translation elongation factor EF-P. *Mol. Cell* **68**, 515–527.e516 (2017).
103. Bernetti, M. & Bussi, G. Pressure control using stochastic cell rescaling. *J. Chem. Phys.* **153**, 114107 (2020).
104. Kabsch, W. Automatic processing of rotation diffraction data from crystals of initially unknown symmetry and cell constants. *J. Appl. Cryst.* **26**, 795–800 (1993).

Acknowledgements

We would like to thank Keitaro Yamashita for help with refinement, Machiko Murata and Naoko Muraki for their technical support. This work was supported by the Deutsche Forschungsgemeinschaft (DFG) (grant WI3285/11-1 to D.N.W.), JSPS Grant-in-Aid for Scientific Research (Grant No. 16H04788, 26116008, 20H05926, and 21K06053 to S.C., 19K16044, and 21K15020 to K.F.), and under Germany's Excellence Strategy grant no. EXC 2067/1-390729940 (L.V.B.). We acknowledge financial support from the Open Access Publication Fund of Universität Hamburg. Cryo-EM data collection was performed at the Multi-User CryoEM Facility at the Centre for Structural Systems Biology, Hamburg, supported by the Universität Hamburg and DFG grant numbers (INST 152/772-1|152/774-1|152/775-1|152/776-1|152/777-1 FUGG).

Author contributions

F.G. generated the SecM-SRC sample and H.S. prepared and screened the cryo-EM grids and collected high resolution data. F.G. and M.M. processed the cryo-EM data, as well as generated and refined the molecular models. H.P. helped with data processing, model building and refinement. K.F. and S.C. performed the biochemical stalling assays. S.G. and L.V.B. performed the MD simulations. D.N.W. and F.G. wrote the manuscript with input from all authors. D.N.W. conceived and supervised the project.

Funding

Open Access funding enabled and organized by Projekt DEAL.

Competing interests

The authors declare no competing interests.

Additional information

Supplementary information The online version contains supplementary material available at <https://doi.org/10.1038/s41467-024-46762-2>.

Correspondence and requests for materials should be addressed to Daniel N. Wilson.

Peer review information *Nature Communications* thanks Matthieu Gagnon and the other, anonymous, reviewer(s) for their contribution to the peer review of this work. A peer review file is available.

Reprints and permissions information is available at <http://www.nature.com/reprints>

Publisher's note Springer Nature remains neutral with regard to jurisdictional claims in published maps and institutional affiliations.

Open Access This article is licensed under a Creative Commons Attribution 4.0 International License, which permits use, sharing, adaptation, distribution and reproduction in any medium or format, as long as you give appropriate credit to the original author(s) and the source, provide a link to the Creative Commons licence, and indicate if changes were made. The images or other third party material in this article are included in the article's Creative Commons licence, unless indicated otherwise in a credit line to the material. If material is not included in the article's Creative Commons licence and your intended use is not permitted by statutory regulation or exceeds the permitted use, you will need to obtain permission directly from the copyright holder. To view a copy of this licence, visit <http://creativecommons.org/licenses/by/4.0/>.

© The Author(s) 2024, corrected publication 2024

Structural basis for translation inhibition by the glycosylated drosocin peptide

Received: 6 October 2022

Accepted: 14 February 2023

Published online: 30 March 2023

Check for updates

Timm O. Koller^{1,4}, Martino Morici^{1,4}, Max Berger^{1,4}, Haaris A. Safdari¹,
Deepti S. Lele², Bertrand Beckert³, Kanwal J. Kaur² & Daniel N. Wilson¹✉

The proline-rich antimicrobial peptide (PrAMP) drosocin is produced by *Drosophila* species to combat bacterial infection. Unlike many PrAMPs, drosocin is O-glycosylated at threonine 11, a post-translation modification that enhances its antimicrobial activity. Here we demonstrate that the O-glycosylation not only influences cellular uptake of the peptide but also interacts with its intracellular target, the ribosome. Cryogenic electron microscopy structures of glycosylated drosocin on the ribosome at 2.0–2.8-Å resolution reveal that the peptide interferes with translation termination by binding within the polypeptide exit tunnel and trapping RF1 on the ribosome, reminiscent of that reported for the PrAMP apidaecin. The glycosylation of drosocin enables multiple interactions with U2609 of the 23S rRNA, leading to conformational changes that break the canonical base pair with A752. Collectively, our study reveals novel molecular insights into the interaction of O-glycosylated drosocin with the ribosome, which provide a structural basis for future development of this class of antimicrobials.

The host defense systems of mammals and higher insects produce a battery of potent antimicrobial peptides (AMPs) in response to bacterial infection. Unlike most AMPs that kill bacteria using a lytic mechanism, proline-rich AMPs (PrAMPs) pass through the bacterial membrane and target intracellular processes, such as protein synthesis^{1–3}. Two types of PrAMPs have been identified and classified based on their mechanism of action to inhibit protein synthesis—namely, type I PrAMPs that block the accommodation of the aminoacyl-tRNA directly after translation initiation and type II PrAMPs that do not interfere with initiation and elongation but prevent dissociation of the release factors RF1 and RF2 during the termination phase³. Structures on the ribosome of a variety of type I PrAMPs from both insect (oncocin, metalnikowin I and pyr-rhocoricin) and mammalian (Bac7 and Tur1A) origin have revealed overlapping binding sites that span from the ribosomal exit tunnel to the A-site of the peptidyltransferase center (PTC)^{4–9}. It has been proposed that, by occluding the A-site at the PTC on the ribosome, type I PrAMPs prevent the binding of the aminoacylated CCA-end of the incoming A-site tRNA and, thereby, arrest translation^{3–7}. Structures on the ribosome with the type II PrAMP Api137, a synthetic derivative of

the natural PrAMP apidaecin, have revealed a binding site within the ribosomal exit tunnel that overlaps with type I PrAMPs^{10,11}. However, the binding mode of Api137 is completely different, with a reversed orientation compared to type I PrAMPs, and also Api137 does not encroach so markedly on the A-site of the PTC. Instead, Api137 inhibits translation by trapping the termination release factors on the ribosome after peptidyl-tRNA hydrolysis^{10,11}.

In addition to the classical membrane-targeting AMPs, such as defensins, cecropins and dipterocins, *Drosophila* also produce a PrAMP called drosocin^{12,13}. Drosocin is 19 amino acids long, rich in proline and arginine residues¹² (Fig. 1a) and displays excellent activity against Gram-negative bacteria, such as *Escherichia coli*^{12,13}. However, unlike most PrAMPs, drosocin carries an O-glycosylation on residue Thr11, consisting of either the monosaccharide N-acetylgalactosamine (α -D-GalNAc) or a disaccharide comprising galactose linked to an N-acetylgalactosamine (β -Gal(1 \rightarrow 3)- α -D-GalNAc) (Fig. 1a,b)^{12,14}. A double-glycosylated form of drosocin bearing the monosaccharide on Ser7 as well as Thr11 has also been reported¹⁵. Both the monosaccharide and disaccharide forms of drosocin appear in *Drosophila*

¹Institute for Biochemistry and Molecular Biology, University of Hamburg, Hamburg, Germany. ²National Institute of Immunology, Aruna Asaf Ali Marg, New Delhi, India. ³Dubochet Center for Imaging (DCI) at EPFL, EPFL SB IPHY DCI, Lausanne, Switzerland. ⁴These authors contributed equally: Timm O. Koller, Martino Morici, Max Berger. ✉e-mail: daniel.wilson@chemie.uni-hamburg.de

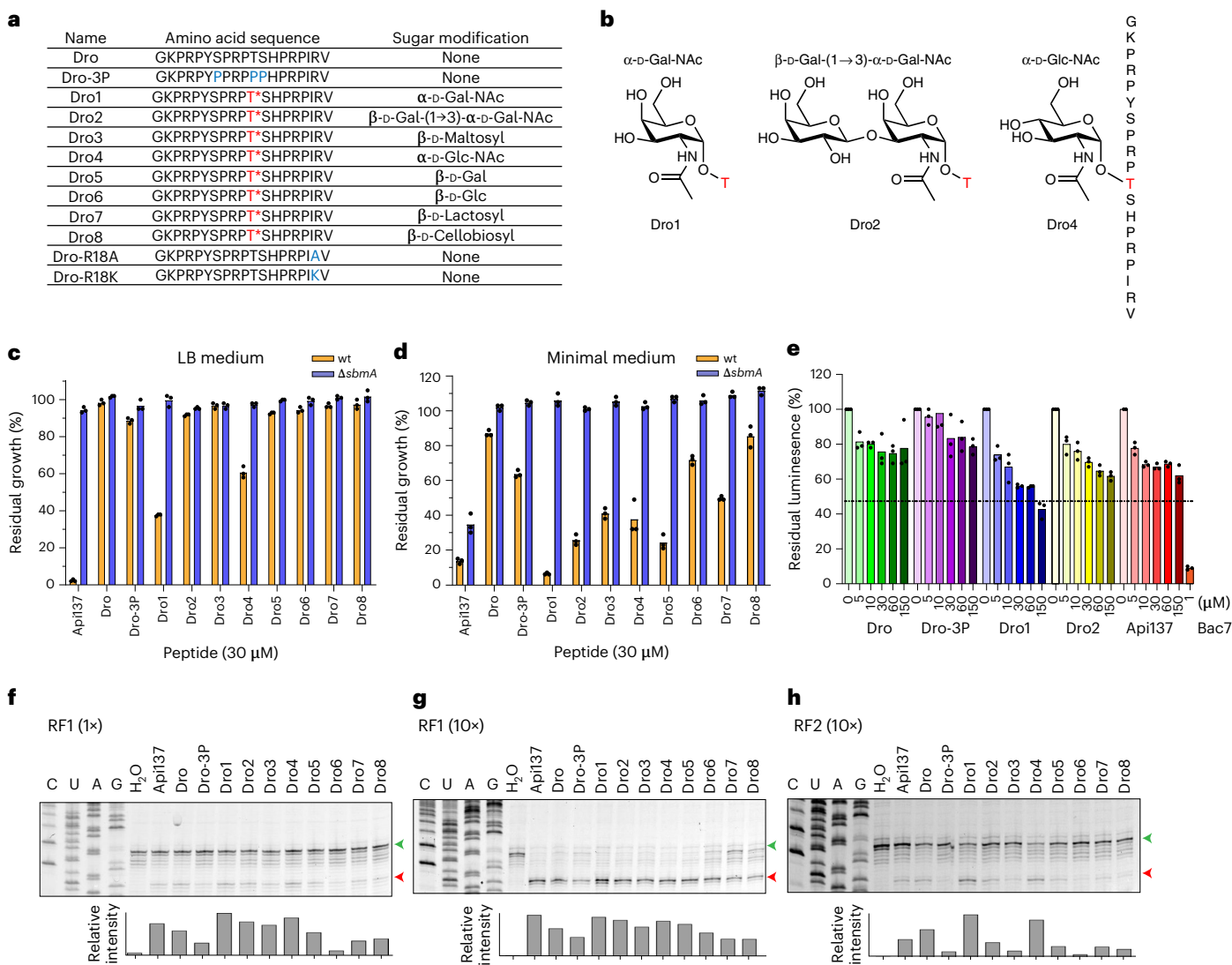


Fig. 1 | Characterization of inhibitory activity of drosocin derivatives.

a, Amino acid sequences of the drosocin peptides used in this study. Drosocin peptides carrying a modification on Thr11 are indicated with T*, whereas the mutated positions are shown in blue. **b**, Chemical structures of the Thr11 modifications of Dro1, Dro2 and Dro4. **c, d**, *In vivo* inhibitory activity of 30 μ M Api137 and drosocin derivatives on the growth of *E. coli* wild-type (yellow) and Δ *sbmA* (blue) strains in rich LB (**c**) or minimal medium (**d**). Histograms represent the averages from three biological replicates, individually plotted as dots, and results are normalized to growth in the absence of peptide, which was assigned as 100%. **e**, Inhibitory activity of increasing concentrations of Dro (green), Dro-3P

(purple), Dro1 (blue), Dro2 (yellow), Api137 (red) and 1 μ M Bac7 (orange) on *in vitro* translation using Fluc as a reporter. The luminescence in the absence of compounds was normalized to 100%; experiments were performed in triplicate, individually plotted as dots, and the bars represent the mean. **f–h**, Toeprinting assays monitoring the position of ribosomes on an MLIF* mRNA in the presence of 30 μ M Api137 and drosocin derivatives and 1 \times RF1 (**f**), 10 \times RF1 (**g**) or 10 \times RF2 (**h**). Bands corresponding to ribosomes present at the start and stop codons are indicated by green and red arrows, respectively. The histogram represents the proportion of relative intensity of stop codon band for the different peptides. Toeprinting assays were performed in duplicate. wt, wild-type.

hemolymph within 6 hours after infection and increase in concentration (to 40 μ M) for up to 24 hours¹⁴. Although the disaccharide form disappears 2 weeks after infection, the monosaccharide persists for up to 3 weeks¹⁴. Synthetic drosocin lacking O-glycosylation is less active than the native compounds, suggesting that the post-translational modification is necessary for full activity^{12,13,16,17}. Indeed, many studies have demonstrated that a variety of synthetic drosocin derivatives with varying sugar moieties maintain good antimicrobial activity, generally better than the unmodified form^{17–24}. Although nuclear magnetic resonance and circular dichroism experiments suggest that both the modified and unmodified forms of drosocin adopt extended conformations in solution^{17,23,24}, the presence of the modification has nevertheless been proposed to help drosocin maintain an extended conformation to facilitate binding to its intracellular target^{13,17}. Additionally,

glycosylation can also increase solubility and serum stability and broaden the biological activity spectrum¹³; however, the exact role of glycosylation for drosocin is unknown.

Although drosocin inhibits protein synthesis *in vivo* and *in vitro*^{25,26}, the exact mechanism remains unclear. Interestingly, the type I insect PrAMP pyrrococin is O-glycosylated with N-acetylgalactosamine on Thr11, and a minor disaccharide form with the additional galactose has also been detected²⁷. Together with the reported sequence similarity, drosocin was proposed to act analogously to pyrrococin and metanikowins rather than apidaecins and abaecins¹³. However, several subsequent observations support similarity between drosocin and apidaecin rather than type I PrAMPs. First, in contrast to drosocin, unmodified pyrrococin is slightly more active than the modified form¹⁶. Second, drosocin was suggested to belong to the apidaecin-like

PrAMPs based on similarity in terms of ribosome-binding antibiotic competition assays—that is, drosocin competes better with Api137 than with the oncocin derivative Onc112 (ref. ²⁸). Finally, drosocin lacking the carboxy-terminal Arg18–Val19 almost completely loses antimicrobial activity¹⁶, analogous to Api137 (ref. ²⁹), whereas N-terminal, rather than C-terminal, truncations inactivate type I PrAMPs, such as Bac7 (refs. ^{6,30}).

In this study, we employed biochemical and structural approaches to dissect the mechanism by which drosocin interacts with the ribosome and inhibits protein synthesis, and we shed light on the role of the critical O-glycosylation on Thr11.

Results

Characterization of the activity of drosocin derivatives

Many PrAMPs use the SbmA transporter to pass through the *E. coli* inner membrane^{4,10,31}; however, whether drosocin also uses SbmA remains, to our knowledge, unknown. To address this, we monitored the effect of the presence of diverse drosocin peptides (Fig. 1a,b and Supplementary Fig. 1a) on the growth of the wild-type *E. coli* strain BW25113 containing SbmA or lacking SbmA ($\Delta sbmA$) (Fig. 1c,d). We compared unmodified drosocin (Dro) with various modified forms (Fig. 1a,b). The modified forms included the naturally occurring Dro1 and Dro2 that carry either a monosaccharide (α -D-GalNAc) or disaccharide (β -D-Gal(1 \rightarrow 3)- α -D-GalNAc) attached to Thr11, respectively (Fig. 1b). In addition, we examined the previously reported^{23,24} drosocin derivatives bearing β -D-Maltosyl (Dro3), α -D-GlcNAc (Dro4), β -D-Gal (Dro5), β -D-Glc (Dro6), β -D-Lactosyl (Dro7) and β -D-Cellobiosyl (Dro8) modifications on Thr11 (Fig. 1a,b and Supplementary Fig. 1a). Finally, we also included in our analysis the synthetic unmodified drosocin derivative with proline substitutions at positions 7, 11 and 12 (Dro-3P) (Fig. 1a), which was previously reported to have similar antimicrobial activity to the monosaccharide form of drosocin²⁵. Growth was monitored in both rich (LB) and minimal medium in the presence of 30 μ M of each peptide and normalized with the growth in the absence of the compounds (Methods). In rich medium, we observed growth inhibition only with Dro1 and Dro4 (Fig. 1c). Because no inhibition was observed with the monosaccharide β -D-Gal (Dro5) or β -D-Glc (Dro6) drosocins, this suggests that, under these conditions, the stereochemistry of the anomeric carbon on the sugar is more important than the type of sugar itself. We also observed no inhibition for Dro2 nor for any of the β -linked disaccharides (Dro3, Dro6 or Dro7). Similarly, the unmodified drosocin and Dro-3P variant were inactive under these conditions (Fig. 1c). By contrast, all drosocin peptides inhibited growth of the *E. coli* BW25113 strain in minimal medium, albeit to different extents (Fig. 1d). The trends were similar to that reported previously^{23,24}—namely, with the highest inhibition observed using Dro1 and the lowest with the unmodified peptide—whereas the other glycosylated variants lay in between (Fig. 1d). We did not observe similar activity between Dro1 and Dro-3P, as reported previously²⁵, which may arise due to differences in the *E. coli* strains and/or growth conditions used. Strikingly, we note that any inhibition observed with the *E. coli* BW25113 strain was lost when performed with the BW25113 $\Delta sbmA$ strain, indicating that SbmA plays a major role in the cellular uptake of all drosocin peptides.

Drosocin traps ribosomes on stop codons during translation

Unmodified wild-type drosocin and Dro-3P have been reported to inhibit in vitro translation reactions^{25,26}; however, the naturally occurring glycosylated forms of drosocin have not been previously tested. To investigate this, we compared the effect of increasing concentrations (0–150 μ M) of modified Dro1 and Dro2 with unmodified Dro, Dro-3P and Api137 using a cell-free in vitro translation system and firefly luciferase (Fluc) mRNA as a template (Fig. 1e), as we have used previously for assessing the activity of other PrAMPs^{4,6,8,9,32,33}. Dro1 exhibited dose-dependent inhibition, with a half maximal inhibitory concentration (IC₅₀) of 78 \pm 13 μ M and reaching a maximum of 60% inhibition at

the highest concentration tested of 150 μ M. By contrast, both Dro and Dro-3P were poor inhibitors, reaching a maximum of 20% inhibition at 150 μ M, whereas Dro2 and Api137 were slightly more effective, with 40% inhibition observed at 150 μ M. This contrasts with type I PrAMPs, such as Bac7 (Fig. 1e) and Onc112, that display IC₅₀ of <1 μ M using the same system^{4,6}, suggesting that drosocin may inhibit translation similarly to Api137, as proposed previously²⁸.

To ascertain which step during protein synthesis is affected by drosocin, we performed toeprinting assays, where reverse transcription is used to monitor the position of ribosomes on a defined mRNA³⁴. In the absence of PrAMP, but the presence of RF1, we observed no band corresponding to ribosomes at the UAA stop codon of the mRNA, whereas, in the presence of 25 μ M Api137 and RF1, ribosomes become stuck at the stop codon (Fig. 1f and Supplementary Fig. 1b), as expected¹⁰. Similarly, the same termination band was also observed in the presence of 30 μ M of each of the tested drosocin derivatives, albeit with differing intensities (Fig. 1f). Increasing the concentration of RF1 by ten-fold in the reactions led to more intense termination bands (Fig. 1g and Supplementary Fig. 1c), consistent with a role of drosocin acting during the termination phase, as reported for Api137 (refs. ^{10,11}). We performed the same toeprinting reactions in the presence of ten-fold RF2, rather than ten-fold RF1, and also observed stalling of ribosomes at the stop codon, albeit with much lower efficiency (Fig. 1h and Supplementary Fig. 1d). The weaker stalling with RF2 is likely due to the endemic A246T mutation found in RF2 from K12 strains, which likely confers some resistance to drosocin, as was shown previously for Api137 (ref. ¹⁰). The strongest stalling was observed in the presence of Dro1 and, to a lesser extent, with Dro4, a trend that was particularly evident in the presence of ten-fold RF2 (Fig. 1h). Both Dro1 and Dro4 were also the most active in our whole-cell assays (Fig. 1c,d). By contrast, weak stalling was observed with Dro-3P, consistent with the lack of activity in the whole-cell (Fig. 1c,d) and in vitro translation assays (Fig. 1e). Interestingly, we observed good activity for Dro in the toeprinting assay (Fig. 1f–h), suggesting that the poor activity observed in the whole-cell assays (Fig. 1c,d) may be due to cellular uptake.

Cryogenic electron microscopy structures of drosocin-bound ribosome complexes

To investigate how drosocin inhibits translation and to provide insight into the role of the O-glycosylation, we set out to determine a cryogenic electron microscopy (cryo-EM) structure of a ribosome–drosocin complex. Rather than forming complexes with vacant ribosomes or pre-defined functional states, we instead performed translation reactions with the same mRNA template used for the toeprinting assays in the presence of ten-fold RF1 and 30 μ M Dro1 (Fig. 1g). Reactions were subsequently pelleted through sucrose cushions, and the pelleted ribosomal complexes were subjected to single-particle cryo-EM analysis. In silico sorting of the data revealed three main populations of ribosomal states—namely, 70S ribosomes with RF1 and P-site tRNA (26%) or with A-site and P-site tRNAs (16%) as well as a population containing only large 50S subunits (30%) (Supplementary Fig. 2), which, after refinement, yielded final reconstructions at 2.3 Å, 2.8 Å and 2.0 Å, respectively (Fig. 2a–c and Extended Data Fig. 1). In all three reconstructions, additional density was observed within the ribosomal exit tunnel that could be unambiguously assigned to the drosocin peptide (Fig. 2a–i). The density for drosocin was particularly well resolved in the RF1-containing 70S map enabling all 19 amino acids to be modeled with sidechains (Fig. 2d and Extended Data Fig. 1), including the α -D-GalNAc modification linked to Thr11 (Fig. 2g). Similarly, the density for drosocin in the cryo-EM map of the 50S subunit was generally well resolved, except for the N-terminal and C-terminal regions (Fig. 2f,i and Extended Data Fig. 1). By contrast, the density for drosocin in the cryo-EM map of the complex containing A-site and P-site tRNAs was less well resolved (Fig. 2e and Extended Data Fig. 1) and was particularly poor for the α -D-GalNAc modification (Fig. 2h), suggesting that the

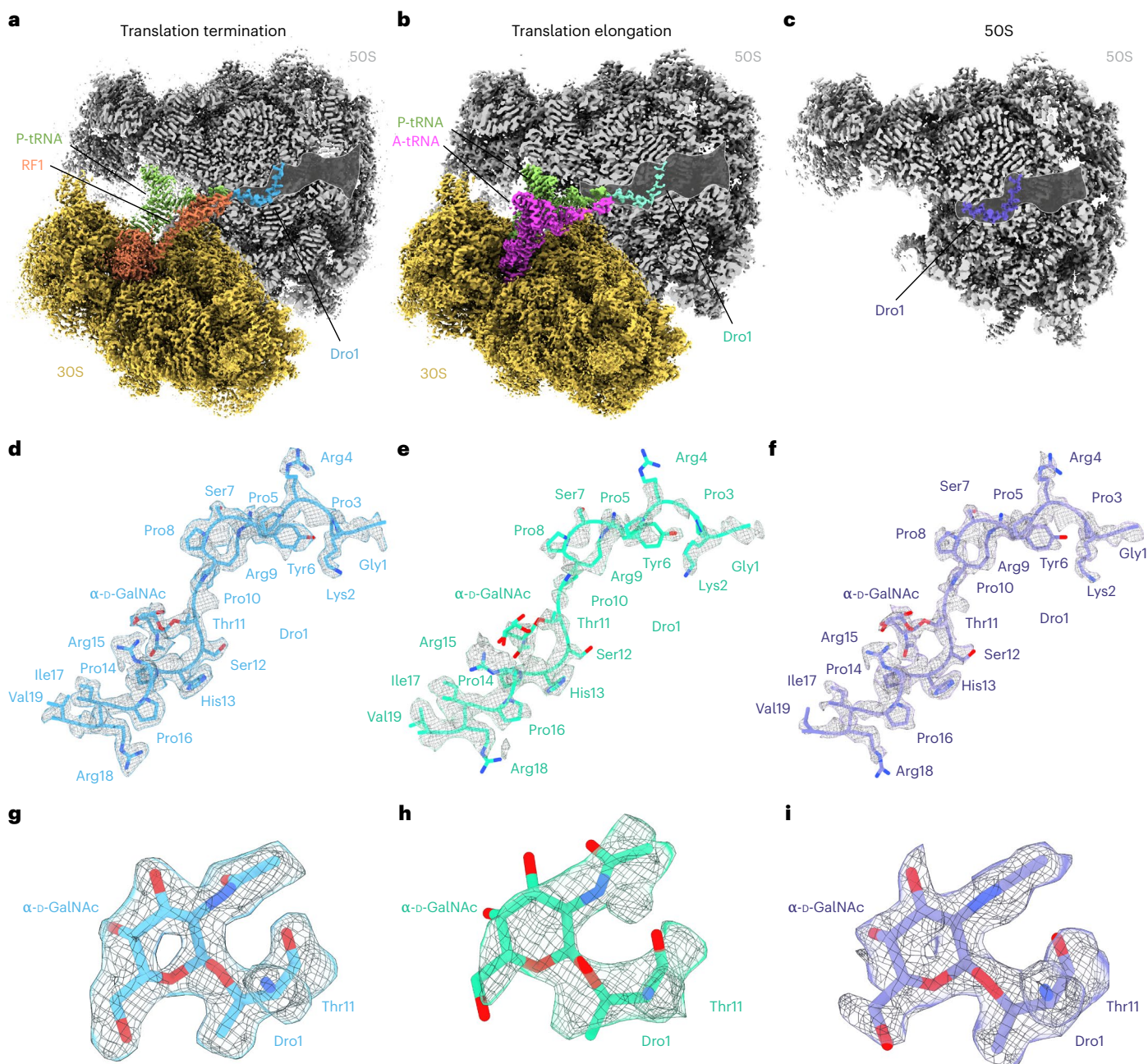


Fig. 2 | Cryo-EM structures of drosocin-bound ribosomal complexes.

a–c, Cryo-EM maps of Dro1 bound to termination (**a**) and elongation (**b**) complexes as well as the large 50S subunit (**c**), with transverse section of the 50S (gray) to reveal the Dro1 binding site within the exit tunnel. In **a**, the P-tRNA, RF1 and Dro1 are colored green, orange and cyan, respectively. In **b**, the A-tRNA, P-tRNA and Dro1 are colored pink, green and teal, respectively, whereas, in **c**, Dro1

is purple. **d–f**, Cryo-EM density (gray mesh) with molecular model for Dro1 (cyan) (**d**) from termination complex as in **a**, Dro1 (teal) (**e**) from elongation complex as in **b** and Dro1 (purple) (**f**) from the 50S subunit as in **c**. **g–i**, Cryo-EM density (gray mesh) with molecular model for α -D-GalNAc modification at Thr11 of Dro1 in the termination (**g**) and elongation (**h**) complexes as well as the 50S subunit (**i**).

peptide is bound less stably within this complex. Nevertheless, in all three structures, the overall orientation of the drosocin peptide within the exit tunnel was identical, with the C-terminus located at the PTC and the N-terminus extending into the exit tunnel, analogous to an elongating nascent polypeptide chain (Fig. 2a–f and Extended Data Fig. 2a). This orientation is also the same as that observed for the type II PrAMP Api137 (refs. 10,11) but opposite to that of type I PrAMPs, such as Bac7 and pyrrolicorin (Extended Data Fig. 2b–d)^{4–9}.

Cryo-EM structure of drosocin on an elongating ribosome

For the drosocin–ribosome complex containing A-site and P-site tRNAs, comparison of the cryo-EM density (Fig. 3a) with pre-attack

and post-attack states³⁵ (Fig. 3b,c) indicates that the P-site tRNA is deacylated, whereas the A-site tRNA carries a nascent chain (Fig. 3a). Thus, drosocin is bound to an elongating ribosome state that is post-peptide bond formation but pre-translocation. Inspection of the cryo-EM density for the anticodon–codon interactions suggested the presence of initiator tRNA^{Met} and tRNA^{Leu} decoding the AUG and UUC codons in the first and second positions of the mRNA, respectively (Supplementary Fig. 3a,b). In this case, the nascent chain should comprise the dipeptide fMet-Leu, which is consistent with the limited space due to the presence of drosocin blocking the PTC and exit tunnel. However, because the density for the nascent chain was poorly resolved and, thus, could not be modeled de novo, only a tentative model for

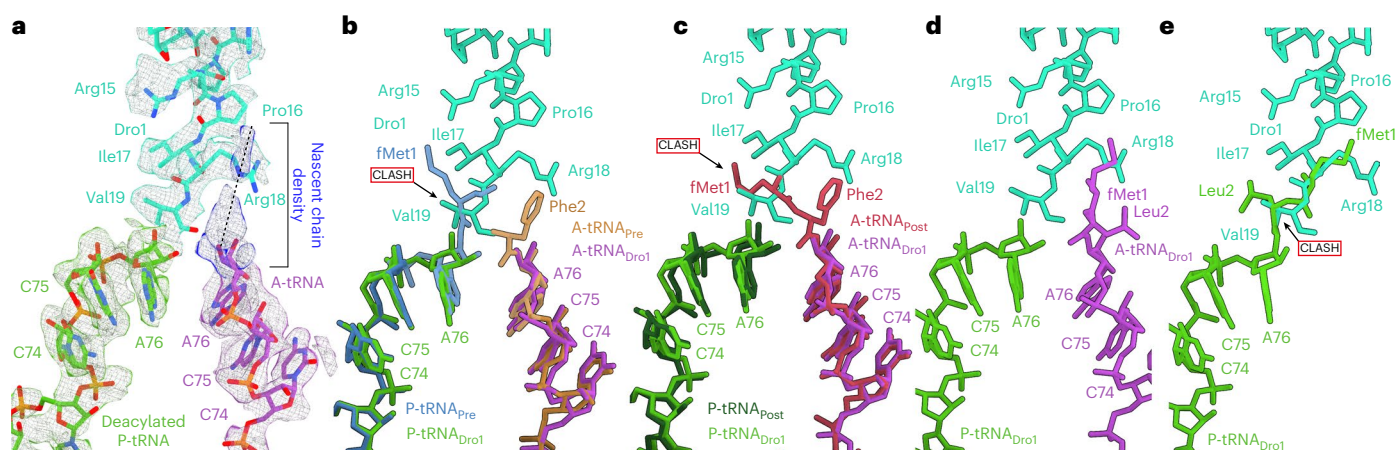


Fig. 3 | Cryo-EM structure of the drosocin-bound translation elongation complex. **a**, Isolated cryo-EM densities (mesh) with molecular models for P-tRNA (light green), A-tRNA (magenta) and Dro1 (teal) within the translation elongation complex. Additional density connected to the A-site tRNA is attributed to the nascent chain but cannot be modeled due to flexibility. **b**, Superimposition of P-tRNA_{Dro1} (light green), A-tRNA_{Dro1} (purple) and Dro1 (teal) from **a**, with P-tRNA_{Pre} (blue) and A-tRNA_{Post} (brown) from PRE-state (PDB ID: 1VY4)³⁵. Alignment is based on the 23S rRNA. The fMet attached to the P-site tRNA would be predicted to

clash with the C-terminus of Dro1 (teal). **c**, Superimposition of P-tRNA_{Dro1} (light green), A-tRNA_{Dro1} (purple) and Dro1 (teal) from **a**, with P-tRNA_{Post} (dark green) and A-tRNA_{Post} (red) from POST-state (PDB ID: 1VY5)³⁵. Alignment is based on the 23S rRNA. The fMet from the fMet-Phe, attached to the A-tRNA_{Post}, would be predicted to clash with the C-terminus of Dro1 (teal). **d**, Hypothetical molecular model of the fMet-Leu nascent chain connected to the A-tRNA (based on POST-state PDB ID: 1VY5)³⁵. **e**, Steric clash of the fMet-Leu nascent chain in the P-site after translocation (based on PDB ID: 7RQE).

fMet-Leu could be generated to illustrate that the position is different than fMet-Phe in the post-peptide bond formation state reported previously (Fig. 3c,d)³⁵. In the latter, we would predict steric clashes between the fMet moiety and the N-terminal Val19 of drosocin (Fig. 3c), which appears to have forced the fMet moiety to shift toward Arg18 (Fig. 3d), providing a likely explanation as to why both regions are poorly ordered in this complex (Fig. 3a). For the elongating complex to exist, drosocin allows initiation (despite predicted clashes between the fMet and Val19, as seen in Fig. 3b), aminoacyl-tRNA binding to the A-site and subsequent peptide bond formation, but it interferes with the first translocation step. To mimic the translocated state, we modeled fMet-Leu-tRNA bound in the P-site based on available P-site peptidyl-tRNAs³⁶, which revealed even larger steric clashes with drosocin (Fig. 3e), providing a structural explanation for the observed translocation inhibition. We note that, although apidaecin strongly interferes with termination, moderate effects on initiation have also been reported in vivo and in vitro³⁷. Given the similarity in the binding position of the C-terminus of Api137 and drosocin on the ribosome (Extended Data Fig. 2b), it seems likely that apidaecin may also interfere with the first translocation step, as seen here for drosocin, rather than acting like a type I PrAMP to prevent accommodation of the aminoacyl-tRNA at the A-site of the PTC, but this remains to be determined.

Interaction of drosocin within the RF1-bound complex

In the RF1-bound complex, Dro1 is very well resolved, enabling a molecular description of the interactions of the drosocin peptide with components of the ribosomal tunnel as well as RF1 (Supplementary Fig. 4a–g). Overall, there is excellent agreement between the interactions observed here for Dro1 and the extensive mutagenesis performed on Dro in ref.³⁸. In total, there are three stacking interactions observed between sidechains of Dro1 and the 23S rRNA—namely, between Arg9 and A751, His13 and C2611 as well as Arg15 and A2062. Mutation of Arg9 or Arg15 to lysine reduces antimicrobial activity of the Dro peptides by four-fold and eight-fold, respectively³⁹, suggesting that these interactions contribute to drosocin binding. Api137 also stacks with A751 and C2611 (refs.^{10,11}); however, the sidechains and modes of interaction are completely distinct (Extended Data Fig. 3a–d). Compared to the canonical RF1-bound termination complexes^{40,41}, we observed a rotated conformation of A2062, which was also observed in the Api137-bound

ribosome structures^{10,11} (Extended Data Fig. 3e–g). The rotated conformation of A2062 forms interactions with A2503, which is adjacent to A2059, both of which were shown to confer resistance to Api137 when mutated¹⁰. Because Arg15 of Dro1 stacks upon A2062 (Supplementary Fig. 4g and Extended Data Fig. 3h) and is in close proximity to A2503 and A2059, we assessed whether A2503G and A2059G mutations confer resistance to Dro1. Indeed, we observed that, compared to the wild-type strain, both strains bearing the A2503G and A2059G mutations were more resistant to Api137 (Extended Data Fig. 3h), as previously reported¹⁰, but also to Dro1 (Supplementary Fig. 4h). We think that these findings provide strong evidence that the ribosome (and, therefore, translation) is a (if not ‘the’) physiological target for Dro1 within the bacterial cell. This is also supported by the identification of mutations in ribosomal protein uL16 that confer resistance to Api137 also confer resistance to Dro (see ref.³⁸).

C-terminal interactions are critical for drosocin activity

The C-terminus of Dro1 is stabilized by three backbone interactions between residues Ile17–Arg18 and 23S rRNA nucleotides U2506, G2061 and A2062 (Fig. 4a). Additionally, the sidechain of Arg18 inserts into a pocket where it can form direct hydrogen bonds with the nucleobases of C2452 and U2506 (Fig. 4b) as well as via water-mediated interactions with Ψ2504, G2061 and A2451 (Fig. 4b,c). Notably, Arg18 comes within 2.9 Å of Gln235 of the conserved GGQ motif of RF1, and a further water-mediated interaction with Gln235 is also possible (Fig. 4b,c), suggesting that Arg18 plays an important role in stabilizing RF1 on the ribosome. This interaction is reminiscent of that observed previously between Arg17 of Api137 and Gln235 of RF1 (refs.^{10,11}) (Extended Data Fig. 4a–f), the importance of which was shown by Arg17Ala mutations that decrease both the ribosome affinity and inhibitory activity of the peptide². Although deletion of the last two residues (Arg18–Val19) of drosocin completely abolished in vitro biological activity¹⁶, single substitutions of Arg18 have, to our knowledge, not been undertaken. Therefore, we synthesized an unmodified drosocin peptide bearing the Arg18Ala mutation (Fig. 1a) and tested its activity using in vitro translation assays, demonstrating a complete loss of activity for the Dro-R18A peptide (Fig. 4d). By contrast, Dro bearing an Arg18Lys mutation (Dro-R18K; Fig. 1a) displayed similar activity to Dro (Fig. 4d). Unlike Arg18, the very C-terminal Val19 of Dro1 is poorly ordered, but, at lower

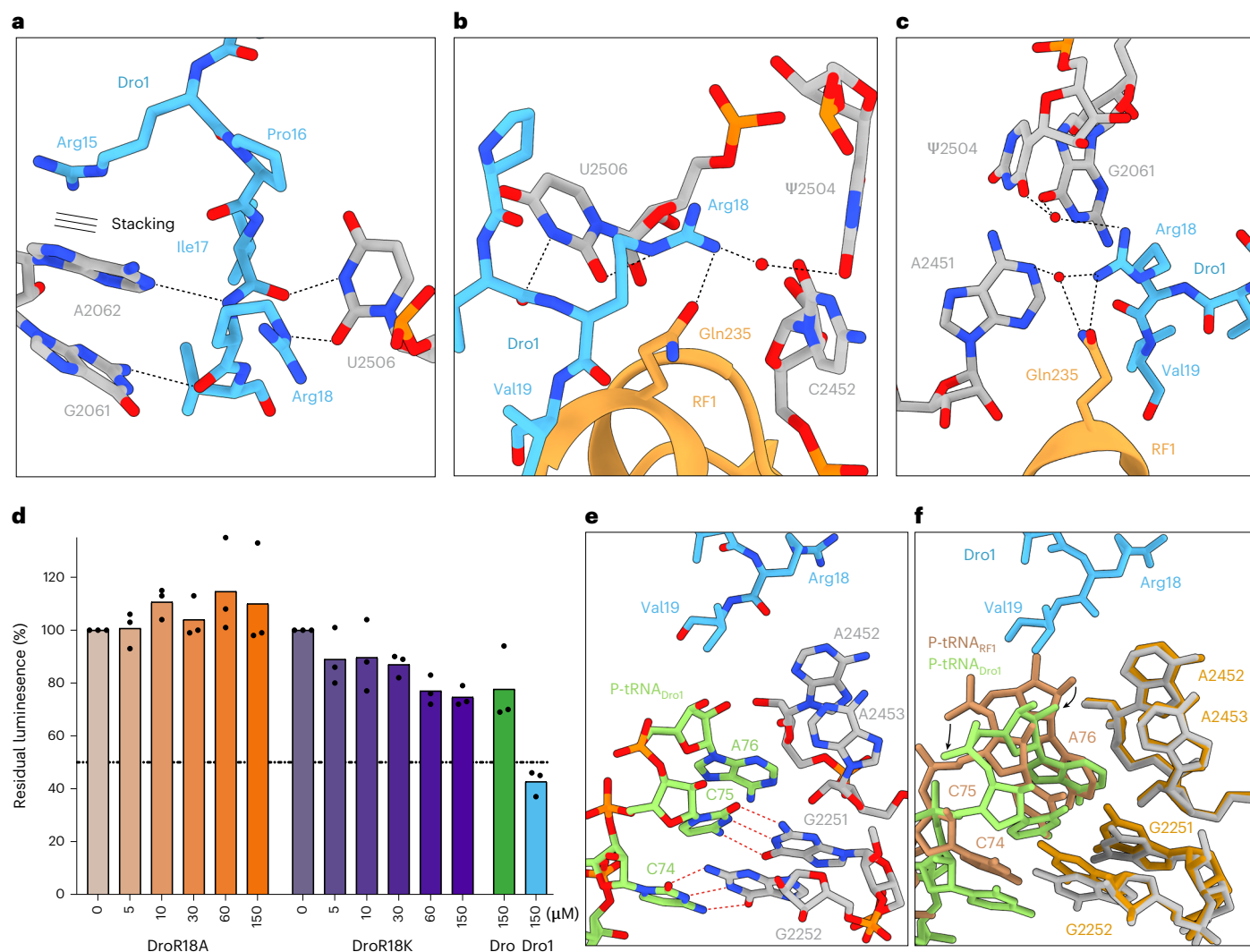


Fig. 4 | Interactions of drosoicin with RF1 and P-tRNA. **a–c**, Interactions of Dro1 (light blue) with 23S rRNA nucleotides (gray) and RF1 (orange). **a**, Stacking interaction of Arg15 (indicated by three lines) and hydrogen bond interactions of G2061, A2062 and U2506 with Ile17 and Arg18 of Dro1. **b,c**, Two views of the water-mediated and direct hydrogen bond interactions of Arg18 of Dro1 with Gln235 of RF1 and 23S rRNA nucleotides Ψ 2504, U2506 and C2452 (**b**) and G2061, A2451 and Ψ 2504 (**c**). **d**, Inhibitory activity of increasing concentrations of Dro R18A (orange), Dro R18K (purple) and 150 μ M Dro (green) or Dro1 (blue), on in

vitro translation using Fluc as a reporter. The luminescence in the absence of compounds was normalized to 100%; experiments were performed in triplicate, individually plotted as dots, and the bars represent the mean. **e**, Deacylated P-tRNA (lime) in the presence of Dro1 (light blue). **f**, Superimposition of **e** with a P-tRNA from a canonical termination complex (brown; PDB ID: 4V63)⁴⁰. Dro1 displaces the CCA-end of the deacylated tRNA while keeping the base-pairing interactions of C74 and C75 with G2252 and G2251 (gray), respectively, which slightly tilts the nucleotides compared to the canonical position (yellow).

thresholds, density is observed to encroach on the P-site of the PTC (Fig. 4e,f). As a consequence, the CCA-end of the P-site tRNA, which is also poorly resolved, is clearly shifted by 2–3 Å from its canonical position observed in RF1 termination complexes^{40,41} (Fig. 4f). The shift is predominantly of the backbone of the CCA-end enabling the nucleobases of C74 and C75 to maintain Watson–Crick base pairs with P-loop nucleotides G2252 and G2251, respectively (Fig. 4e,f). This is distinct from Api137, where the C-terminus was observed to directly interact with the A76 of the P-site tRNA and stabilize the P-site tRNA in its canonical position (Extended Data Fig. 4g–h). By comparison, we did not observe a shifted P-site tRNA in the Dro1-bound elongating state (Extended Data Fig. 4i). Otherwise, the binding position and interactions of RF1 in the Dro1–RF1–ribosome complex are identical to those observed previously for RF1 decoding of stop codons during canonical termination^{40,41} (Supplementary Fig. 5a–c). However, with the higher resolution, we also observed multiple water-mediated interactions between RF1 and the UAA stop codon (Supplementary

Fig. 5d–g), which were not reported in the previous lower-resolution termination complexes^{40,41}.

Interaction of drosoicin O-glycosylation with the ribosome

For the Dro1–RF1–70S and Dro1–50S complexes, the α -D-GalNAc modification linked to Thr11 establishes multiple interactions with U2609 of the 23S rRNA (Fig. 5a). In particular, the C3 hydroxyl comes within 2.6 Å and 2.7 Å of the N3 and O2, respectively, of the base of U2609 (Fig. 5a). Additionally, a hydrogen bond is also possible (3.5 Å) from the C4 hydroxyl to the O4 of U2609 (Fig. 5a). We note that α -D-GlcNAc present in Dro4 would maintain the former interactions and lose only the latter weaker interaction with O4 of U2609 (Extended Data Fig. 5a,b), consistent with the similar activity of Dro4 compared to Dro1 (Fig. 1c,d). By contrast, modifications of β -D-linkage, as in Dro3 and Dro5–Dro8, would be incompatible with the interactions observed with α -D-GlcNAc, providing an explanation for why they exhibit lower activity compared to Dro1 and Dro4 (Fig. 1c,d). Comparison with

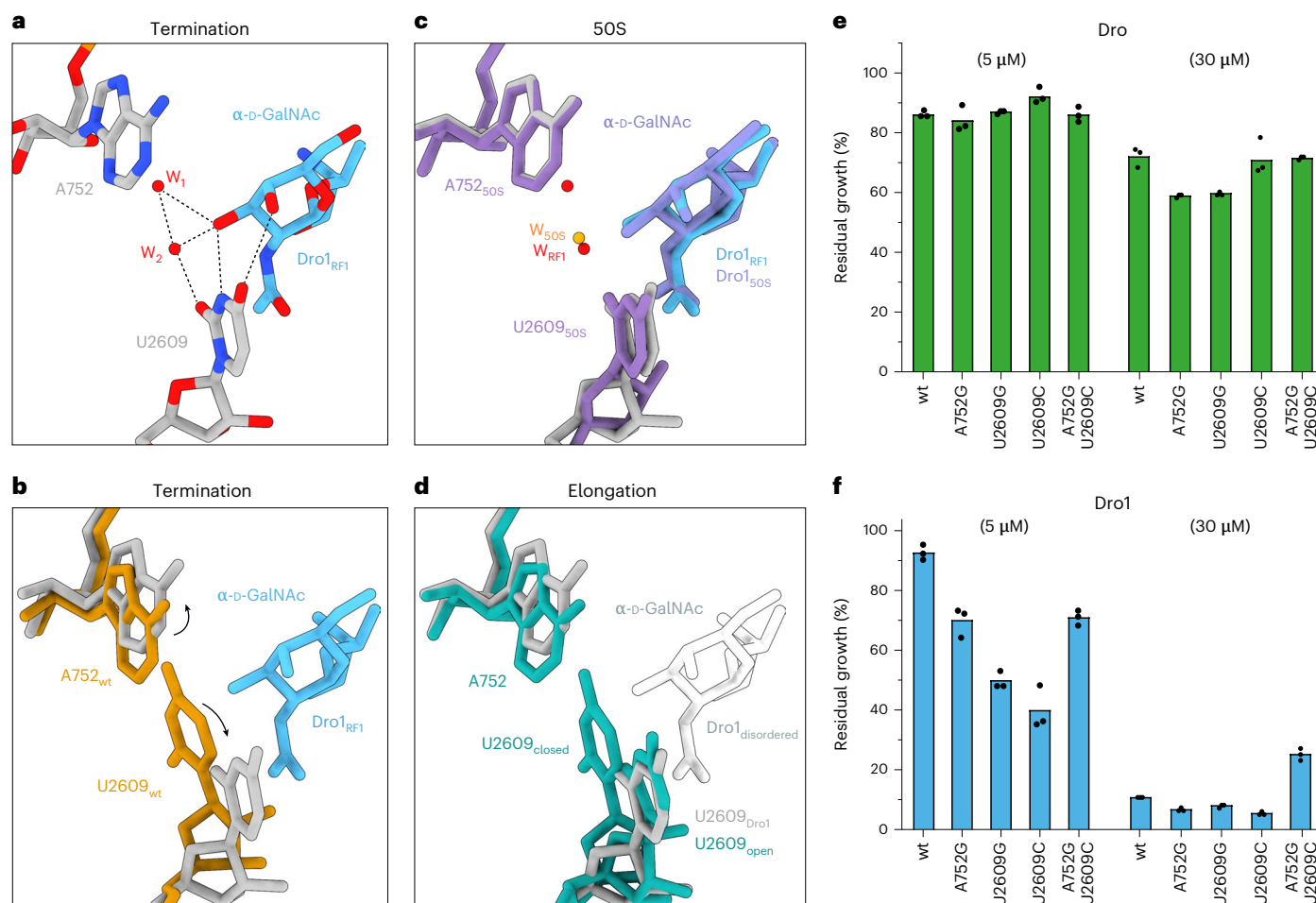


Fig. 5 | Interaction of O-glycosylation of Dro1 with U2609 of the 23S rRNA. **a**, Molecular interactions between the α -D-GalNAc modification on Thr11 of Dro1 (light blue) and the 23S rRNA nucleotide U2609 (gray) of the Dro1-bound termination complex. Two coordinated water molecules (red) stabilize the interactions of α -D-GalNAc of Dro1 with U2609. **b–d**, Superimposition of Dro1_{RF1} (light blue), waters (red) and 23S rRNA (gray) from **a** with 23S rRNA (yellow) from canonical RF1-bound termination complex (PDB ID: 4V63)⁴⁰ (**b**), 23S rRNA (purple) from the Dro1-bound 50S complex (**c**) and 23S rRNA (turquoise) from the Dro1-bound elongation complex with two alternative conformations (open

and closed) of U2609 shown (**d**). α -D-GalNAc modification of Dro1 was poorly ordered in the elongation complex; therefore, the white silhouette indicates the position from Dro1_{RF1} that is incompatible with the closed conformation of U2609. **e, f**, In vivo inhibitory activity of 5 μ M and 30 μ M of Dro (green) (**e**) and Dro1 (blue) (**f**) on the growth of *E. coli* SQ171 wild-type, *E. coli* SQ171 A752G, *E. coli* SQ171 U2609G, *E. coli* SQ171 U2609C and *E. coli* SQ171 A752G/U2609C. Histograms represent the averages from three biological replicates, individually plotted as dots. wt, wild-type.

other *E. coli* 70S ribosome structures, including RF1 termination complexes^{40,41}, reveals that U2609 is usually base paired with A752 (Fig. 5b and Extended Data Fig. 5c), whereas, in the Dro1–RF1–70S and Dro1–50S complexes, α -D-GalNAc occupies the position of U2609, causing the base to shift away from A752 by up to 6 Å (Fig. 5b,c and Extended Data Fig. 5d,e). Moreover, we observed two water molecules located between U2609 and A752 that may also contribute to stabilizing the shifted conformation by establishing indirect interactions between U2609 and α -D-GalNAc (Fig. 5a,c). Interestingly, in the cryo-EM map of Dro1 bound to the elongating ribosome, we observed both the base-paired and shifted conformation of U2609 (Fig. 5d and Extended Data Fig. 5f). As mentioned, the density for α -D-GalNAc is less well resolved in this complex (Fig. 2h and Extended Data Fig. 5f), suggesting that it is highly flexible, presumably because it cannot adopt the preferred position interacting with the shifted conformation of U2609.

Collectively, these findings suggest that the propensity of U2609 and A752 to base pair could influence the ability of Dro1 to bind stably to the ribosome and inhibit translation. To test this, we monitored the antimicrobial activity of Dro1 on strains bearing A752G, U2609G or U2609C mutations, which should perturb Watson–Crick base pairing.

In addition, we also used a strain with a U2609C–A752G double mutation, which would be predicted to restore Watson–Crick base pairing, and with three hydrogen bonds could possibly make breaking the base pair harder than with the canonical two hydrogen bonds for the A–U base pair. As a control, we also tested Dro that lacks the α -D-GalNAc modification, which we predict (assuming that Dro binds analogously to Dro1) should not interact with U2609 and, therefore, not be influenced by the conformation of the U2609–A752 base pair. As seen in Fig. 5e, we observed that there was no significant difference in growth inhibition by 5 μ M Dro and only a modest effect at 30 μ M Dro, when comparing the wild-type strain and strains bearing single or double mutations. By contrast, we observed that the growth of the strains bearing the single point mutations was more susceptible to Dro1 than the wild-type strain, especially for the U2609C mutation, although this effect became less evident at higher (30 μ M) drug concentrations (Fig. 5f). Although the U2609C–A752G double mutation was also slightly more susceptible than the wild-type to Dro1 at 5 μ M, it was still less susceptible than most single point mutations and appeared to be 2.5-fold more tolerant to Dro1 than the wild-type strain at 30 μ M (Fig. 5f). Collectively, these findings support a role for the U2609–A752

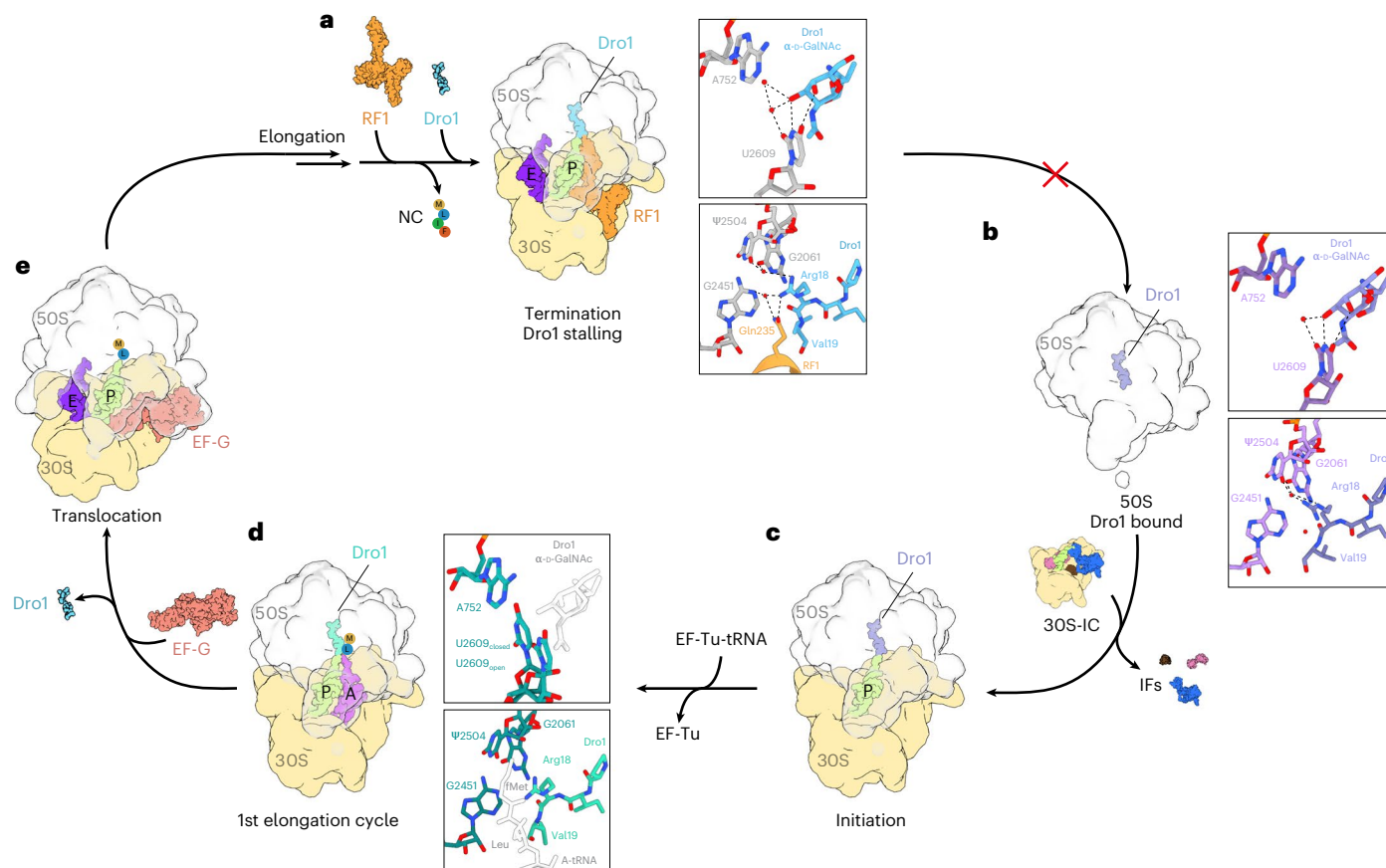


Fig. 6 | Model for the mechanism of action of Dro1 inhibition during translation. **a**, Appearance of a stop codon in the A-site is recognized by RF1 (or RF2, orange), which catalyzes release of the nascent chain (NC) from the P-site tRNA (lime). After NC release, Dro1 (light blue) binds within the exit tunnel, separating the A752–U2609 base pair (gray) with Dro1 α -D-GalNAc modification and becomes stabilized via water-mediated and direct interactions between Arg18 of Dro1 and the Gln235 of the conserved GGQ motif of RF1 and surrounding 23S rRNA nucleotides. This interaction stabilizes RF1 on the post-release complex, preventing its dissociation and, thereby, blocking subsequent ribosome recycling steps and re-initiation. **b**, Dro1 (purple) binds to free 50S subunits (gray), separating the A752–U2609 base pair (light purple) with Dro1 α -D-GalNAc modification but is not fully stabilized via water-mediated and direct

interactions between Arg18 of Dro1 and surrounding 23S rRNA nucleotides. **c**, Translation initiation complexes can form in the presence of Dro1 (purple), despite slight overlap between Dro1 and the fMet moiety of the P-tRNA (lime), suggesting that fMet might displace the C-terminal part of Dro1. **d**, After peptide bond formation, the presence of Dro1 (teal) appears to interfere with translocation of the dipeptidyl-tRNA in the A-site (purple) into the P-site (lime). The α -D-GalNAc modification (white) is disordered, and both the open and closed conformation of the U2609 base (dark teal) is observed. The dipeptidyl moiety (white) on the A-tRNA interferes with the stabilization of Dro1 in the PTC. **e**, For translocation to occur, and subsequent steps of elongation to occur, Dro1 must dissociate from the ribosome, followed by elongation until translation termination is reached.

base pair in modulating the ribosome binding and inhibition activity of glycosylated drosocin.

Discussion

Our biochemical and structural analysis allows us to propose a model for the mechanism of action of drosocin, highlighting the role of the O-glycosylation (Fig. 6). Analogous to Api137 (refs. ^{10,11}), we reveal that drosocin interferes with the translation termination by trapping RF1 on the ribosome subsequent to the release of the nascent polypeptide chain (Fig. 6a). Like Api137 (refs. ^{10,11}), the C-terminal Arg18 of Dro directly interacts with Gln235 of the conserved GGQ motif of RF1 (Fig. 6a). Arg18 of Dro is critical because mutation to alanine abolishes all inhibitory activity of the peptide (Fig. 4d), collectively providing a structural basis for how RF1 dissociation is impeded by drosocin. Unlike Api137, drosocin is O-glycosylated on Thr11, and we observed that the α -D-GalNAc modification contributes to the ribosome binding by establishing multiple hydrogen bond interactions with U2609 of the 23S rRNA (Fig. 6a). These interactions rationalize our (Fig. 1) and previous^{17–24} observations that the native modified forms of drosocin generally display enhanced antimicrobial activity compared to the

unmodified peptide. Interestingly, we observed that drosocin causes a shift of U2609 that breaks the base pair that U2609 usually forms with A752 (Fig. 6a). Consistently, we could demonstrate that single and double mutations at these positions could influence the activity of the glycosylated, but not the unmodified, form of drosocin (Fig. 5e,f). To our knowledge, breaking of this base pair has not been observed in *E. coli* previously, although the base pair is important for interaction⁴² and bactericidal activity⁴³ of the ketolide telithromycin and also interacts with the free tryptophan during TnaC-mediated translational stalling⁴⁴ (Extended Data Fig. 5g–i). We note, however, that U2609 and A752 are unpaired in some bacterial ribosomes, such as *Mycobacterium tuberculosis*⁴⁵, raising the question of whether these ribosomes are more susceptible to glycosylated forms of drosocin.

In addition to the termination complex, we observed drosocin bound to two other ribosomal particles—namely, a vacant 50S subunit and an elongating ribosome (Fig. 2b,c). This implies that, in the cell, drosocin could potentially interact with the 50S subunit after termination and ribosome recycling, when the 70S ribosomes are split into their component subunits (Fig. 6b). This is not surprising given that most of the interactions formed by drosocin are identical between

the vacant and terminating ribosome. Indeed, we observed that, on the vacant 50S ribosome, the α -D-GalNAc has also inserted in between the U2609–A752 base pair, causing a shift in U2609 as observed in the termination state (Fig. 6b). By contrast, the C-terminus of drosocin on the vacant 50S subunit appears flexible and less well resolved, presumably because the interaction with Gln235 of RF1 is absent (Fig. 6b). Similarly, binding of Api137 has previously been shown to be stabilized on 70S ribosomes by the presence of RF1 when compared to vacant ones¹⁰. Because we observed no initiation states within our structural ensembles, we presume that the fMet-tRNA can bind at the P-site of the PTC unimpeded by the presence of drosocin (Fig. 6c), possibly by competing with the C-terminus for its binding site at the PTC. Conversely, we observed a major population of drosocin-bound ribosomes that was in an elongation state—namely, a post-peptide bond formation pre-translocation state with deacylated-tRNA^{fMet} in the P-site and a fMet-Leu-tRNA^{Leu} in the A-site (Fig. 6d). This suggests that drosocin can interfere with the first translocation event involving the movement of the fMet-Leu-tRNA^{Leu} into the P-site. We think that this arrest is likely to be temporary because, in our toeprinting experiments, we observed that ribosomes can eventually translate the entire open reading frame (ORF) and become trapped at the termination codon (Fig. 1f–h). In the elongation state, drosocin is particularly flexible and poorly resolved, which is exemplified by the poor density for the α -D-GalNAc and the presence of both closed (base paired) and open (unpaired) conformations of U2609 (Fig. 6d and Extended Data Fig. 5a–f). We favor a model whereby drosocin and the fMet-Leu-tRNA^{Leu} jostle for position at the P-site of the PTC and that occupation by fMet-Leu-tRNA^{Leu} triggers translocation and subsequent rounds of elongation that ultimately cause dissociation of drosocin from the ribosome (Fig. 6e). Once the nascent polypeptide chain becomes extended within the ribosomal tunnel, drosocin cannot rebind until the termination codon is reached and the nascent chain is released by RF1 (or RF2) (Fig. 6a).

It is remarkable that, although both drosocin and apidaecin inhibit translation by trapping RFs on the ribosome in an analogous manner, the binding mode and molecular details of the interactions of these peptides with components of the ribosomal tunnel are completely distinct. This is accentuated by the presence of O-glycosylation that plays a critical role for drosocin but is lacking for apidaecin. Curiously, other AMPs are glycosylated, such as pyrrolicorin¹³, which bears an identical modification to drosocin at exactly the same position—namely, GalNAc on Thr11—and minor forms with an additional galactose on the GalNAc have been also detected²⁷. Although structures of the unmodified pyrrolicorin on the ribosome reveal a reversed orientation compared to drosocin^{6,7}, superimposition reveals that Thr11 of pyrrolicorin and drosocin are in close proximity, raising the possibility that the glycosylation of pyrrolicorin may establish analogous interactions with the ribosome, as observed here for drosocin. Finally, we show that drosocin traps RF1 decoding the UAA stop codon on the ribosome in an analogous manner to that observed during canonical translation. However, the higher resolution observed here enables us to observe many water-mediated interactions that were not possible to observe previously. Thus, our study also provides structural insight into the fundamental mechanism of stop codon recognition during canonical translation termination.

Online content

Any methods, additional references, Nature Portfolio reporting summaries, source data, extended data, supplementary information, acknowledgements, peer review information; details of author contributions and competing interests; and statements of data and code availability are available at <https://doi.org/10.1038/s41589-023-01293-7>.

References

- Mardirossian, M. et al. The host antimicrobial peptide Bac71-35 binds to bacterial ribosomal proteins and inhibits protein synthesis. *Chem. Biol.* **21**, 1639–1647 (2014).
- Krizsan, A. et al. Insect-derived proline-rich antimicrobial peptides kill bacteria by inhibiting bacterial protein translation at the 70S ribosome. *Angew. Chem. Int. Ed. Engl.* **53**, 12236–12239 (2014).
- Graf, M. & Wilson, D. N. Intracellular antimicrobial peptides targeting the protein synthesis machinery. *Adv. Exp. Med. Biol.* **1117**, 73–89 (2019).
- Seefeldt, A. C. et al. The proline-rich antimicrobial peptide Onc112 inhibits translation by blocking and destabilizing the initiation complex. *Nat. Struct. Mol. Biol.* **22**, 470–475 (2015).
- Roy, R. N., Lomakin, I. B., Gagnon, M. G. & Steitz, T. A. The mechanism of inhibition of protein synthesis by the proline-rich peptide oncocin. *Nat. Struct. Mol. Biol.* **22**, 466–469 (2015).
- Seefeldt, A. C. et al. Structure of the mammalian antimicrobial peptide Bac7(1–16) bound within the exit tunnel of a bacterial ribosome. *Nucleic Acids Res.* **44**, 2429–2438 (2016).
- Gagnon, M. G. et al. Structures of proline-rich peptides bound to the ribosome reveal a common mechanism of protein synthesis inhibition. *Nucleic Acids Res.* **44**, 2439–2450 (2016).
- Mardirossian, M. et al. The dolphin proline-rich antimicrobial peptide Tur1A inhibits protein synthesis by targeting the bacterial ribosome. *Cell Chem. Biol.* **25**, 530–539 (2018).
- Mardirossian, M. et al. Peptide inhibitors of bacterial protein synthesis with broad spectrum and SbmA-independent bactericidal activity against clinical pathogens. *J. Med. Chem.* **63**, 9590–9602 (2020).
- Florin, T. et al. An antimicrobial peptide that inhibits translation by trapping release factors on the ribosome. *Nat. Struct. Mol. Biol.* **24**, 752–757 (2017).
- Graf, M. et al. Visualization of translation termination intermediates trapped by the apidaecin 137 peptide during RF3-mediated recycling of RF1. *Nat. Commun.* **9**, 3053 (2018).
- Bulet, P. et al. A novel inducible antibacterial peptide of *Drosophila* carries an O-glycosylated substitution. *J. Biol. Chem.* **268**, 14893–14897 (1993).
- Bulet, P., Hetru, C., Dimarcq, J. L. & Hoffmann, D. Antimicrobial peptides in insects; structure and function. *Dev. Comp. Immunol.* **23**, 329–344 (1999).
- Uttenweiler-Joseph, S. et al. Differential display of peptides induced during the immune response of *Drosophila*: a matrix-assisted laser desorption ionization time-of-flight mass spectrometry study. *Proc. Natl Acad. Sci. USA* **95**, 11342–11347 (1998).
- Rabel, D. et al. Primary structure and in vitro antibacterial properties of the *Drosophila melanogaster* attacin C pro-domain. *J. Biol. Chem.* **279**, 14853–14859 (2004).
- Hoffmann, R., Bulet, P., Urge, L. & Otvos, L. Jr. Range of activity and metabolic stability of synthetic antibacterial glycopeptides from insects. *Biochim. Biophys. Acta* **1426**, 459–467 (1999).
- Gobbo, M. et al. Antimicrobial peptides: synthesis and antibacterial activity of linear and cyclic drosocin and apidaecin 1b analogues. *J. Med. Chem.* **45**, 4494–4504 (2002).
- Marcaurette, L. A., Rodriguez, E. C. & Bertozzi, C. Synthesis of an oxime-linked neoglycopeptide with glycosylation-dependent activity similar to its native counterpart. *Tetrahedron Lett.* **39**, 8417–8420 (1998).
- Rodriguez, E. C., Winans, K. A., King, D. S. & Bertozzi, C. R. A strategy for the chemoselective synthesis of O-linked glycopeptides with native sugar–peptide linkages. *J. Am. Chem. Soc.* **113**, 9905–9906 (1997).
- Otvos, L. Jr. et al. Interaction between heat shock proteins and antimicrobial peptides. *Biochemistry* **39**, 14150–14159 (2000).
- Ahn, M. et al. Substitution of the GalNAc- α -O-Thr¹¹ residue in drosocin with O-linked glyco-peptoid residue: effect on antibacterial activity and conformational change. *Bioorg. Med. Chem. Lett.* **21**, 6148–6153 (2011).

22. Ahn, M. et al. Functional and structural characterization of drosocin and its derivatives linked O-GalNAc at Thr¹¹ residue. *Bull. Korean Chem. Soc.* **32**, 3327–3332 (2011).
23. Talat, S., Thiruvikraman, M., Kumari, S. & Kaur, K. J. Glycosylated analogs of formaecin I and drosocin exhibit differential pattern of antibacterial activity. *Glycoconj. J.* **28**, 537–555 (2011).
24. Lele, D. S., Dwivedi, R., Kumari, S. & Kaur, K. J. Effect of distal sugar and interglycosidic linkage of disaccharides on the activity of proline rich antimicrobial glycopeptides. *J. Pept. Sci.* **21**, 833–844 (2015).
25. Lele, D. S., Talat, S., Kumari, S., Srivastava, N. & Kaur, K. J. Understanding the importance of glycosylated threonine and stereospecific action of drosocin, a proline rich antimicrobial peptide. *Eur. J. Med. Chem.* **92**, 637–647 (2015).
26. Ludwig, T., Krizsan, A., Mohammed, G. K. & Hoffmann, R. Antimicrobial activity and 70S ribosome binding of apidaecin-derived Api805 with increased bacterial uptake rate. *Antibiotics (Basel)* **11**, 430 (2022).
27. Cociancich, S. et al. Novel inducible antibacterial peptides from a hemipteran insect, the sap-sucking bug *Pyrrhocoris apterus*. *Biochem. J.* **300**, 567–575 (1994).
28. Krizsan, A., Prah, C., Goldbach, T., Knappe, D. & Hoffmann, R. Short proline-rich antimicrobial peptides inhibit either the bacterial 70S ribosome or the assembly of its large 50S subunit. *ChemBioChem* **16**, 2304–2308 (2015).
29. Berthold, N. & Hoffmann, R. Cellular uptake of apidaecin 1b and related analogs in Gram-negative bacteria reveals novel antibacterial mechanism for proline-rich antimicrobial peptides. *Protein Pept. Lett.* **21**, 391–398 (2014).
30. Benincasa, M. et al. Antimicrobial activity of Bac7 fragments against drug-resistant clinical isolates. *Peptides* **25**, 2055–2061 (2004).
31. Mattiuzzo, M. et al. Role of the *Escherichia coli* SbmA in the antimicrobial activity of proline-rich peptides. *Mol. Microbiol.* **66**, 151–163 (2007).
32. Mardirossian, M. et al. Fragments of the Nonlytic Proline-Rich Antimicrobial Peptide Bac5 Kill *Escherichia coli* Cells by Inhibiting Protein Synthesis. *Antimicrob. Agents Chemother.* **62**, e00534–18 (2018).
33. Mardirossian, M. et al. Proline-rich peptides with improved antimicrobial activity against *E. coli*, *K. pneumoniae*, and *A. baumannii*. *ChemMedChem* **14**, 2025–2033 (2019).
34. Hartz, D., McPheeters, D. S., Traut, R. & Gold, L. Extension inhibition analysis of translation initiation complexes. *Methods Enzymol.* **164**, 419–425 (1988).
35. Polikanov, Y. S., Steitz, T. A. & Innis, C. A. A proton wire to couple aminoacyl-tRNA accommodation and peptide-bond formation on the ribosome. *Nat. Struct. Mol. Biol.* **21**, 787–793 (2014).
36. Syroegin, E. A., Aleksandrova, E. V. & Polikanov, Y. S. Structural basis for the inability of chloramphenicol to inhibit peptide bond formation in the presence of A-site glycine. *Nucleic Acids Res.* **50**, 7669–7679 (2022).
37. Mangano, K. et al. Genome-wide effects of the antimicrobial peptide apidaecin on translation termination in bacteria. *eLife* **9**, e62655 (2020).
38. Mangano, K. et al. Inhibition of translation termination by the antimicrobial peptide drosocin. *Nat. Chem. Biol.* <https://doi.org/10.1038/s41589-023-01300-x> (2023).
39. Lele, D. S., Talat, S. & Kaur, K. J. The presence of arginine in the Pro-Arg-Pro motif augments the lethality of proline rich antimicrobial peptides of insect source. *Int. J. Pept. Res. Ther.* **19**, 323–330 (2013).
40. Laurberg, M. et al. Structural basis for translation termination on the 70S ribosome. *Nature* **454**, 852–857 (2008).
41. Zhou, J., Korostelev, A., Lancaster, L. & Noller, H. F. Crystal structures of 70S ribosomes bound to release factors RF1, RF2 and RF3. *Curr. Opin. Struct. Biol.* **22**, 733–742 (2012).
42. Dunkle, J. A., Xiong, L., Mankin, A. S. & Cate, J. H. Structures of the *Escherichia coli* ribosome with antibiotics bound near the peptidyl transferase center explain spectra of drug action. *Proc. Natl Acad. Sci. USA* **107**, 17152–17157 (2010).
43. Svetlov, M. S., Cohen, S., Alsuhebany, N., Vazquez-Laslop, N. & Mankin, A. S. A long-distance rRNA base pair impacts the ability of macrolide antibiotics to kill bacteria. *Proc. Natl Acad. Sci. USA* **117**, 1971–1975 (2020).
44. van der Stel, A. X. et al. Structural basis for the tryptophan sensitivity of TnaC-mediated ribosome stalling. *Nat. Commun.* **12**, 5340 (2021).
45. Yang, K. et al. Structural insights into species-specific features of the ribosome from the human pathogen *Mycobacterium tuberculosis*. *Nucleic Acids Res.* **45**, 10884–10894 (2017).

Publisher's note Springer Nature remains neutral with regard to jurisdictional claims in published maps and institutional affiliations.

Open Access This article is licensed under a Creative Commons Attribution 4.0 International License, which permits use, sharing, adaptation, distribution and reproduction in any medium or format, as long as you give appropriate credit to the original author(s) and the source, provide a link to the Creative Commons license, and indicate if changes were made. The images or other third party material in this article are included in the article's Creative Commons license, unless indicated otherwise in a credit line to the material. If material is not included in the article's Creative Commons license and your intended use is not permitted by statutory regulation or exceeds the permitted use, you will need to obtain permission directly from the copyright holder. To view a copy of this license, visit <http://creativecommons.org/licenses/by/4.0/>.

© The Author(s) 2023

Methods

Drosocin peptides

Api137, Dro, Dro-3P, Dro-R18A and Dro-R18K were synthesized by Novo-Pro (<https://www.novoprolabs.com>). The glycosylated Dro1–Dro8 peptides were synthesized as described^{23–25,46}.

Bacterial strains

Strains *E. coli* Keio wild-type and *E. coli* Keio $\Delta sbmA$ used from the Keio knockout collection (Horizon, <https://horizondiscovery.com>). Wild-type *E. coli* SQ110 ($\Delta rrnGADBHC$ (ptRNA67))⁴⁷ and SQ171 ($\Delta rrnGADEHBC$ (pKK3535, ptRNA67))⁴⁷ strains and related mutants *E. coli* SQ110 A2059G and *E. coli* SQ171 A2503G were obtained from the previous Api137 study¹⁰. *E. coli* strains SQ171 bearing A752G, U2609C and A752G:U2609C mutations⁴³ and *E. coli* SQ171 U2609G⁴⁸ were generated previously.

Antibiotic susceptibility assays

The susceptibility of *E. coli* strains to compounds was evaluated by monitoring the bacterial growth in presence of increasing concentrations of the compound of interest. In brief, bacteria were inoculated in a total volume of 100 μ l of medium contained in a well of a 96-well microplate (round bottom, with cap, sterile; Sarstedt). The medium used was either LB, as rich medium, or ATCC medium (778 Davis and Mingioli glucose minimal medium), as minimal medium. Before inoculation, bacteria were grown up to exponential phase and then inoculated into the culture mix, containing selective antibiotic if necessary, with an initial optical density at 600 nm (OD₆₀₀) of 0.05. Values measured from wells containing just the medium were used as a blank. The growth in each well was monitored by measuring the OD₆₀₀ every 10 minutes for a total of 20 hours at 37 °C with shaking using a plate reader (Tecan Infinite 200 PRO). The inhibition resulting from a compound's concentration was evaluated by normalizing the OD₆₀₀ at $t = 12$ hours (corresponding to the end of the log phase) from the treated culture to the untreated one. For each compound, the concentrations tested were 5 μ M, 10 μ M and 30 μ M. Each single titration assay was done in triplicate with individually prepared culture mixes. For each concentration, the standard deviation was calculated, taking into account each single replica and its specific technical error from the plate reader.

Data analysis

Data from the in vivo assay were normalized and statistically analysed by GraphPad Prism version 9.4.0.

In vitro translation assays

The in vitro translation assay was carried out as described previously^{4,8} using the *E. coli* PURExpress system (New England Biolabs (NEB), E6800S). Then, 1 μ l of antibiotic solution was added to 5 μ l of PURExpress reaction mix. Each reaction contained 10 ng μ l⁻¹ of mRNA encoding the Fluc, which was in vitro transcribed from a pIVEX-2.3MCS vector containing the Fluc gene using T7 polymerase (Thermo Fisher Scientific). The reaction mix was incubated for 30 minutes at 32 °C while shaking (600 r.p.m.). Reactions were stopped with 5 μ l of kanamycin (50 mg ml⁻¹) and transferred into a 96-well microplate (Greiner Lumitrac, non-binding, white, chimney). Next, 40 μ l of luciferase assay substrate solution (Promega, E1501) was added, and luminescence was measured using a plate reader (Tecan Infinite 200 PRO). Nuclease-free water was added instead of antibiotic as control. Absolute luminescence values were normalized using reactions without antibiotic. All assays were done as triplicates with individually prepared reaction mix.

Toeprinting assays

Toeprinting reactions were performed as described previously⁴. In brief, reactions were performed with 6 μ l of PURExpress Δ RF123 in vitro protein synthesis system (NEB) in the presence of 1 \times RF3 and either 1 \times or 10 \times of RF1 or RF2 (relative to the manufacturer's recommendation).

The reactions were carried out on an MLIF-UAA-toeprint template (5'-TAATACGACTCACTATAGGAGACTTAAGTATAAGGAGGAAAAAATATGATATCTTTGTAATGCGTAATGTAGATAAAACATCTACTATTTAAGTGATAGAATTCTATCGTTAATAAGCAAATTCATTATAACC-3', ORF start codon and stop codon are underlined bold), containing T7 promoter, a ribosome binding site, an MLIF-coding ORF and the NVI* primer binding site. The template is a version of the ErmBL template with a truncated ORF and addition of a isoleucine coding codon at the third position in the ORF. The template was generated by polymerase chain reaction of two overlapping 77-nt- and 78-nt-long primers. The reactions contained 30 ng of the MLIF-UAA-toeprint DNA template. The reactions were supplemented with Api137, thiostrepton or one of the drosocin derivatives as specified. The transcription–translation reactions were incubated for 15 minutes at 37 °C. The reverse transcription on the MLIF-short-UAA toeprint template was carried out using AMV RT and primer NV*1-Alexa 647 (5'-GGTTATAATGAATTTGCTTATTAAC-3'). The transcription–translation reactions were incubated with AMV RT and NV*1-Alexa 647 for 20 minutes at 37 °C. mRNA degradation was carried out by the addition of 1 μ l of 5 M NaOH. The reactions were neutralized with 0.7 μ l of 25% HCl, and nucleotide removal was performed with the QIAquick Nucleotide Removal Kit (Qiagen). The samples were dried under vacuum for 2 hours at 60 °C for subsequent gel electrophoresis. The 6% acrylamide gels were scanned on a Typhoon scanner (GE Healthcare).

Preparation of complexes for structural analysis

Drosocin–ribosome complexes were generated by in vitro transcription–translation reactions in PURExpress Δ RF123 in vitro protein synthesis system (NEB) with the same reaction mix as described earlier in the toeprinting assays. Complex formation reactions were carried out on an MLIF-UAA toeprint DNA template in a 48- μ l reaction with 1 \times RF3 and 10 \times RF1 (amounts relative to the manufacturer's recommendation) in the presence of 30 μ M Dro1. The reaction was incubated for 15 minutes at 37 °C. The reaction volume was then split: 42 μ l was used for complex generation, and 6 μ l was used for toeprinting analysis. Ribosome complexes were isolated by centrifugation in 900 μ l of sucrose gradient buffer (containing 40% sucrose, 50 mM HEPES-KOH pH 7.4, 100 mM KOAc, 25 mM Mg(OAc)₂ and 6 mM 2-mercaptoethanol) for 3 hours at 4 °C and 80,000g in an Optima Max-XP Tabletop Ultracentrifuge with a TLA 120.2 rotor. The pelleted complex was resuspended in Hico buffer (50 mM HEPES-KOH pH 7.4, 100 mM KOAc and 25 mM Mg(OAc)₂ supplemented with RF1, RF3 and Dro1 at the same concentrations used in the in vitro translation reaction) and then incubated for 15 minutes at 37 °C.

Preparation of cryo-EM grids and data collection

Grids (Quantifoil R3/3 Cu300 with 3-nm holey carbon) were glow discharged, and 4 μ l of sample (8 OD₂₆₀ per milliliter) was applied using a Vitrobot Mark IV (FEI) and snap-frozen in ethane/propane. Frozen cryo-EM grids were imaged on a TFS 300 kV Titan Krios at the Dubochet Center for Imaging EPFL (Lausanne, Switzerland). Images were collected on a Falcon IV direct detection camera in counting mode using the EPU and AFIS data collection scheme with a magnification of $\times 96,000$ and a total dose of 40 electrons per square angstrom ($e^-/\text{\AA}^2$) for each exposure and defocus ranging from $-0.4 \mu\text{m}$ to $-0.9 \mu\text{m}$. In total, 8,861 movies were produced in electron event representation format.

Single-particle reconstruction of drosocin–ribosome complexes

RELION version 4.0 (ref. ⁴⁹) was used for processing, unless otherwise specified. For motion correction, RELION's implementation of MotionCor2 with 4 \times 4 patches, and, for initial contrast transfer function (CTF) estimation, CTFFIND version 4.1.14 (ref. ⁵⁰), were employed. From 8,861 micrographs, 715,455 particles were picked using crYOLO with a general model⁵¹. In total, 529,600 ribosome-like particles were

selected after two-dimensional (2D) classification and extracted at 3× decimated pixel size (2.4 Å per pixel) (Supplementary Fig. 2). An initial three-dimensional (3D) refinement was done using an *E. coli* 70S reference map (EMD-12573) and followed by initial 3D classification without angular sampling with six classes. Two classes containing 70S ribosomes were combined (356,671 particles) and subsorted. A class containing 50S subunits (159,749 particles) was further processed. We observed no classes containing RF3, despite the presence of RF3 in the translation reactions. However, unlike our previous study¹¹, we did not use non-hydrolysable GTP analogs. The subsorting was done using particle subtraction with a circular mask around the A-site with four classes. One class containing density that could be assigned RF1 (137,449 particles), and one class with A-tRNA density (84,697 particles), were further processed. All resulting classes were 3D refined and CTF refined (4th order aberrations, beam tilt, anisotropic magnification and per-particle defocus value estimation). The termination complex was additionally subjected to Bayesian polishing and another round of CTF refinement. For the termination, elongation and 50S complexes, final resolutions (gold-standard FSC_{0.143}) of masked reconstructions of 2.3 Å, 2.8 Å and 2.0 Å were achieved, respectively (Extended Data Fig. 1a–c). To estimate local resolution values, Bsoft⁵² was used on the half-maps of the final reconstructions (bloccres -sampling 0.8 -maxres -boc 20 -cutoff 0.143 -verbose 1 -origin 0,0,0 -Mask half_map1 half_map 2) (Extended Data Fig. 1d–i).

Molecular modeling of the drosocin–ribosome complexes

The molecular models of the 30S and 50S ribosomal subunits were based on the *E. coli* 70S ribosome (Protein Data Bank (PDB) ID: 7K00)⁵³. Drosocin was modeled de novo, and the 2-acetamido-2-deoxy- α -D-galactopyranose was taken from the Ligand Expo database A2G (PDB ID: ID0H) and linked through REFMAC 5 (ref.⁵⁴). Restraint files for modified residues were created using aceDRG⁵⁵. The termination complex was assembled with an RF1 AlphaFold model (AF-POA710-F1) and a crystal structure of a deacylated phenylalanine tRNA (PDB ID: 6Y3G) in the P-site. The elongation complex was assembled with an initiator fMet-tRNA (PDB ID: 1VY4)³⁵ in the P-site and a Leu-tRNA (PDB ID: 7NSQ) in the A-site. Starting models were rigid body fitted using ChimeraX⁵⁶ and modeled using Coot 0.9.8.3 (ref.⁵⁷) from the CCP4 software suite version 8.0 (ref.⁵⁸). The sequence for the tRNAs was adjusted based on the appropriate anticodons corresponding to the mRNA. Final refinements were done in REFMAC 5 (ref.⁵⁴) using Servalcat⁵⁹. The molecular models were validated using Phenix comprehensive cryo-EM validation in Phenix 1.20–4487 (ref.⁶⁰).

Figures

UCSF ChimeraX 1.3 was used to isolate density and visualize density images and structural superpositions. Models were aligned using PyMol version 2.4 (Schrodinger). Figures were assembled with Adobe Illustrator and Inkscape (latest development release, regularly updated).

Reporting summary

Further information on research design is available in the Nature Portfolio Reporting Summary linked to this article.

Data availability

Micrographs have been deposited as uncorrected frames in the Electron Microscopy Public Image Archive with accession code [EMPIAR-11388](#). Cryo-EM maps have been deposited in the Electron Microscopy Data Bank with accession codes [EMD-15488](#) (drosocin termination complex), [EMD-15523](#) (drosocin elongation complex) and [EMD-15533](#) (drosocin 50S complex). Molecular models have been deposited in the Protein Data Bank with accession codes [8AKN](#) (drosocin termination complex), [8AM9](#) (drosocin elongation complex) and [8ANA](#) (drosocin 50S complex). Source data are provided with this paper.

References

46. Lele, D. S., Kaur, G., Thiruvikraman, M. & Kaur, K. J. Comparing naturally occurring glycosylated forms of proline rich antibacterial peptide, drosocin. *Glycoconj. J.* **34**, 613–624 (2017).
47. Quan, S., Skovgaard, O., McLaughlin, R. E., Buurman, E. T. & Squires, C. L. Markerless *Escherichia coli* *rrn* deletion strains for genetic determination of ribosomal binding sites. *G3 (Bethesda)* **5**, 2555–2557 (2015).
48. Osterman, I. A. et al. Tetracenomycin X inhibits translation by binding within the ribosomal exit tunnel. *Nat. Chem. Biol.* **16**, 1071–1077 (2020).
49. Kimanius, D., Dong, L., Sharov, G., Nakane, T. & Scheres, S. H. W. New tools for automated cryo-EM single-particle analysis in RELION-4.0. *Biochem. J.* **478**, 4169–4185 (2021).
50. Zheng, S. Q. et al. MotionCor2: anisotropic correction of beam-induced motion for improved cryo-electron microscopy. *Nat. Methods* **14**, 331–332 (2017).
51. Wagner, T. et al. SPHIRE-crYOLO is a fast and accurate fully automated particle picker for cryo-EM. *Commun. Biol.* **2**, 218 (2019).
52. Heymann, J. B. Guidelines for using Bsoft for high resolution reconstruction and validation of biomolecular structures from electron micrographs. *Protein Sci.* **27**, 159–171 (2018).
53. Watson, Z. L. et al. Structure of the bacterial ribosome at 2 Å resolution. *eLife* **9**, e60482 (2020).
54. Vagin, A. A. et al. REFMAC5 dictionary: organization of prior chemical knowledge and guidelines for its use. *Acta Crystallogr. D* **60**, 2184–2195 (2004).
55. Long, F. et al. AceDRG: a stereochemical description generator for ligands. *Acta Crystallogr. D* **73**, 112–122 (2017).
56. Pettersen, E. F. et al. UCSF ChimeraX: structure visualization for researchers, educators, and developers. *Protein Sci.* **30**, 70–82 (2021).
57. Emsley, P., Lohkamp, B., Scott, W. G. & Cowtan, K. Features and development of Coot. *Acta Crystallogr. D* **66**, 486–501 (2010).
58. Winn, M. D. et al. Overview of the CCP4 suite and current developments. *Acta Crystallogr. D* **67**, 235–242 (2011).
59. Yamashita, K., Palmer, C. M., Burnley, T. & Murshudov, G. N. Cryo-EM single-particle structure refinement and map calculation using Servalcat. *Acta Crystallogr. D* **77**, 1282–1291 (2021).
60. Liebschner, D. et al. Macromolecular structure determination using X-rays, neutrons and electrons: recent developments in Phenix. *Acta Crystallogr. D* **75**, 861–877 (2019).
61. Chan, K. H. et al. Mechanism of ribosome rescue by alternative ribosome-rescue factor B. *Nat. Commun.* **11**, 4106 (2020).

Acknowledgements

We thank A. Myasnikov, S. Nazarov and E. Ushikawa from the Dubochet Center for Imaging (an EPFL, UNIGE, UNIL initiative in Lausanne, Switzerland) for help with cryo-EM data collection, live data processing and IT support for data collection. We thank S. Mankin and coworkers for sharing unpublished data on the activity of drosocin derivatives. D.N.W. is supported by the Deutsche Zentrum für Luft- und Raumfahrt (DLR01K1820) within the RIBOTARGET consortium under the framework of the Joint Programming Initiative on Antimicrobial Resistance.

Author contributions

D.S.L. and K.J.K. synthesized modified drosocin peptides. M.M. performed all growth assays and in vitro translation assays. M.B. prepared cryo-EM samples and performed toeprinting analysis. H.S. prepared cryo-EM grids, and B.B. collected the cryo-EM data. T.O.K. processed the microscopy data and generated and refined the molecular models. T.O.K., M.M. and M.B. prepared the figures. D.N.W.

wrote the paper, with input from all authors. D.N.W. conceived and supervised the project.

Funding

Open access funding provided by Universität Hamburg.

Competing interests

The authors declare no competing interests.

Additional information

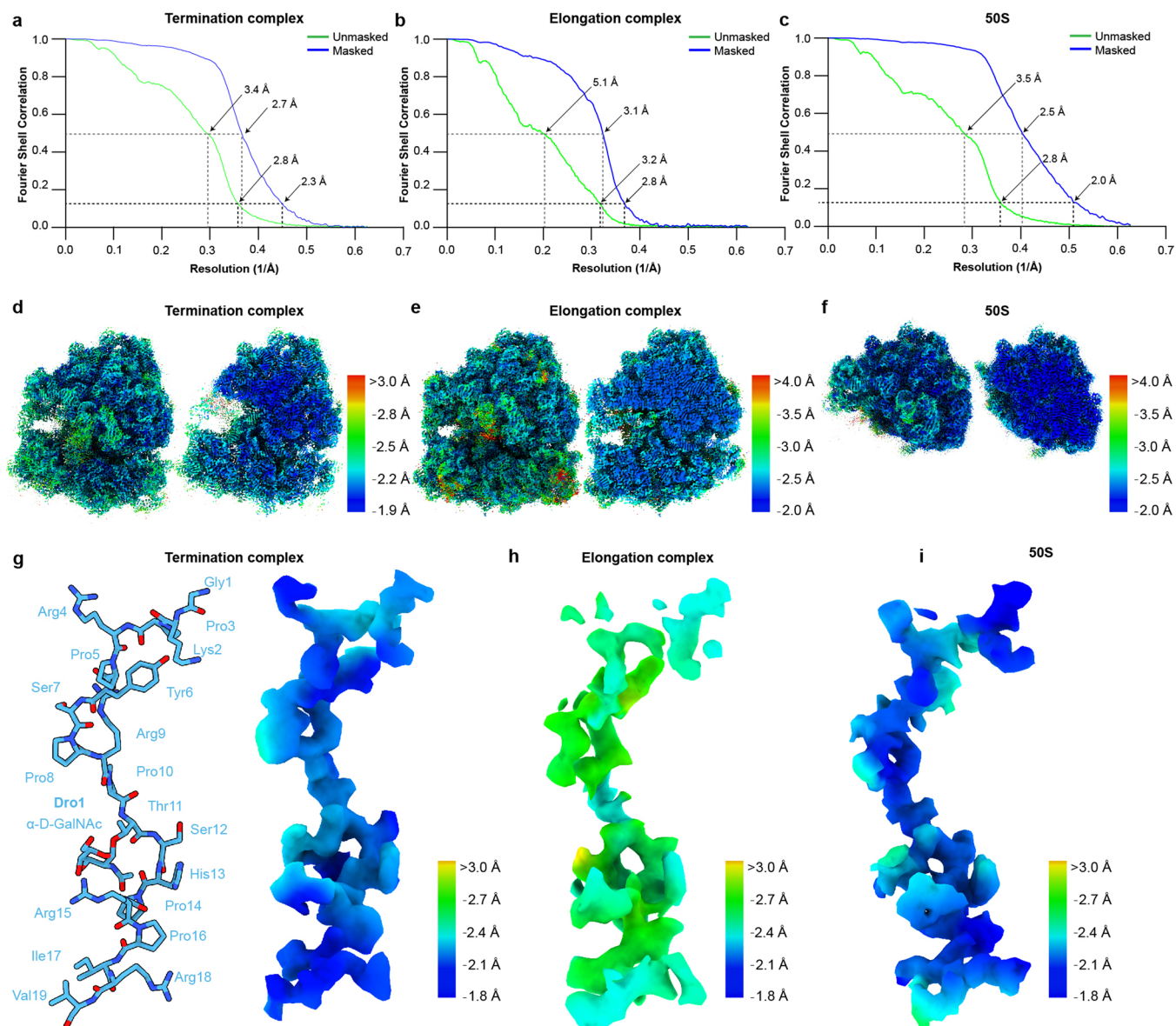
Extended data is available for this paper at <https://doi.org/10.1038/s41589-023-01293-7>.

Supplementary information The online version contains supplementary material available at <https://doi.org/10.1038/s41589-023-01293-7>.

Correspondence and requests for materials should be addressed to Daniel N. Wilson.

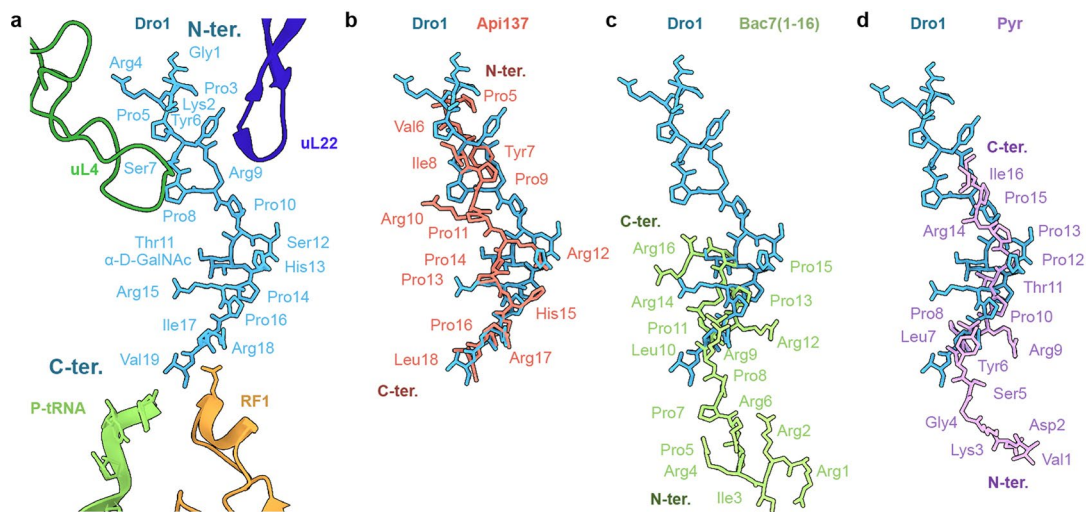
Peer review information *Nature Chemical Biology* thanks the anonymous reviewers for their contribution to the peer review of this work.

Reprints and permissions information is available at www.nature.com/reprints.



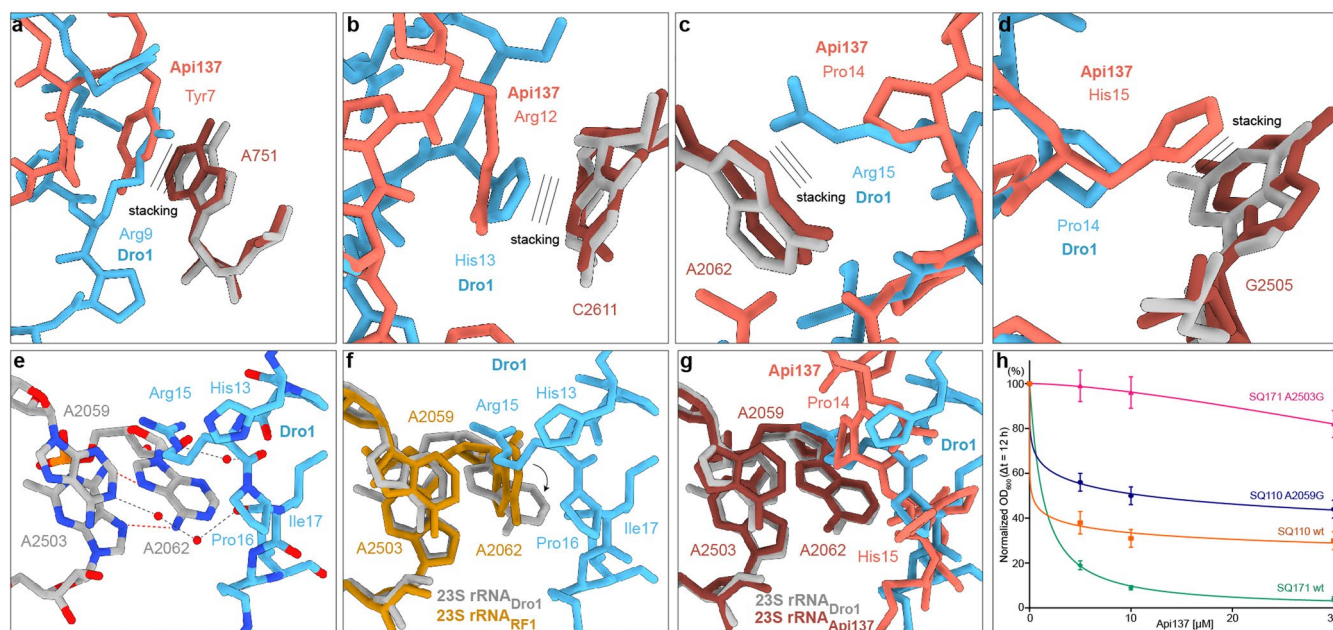
Extended Data Fig. 1 | Cryo-EM data processing. **a-c**, Fourier shell correlation (FSC) curve of the **(a)** termination, **(b)** elongation and **(c)** 50S complexes, with unmasked (green) and masked (blue) FSC curves plotted against the resolution (1/Å). **d-f**, Cryo-EM density colored according to local resolution and transverse

section for the **(d)** termination, **(e)** elongation and **(f)** 50S complexes. **g-i**, Molecular model of Dro1 (light blue) and corresponding cryo-EM density colored according to local resolution for the **(g)** termination, **(h)** elongation and **(i)** 50S complex.



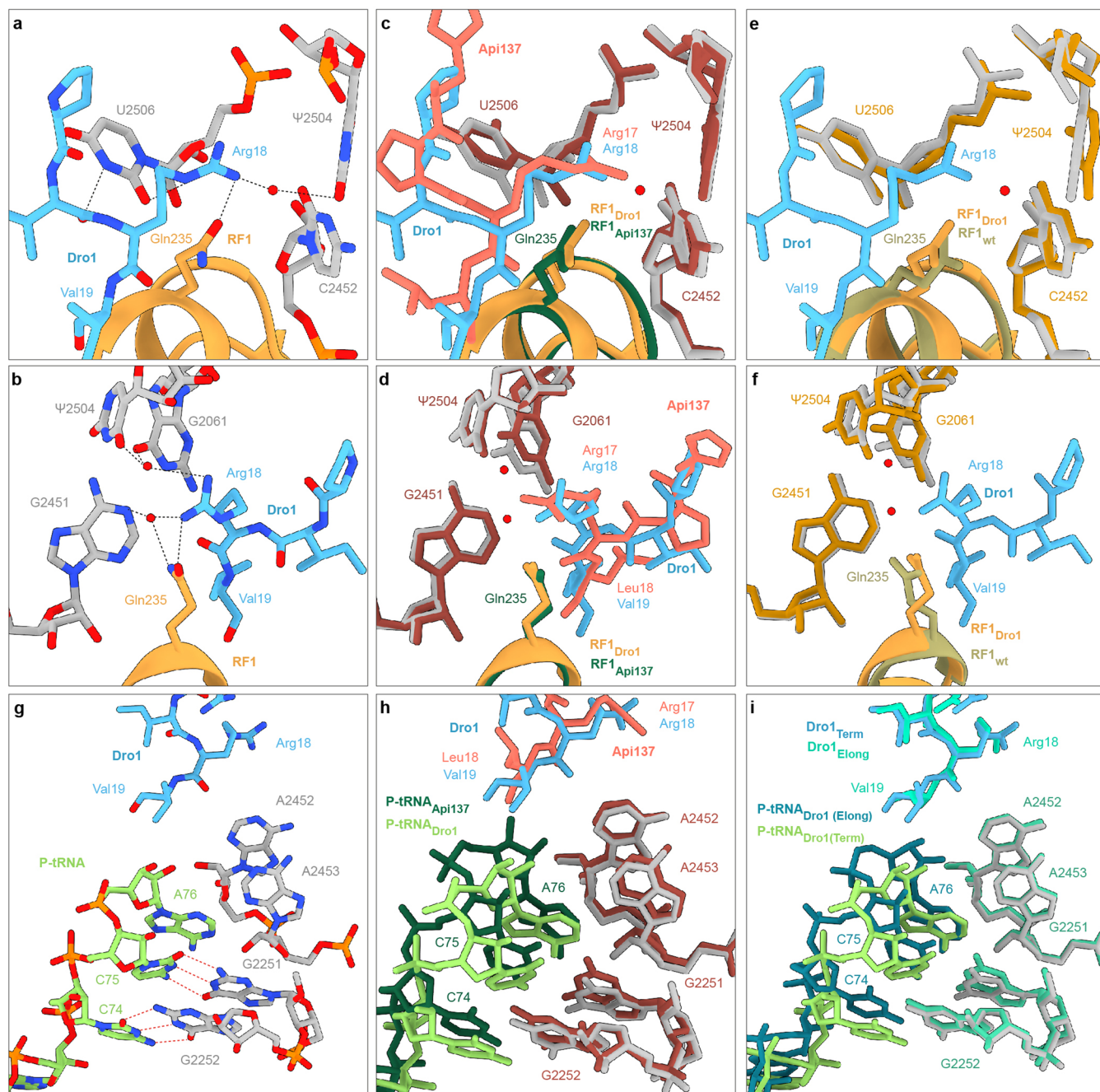
Extended Data Fig. 2 | Dro1 binds with same orientation as Api137, which is distinct from Bac7 and Pyr. a, Relative position of Dro1 (light blue) compared to P-tRNA (lime), RF1 (orange), uL4 (green) and uL22 (dark blue) within the Dro1-bound termination complex. **b-d**, Superimposition of Dro1 (light blue)

from **(a)** with **(b)** Api137 (salmon) from the Api137-ArfB complex (PDB ID [6YSS](#))⁶¹, **(c)** Bac7(1–16) (lime) from the Bac7-70S complex (PDB ID [5F8K](#))⁶ and **(d)** Pyrrocoricin (Pyr, purple) from the Pyr-70S complex (PDB ID [5FDV](#))⁶.



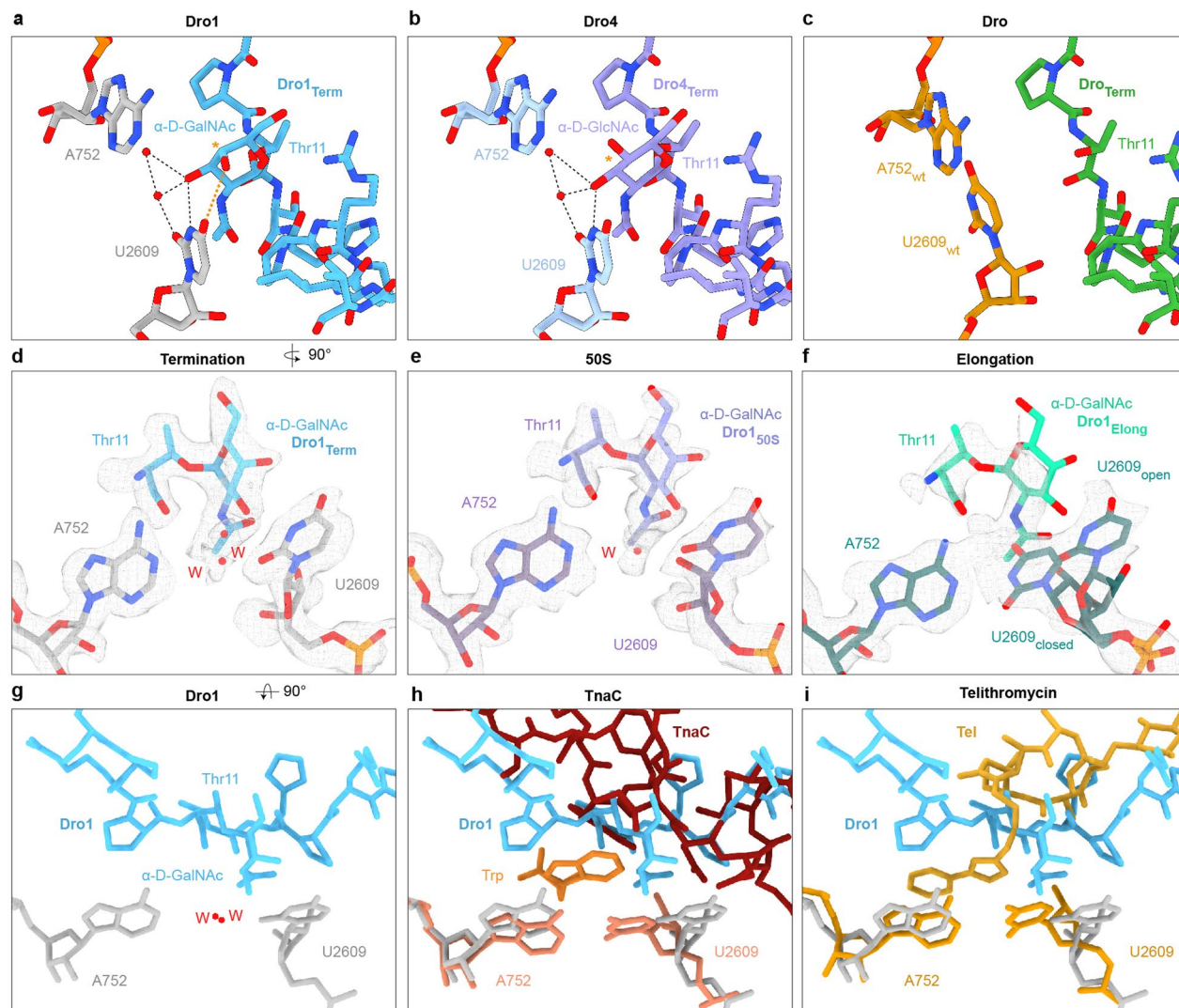
Extended Data Fig. 3 | Comparison of Dro1 and Api137 interactions with the exit tunnel. a-d, Stacking interactions (indicated as three lines) of sidechains of Api137 (light red, PDB ID 5O2R)¹⁰ with 23S rRNA nucleotides (dark red) compared to Dro1 (light blue) stacking interactions with 23S rRNA nucleotides (grey). **e**, Water-mediated interactions of Dro1 (light blue) with surrounding 23S rRNA nucleotides (grey). **(f-g)** Comparison of Dro1 from **(e)** with **(f)** a canonical termination complex (PDB ID 4V63)⁴⁰ and **(g)** Api137 (light red) and corresponding 23S rRNA nucleotides (dark red, PDB ID 5O2R)¹⁰. **h**, *in vivo*

inhibitory activity of 5 μM, 10 μM and 30 μM Api137 on the growth of *E. coli* SQ110 wt (orange), *E. coli* SQ110 A2059G (blue), *E. coli* SQ171 wt (green) and *E. coli* SQ171 A2503G (pink) in LB medium. For each concentration, inhibition values are the OD₆₀₀ at t = 12 h of the treated culture normalized to the untreated one, considered as 100%. The plotted points represent the mean for three independent biological replicas, the error bars represent the standard deviation and the technical measurement error of the plate reader. The curves were calculated and plotted by non-linear regression.



Extended Data Fig. 4 | Interaction of RF1 and P-tRNA with Dro1. **a-b**, Water-mediated and direct hydrogen bond interactions of Arg18 of Dro1 (light blue) with surrounding 23S rRNA nucleotides (grey) and Gln235 of RF1 (orange) from two views. **c-f**, Comparison of **(a-b)** with **(c-d)** Api137 (light red, PDB ID 5O2R)¹⁰ with RF1 (dark green) and 23S rRNA (dark red) and with **(e-f)** a canonical termination complex RF1 (olive, PDB ID 4V63)⁴⁰ and surrounding 23S rRNA

nucleotides (yellow). **g**, CCA-end of a deacylated tRNA (lime) in the P-site in presence of Dro1 is shifted while still establishing base-pairing interactions with G2251 and G2252. **h-i**, Comparison of **(g)** with superimposed deacylated tRNA in the P-site (**h**) with superimposed deacylated tRNA in the P-site (dark green) and **(h)** the presence of Api137 (light red, PDB ID 5O2R)¹⁰ or **(i)** the drosocin-bound elongation complex with deacylated tRNA in the P-site (dark teal) and Val19 of Dro1 poorly ordered (teal).



Extended Data Fig. 5 | Sugar modification of drosocin. **a-c**, Comparison of **(a)** the α -D-GalNAc modification of Dro1 (light blue) in the termination complex with **(b)** an *in silico* model for the α -D-GlcNAc modification of Dro4 **(b)**, light purple) indicating potential loss of a weak hydrogen bond (orange) of C4 hydroxy group of the sugar with C4 hydroxy group of U2609 (grey) as well as **(c)** comparison with an *in silico* model for the unmodified Dro that lacks the Thr-11 glycosylation (green). **d-f**, Isolated density (mesh) for Thr-11 with sugar modification and 23S rRNA nucleotides A752 and U2609 in an open

conformation for the **(d)** termination (grey) and **(e)** 50S complexes and **(f)** both open and closed conformations for the elongation complex (dark green). **g-i**, Dro1 (light blue) with 23S rRNA nucleotides A752 and U2609 (grey) and waters (red) in the termination complex superimposed with **(h)** TnaC (red) with 23S rRNA nucleotides (salmon) and Tryptophan (orange) from the TnaC-stalled *E. coli* ribosome complex (PDB ID 7O19)⁴⁴, and with **(i)** telithromycin (Tel, yellow, PDB ID 4V7S)⁴² with 23S rRNA nucleotides (orange).

Reporting Summary

Nature Portfolio wishes to improve the reproducibility of the work that we publish. This form provides structure for consistency and transparency in reporting. For further information on Nature Portfolio policies, see our [Editorial Policies](#) and the [Editorial Policy Checklist](#).

Statistics

For all statistical analyses, confirm that the following items are present in the figure legend, table legend, main text, or Methods section.

- | n/a | Confirmed |
|-------------------------------------|--|
| <input type="checkbox"/> | <input checked="" type="checkbox"/> The exact sample size (n) for each experimental group/condition, given as a discrete number and unit of measurement |
| <input type="checkbox"/> | <input checked="" type="checkbox"/> A statement on whether measurements were taken from distinct samples or whether the same sample was measured repeatedly |
| <input checked="" type="checkbox"/> | <input type="checkbox"/> The statistical test(s) used AND whether they are one- or two-sided
<i>Only common tests should be described solely by name; describe more complex techniques in the Methods section.</i> |
| <input checked="" type="checkbox"/> | <input type="checkbox"/> A description of all covariates tested |
| <input checked="" type="checkbox"/> | <input type="checkbox"/> A description of any assumptions or corrections, such as tests of normality and adjustment for multiple comparisons |
| <input type="checkbox"/> | <input checked="" type="checkbox"/> A full description of the statistical parameters including central tendency (e.g. means) or other basic estimates (e.g. regression coefficient) AND variation (e.g. standard deviation) or associated estimates of uncertainty (e.g. confidence intervals) |
| <input checked="" type="checkbox"/> | <input type="checkbox"/> For null hypothesis testing, the test statistic (e.g. F , t , r) with confidence intervals, effect sizes, degrees of freedom and P value noted
<i>Give P values as exact values whenever suitable.</i> |
| <input checked="" type="checkbox"/> | <input type="checkbox"/> For Bayesian analysis, information on the choice of priors and Markov chain Monte Carlo settings |
| <input checked="" type="checkbox"/> | <input type="checkbox"/> For hierarchical and complex designs, identification of the appropriate level for tests and full reporting of outcomes |
| <input checked="" type="checkbox"/> | <input type="checkbox"/> Estimates of effect sizes (e.g. Cohen's d , Pearson's r), indicating how they were calculated |

Our web collection on [statistics for biologists](#) contains articles on many of the points above.

Software and code

Policy information about [availability of computer code](#)

Data collection CryoEM data were collected using the EPU 2.6.1 software (FEI, Netherlands)

Data analysis RELION v4 with MotionCor2 v1.2.1, CTFIND 4.1.14, and crYOLO v1.8.4 were used for processing micrographs, picking particles, classification and refining cryo-EM maps. BSoft 2.1.1 was used to calculate local resolution. Coot v0.9.8.3 from the CCP4 software suit v8.0, for model building and Phenix (1.20-4487) and ServalCat in REFMAC 5 for model refinement and statistics. Figures were generated using Pymol v2.4 and ChimeraX v1.3.

For manuscripts utilizing custom algorithms or software that are central to the research but not yet described in published literature, software must be made available to editors and reviewers. We strongly encourage code deposition in a community repository (e.g. GitHub). See the Nature Portfolio [guidelines for submitting code & software](#) for further information.

Data

Policy information about [availability of data](#)

All manuscripts must include a [data availability statement](#). This statement should provide the following information, where applicable:

- Accession codes, unique identifiers, or web links for publicly available datasets
- A description of any restrictions on data availability
- For clinical datasets or third party data, please ensure that the statement adheres to our [policy](#)

Cryo-EM maps have been deposited in the Electron Microscopy Data Bank (EMDB) with accession codes EMD-15488 [<https://www.ebi.ac.uk/pdbe/entry/emdb/EMD-15488>] (Drosocin-termination complex), EMD-15523 [<https://www.ebi.ac.uk/pdbe/entry/emdb/EMD-15523>] (Drosocin-elongation complex), and EMD-15533 [<https://www.ebi.ac.uk/pdbe/entry/emdb/EMD-15533>] (Drosocin-50S complex). Molecular models have been deposited in the Protein Data Bank with accession codes 8AKN [<https://doi.org/10.2210/pdb8AKN/pdb>] (Drosocin-termination complex), 8AM9 [<https://doi.org/10.2210/pdb8AM9/pdb>] (Drosocin-elongation

complex), 8ANA [<https://doi.org/10.2210/pdb8ANA/pdb>] (Drosocin-50S complex). For model building: Starting model E. coli 70S (Protein Data Bank accession code 7k00 [10.2210/pdb7K00/pdb]), E. coli Release Factor 1 (AlphaFold AF514 POA710-F1), 2-acetamido-2-deoxy511 alpha-D-galactopyranose (Protein Data Bank accession code 1D0H [10.2210/pdb1D0H/pdb]), Phenylalanine-tRNA (Protein Data Bank accession code 6Y3G [10.2210/pdb6Y3G/pdb]), Leucine-tRNA (Protein Data Bank accession code 7NSQ [10.2210/pdb7NSQ/pdb]), fMet-tRNA (Protein Data Bank accession code 1VY4 [10.2210/pdb1VY4/pdb]).

Field-specific reporting

Please select the one below that is the best fit for your research. If you are not sure, read the appropriate sections before making your selection.

Life sciences Behavioural & social sciences Ecological, evolutionary & environmental sciences

For a reference copy of the document with all sections, see [nature.com/documents/nr-reporting-summary-flat.pdf](https://www.nature.com/documents/nr-reporting-summary-flat.pdf)

Life sciences study design

All studies must disclose on these points even when the disclosure is negative.

Sample size	MIC and IC50 experiments were done in triplicates using three individual bacterial cultures/reactions. This meets the standard agreed on in the field.
Data exclusions	Micrographs with low estimated resolution or poorly fitted CTFs were discarded, as were particles that clustered into poorly defined classes during 2D and 3D classification.
Replication	For MIC and IC50 experiments individual independent cultures/reactions were used to generate independent biological replicates. MIC and IC50 triplicates were successful and presented in Figure 1c-e, 4h, 5d and 6e,f, also sup Figure 6h. Toeprinting assays were performed in duplicate and were successful, a single replica representative of the duplicate is shown in Fig 1f-h and Supplementary Fig. 1b-d.
Randomization	For 3D refinement in RELION, particles are randomly placed in one of two subsets and half-reconstructions are processed independently employing the gold-standard. These subsets are maintained for CTF refinement. Otherwise, no randomization was performed.
Blinding	No blinding was performed as blinding is not possible or not applicable for the experiments.

Reporting for specific materials, systems and methods

We require information from authors about some types of materials, experimental systems and methods used in many studies. Here, indicate whether each material, system or method listed is relevant to your study. If you are not sure if a list item applies to your research, read the appropriate section before selecting a response.

Materials & experimental systems

n/a	Involved in the study
<input checked="" type="checkbox"/>	<input type="checkbox"/> Antibodies
<input checked="" type="checkbox"/>	<input type="checkbox"/> Eukaryotic cell lines
<input checked="" type="checkbox"/>	<input type="checkbox"/> Palaeontology and archaeology
<input checked="" type="checkbox"/>	<input type="checkbox"/> Animals and other organisms
<input checked="" type="checkbox"/>	<input type="checkbox"/> Human research participants
<input checked="" type="checkbox"/>	<input type="checkbox"/> Clinical data
<input checked="" type="checkbox"/>	<input type="checkbox"/> Dual use research of concern

Methods

n/a	Involved in the study
<input checked="" type="checkbox"/>	<input type="checkbox"/> ChIP-seq
<input checked="" type="checkbox"/>	<input type="checkbox"/> Flow cytometry
<input checked="" type="checkbox"/>	<input type="checkbox"/> MRI-based neuroimaging